R.F.A. van Noort June 2017

Bow thruster velocities at multiple bank slope configurations and the stability of slope material

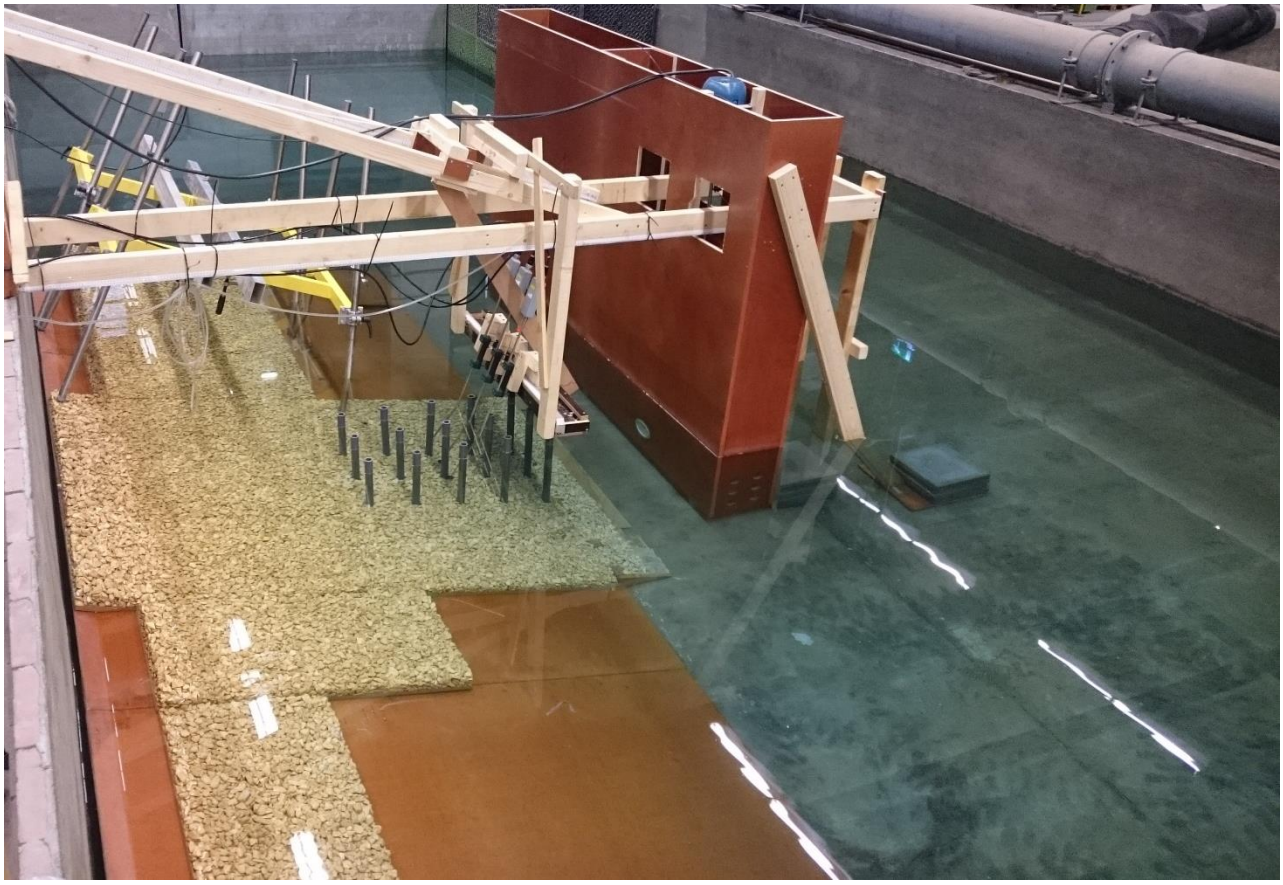

TU Delft

Bow thruster velocities at multiple bank slope configurations and the stability of slope material

By

R.F.A. van Noort

MSc Thesis

June 2017

Supervisor:	Prof. dr. ir. T. Vellinga,	TU Delft
Thesis committee:	Ir. H.J. Verheij,	TU Delft
	Ir. H.J. Verhagen	TU Delft
	Ir. T. Blokland	Municipality of Rotterdam
	Ir. A. van der Hout	Deltares

TU Delft

Abstract

Nearby several mooring locations for both sea-going vessels and inland vessels damage to embankments can be observed. Most times this damage is caused by the main propeller or the bow or stern thruster that is used when the vessel manoeuvres in order to berth or to de-berth. This research only focuses on the damage and velocities that are induced by the bow thruster. When a vessel uses its bow thruster to manoeuvre nearby a mooring location it creates a propeller jet. If this propeller jet is directed towards a bank, or slope that is part of for example an open quay structure it creates a hydraulic load on this slope. When the stability of the slope material or of the slope protection is not high enough erosion occurs and this might lead to instabilities of the entire slope and possibly also to nearby constructions if these are present. That is why a properly and stable enough slope protection is essential at locations where frequently hydraulic loads induced by propeller jets affect the slope. In order to design such a slope protection the Dutch engineering guidelines can be followed. For this first a calculation method to determine the maximum hydraulic bed load should be applied and after that a calculation method to determine the median stone diameter for a riprap or armourstone revetment is applied as well.

Within this research both the design method for the hydraulic bed loads and the design method for the stability calculation according to the current Dutch engineering guidelines are considered and checked with scale model tests performed at the facilities of Deltares. The main goal of this research is to extend and to validate methods 1) to calculate the hydraulic bed loads as is proposed by a research by Van Doorn (2012) and 2) to calculate the stability of slope material as is proposed by a research by Roelse (2014). To fulfil this main goal it is important to get to know the differences between the measured maximum slope velocities and the theoretical maximum slope velocities according to the unconfined jet method for all test scenarios and for variations in slope angle, axial distance to the slope and different pile configurations. Next to that, it is important to get to know the consequences of these differences on the design of a slope protection. Furthermore, a stability relation is derived from the equilibrium scour depth equation that is proposed by Roelse (2014) for the design of a riprap revetment affected by a propeller jet. In addition, to validate this newly proposed stability relation which is based on the stability relation by Pilarczyk (1995) it is important to determine the stability parameters with the performed stability tests.

In order to answer the research questions scale model tests are conducted and ten different test scenarios are tested. All test scenarios contained velocity measurements except for one test scenario which contained stability measurements. Besides also the outflow velocities were measured. Within the scenarios with velocity measurements the roughness, slope angle, axial distance and the pile configuration are varied. The model set ups of the test scenarios included slopes of 1 : 2.5 with a rough and a smooth slope and slopes of 1 : 3 with and without piles. The variation in pile configuration included also a variation in location of jet axis with respect to the piles. For the velocity measurements an Electro Magnetic velocity Sensor is used which measured the velocities in front of the outflow opening, at multiple locations just above the center of the slope and sideward at the top of the slope. From these velocity measurements in time at a fixed location the time-averaged slope velocity and the turbulence intensity are determined for every measurement point. For the stability measurements an underwater camera is used to record all the stone movements while the rotational speed of the propeller was increased in small steps for five runs.

From the analyzed results of the velocity measurements it became clear that the relative turbulence intensities that are measured in the propeller jet and just above the slope are smaller than according to the literature and measurements performed by Van Doorn (2012). This can be explained by the fact that different measurement equipment is used that has a larger measurement volume and lower effective measuring frequency and due to that the smaller turbulent vortices can not be measured. This leads to smaller absolute turbulence intensities. Furthermore, the unconfined jet calculation method underestimates the maximum slope velocities with a correction factor ‘f’ of 1.22 to 1.64 for slopes of 1 : 2.5 and slopes of 1 : 3 without piles. For 1 : 3 slopes with piles the unconfined jet calculation method underestimates the maximum slope velocities with a correction factor ‘f’ of 1.46 to 1.67. Next to these conclusions, it is also concluded that the locations of the maximum slope velocities for all scenarios with and without piles are located higher on the

slope and closer to the point of intersection than according to the unconfined jet method. Besides, when these correction factors ‘f’ for the maximum slope velocity are applied when designing a slope structure this leads to larger median stone diameters for the riprap revetment. However, the current Dutch engineering guidelines use a larger stability parameter to correct the underestimation of the hydraulic bed loads on the slope.

Within the literature study a stability relation for the design of riprap and armourstone revetments is derived from the equilibrium scour depth equation proposed by Roelse (2014). This relation together with the original Izbash type stability relation and the modified Izbash type stability relation are tested with the scale model tests. The results show that the calculated stability parameters of the original Izbash type stability relation are smaller than the recommended values and therefore when the recommended Izbash stability parameter is used the d_{50} is overestimated. Also, the results show that the calculated stability parameters of the modified Izbash type stability relation are larger than the recommended values for the criterion of initiation of motion of no movement and little movement. This means that when using the recommended modified Izbash stability parameter the d_{50} is underestimated. Next to that, the results show that the calculated mobility parameter of the Pilarczyk type stability relation is smaller than the recommended value for the criterion of no movement and larger than the recommended value for the criterion of little movement. Therefore when using the recommended mobility parameter it underestimates the d_{n50} for the criterion of no movement and it overestimates the d_{n50} for little movement. After all, the location of maximum damage was determined and observed just above the toe of the slope and when comparing this to the results of the velocity measurements of test scenario T5 it shows that the largest turbulence intensities which make up the largest peak velocities together with the time-averaged velocity are most responsible for this damage.

Further research into the stability relation and thereby more lab experiments to validate also the jet diffusion mechanism in combination with the pile obstruction mechanism is recommended. In addition, it is recommended to conduct more research to define a function for the correction factor ‘f’ for the hydraulic bed loads that can be applied in more scenarios and that is dependent on parameters that are not taken into account in the present calculation method. Parameters such as the jet confinement due to the slope, the roughness and the influence of piles on the slope.

Preface

This research report is carried out in order to finish the Master Hydraulic Engineering at Delft University of Technology. It focuses on the flow velocities at multiple slope configurations induced by a bow thruster and the stability of slope material. Part of this research was to perform scale model tests at the laboratory of Deltares.

For the professional guidance I would like to thank each member of the graduation committee that is formed by Prof. dr. ir. T. Vellinga, ir. H.J. Verheij, ir. H.J. Verhagen, ir. A. van der Hout and ir. T. Blokland. Their feedback and enthusiastic support helped me during the entire project.

Secondly, I would like to thank the employees of the TU Delft and Deltares that helped me with setting up and performing the scale model tests. Especially Arno Doorn, Piet Doorn, Sander de Vree, Jaap van Duin, Hans Tas, Rob van Dijk, Richard Boele, Frans de Vreede and Wim Taal. Their support made me finish the measurement campaign successfully.

After all, I would like to thank all colleague students, friends, girlfriend and family that supported and motivated me.

Delft, June 2017

Roel van Noort

Table of Contents

List of Figures

List of Tables

List of Symbols

Symbol	Parameter	Value	Dimension
a	Exponent in formula hydraulic bed load	1	-
A	Coefficient in formula hydraulic bed load	2.8	-
b	Coefficient in formula hydraulic bed load	15.43	-
C	Coefficient in formula for velocity distribution	-	-
C_1	Coefficient in formula for velocity distribution	-	-
C_2	Coefficient in formula for velocity distribution	-	-
d_{n50}	Median stone diameter by weighing	-	m
d_{50}	Median stone diameter by sieving	-	m
D_0	Jet diameter at start	-	m
D_p	Propeller diameter	-	m
$D_{thruster}$	Thruster diameter	-	m
D_{pile}	Diameter of pile		
f	Correction factor formula hydraulic bed load	-	-
f_n	Percentage of maximum number of rotations per minute	-	-
$f_{thruster}$	Coefficient formula outflow velocity	1.02 – 1.05	-
Fr	Froude number	-	-
$Fr_{slope,crit}$	Critical densimetric slope Froude number	-	-
g	Gravitational constant	9.81	m/s^2
G_{pile}	Gap width between piles or centre to centre distance	-	m
k_h	Velocity profile factor	-	-
k_{sl}	Side slope factor	-	-
k_t	Turbulence factor	-	-
K_T	Thrust coefficient	-	-
L	Axial distance between outflow and slope	-	m
L_m	Length in scale model	-	m
L_p	Length in prototype	-	m
m_h	Slope factor	-	-
M	Momentum	-	Nm
M_0	Initial momentum	-	Nm
n_l	Scale factor for dimensions	-	-
n_u	Scale factor for velocities	-	-
n_{max}	Maximum number of rotations per minute	-	s^{-1}
N	Amount of measurements	-	-
p	Measure for the amount of standard deviations	-	-
$P_{thruster}$	Maximum installed engine power on ship	-	W
r	1. Radial distance from jet axis	-	m
	2. Relative turbulence intensity	-	-
$r_{uniform}$	Relative turbulence intensity in uniform flow	-	-
$Re_{jet-flow}$	Reynolds number of jet flow	-	-
RPM	Rotations per minute	-	min^{-1}
$\bar{U}$	Averaged flow velocity	-	m/s
U'	Flow velocity fluctuation	-	m/s
$U_{1\%}$	Velocity that is exceeded by 1% of the velocities	-	m/s
$U_{b,max}$	Maximum bed velocity	-	m/s

$U_{slope,crit}$	Critical slope velocity	-	m/s
U_0	Efflux velocity	-	m/s
$U_{approach}$	Approach flow velocity in front of the piles	-	m/s
U_{axis}	Axial flow velocity	-	m/s
U_{pile}	Flow velocity next to pile	-	m/s
$U_{slope,max}$	Maximum flow velocity above slope	-	m/s
$U_{x,r}$	Flow velocity at location x, r in jet	-	m/s
U_*	Near bed shear velocity	-	m/s
x	Horizontal distance from outflow point of jet	-	m
$X_{U,max}$	Distance between outflow and point of maximum load	-	m
α	Slope angle	-	°
α_p	Coefficient in formula for velocities between piles	-	-
$\beta_{Iz,cr}$	Izbash type stability parameter	-	-
$\beta_{Iz,modified}$	Modified Izbash type stability parameter	-	-
$\beta_{Iz,cr,uniform}$	Critical Izbash stability parameter for uniform flow	0.7	-
Δ	Relative density	-	-
θ_u	Angle of velocity vector	-	°
ν	Kinematic viscosity	-	m^2/s
σ	Absolute turbulence intensity	-	m/s
φ	Angle of internal friction of stones	-	°
Φ_{sc}	Stability correction factor	-	-
Ψ_{cr}	Shields type mobility parameter	-	-

1. Introduction

During a procedure for berthing or de-berthing of a ship the navigation speed is reduced and is low in order to increase the controllability of the ship. While carrying out the berthing process using only the rudder is insufficient and other propulsion systems or tugboat assistance is needed. Another propulsion system is most likely to be the transverse thruster at the bow or at the stern. Nowadays the bow thruster is most applied to ease the berthing and departure procedure. However the use of such a bow thruster has an effect on the banks and several types of constructions that are nearby the vessel. The jet that is formed affects the stability of these banks and constructions as is shown in Figure 1.

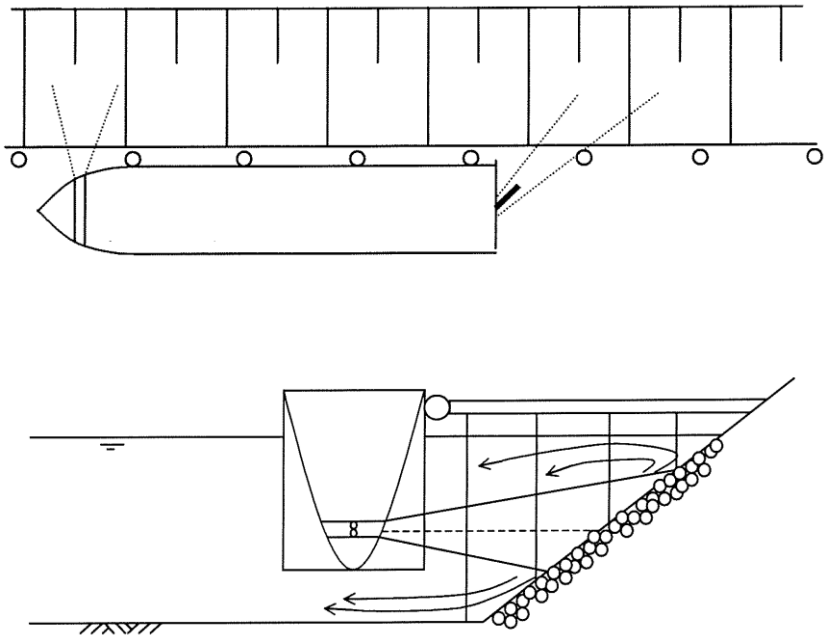

Figure 1 - Bow thruster jet induced by a vessel near an open quay wall or bank. A top view (top) and a side view (bottom)

In this research the currents on a bank or an open quay structure induced by a bow thruster are investigated with scale model tests. This chapter introduces the problem that will be investigated and presents the formulated research goal and research questions. Besides some background researches are discussed shortly which this research goes on with.

1.1 Problem formulation

Banks along port basins, rivers or canals are affected by bow thruster currents at several locations due to manoeuvering vessels. Both sea-going ships and the smaller inland waterway vessels may induce damage to the banks when the bow thrusters are used and transversal bow thruster jets reach the banks. Especially at locations where vessels moor frequently the damage may be large and probably cause instability of the slope. Usually the banks are designed with bank protection to avoid erosion. However, there is a need to avoid under- and overestimating of the loads and design a more adequate protection. Especially with the increasing size and the better equipped vessels nowadays.

For example, along open quay walls in ports several sea-going ships manoeuvre with their bow thrusters generating hydraulic forces on the slope. These hydraulic forces can lead to the movement or structural damage of the protection material. The forces are dependent on the used bow thruster power of the vessel. Larger vessels have the ability to use a larger bow thruster power and therefore are able to induce more damage.

Besides the problems near open quay walls, situations where vessels equipped with bow thrusters moor along a jetty close to an embankment occur a lot in the port of Rotterdam and at several other sea-ports all over the world. Nearby these locations bow thruster damage is also a problem to take into mind.

Additionally there are multiple situations where inland waterway traffic caused damage to the river or canal banks. Inland waterway vessels perform several manoeuvres during the navigation within an inland waterway. Most manoeuvres of the vessels have a short duration and are not of considerable influence on the stability of the bank and bed protection. However when a lot of manoeuvres occur at the same location repetitively there could be severe damage to the protection. Especially at mooring places for roll-on and roll-off vessels (mainly ferries), nearby locks and bridges where inland waterway traffic have to wait, at locations where mainly tugboats (relative powerful engines in small vessels) are used and at mooring locations along a waterway or side channel for other purposes

1.2 Bow thrusters

A propulsion system enables a vessel to manoeuvre and navigate through the waterways, in harbors and other locations. The type of propulsion system that is mostly applied is the propeller. In most cases vessels contain a main propeller to navigate and a thruster at the bow and/or at the stern to manoeuvre. Within this research only the bow thruster is considered.

The propeller of a bow thruster usually consists of 4 or 5 blades that are symmetrically attached to the propeller hub. This propeller hub is rotating in a vertical plane around the shaft that is driven by an engine. In order to provide a force that is pushing the vessel sideways the blades are 3-dimensional and have a wing-type profile. Characterizations of a propeller are the power and thrust delivered at standard regime, the rotational speed and direction, the amount and angle of the blades and the external diameter. More about the characteristics of bow thrusters is discussed in Appendix A - Bow thrusters.

A transverse thruster has to be worthwhile to build on a vessel because ships are only for a short duration performing a berthing or de-berthing operation. Therefore it is mainly applied on the following type of vessels:

- Ferries
- RoRo vessels
- Cruise ships
- Container vessels
- Smaller bulk carriers and tankers
- Inland waterway vessels

While operating the berthing of a ship it is of high importance to have enough control over the movements of the ship and to avoid damage to any structure. The vessel will move large masses of water and the flowing away of this water takes time. Especially during the movement towards the quay or bank the water body in between the vessel and the quay should have time to move away. For this reason the thruster is activated for short periods of about 30 seconds after which the captain has the possibility to break and observe to improve the operation.

1.3 Research goal

Still some research has to be done within the subject of bow thruster currents and the effect of that on the stability of slope material. This is of importance for slopes close to mooring locations and slopes as part of open quay wall structures. In the past several researches are performed about bow thruster currents at slopes and at slopes of open quay walls, however there still can be improvement and there is still more data related to this subject needed.

The main objective of this research project is formulated as:

- Extend and validate methods to calculate (1) the hydraulic loads from a bow thruster on a slope as proposed by Van Doorn (2012) and (2) the stability of slope material as proposed by Roelse (2014) for multiple bank slope configurations with and without piles.

In order to try to answer this main objective some sub-research questions have to be formulated and needs to be answered during the research process. The sub-research questions are:

1. If there are any differences, what are the differences between the measured and the theoretical maximum hydraulic bed loads for lab test set ups:
    - With varying distances between the outflow opening and the slope?
    - With varying slope angles?
    - With varying pile configurations on the slope?

2. What are the effects of any differences between the measured and the theoretical maximum hydraulic bed loads on the design of a slope protection?

3. How can the method to calculate equilibrium scour depth proposed by Roelse (2014) be changed into a stability formula for riprap revetments?

4. Which values can be found for the stability parameters of the original Izbash type stability relation, the modified Izbash type stability relation and the stability relation derived from the method proposed by Roelse (2014) for the test scenario tested in this research?

1.4 Background

As can be concluded from the research questions some research into this problem is already conducted in the past. Therefore this research project will continue on the obtained results and recommendations from these researches.

A master thesis research about bow thruster currents at open quay wall structures was performed earlier by Van Doorn (2012). This research introduced a correction factor that can be applied to a method to determine the hydraulic loads by a bow thruster on the slope of an open quay wall. The original method is based on research by Blaauw and Van de Kaa (1978), Verheij (1983) and Blokland (1997). During Van Doorn's research lab experiments were conducted and the results showed that the guidelines from PIANC (1997) underestimate the hydraulic loads. With this conclusion correction factors for the hydraulic loads are defined. However further research is needed into this method and the calculation method for the hydraulic loads should be checked for more configurations than done within that research. The thesis recommended that more slope configurations and more data have to be obtained with new lab experiments.

Secondly, in 2014 Roelse conducted a research to predict the equilibrium scour depth for a slope as part of an open piled quay structure. The method makes use of the same method as used with the other research to calculate the hydraulic load on slopes. The equilibrium scour depth equation follows from a literature study focused on the available theories on bow thruster induced currents, their influence on the stability and the scouring process. The equation is a combination of the scour induced by the jet flow and the additional scour induced by the presence of piles on the slope. During his research no lab experiments were conducted and the proposed scour equation is not validated yet. Part of this research by Roelse is used to propose a stability relation for an armourstone or riprap revetment.

A more detailed overview of the theory that will be used for this thesis and the calculation methods described above are discussed in the next chapter that contains a literature study.

1.5 Outline thesis

First the literature study of the different aspects of this research is presented in chapter 2. Present calculation methods are given for subsequently outflow velocities of a bow thruster, hydraulic bed loads on a slope and after all for the stability of bed material on a slope.

In chapter 3 the research method and therefore the experimental model set-up is described. A scale model was built at the test facilities of Deltares that could deliver the research data needed to answer the research questions. The most important test results obtained are presented in chapter 4 and a distinction is made between the outflow velocity measurements, the slope velocity measurements and the stability measurements.

The remaining part of this report contains the velocity analysis, the stability analysis, discussion and the conclusion supplemented by recommendations. In chapter 5 first the test results of the outflow velocity measurements are analyzed and after that the analysis of the slope velocity measurements is presented. For this part of the analysis the methods described in the literature study are used. In chapter 6 first the initiation of motion is analyzed and for this the stability relations described in the literature study are used. Besides the location of maximum damage is determined from the stability test results and discussed. In chapter 7 all findings and possible contributions for present methods are summed up and evaluated. Finally, chapter 8 includes the conclusions and therefore the answers to the sub-research questions that are formulated. Also, recommendations are formulated concerning all subjects mentioned.

In several sections of this report cross-references to appendices are given. The appendices at the end of this report contain subsequently supplements to the literature study, a plan view and cross section of the model set up, a sieve analysis of the stones used for the stability tests, all test results for each test scenario, a comparison of the test results of test scenario 1 with the results of test scenario 1 by Van Doorn (2012) and the derivation of the equation of the unconfined jet method for slopes.

2. Literature study

A literature study is conducted in order to make an overview of all the theory needed to set up the research method, analyze the results and finally answer the research questions.

In general when designing a slope protection a design procedure is followed as presented in Figure 2. This procedure presents all the important steps that lead to a stable design for a slope protection when correct assumptions are made and the correct equations are used.

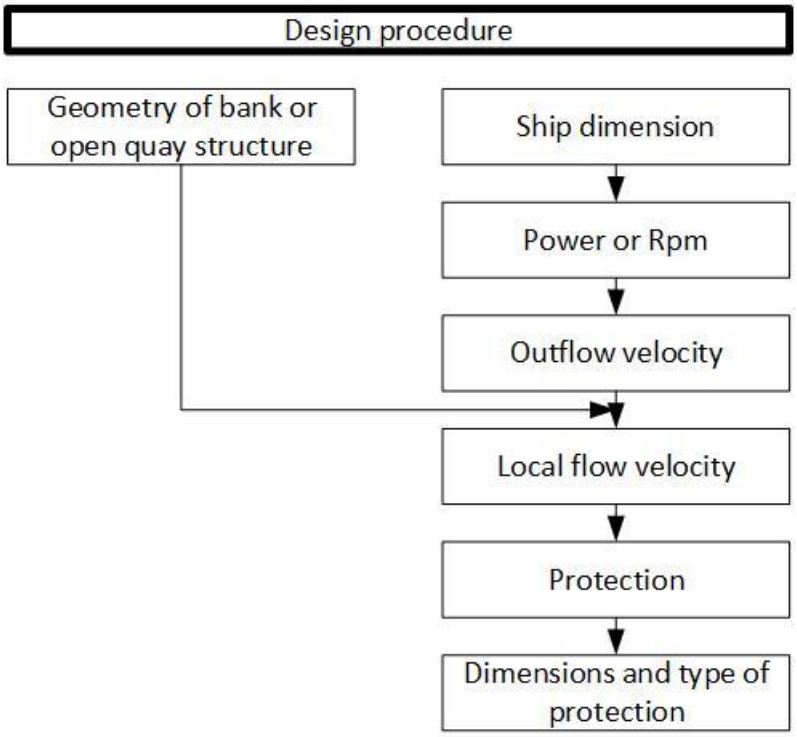

Figure 2 - Design procedure to design a stable slope protection

Following this design procedure leads to several topics that have to be studied in detail. These topics are mentioned in Figure 3. In the next sections within this chapter all the relevant theory related to these topics are discussed and described.

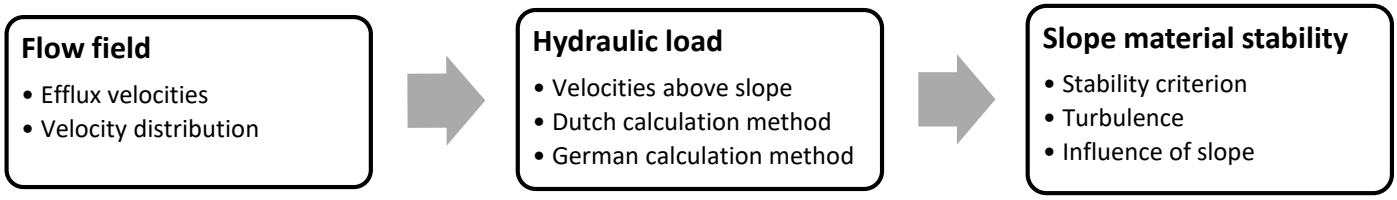

Figure 3 – Overview of the topics discussed in the literature review

2.1 Flow field

The propulsion systems of ships create water jets that can have influence on the stability of bed material, slope material or all kind of structures placed in the water. During this research only the stability of the slope material affected by the forces of the water jet of the bow thruster is considered. Especially when manoeuvring nearby open quay walls and banks of a canal or a port basin. In this section the propeller jet created by the bow thruster is explained in detail.

2.1.1 Velocity distribution in propeller jet

For the velocity distribution within a water jet initially Albertson et al (1950) determined a formula for a free jet. In the case of a free jet water is flowing out of an orifice into an unrestricted volume of water. It means that the submerged flow is not disturbed by any structure, bottom, surface or another type of boundary. The equations for a free jet as shown in (Eq. 2-1) and (Eq. 2-2) are valid for the zone of established flow and describe a velocity distribution that has a normal distribution around the jet axis as shown in Figure 4. The zone of established flow is the zone at the right of X_0 in this figure.

$$U_{axis} = \frac{1}{2C} U_0 (D_0/x) \qquad \textit{(Eq. 2-1)}$$

With: U_{axis}: $Axial\ flow\ velocity\ [m/s]$
C: $Coefficient\ [-]$
U_0: $Efflux\ velocity\ [m/s]$
D_0: $Jet\ diameter\ at\ start\ jet\ [m]$
x: $Horizontal\ distance\ from\ outflow\ of\ jet\ [m]$

$$\frac{U_{x,r}}{U_{axis}} = exp\left[-\frac{1}{2C^2}\frac{r^2}{x^2}\right] \qquad \textit{(Eq. 2-2)}$$

With: $U_{x,r}$: $Flow\ velocity\ at\ location\ x,r\ in\ jet\ [m/s]$
r: $Radial\ distance\ from\ jet\ axis\ [m]$

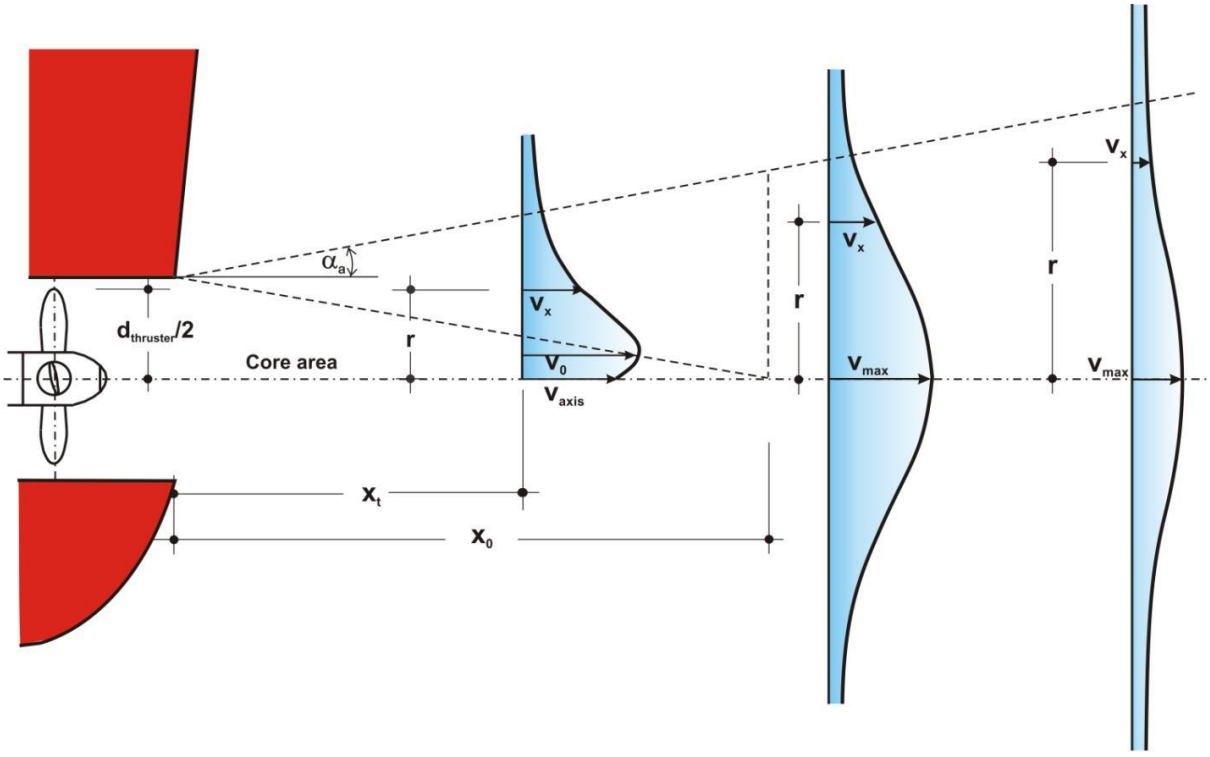

Figure 4 - Velocity distribution within the jet created by a transverse thruster (PIANC, 2015)

It has been proved in further research by Hamill & Johnston (1996) that in the non-established flow zone the jet created by a propeller differs from the free jet. Due to the rotating movement of a propeller more turbulence is created together with a wider spread of the velocities. Next to that, the characteristics are a shorter zone for the flow to establish and a radial component of the velocity as can be seen in Figure 5, Figure 6 and Figure 7. Therefore the formulas by Albertson et al (1950) can only be used for the established flow zone and closer to the tunnel gap other equations should be used.

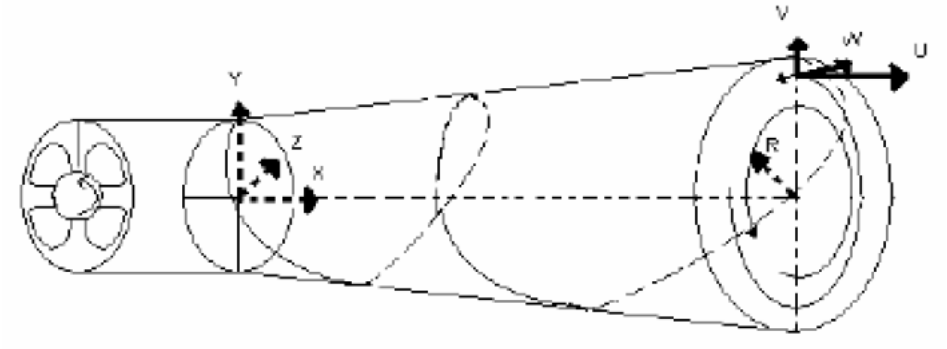

Figure 5 - Induced radial component of velocity by propeller (PIANC, 2015)

A shorter length of the establishment zone is shown in Figure 6. Due to the rotating propeller the water in the jet is already turbulent near the outflow of the propeller and this makes the establishment zone of the jet shorter. As can be concluded from the figure the relative turbulence intensities within the free jet and the propeller jet are around 0.3 in the developed zone of the jet. Therefore according to Verhagen (2001) it can be concluded that the expectation is that the propeller jet is diverging more. This is also proven with the results presented in Figure 7.

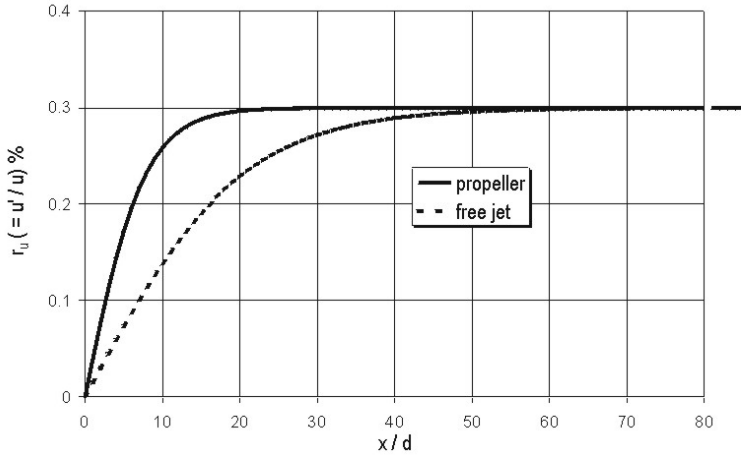

Figure 6 - Comparison of the relative turbulence in the propeller jet and the circular free jet (Verheij, 1985)

As is shown in the left graph of Figure 7 the maximum velocities within the propeller jet start to reduce closer to the outflow point than the velocities within the free jet. It can be concluded that this is related to the divergence of the propeller jet as is shown in the right graph of Figure 7.

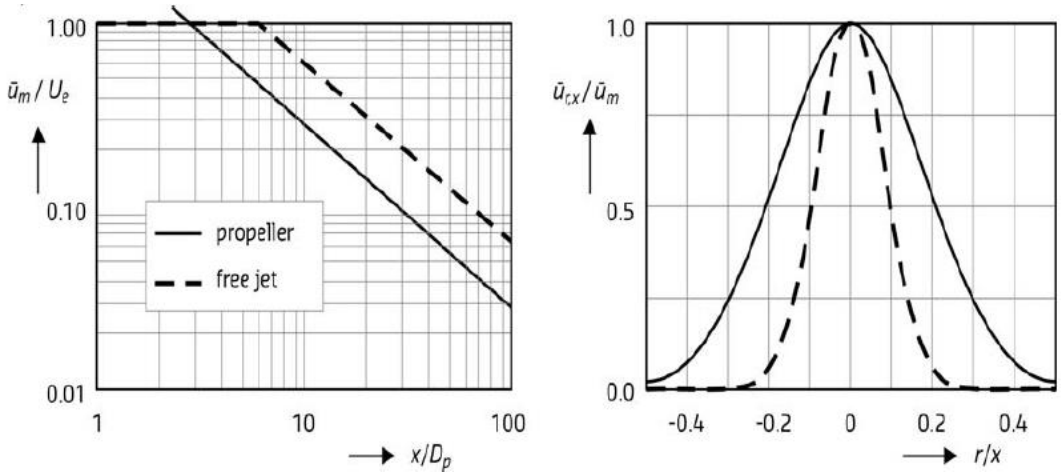

Figure 7 - Different flow velocities for propeller jets and free jets (Verheij, 1983 & Verheij, 1985)

When taking into account the differences between the free jet and the jet of a transverse thruster the general equation (Eq. 2-3) (PIANC, 2015) is derived for the distribution of the flow velocities within a propeller jet.

$$U_{x,r} = A\left(\frac{D_p}{x}\right)^a U_0 exp\left(-\frac{1}{2C_2^2}\frac{r^2}{x^2}\right) \qquad \textit{(Eq. 2-3)}$$

With:
U_0: $Efflux\ velocity\ [m/s]$
f_n: $Percentage\ of\ maximum\ number\ of\ rotations\ per\ minute\ [-]$
n_{max}: $Maxium\ number\ of\ rotations\ per\ minute\ [s^{-1}]$
D_p: $Propeller\ diameter\ [m]$
K_T: $Thrust\ coefficient\ [-]$
C_1, C_2: $Coefficients\ [-]$
A: $Coefficient\ [-]$
a: $Exponent\ [-]$

2.1.2 Efflux velocity

To derive a formula for the outflow velocity (V_0 in Figure 4 which is equal to U_0) several researches are performed and one of the empirical relations derived is by Blaauw and Van de Kaa (1978). This relationship is presented in (Eq. 2-4) where it is empirically determined that $C_1 * f_n = 1.60$.

$$U_0 = C_1 f_n n_{max} D_p \sqrt{K_T} \qquad \textit{(Eq. 2-4)}$$

For thrusters the empirical relationship presented above is modified to a better applicable equation with physical parameters that are provided by the manufacturer. This more practical equation is given in (Eq. 2-5) and has according to PIANC (2015) sufficient accuracy in the case of transverse thrusters.

$$U_0 = 1.15\left(\frac{P_{thruster}}{\rho_w D_{thruster}^2}\right)^{0.33} \qquad \textit{(Eq. 2-5)}$$

$$D_{thruster} = f_{thruster} * D_p$$

With:
$P_{thruster}$: $Max\ installed\ thruster\ engine\ power\ [W]$
$D_{thruster}$: $Thruster\ diameter\ [m]$
$f_{thruster}$: $1.02 - 1.05$

Axial momentum theory

This theory is formulated by Albertson et al. (1948) after which it is adapted by several other researchers. The method considers no tangential and rotational effects, only velocities in axial direction as can also be concluded from (Eq. 2-7). For the calculation of the representative efflux velocity U_0 this method is very useful and quite accurate as well.

The equation (Eq. 2-6) assumes that the momentum at some distance behind the propeller (M) is equal to the momentum at the outflow point (M_0).

$$M = M_0 \qquad \textit{(Eq. 2-7)}$$

$$\int_0^\infty U_{x,r}^2 dA = U_0^2 \frac{1}{4}\pi D_0^2$$

With: $\int_0^\infty U_{x,r}^2 dA = 2\pi \int_0^\infty r U_{x,r}^2 dr$

Within this theory a propeller is schematized as an actuator disk. For this schematization some assumptions are made. These include that the number of blades is infinite. Also there is a constant load of every blade over the radius. In addition, the rotating velocity is infinite and the most important assumption is that the thrust delivered by the actuator disc is equal to the thrust delivered by the propeller.

2.1.3 German calculation method

Researches by the Germans are performed to develop prediction methods for the flow field within jets created by propellers. In this paragraph only the situation for transverse thrusters nearby slopes is discussed. As mentioned before the flow field is not only a function of the propeller characteristics. It will also be determined by the dimensions of the restrictions within the flow area like the slope of a riverbank or the inclination of an open quay wall.

The German method is based on research on jet flow velocities above a slope of 1 : 3 by Schokking (2002) and Römisch (2006) and resulted in equation (Eq. 2-8). Distinction is made between some axial distances 'x' from the thruster outlet point. In addition it shows a reduction of the flow velocity towards the slope due to the slope and the smaller water level. The presented equation only provides axial flow velocities and does not give the slope velocities.

$$U_{axis} = U_0 \qquad \text{For: } \frac{x}{D_{thruster}} < 1 \qquad \textit{(Eq. 2-8)}$$

$$U_{axis} = U_0 \left(\frac{x}{D_{thruster}}\right)^{-0.33} \qquad \text{For: } 1 < \frac{x}{D_{thruster}} < 5.375$$

$$U_{axis} = 2.3 U_0 \left(\frac{x}{D_{thruster}}\right)^{-0.825} \qquad \text{For: } \frac{x}{D_{thruster}} > 5.375$$

2.1.4 Dutch calculation method

The German method is already discussed and a prediction method for the same situation is also developed by Dutch researchers. Results of both methods show differences and therefore both methods are mentioned. The original equations are formulated based on research by Blaauw and Van de Kaa (1977), Verheij (1983) and Blokland (1997). After that further research is performed in 2012 by Van Doorn and this led to correction factors for the Dutch calculation method. The original method shows how to calculate the maximum jet flow velocity above the slope in the case of a free extending and unconfined thruster jet. The method is in more detail discussed in section 2.2.

2.1.5 Flow field around vertical piles

When an open quay wall on piles is considered the influence of the vertical piles and the slope on the flow field should be studied. The influence of the slope is already discussed above. When investigating the flow pattern around a pile it results that the flow is contracting next to the pile (this is presented in Figure 9). As a consequence of the flow contraction the local velocity increases next to a single pile and between two piles. According to Breusers et al. (1977) the velocity next to a single pile is estimated with (Eq. 2-9).

$$V_{pile} = 2 * V_{approach} \qquad \textit{(Eq. 2-9)}$$

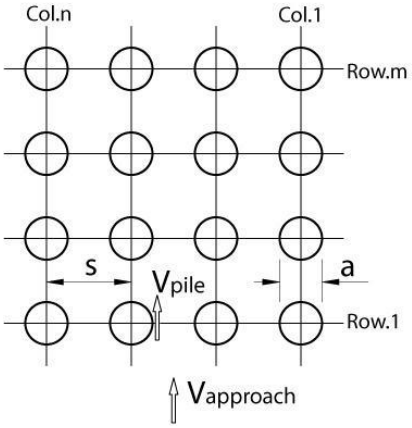

Figure 8 - Locations to determine the velocity parameters of (Eq. 2-9) for the situation with multiple piles

Piles that are located at the slope of an open quay structure influence the impact of the jet flow on the bed slope material. The flow pattern changes due to the piles and as shown in Figure 9 horse shoe vortices are induced around the pile.

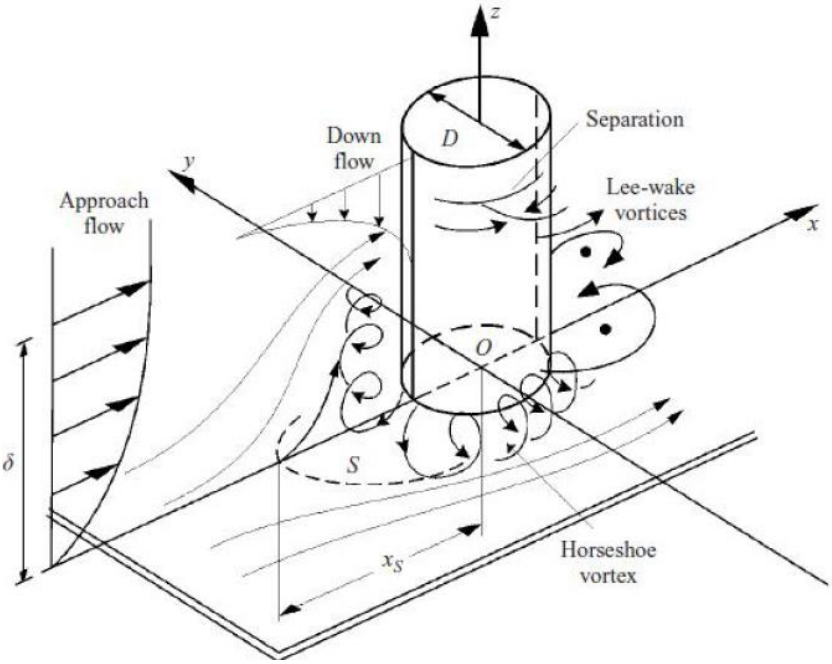

Figure 9 - Flow pattern around vertical pile (Roulund, 2005)

Bed scour around a pile is initiated due to the flow pattern around a pile. In front of the pile the difference in the vertical direction of the horizontal velocity causes a down flowing water jet. Also an acceleration of the flow occurs next to the pile due to flow contraction. Both mechanisms initiate erosion in front of and next to the pile. When a scour hole is formed a circulating current is formed in that hole and these circulations are travelling together with the flow downstream. This erodes even more bed slope material.

2.2 Hydraulic load on a slope

According to PIANC (2015) originally there are two methods to estimate the hydraulic loads on an inclining slope. That is the German method and the Dutch method which in short are both described before. For this research only the Dutch calculation method is considered and therefore discussed in more detail. Originally the Dutch method does not take into account the confinement of the propeller jet, however Van Doorn (2012) proposed a correction factor 'f'. One of the things this factor takes into account is the jet confinement for some scenarios that are described in this paragraph. However, in this research different type of scenarios are investigated and therefore this calculation method for the hydraulic bed load on a slope is defined as the unconfined jet method for slopes. This definition is therefore used for the following part of this report.

2.2.1 Unconfined jet method for slopes

The Dutch method to calculate the maximum slope velocity (Eq. 2-10) is based on research by Blaauw and Van de Kaa (1978), Verheij (1983), Blokland (1997) and Van Doorn (2012). A representation of this method and its parameters is shown in Figure 10. Originally the calculation method was valid for free extending and unconfined propeller jets. Anyhow after the research in 2012 by Van Doorn, a correction factor 'f' is added and with this factor the influence of the confinement due to the slope is taken into account.

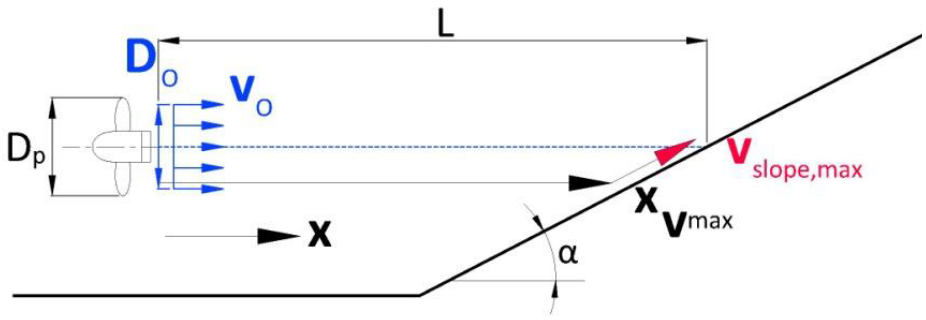

Figure 10 - Representation of the Dutch calculation method for maximum slope velocity (PIANC, 2015)

$$U_{slope,max} = f * A * \left(\frac{D_0}{L} * \frac{L}{X_{U,max}}\right)^a * U_0 * exp\left[-b * \left(\frac{\frac{L}{X_{U,max}} - 1}{\cot(\alpha)}\right)^2\right] \quad \textit{(Eq. 2-10)}$$

$$\frac{X_{U,max}}{L} = K * \left(\sqrt{1 + \frac{2}{K}} - 1\right)$$

$$K = \frac{b}{a * (\cot(\alpha))^2}$$

With:
$U_{slope,max}$: $Flow\ velocity\ just\ above\ slope\ [m/s]$
f: $Correction\ factor$ [-]
A: $(= 2.8)\ Coefficient\ [-]$
D_0: $Jet\ diameter\ [m]$
L: $Axial\ distance\ between\ slope\ and\ propeller\ plane\ [m]$
$X_{U,max}$: $Distance\ between\ propeller\ and\ point\ of\ maximum\ load\ [m]$
a: $(= 1)\ Coefficient\ [-]$
U_0: $Efflux\ velocity\ [m/s]$
b: $(= 15.43)\ Coefficient\ [-]$
α: $Slope\ angle\ [°]$

The obstructions on the slope and the slope conditions determine the location of the maximum slope velocity. According to this method the location of the maximum hydraulic load on the slope is located below the point of intersection of the jet axis with the slope. However in practice this location can deviate from the location according to the unconfined jet method for slopes.

Correction factor

According to the research by Van Doorn (2012) the original Dutch method as mentioned in PIANC (1997) underestimated the hydraulic loads. Therefore a correction factor 'f' is proposed. This factor takes into account the confinement of the propeller jet above the slope, the roughness of the slope and the effect of multiple piles if present.

That research consisted of scale model tests with slopes of 1:1.5 and 1:2.5. Experiments were performed for ten test scenarios. The model set ups for these scenarios contain configurations with and without piles, with a rough or a smooth slope, axial distances of the vessel to the slope of $6.2D_0$ and $4.0D_0$ and configurations where a displacement parallel to the slope is applied. The slope configurations with piles should simulate an open quay wall structure. A prototype model with a 7000 TEU container vessel with a bow thruster diameter of 2.75m was scaled with a scale factor of 25.

Further research into this subject of bow thruster velocities by De Jong (2014) states that the maximum velocities presented by the research by Van Doorn (2012) are calculated in a wrong manner. A different formula should be used to transform the measured maximum velocities in the horizontal and vertical plane into maximum flow velocities parallel and perpendicular to the slope. This leads to a reduction of the velocities at the slope up to 30% and therefore also to a reduction of the correction factor 'f'. In order to determine new correction factors 'f' the correct transformation is applied to the x- and y-velocities measured by Van Doorn (2012).

A second correction is applied to the maximum slope velocities according to the unconfined jet method with 'f' equal to 1 (Eq. 2-10) that are determined by Van Doorn (2012). It is found that the rotational speed of the propeller as reported in the report by Van Doorn (2012) is incorrect. Similar equipment and similar settings were used during this research however it was checked that the rotational speed should be 1091 RPM instead of the 1021 RPM reported by Van Doorn (2012). Van Doorn has applied 1091 RPM, but he has wrongly reported 1021 RPM. In addition, he used the provided thrust coeffcient K_T of 0.28 provided by the manufacturer instead of the thrust coeffcient of 0.22 determined in section 5.1.3 Thrust coefficient and based on the outflow measurements. For this reason he has also calculated incorrect maximum slope velocities, based on an efflux velocity U_0 occuring at 1021 RPM and for a K_T of 0.28. When applying the correct rotational speed of 1091 RPM and the correct thrust coefficient of 0.22 it leads to a small increase of the correction factor that was already corrected with the first correction.

The new and improved correction factors 'f' are determined taking into account both corrections and these are presented in Table 1.

Slope angle (1:m)	**Slope configuration**	**New correction factor [-]**	**Correction factor by Van Doorn (2012) [-]**
Slope of 1 : 2.5	Smooth surface	f = 1.15	f = 1.11
Slope of 1 : 1.5	Smooth surface	f = 1.08 - 1.23	f = 1.07 – 1.19
Slope of 1 : 1.5	Rough surface (rock protection)	f = 1.06 – 1.18	f = 1.26
Slope of 1 : 1.5	Smooth surface with open quay piles	f = 1.24 – 1.28	f = 1.36 – 1.41
Slope of 1 : 1.5	Rough surface with open quay piles	f = 1.31 – 1.57	f = 1.58 – 1.72

Table 1 – Improved correction factors 'f' for the unconfined jet method taking into account the correction by De Jong (2014) and the incorrect propeller rotational speed and thrust coefficient

2.3 Slope material stability

The hydraulic load produced by the thruster on the slope material can induce an unstable situation. This is undesirable and can lead to damage of the slope or of the slope protection. There are several empirical relations that describe the stability of loose grains. The well-known theories by Izbash, Shields and Hoan are discussed in Appendix B - Material stability. First the original Izbash type stability relation that generally is used for the design of slope protections is presented. The most important conditions to take into account in a stability relation for the stability of slope material are discussed in the second and third part of this section. After that the modified Izbash type stability relation that contains those important conditions is described.

Also, a method by Pilarczyk (1995) is described which can be used for the stability of slope material that is attacked by currents. This method is discussed because it is the basis for a stability relation that can be derived from the equilibrium scour depth equation proposed by Roelse (2014). At the end, this derived Pilarczyk type stability relation for riprap revetments affected by propeller jets is presented. This last method, the original Izbash type stability relation and the modified Izbash type stability relation are exercised in the analysis of the results of the performed scale model tests.

2.3.1 Original Izbash type stability relation

The original Izbash type design equation for the median stone diameter for slope protections is equation (Eq. 2-11) and includes a stability parameter and the maximum bed velocity. Also a slope coefficient is part of the equation. The turbulence is indirectly included in the Izbash type stability parameter $\beta_{Iz,cr}$ and not as an input parameter in the equation. The critical Izbash stability parameters that should be applied when using the Dutch engineering guidelines are given in Table 2.

$$d_{50} \geq \beta_{Iz,cr} * \frac{m_h U_{b,max}^2}{2 * g * \Delta} \qquad \textit{(Eq. 2-11)}$$

With: $d_{50}: Median\ stone\ diameter\ [mm]$
$\beta_{Iz,cr}: Izbash\ stability\ parameter\ [-]$
$m_h: Slope\ factor\ [-]$
$U_{b,max}: Maximum\ bed\ velocity\ [m/s]$

$\beta_{Iz,cr}$	Conditions	Equation	Type of flow	Recommended by
2.5	Some movement of stones	(Eq. 2-11), turbulence intensity not included in formula	Propeller jet	Blokland (1997)
3.0	No movement of stones	(Eq. 2-11), turbulence intensity not included in formula	Propeller jet	Blokland (1997)

Table 2 - Recommendations for $\beta_{Iz,cr}$ of the original Izbash type stability relation (Eq. 2-11)

2.3.2 Slope conditions

The conditions of the original experiments contain a horizontal bed. However for the case of stability of armor stones on a slope it should be a sloping bed. Therefore the stability criterion has to contain a coefficient to take into account the effect of a sloping bed on the stability. Correction factor m_h, given in equation (Eq. 2-12), represents the influence of the slope and the direction of approach of the velocity and leads to a reduction of the strength of the slope material.

$$m_h = \frac{\tan(\varphi)}{\cos(\theta_u)*\sin(\alpha)+\sqrt{cos^2(\alpha)*tan^2(\varphi)-sin^2(\theta_u)sin^2(\alpha)}} \qquad \textit{(Eq. 2-12)}$$

With: θ_u: $Angle\ of\ velocity\ vector\ (= 0\ when\ upwards\ the\ slope)$ [°]
φ: $Angle\ of\ internal\ friction\ of\ stones$ [°]
α: $Angle\ of\ slope$ [°]

2.3.3 Turbulence

The influence of turbulence on the stability is high and therefore a coefficient for this phenomenon is included as well in the modified stability relation presented in the section hereafter (Eq. 2-17). The correction factor for the turbulence increases the load on the stone. It is possible to measure the amount of turbulence by measuring the flow velocities in time at a fixed point. The flow velocities in a fixed point consist of the time-averaged velocity and the velocity fluctuations (Eq. 2-13). These turbulent fluctuations are a measure for the turbulence intensity.

$$U = \overline{U} + U' \qquad \textit{(Eq. 2-13)}$$

With: $\overline{U}$: $Time-averaged\ flow\ velocity\ [m/s]$
U': $Flow\ velocity\ fluctuation\ [m/s]$

To calculate the relative turbulence intensity the absolute turbulence intensity is divided by the time-averaged velocity, as shown in equation (Eq. 2-14). Taking the standard deviation of the measured flow velocities in a fixed point gives the absolute turbulence intensity.

$$\sigma = \sqrt{(U')^2} = \left[\lim_{N\to\infty} \frac{1}{N} \sum_{n=1}^{N} \left(U'^{(n)}\right)^2\right]^{1/2} \qquad \textit{(Eq. 2-14)}$$

$$r = \frac{\sigma}{\overline{U}}$$

With: σ: $Turbulence\ intensity\ [m/s]$
N: $Amount\ of\ measurepoints\ [-]$
r: $Relative\ turbulence\ intensity\ [-]$

When the relative turbulence intensity is determined the influence of the turbulence on the stability can be included. According to Verheij (1985) only the highest velocity fluctuations cause instability of the stones. If it is assumed that the measured velocities in time are normally distributed a velocity can be defined that is exceeded by only a few percent of the total amount of measured velocities. The standard deviation of the distribution of the measured velocities is the turbulence intensity. When taking 3 times the standard deviation (p=3 in equation (Eq. 2-15)) an exceedance percentage of 0.13 % is achieved. This is recommended by Schiereck and Verhagen (2012) as a representation of the peak velocities which cause instabilities (Figure 11 and equation (Eq. 2-15)).

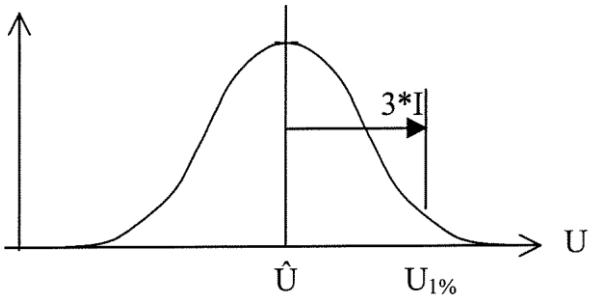

Figure 11 - Normal distribution of measured flow velocities in time with 3 times standard deviation

$$U_{1\%} = \overline{U}(1 + p * r) \qquad \textit{(Eq. 2-15)}$$

With: $U_{1\%}$: $Flow\ velocity\ with\ exceedance\ percentage\ of\ 1\%\ [m/s]$
p: $= 3\ (when\ exceedance\ percentage\ of\ 1\%)\ [-]$

An approach to include the turbulence into the stability relation is described by Verhagen (2001). The stability relations presented by Izbash and Shields both contain the velocity squared. This means that the

equation for velocity presented in equation (Eq. 2-13) should be squared and time-averaged as is shown in equation (Eq. 2-16). The velocity fluctuations added to the average velocity gives the local velocity. These velocity fluctuations are very important for the stability of the grains and are described with the relative turbulence intensity 'r'. Furthermore concluding from Verhagen (2001) it is of higher importance to measure the turbulence intensity in the jet flow than the average velocities.

$$U^2 = (\overline{U} + U')^2 \qquad \textit{(Eq. 2-16)}$$

Time averaged:
$\overline{U^2} = (1 + r^2)\overline{U}^2$

2.3.4 Modified Izbash type stability relation

Both influences of the slope and the turbulence are included in correction factors as already described. The original Izbash type stability relation already contains a correction factor for the slope however not for the for turbulence. When including the correction factor for the turbulence in the original Izbash type stability relation a new relation is achieved which is the modified Izbash type stability relation, shown in (Eq. 2-17).

$$\Delta d_{50} = \beta_{Iz,cr,mod} * \frac{m_h * U_{b,max}^2 * (1+p*r)^2}{2*g} \qquad \textit{(Eq. 2-17)}$$

The modified Izbash stability parameter $\beta_{Iz,cr,modified}$ is not the same stability coefficient as in the original Izbash type stability relation ($\beta_{Iz,cr}$) in equation (Eq. 2-11). The original Izbash type stability relation includes indirectly the influence of the turbulence in the critical Izbash stability parameter $\beta_{Iz,cr}$. Whereas in (Eq. 2-17) the influence of the turbulence is included as an extra parameter in the equation, the relative turbulence intensity 'r'. Also a coefficient 'p' is applied to take into account 'p' times the standard deviation (in most cases p=3, as discussed before).

Blokland (1997) recommended to apply a stability coefficient as presented in Table 2 for the original stability equation (Eq. 2-11). These values are validated by measurements during prototype tests at the Benelux haven in Rotterdam, the Netherlands. The relation between the modified stability parameter and the provided stability parameter is presented in equation (Eq. 2-18). According to Blokland (personal communication) the stability parameter $\beta_{Iz,cr,uniform}$ is assumed to be 0.7 and the relative turbulence intensity $r_{uniform}$ is generally in the range between 0.075 to 0.12, both for uniform flow conditions. Assuming $r_{uniform}$ = 0.1 and p =3 (see previous section) this leads to a recommended modified stability parameter $\beta_{Iz,cr,mod}$ of 0.414.

Combining equation (Eq. 2-11) and equation (Eq. 2-17) results in equation (Eq. 2-18).

$$\beta_{Iz,cr} = \beta_{Iz,cr,mod}(1 + p * r)^2 \qquad \textit{(Eq. 2-18)}$$

For uniform flow (with low turbulence level) equation (Eq. 2-19) is formulated.

$$\beta_{Iz,cr,uniform} = \beta_{Iz,cr,mod}\left(1 + p * r_{uniform}\right)^2 \qquad \textit{(Eq. 2-19)}$$

This results in the following equation (Eq. 2-20) for $\beta_{Iz,cr,mod}$.

$$\beta_{Iz,cr,mod} = \frac{\beta_{Iz,cr,uniform}}{\left(1 + p * r_{uniform}\right)^2} \qquad \textit{(Eq. 2-20)}$$

2.3.5 Stability relation by Pilarczyk (1995)

For the stability of stones on an embankment under current attack Pilarczyk (1995) formulated the equation given in (Eq. 2-21). It shows a relationship between parameters representing properties of the armor stones and the hydraulic parameters of the current attack.

$$d_{n50} = \frac{\Phi_{sc}}{\Delta} \frac{0.035}{\Psi_{cr}} k_h k_{sl}^{-1} k_t^2 \frac{U^2}{2g} \qquad \textit{(Eq. 2-21)}$$

When reformulating the equation it is similar to the Shields equation and some extra parameters to take the effects of the slope, the turbulence, the mobility and the location where the velocity is determined into account. The formula contains several parameters including a stability correction factor (Φ_{sc}), a mobility parameter of the protection element (Ψ_{cr}), velocity profile factor (k_h), turbulence factor (k_t) and a side slope factor (k_{sl}).

$$\frac{U^2}{g\Delta d_{n50}} = \frac{\Psi_{cr}}{0.035} * \frac{2k_{sl}}{\Phi_{sc} k_h k_t^2} \qquad \textit{(Eq. 2-22)}$$

The stability correction factor takes into account the transitions and edges of the armor stone top layer because in practice it will never be an endless continuous layer. Due to that there might be different hydraulic loads at edges and transitions. For these edges and transitions this factor is higher than 1. This means a larger stone diameter is required to create a larger strength. According to CIRIA (2007) the factor Φ_{sc} should be 0.75 for continuous rock protection and 1.5 for exposed edges or transitions for riprap protection.

The mobility parameter for the armor stones is related to the critical Shields criterion. For this case the critical Shields parameter is defined for initial movement of loose stones, so when the first stone moves and not for 'some' movement. Therefore the Ψ_{cr} is defined as 0.035. The mobility parameter compares the stability of the system with this critical value defined by Shields and is a relative parameter.

The velocity profile factor is representing a factor to calculate the velocity near the bed or the sloping bed and depends on the water depth and the type of flow which make the vertical velocity profile. In the case with propellers and where the velocity is determined near the sloping bed a factor of k_h equal to 1.0 is valid.

Pilarczyk recommends a turbulence factor kt^2 between 2.9 and 4.0 for loads induced by screw jets. There is a relation between the relative turbulence intensity and the turbulence factor (Eq. 2-23). The relative turbulence intensities used in this approach is still a point of discussion. Pilarczyk (1995) proposed values of 0.4 to 0.53 for jets created by screws. In 1978 Blaauw & Van de Kaa found values of 0.25 to 0.3 in the jet axis and values up to 0.6 nearby the bed. In 2012 Van Doorn found values of 0.3 to 0.55. PIANC (2015) mentioned that the proposed values by Blaauw and Van de Kaa (1978) are underestimated because the confinement of the propeller jet was not taken into account. In addition, Schiereck (2012) recommended values of 0.30 for propeller jets.

$$k_t = \frac{1 + 3r}{1.3} \qquad \textit{(Eq. 2-23)}$$

The slope factor is already discussed in section 2.3.2 Slope conditions and is given by equation (Eq. 2-12).

When using the values of the correction factors described above the equation (Eq. 2-24) can be derived. A continuous rock protection is assumed for this relation. During the research by Roelse (2014) this formulation is used to formulate the densimetric slope Froude number, which is part of his equilibrium scour depth equation. This relation is therefore also the basis for the stability relation that is derived and proposed in the next paragraph.

$$\frac{U^2}{g\Delta d_{n50}} = \frac{\Psi_{cr}}{0.035} * \frac{2}{0.75 m_h k_t^2} \qquad \textit{(Eq. 2-24)}$$

$$k_{sl} = \frac{1}{m_h}$$

2.3.6 Stability relation derived from the method by Roelse (2014)

In 2014 Roelse conducted a research to develop a method to predict the equilibrium scour depth at a slope with piles that is affected by a bow thruster current. The equation that is formulated consists of two parts, the jet diffusion mechanism and the pile obstruction mechanism. The hydraulic bed load on the sloping bed that causes scour is determined with the Dutch calculation method to calculate the hydraulic loads on a slope.

This scouring process begins when the bed slope velocity becomes above a critical value and that critical value is defined by the bed strength, that means the particle size and density. This bed slope velocity has fluctuations around an average value. These fluctuations determine the turbulence intensity and mainly influence the stability of the slope material. Eventually the equilibrium scour depth is reached when the depth of the scour hole has stopped increasing. The equation for equilibrium scour depth is presented and discussed in Appendix C - Equilibrium scour depth.

The critical densimetric slope Froude number (Eq. C-1) that is part of the equilibrium scour depth equation is indicated as a stability parameter for the stability of the grains under influence of the slope velocity of the propeller jet. Originally the equation presented by (Eq. 2-25) is formulated from the design method of Pilarczyk (Eq. 2-24) for the conditions mentioned in the section before. Which is a bed slope protection induced by a current. Effects due to the fact that it is a screw jet are taken into account in the turbulence factor of the equation.

The jet diffusion mechanism is the first part of the equilibrium scour depth equation (Eq. C-3) and this mechanism is initiated when a propeller jet is considered without obstructions that affect the flow. This first part contains the critical densimetric slope Froude number and is therefore the stability relation when only this mechanism is initiated and is given at part 1) in equation (Eq. 2-25).

However when piles are situated at the scouring location, part of the stability of the grains on the slope is also affected by the pile obstruction mechanism which is the second part of the equilibrium scour depth equation (Eq. C-3). That is because this mechanism is already initiated when the densimetric slope Froude number is half times the critical densimetric slope Froude number. This means that the stability parameter Δd_{n50} becomes two times higher and therefore a grain size that is two times larger is recommended. The stability equation for that is given at part 2) in (Eq. 2-25). This equation is in this research named as the Pilarczyk type stability relation.

$$Fr^2{}_{slope,crit} = \frac{U^2{}_{slope,crit}}{g * \Delta * d_{n50}} \approx \frac{\Psi_{cr}}{0.035} * \frac{2}{m_h * k_t^2} \qquad \textit{(Eq. 2-25)}$$

1) Jet diffusion mechanism:

$$\Delta d_{n50} = \frac{0.035 * U_{slope,max}^2 * m_h * k_t^2}{2 * g * \Psi_{cr}}$$

2) Pile obstruction mechanism and jet diffusion mechanism:

$$\Delta d_{n50} = 2 * \frac{0.035 * U_{slope,max}^2 * m_h * k_t^2}{2 * g * \Psi_{cr}}$$

3. Research method

This chapter discusses the method that is used to collect all the test data that is needed to answer the research questions. First some general remarks are discussed. Secondly a prototype situation is defined after which this situation is scaled into a scale model. In addition the test program and test equipment is described. After that also the measurement program is presented.

3.1 General

This research is actually an extension of the research performed by Van Doorn in 2012 and that is why the model set-up of Van Doorn (2012) as shown in the left picture in Figure 12 will be rebuild with several changes. It will include stability measurements and more test configurations. The scale model that is built for this research is shown in the left picture of Figure 12 and all the characteristics and dimensions of it are discussed in the following paragraphs.

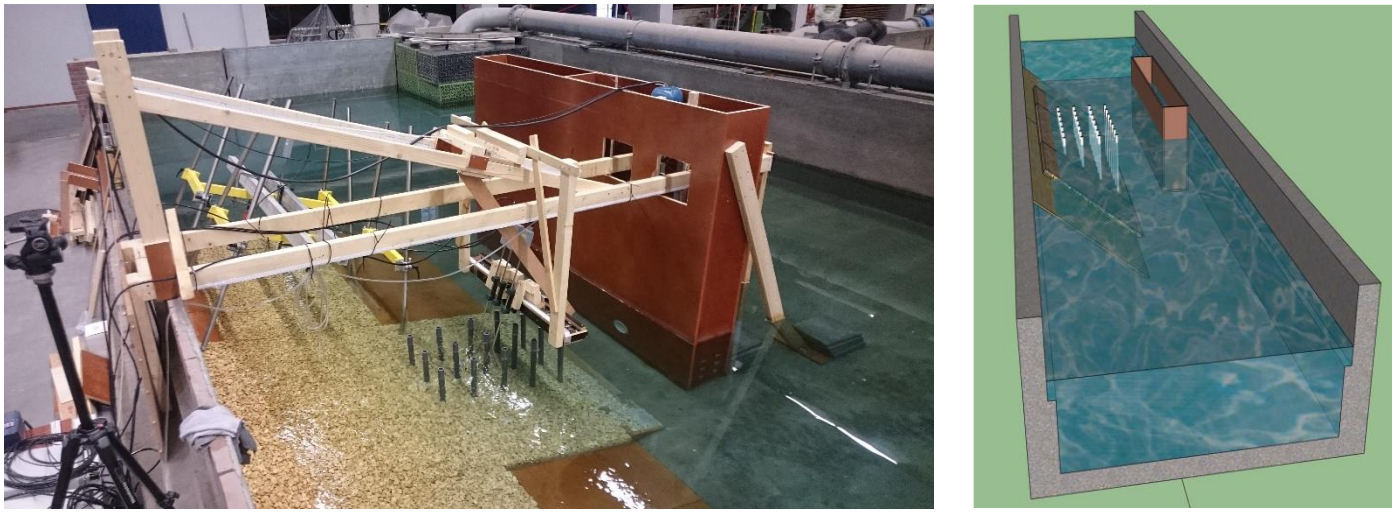

Figure 12 - Model setup for this research (left) and model set up by Van Doorn (2012) (right)

The research method is largely dependent on the facilities that are available and especially the basin that is available to perform the tests in. The tests will be conducted at Deltares where a basin of 15 meter long and 6 meter wide was available for this research. The fact that this basin is that large is beneficial because it was concluded that during researches in the past the circulation within the basin might have influenced the test results.

For example Van Veldhoven (2002) and Schokking (2002) performed lab tests with a similar subject and used a basin of 2 meter by 2 meter which was too small as follows from their conclusions. Also Van Doorn (2012) performed lab tests with a similar subject and used a basin with a length of 10 meter. Within that research it was assumed the circulation is negligible however it is mentioned that further research in the circulation is needed. An overview of the differences in circulation of the water flow between a prototype situation and the different model set ups used is presented in Figure 13. Another restriction within the research of Van Doorn (2012) was the width of the basin. This was 2 meter and gentle slopes did not fit into the basin and for this reason it is also beneficial for this research that a wider basin is available.

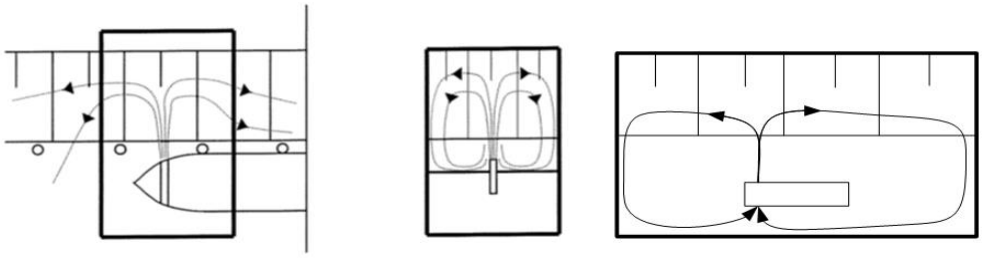

Figure 13 – Circulation in prototype situation (left), model situation (Van Veldhoven, 2002) (middle) and model situation (Van Doorn, 2012) (right)

3.2 Prototype situation

In this paragraph the characteristics and dimensions that are relevant to form a prototype situation are mentioned. A distinction is made between the vessel considered, the bow thruster considered and the open quay structure, bank or jetty considered. A large part of the prototype situation is similar to the prototype situation considered by Van Doorn (2012) because it is assumed this is a representative situation for the scenarios of interest in this research.

3.2.1 Prototype vessel

In order to extent the results of the research by Van Doorn (2012) the same vessel dimensions are also used for this research. These are the dimensions of two Maersk vessels, the Regina and the Sovereign Maersk. Dimensions and characteristics are given in Table 3.

3.2.2 Prototype bow thruster

The characteristics of the bow thrusters that are installed on the prototype vessels are mentioned in Table 3. This information is according to the database for vessels of the Ingenieursbureau Gemeentewerken Rotterdam (IGWR).

	Dimensions / Characteristics
Vessel	
Length	332 m
Draught	14.25 m
Beam	42.8 m
Thruster tunnel to bow distance	23.6 m
Thruster tunnel to keel distance	4.6 m
Bow thruster	
Bow thruster power	2 210 kW
Bow thruster tunnel diameter	2.75 m
V_0 of thruster	7.5 m/s
Bow thruster tunnel length	5.8 m

Table 3 - Prototype vessel and thruster dimensions and characteristics

3.2.3 Prototype open quay wall, bank and jetty.

The most applied slopes for open quay walls and banks with an riprap revetment or armor stone top layer ranges from 1:1.25 to 1:4.0. Due to the fact that open quay walls are rarely applied in the Netherlands the scale model tests will focuses more on banks than on open quay walls. Slopes of 1:3.0 are most often applied for banks, at open quay walls and for slopes close to jetties in the Netherlands according to Blokland (personal communication).

Generally the choice for a specific slope angle depends on the costs and the geotechnical stability of the subsurface. In order to make the costs as low as possible it should be as steep as possible. However due to the geotechnical stability it can not be too steep. For example when an armourstone revetment is applied the limit is 1 : 1.5 due to the geotechnical stability. Also, for the case the slopes become gentler than 1 : 3 for most cases it would become too expensive due to the fact that too much stones and space have to be used.

	Dimensions / Characteristics
Slopes of bank, open quay wall and jetty	
Applied range for slopes (1 : m)	2.5 and 3.0
Slope material	Stones
Layer thickness	2 * D_{n50}
Stone class[1)]	100 to 200 kg
Water depth	15.75 m
Pile configuration for open quay walls	
Pile diameter	0.75 m
Pile shape	Round
C-t-c distance 'y' direction	5.0 m
C-t-c distance 'x' direction	5.0 m
Pile configuration for jetties	
Pile diameter	1.00 – 1.80 m
Pile shape	Round
C-t-c distance 'y' direction	9.0 m
C-t-c distance 'x' direction	9.0 m

Table 4 - Prototype characteristics and dimensions for banks, open quay walls and jetties

Remark:

1) The stone class mentioned is assumed to be the class LM_A 60-300 of standard gradings in EN13383 with a d_{n50} of 38 cm and the range of W_{50} for category A 120 – 190 kg.

3.3 Scaling and scale effects

In order to set up a proper scale model all the objects and dynamics that are part of the prototype situation need to be scaled. Therefore to ensure that processes act in the same way and with the same influence in prototype and on model scale, some scale rules are applied. These scale rules are formulated to approach geometrical and dynamic similarity as good as possible. However in scale models it is impossible to scale all length dimensions and scale all dynamic forces to achieve exactly the same situation as in the prototype model.

Geometrical similarity means that each geometrical dimension is modelled with the same scale. This applies for example to the length, width and height of the objects used in the model set-up. Dynamic similarity means that the forcing of all movements of the objects and bodies of water are modelled on the same scale as well.

3.3.1 Geometrical similarity

The factor which represents the ratio between the prototype dimensions and the model dimensions is the scale factor. The scale factor is defined as shown in equation (Eq. 3-1). Only one scale factor is applied on all the dimensions in order to achieve geometrical similarity.

$$n_L = \frac{L_p}{L_m} \qquad \textit{(Eq. 3-1)}$$

With: n_L: $Scale\ factor\ for\ length$ $[-]$
L_p: $Length\ in\ prototype$ $[m]$
L_m: $Length\ in\ scale\ model$ $[m]$

3.3.2 Dynamic similarity

When applying scale rules to models with fluid motion in combination with a flow around structures, the Reynolds number and Froude number are the main criteria according to Schiereck (2007). These are dimensionless numbers, the Froude number gives the ratio of inertia to gravity and the Reynolds number gives the ratio of inertia to viscosity. The equations for both dimensionless numbers are shown in equation (Eq. 3-2) and equation (Eq. 3-3).

$$Fr = \frac{u^2}{g*h} \qquad \textit{(Eq. 3-2)}$$

With: Fr: $Froude\ number$ $[-]$

$$Re = \frac{u*L}{v} \qquad \textit{(Eq. 3-3)}$$

With: Re: $Reynolds\ number$ $[-]$
v: $Kinematic\ viscosity$ $[m^2/s]$

To accomplish dynamic similarity Froude and Reynolds numbers must have the same value in prototype as on model scale. This is however impossible and therefore viscous scale effects can be expected. Nevertheless the viscous scale effects should be minimized by making the Reynolds number high enough. According to Verheij (1985) the scaling effects caused by viscosity are negligible when the Reynolds number of the jet flow is larger than 3,000. The equations for the Reynolds numbers of the jet flow is given in equation (Eq. 3-4).

$$Re_{jet-flow} = \frac{U_0 * D_p}{v} \quad \textit{(Eq. 3-4)}$$

With: $Re_{jet-flow}$: $Reynolds\ number\ of\ jet\ flow\ [-]$

Furthermore scale effects within the flow near the bed should be avoided. To accomplish this the Reynolds criterion given in equation (Eq. 3-5) is used. The flow conditions just above the bed and the turbulent pressure forces on the bed material are mainly determined by the interaction of the viscous sub layer and the size of the bed material. A distinction is made between a hydraulically smooth bed, when $Re_* < 5$, a hydraulically rough bed, when $Re_* > 70$ and the case where the influence of the viscous sub-layer is negligible, when $Re_* > 600$. Hydraulically smooth indicates that the viscous forces completely determine the resistance of the grains and hydraulically rough indicates that the grains are large compared to the laminar sub layer. In the last case, where the influence of the viscous forces is negligible, it means that the $d_{50} \geq$ 5mm.

$$Re_* = \frac{U_* * d_{50}}{v} \quad \textit{(Eq. 3-5)}$$

With: Re_*: $Reynolds\ number\ [-]$
U_*: $Near\ bed\ velocity\ [m/s]$

Van der Schriek (2011) recommended to use a stone diameter in the scale model that is not smaller than approximately 10 mm due to another possible problem, which is the turbulent flow in the pores. In the prototype the pores between the armor stones are large and therefore the flow is turbulent. However in the scale model the pores will be smaller due to the smaller armor stones used and therefore the pore size should not be too small otherwise no turbulent flow will occur.

3.3.3 Scale factor

As follows from the scale rules for geometric similarity all the dimensions within the scale model have to be dimensioned with the same scale factor. The value for the scale factor depends on the available basin to test the model situation and the available equipment. All the objects within the prototype model situation have to fit in the scale model. Some objects like the stones have limitations because of the smallest available stone class. Also the bow thruster is normative for the scale factor, the smallest available bow thruster is described below at the equipment part. Moreover because of dynamic similarity it is better to apply a scale model with the largest dimensions possible so that the dynamic and kinematic processes occurring in the prototype situation do not lead to scale effects in the scale model. In Table 5 the dimensions of the prototype model and the scale model are given for a scale factor (SF) of 25.

	Prototype dimensions	SF of 25	Scale model dimensions
Vessel			
Length	332.00 m	13.280 m	2.500 m
Draught	14.25 m	0.570 m	0.570 m
Beam	42.80 m	1.710 m	0.300 m
Bow thruster tunnel diameter	2.75 m	0.110 m	0.110 m
Bow thruster tunnel length	5.80 m	0.230 m	0.300 m
Thruster tunnel to bow distance	23.60 m	0.940 m	0.600 m
Thruster tunnel to keel distance	4.60 m	0.180 m	0.180 m
Outflow velocity U_0	8.0 m/s	1.6 m/s	1.6 m/s
Keel clearance	1.50 m	0.064 m	0.064 m
Propeller axis to bed distance	6.10 m	0.244 m	0.244 m
Local situation			
Water depth	15.75 m	0.630 m	0.630 m
Armor stones (d_{n50})	~ 0.38 m	0.016 m	0.016 m
Open quay wall			
Pile diameter	0.75 m	0.030 m	0.030 m
C-t-c distance 'y' direction	5.00 m	0.200 m	0.200 m
C-t-c distance 'x' direction	5.00 m	0.200 m	0.200 m
Jetty			
Pile diameter	1.50 m	0.060 m	0.060 m
C-t-c distance 'y' direction	9.00 m	0.360 m	0.360 m
C-t-c distance 'x' direction	9.00 m	0.360 m	0.360 m

Table 5 - Prototype dimensions and scale model dimensions (continued)

Some dimensions are scaled smaller considering that it is without any negative consequences on the results. These dimensions are marked in Table 5 with a red color. This is the case for the length and width of the vessel and the shape of the bow. The reason for each deviating scaled dimension is discussed below.

Scaled vessel

When the ship is scaled with a factor of 25 it is too large to handle, as shown in Table 5, and then it blocks a considerable amount of the recirculating flow within the basin. It is assumed that the smaller length and width of the ship do not influence the results in a considerable way. This is because the flow velocities are considered to be small beneath and besides the ship according to Van Doorn (2012).

Bow thruster tunnel

The shape of the scaled ship will be rectangular and therefore the bow has a different shape as in reality. In reality it is a bulb-shaped bow. This makes the bow thruster tunnel longer than the actual scaled length. The difference in this situation is small and therefore not of considerable influence. Furthermore the distance between the bow and the tunnel is taken smaller due to the rectangular shape of the bow and therefore to compensate for the distance that the water has to flow around the bulb of the vessel.

Efflux velocity

When using Reynolds numbers as indicated in section 3.2, viscosity effects are small enough that they can be neglected. Therefore when applying these conditions only the Froude number is considered. Since the gravity is the same in the scale model as in the prototype situation, following from the formulas in (Eq. 3-6), the efflux velocity in the scale model is scaled to 1.5 m/s. The Reynolds number for the jet flow is much larger than the criterion of 3,000 for this outflow velocity and that minimizes the scale effects considerably.

$$Fr_{prototype} = Fr_{model} \qquad \textit{(Eq. 3-6)}$$

$$\frac{u^2_{prototype}}{g * l_{prototype}} = \frac{u^2_{model}}{g * l_{model}}$$

$$u^2_{prototype} = n_l * u^2_{model}$$

$$n_u = \sqrt{n_l}$$

n_u: $Scale\ factor\ for\ velocities$ $[-]$
n_l: $Scale\ factor\ for\ dimensions$ $[-]$

3.4 Test program

Now that the prototype situation and the scale model dimensions are discussed it is important to define the test program. The parameters that are varied and investigated and therefore the scenarios that are tested are discussed in this section. Set ups that are representative for situations where a vessel is in bollard-pull condition along a bank, an open quay wall on piles and a jetty are considered. A distinction is made between a type I test where the outflow velocities are measured, type II tests where the slope velocities are measured and a type III test with stability measurements.

It is important to measure the outflow velocities of this bow thruster as this is important to determine the representative efflux velocity U_0. Therefore the first velocity measurements of the type I test are conducted nearby the outflow opening and are part of test scenario T0. For this test scenario velocity measurements are conducted in the vertical plane above a flat bottom and no measurements are conducted above the slope. This is why a large axial distance to the slope is chosen. This test scenario is presented in Table 7 with a blue color.

The test scenarios for the type II tests with the slope velocity measurements should be an extension to the research by Van Doorn (2012) and that is why other configurations than tested during that research should be used. In addition there is a strict deadline and this means that it has to be assessed which parameters should be varied that give the most valuable data but do not cost too much time and money. For example changing the slope angle costs a lot of time and therefore only two slope angles are tested, although the slope angle is an important parameter in the calculation method for hydraulic bed loads. Changing the axial distance costs less time and is an important input parameter in the hydraulic bed load calculation method as well. Also piles on a slope is a situation that can be seen regularly and therefore an important obstruction on the slope. The construction however costs much time but this is compensated by the importance and the high influence on the flow pattern of it. Next to that changing a bow thruster is not an option because it costs a lot of money and a lot of time. In addition it is important to make a comparison with the measured velocities by Van Doorn (2012) and that is why one test set up is similar to one of the set ups used during that research. This is a set up with a smooth slope and a slope angle of 1 in 2.5. To sum things up, the parameters that will be varied during the model tests for the type II tests with slope velocity measurements are presented in Table 6.

Varied parameters	**Parameter in unconfined jet method for hydraulic bed loads (Eq. 2-10)**
Slope angle	α
Axial distance of outflow opening to point of intersection	L
Roughness of the slope	(none)
Pile configuration	(none)
Lateral distance with respect to a pile	(none)

Table 6 - Parameters that are varied in the test set ups of the type II tests.

With these parameters that are varied multiple test scenarios are created for the type II tests. It is important that the achieved data from the different test scenarios can be compared properly. It should be noted that all test scenarios of the type II tests contain slope velocity measurements and are marked with a red color in Table 7.

For the type III tests stability measurements are performed. The test scenario for these measurements is named as test scenario T6 and marked with a green color in Table 7. The reason that it contains only one scenario is because of the strict deadline. For the scenario with the stability tests it is also important that velocity measurements are performed in a scenario with a similar model set up in order to compare the two type of measurements and therefore a similar set up as with test scenario T5 is used. The only difference is that loose stones are used for the top layer on the slope for the stability measurements. For the velocity measurements the top layer consists of glued stones because otherwise the measurement equipment might be damaged.

Piles		Axial distance	Lateral shift		1/2.5 Stones		1/3.0 Stones	
Number	Diameter in D_{pile}/D_0 [-]	Outflow – Jet axis intersection with slope in x/D_0 [-]	Distance in positive y-direction to jet axis in y/D_0 [-]	Smooth	Glued	Loose	Glued	Loose
0	0	11.5	0	T0				
0	0	6.2	0	T1	T2		T3	
		9.5	0				T5	T6
		11.5	0				T4	
6	0.57	6.2	0					
		9.5	0				T7	
			0.82				T8	
		11.5	0					
15	0.29	6.2	0					
		9.5	0				T10	
			0.82				T9	
		11.5	0					

Table 7 - Test program of type I, type II and type III tests

For the type II tests, the choice for the 1 in 3 slope and the 1 in 2.5 slope is because that are the most applied slopes for banks of port basins, rivers or canals. The 1 in 2.5 slope is also chosen to make the comparison with the results of test scenario 1 by Van Doorn (2012).

The chosen axial distances for the type II tests are based on observations of real situations and earlier performed tests. The tests performed in 2012 contain axial distances of the jet to the slope (variable L in (Eq. 2-10) of 4.0 D_0 and 6.2D_0, this is respectively 440 mm and 682 mm. The axial distance of 6.2D_0 is used in these model set ups so that the data from this research can be compared with the already available data. Smaller axial distances are not possible due to the more gentle slope and the small keel clearance. In order to check if these distances are comparable to real situations, situations at the Port of Rotterdam and at the river Waal and the river Rhine are observed as indicated in Appendix A.3 Distance bow thruster to quay wall. It is nearly impossible to determine the exact real axial distances and therefore only used to see if the range of distances used is realistic. The smallest observed distance is comparable to the distance 6.2D_0 and therefore this axial distance is used as smallest distance. As largest distance the approximate diffusion angle defined by Verheij (1985) and Oebius and Schuster (1975) is used to determine at which distance the lowest part of the propeller jet should hit the slope just above the toe. This was approximately at an axial distance of 11.5 times the propeller diameter. This distance is taken as largest distance and is also comparable to the larger observed distances.

After all two different pile configurations are tested during the type II tests. The first configuration is chosen to investigate the influence of an open quay on piles on the velocities on the slope. The second configuration is chosen to investigate a situation with a jetty and to see what the effect of a larger pile diameter and larger center-to-center distance is on the slope velocities.

A variable which is not considered yet is the outflow velocity or actually the used power of the bow thruster. This can be regulated with the frequency regulator which will be connected to the electromotor of the bow thruster and regulates the amount of rotations per minute. For the type I test three different rotational speeds are used in order to determine a proper relation between the rotational speed and the efflux velocity. For the type II tests the amount of RPM is held constant at 1091 RPM in order to avoid increasing the amount of variables. Another reason for the choice of this rotational speed is that it can be assumed that it represents the maximum outflow velocity of the prototype vessel, which is the representative design condition for the prototype situation. For the type III test, or when testing the initiation of motion this amount of rpm is increased in steps.

3.5 Test equipment

In this paragraph the most important characteristics of the test equipment used during the scale model tests are discussed.

3.5.1 Bow thruster

The selected scale model bow thruster should be a stable, strong and representative thruster. Therefore the Vetus 2512B Bow Thruster is chosen as shown in Figure 14 and this type is usually used for small pleasure crafts. Originally this bow thruster contains an engine of 12 Volt. It is important to control the rotations per minute during the tests and to let the engine run for longer time periods. Therefore the engine is replaced with another electromotor. All the properties of the model thruster are given in Table 8 and are provided by the manufacturer.

This type contains a propeller with six blades. However, generally propellers in thrusters of most vessels are four-bladed. Nevertheless the geometry is equal and no significant influence on the jet velocities is assumed.

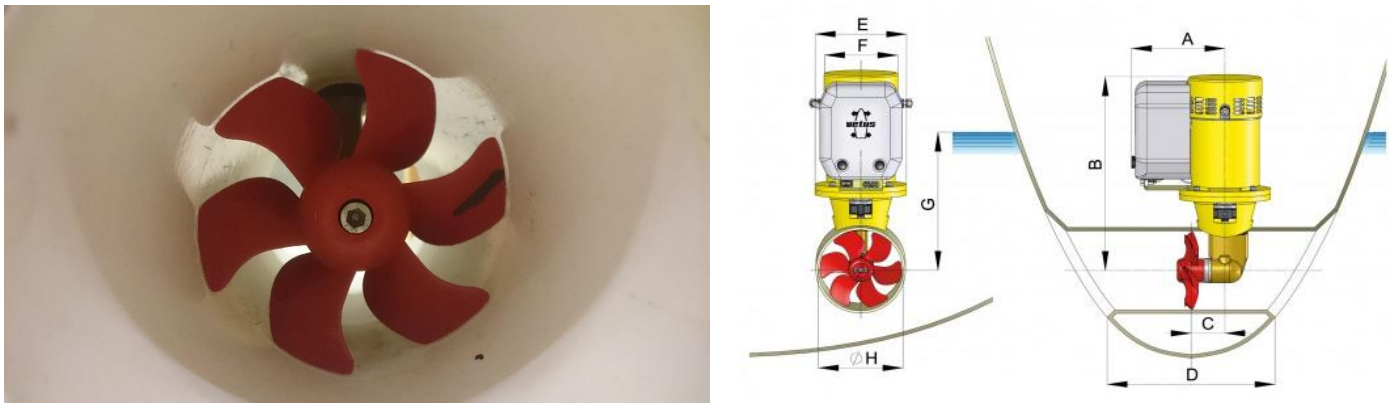

Figure 14 - Bow Thruster of H=110 mm (H=diameter in this case) by Vetus (Vetus, 2016)

It is equipped with a frequency regulator and is therefore able to vary the rotational speed. Equation (Eq. 2-3) is used to calculate the required rotations per minute. The scaled efflux velocity has to be used which is according to the scale rules 1.5 m/s (Eq. 3-6). Together with the thrust coefficient the needed amount of rotations per minute can be calculated. This thrust coefficient of 0.28 is provided by the manufacturer and actually is a value that is optimised for the original electromotor which normally rotates with 3000 rpm.

	Properties
Diameter	0.110 m
Power	1.5 kW
Max rpm	1400
Frequency at max rpm	50 Hz
Thrust coefficient	0.28

Table 8 – Technical specifications of Vetus model bow thruster (Vetus, 2016)

3.5.2 Stone class

One of the scale rules mentioned is that the minimum size of stones in scale models is 10 mm. The class of stones available which is just above this requirement is the stone class of 11 to 22 mm. This class is used for the scale model and is a type of quarry run that is called ‘yellow sun split’ (KPS Delft, 2016). A few layers of yellow sun split are glued on plates which are placed on the slope. For the stability tests with loose stones a layer of these stones with a thickness of $2d_{n50}$ was placed on top of the glued stones.

A sample of the stones used for the stability tests was sieved in order to check the gradation of the stones. The sieve distribution curve is presented in Appendix E - Sieve analysis stones stability tests. From this analysis it was concluded that the d_{50} is equal to 0.015 m and the ratio d_{85}/d_{15} is equal to 1.5.

3.5.3 Pile system

There is a pile system of 3 x 5 piles for test scenario T9 and T10 which is shown on the left side of Figure 15. The scaled situation consists of piles of 32 mm diameter with a centre to centre distance of 200 mm. This system is representative for an open quay wall. For test scenario T7 and T8 the pile configuration is shown on the right side of Figure 15. A configuration of 6 jetty piles are considered. The piles in the scale model have a diameter of 63 mm and a centre to centre distance of 360 mm. This configuration can be representative for jetties.

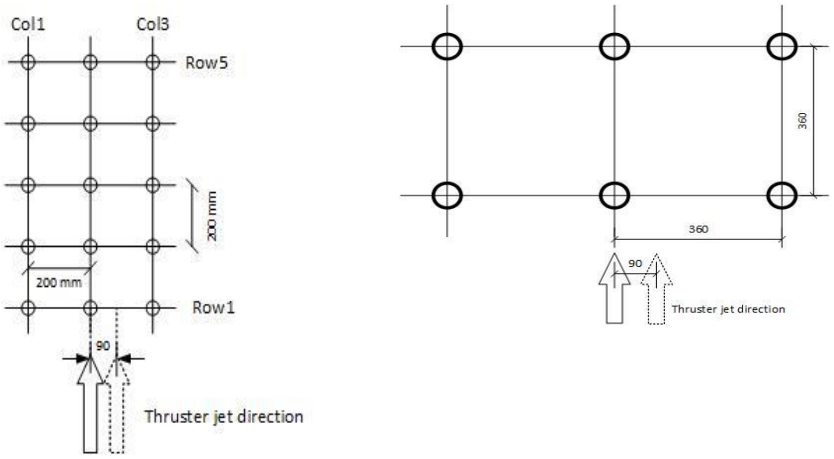

Figure 15 – Pile configuration for scenario T9 and T10 (left) and pile configuration for scenario T7 and T8 (right)

Two scenarios (T7 and T10) are set up in a way that the jet axis intersects with the middle row of piles. The other two scenarios (T8 and T9) contain a lateral shift of the jet axis with respect to the middle row of piles so that there is an eccentric approach of the propeller jet to the piles. This way high slope velocities occur close next to the pile. This lateral shift is 90 mm in negative y-direction. This is 0.25 times the centre to centre distance of the pile configuration with the 63 mm diameter piles and 0.45 times the centre to centre distance of the pile configuration with the 32 mm diameter piles.

3.5.4 Measuring device for velocities

Few measurement equipment are available to measure the velocities within the test basin. These are the Electromagnetic Velocity Sensor (EMS) which was used during the research by Schokking (2002) and Van Veldhoven (2002) or the Acoustic Doppler Velocimeter (ADV) used by Van Doorn (2012).

The ADV is no option because there is no seeding possible in the basin of Deltares and without seeding this measurement does not work properly. This seeding material has to be used for reflecting the signals sent from the velocimeters. A second option remains and that is the EMS which is used during the tests.

Electromagnetic Velocity Sensor

For the velocity measurements within the propeller jet (type I tests) and at locations just above the slope (type II tests) an EMS is used which measures the velocity in two directions, the x-direction and the y-direction for the type I tests and the x'- and y-direction for the type II tests. The used coordinate system is shown in Figure 17. The z-direction and z'-direction can not be measured. It is assumed that the velocity in these directions is relatively small and it has no large consequences when not measuring it.

A measuring probe of an EMS is shown in Figure 16. The working principle is actually based on Faraday's Induction Law and the same principle is also applied at pipe flow meters. An electromagnetic field is developed between the 5 points shown in the picture and the disturbances in this field are caused by the flow velocities. These disturbances are recorded and converted to velocities, taking into account proper calibration.

Figure 16 – An Electromagnetic Velocity Sensor (left), the measuring probe of an EMS (middle) and the dimensions (right)

The electromagnetic velocity sensor has some properties which make it sometimes not the ideal measurement instrument. This however depends on the situation tested and the processes interested in. For example in this scale model the dimensions of the stones are smaller than the dimensions of the EMS and this might influence the results. Velocity measurements close to piles and close to the bed are not possible because the sensor has a relatively large diameter of 33 mm and therefore can influence the flow within the jet. Moreover due to the relatively large measuring probe and the possible influence on the outflow the minimum distance between the outflowing point of the thruster and the EMS is set at 100 mm for the type I test.

The used EMS creates a measuring volume with a thickness of 5 mm and a diameter of 50 mm and this is larger than for example an Acoustic Doppler Velocimeter which has a measuring volume with a diameter of 6 mm and a height of 3 to 15 mm. This can lead to deviations when measuring the turbulence intensities because the length of the vortices that can be measured is partly dependent on the measuring volume. The averaging out of small vortices leads to smaller measured turbulence intensities.

The inaccuracy of the measuring instrument is ± 1% of the measured value or ± 0.01 m/s provided that the tilt angle with respect to the flow direction is smaller than 10 degrees. However, the flow direction on the slope is upwards and parallel to the slope and therefore there is no tilt angle with respect to the flow direction provided proper alignment during installation. The setting of the EMS for the type II tests is perpendicular to the slope as is shown in Figure 18.

3.5.5 Measuring device for stability

The initiation of motion can be measured visually with an underwater camera. A Nikkei Action Cam is used for this. In order to determine the critical velocity the initiation of motion should be defined exactly. Also the location of the initiation of motion is of importance. Next to that it should be determined in what direction the stones move and how much stones move.

In order to measure all this the underwater camera should be on a location where:

- It does not influence the flow induced by the bow thruster
- It can see the movements in x'- and y-direction of the stones
- It has a wide view over the stones in the impact zone of the propeller jet

3.6 Measurement program

The measurement set ups, settings and the methods to process the data for the type I tests, the type II tests and the type III tests are discussed in this paragraph.

The coordinate system that is used is shown in Figure 17. The positive x-direction is in the direction of the jet axis and is zero at the outflow point. At the jet axis the y- and z-coordinates are zero. The y-direction is similar to the lateral direction with respect to the slope. The z-direction is positive towards the water level. It should be noted that above the slope the direction parallel to the slope is defined as the x'-direction and the direction perpendicular to the slope is defined as the z'-direction as shown in Figure 18.

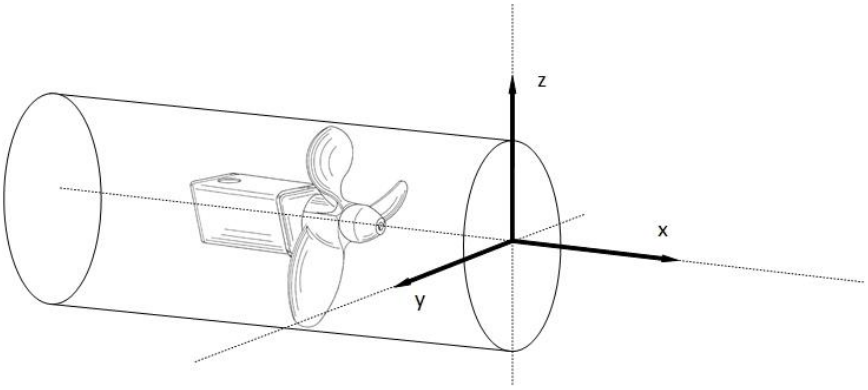

Figure 17 - Coordinate system

3.6.1 Measurement set up

First the measurement set ups for the velocity measurements of the type I and type II tests are discussed and secondly the measurement set up for the stability measurements of the type III test is discussed.

Velocity measurements for type I test

For the outflow velocity measurements of the type I test the EMS is positioned above a flat bottom in a vertical plane that is in line with the jet axis. At multiple distances to the outflow opening and at multiple distances in z-direction to the jet axis the velocities in x- and y-direction are measured. The distances in x-direction applied are 100 mm, 200 mm, 300 mm and 450 mm to the point of outflow. The distances in z-direction to the jet axis applied are 20, 40, 60, 80, 100, 120 and 160 mm in positive and negative z-direction.

Velocity measurements for type II tests

In the model set ups of the type II tests the flow velocities just above the slope at multiple locations and the sideward flow velocities at multiple locations are measured. As already discussed for all type II tests with velocity measurements the EMS is set perpendicular to the slope and measures the velocity in the y-direction and x'-direction.

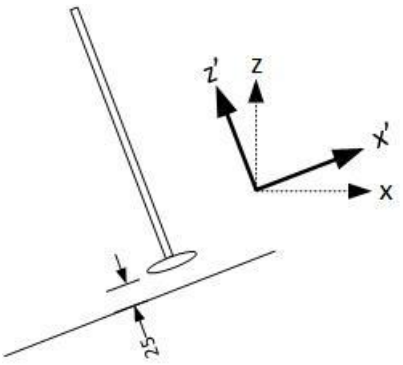

Figure 18 – Position EMS just above the slope and coordinate system above slope

The height of the EMS above the bed is set at 25 mm in z'-direction as is advised in other researches. In addition it is checked in this research that at a height of 25 mm in z'-direction above the bed the largest velocities are measured.

As seems logical the closer the measuring probe to the bed the more influence it has on the flow close to the bed. The effect of the difference in distance might be that when too close to the bed it can block the development of small vortices. As when it is 25 mm from the bed, this is approximately 1.5 times the d_{50}, and according to Hofland (2001) and Booij (1998) this is similar to the size of the vortices which are most effective. After all it is chosen to perform the measurements at a distance of 25 mm to the bed because it is important to determine the flow field as close as possible to the bed.

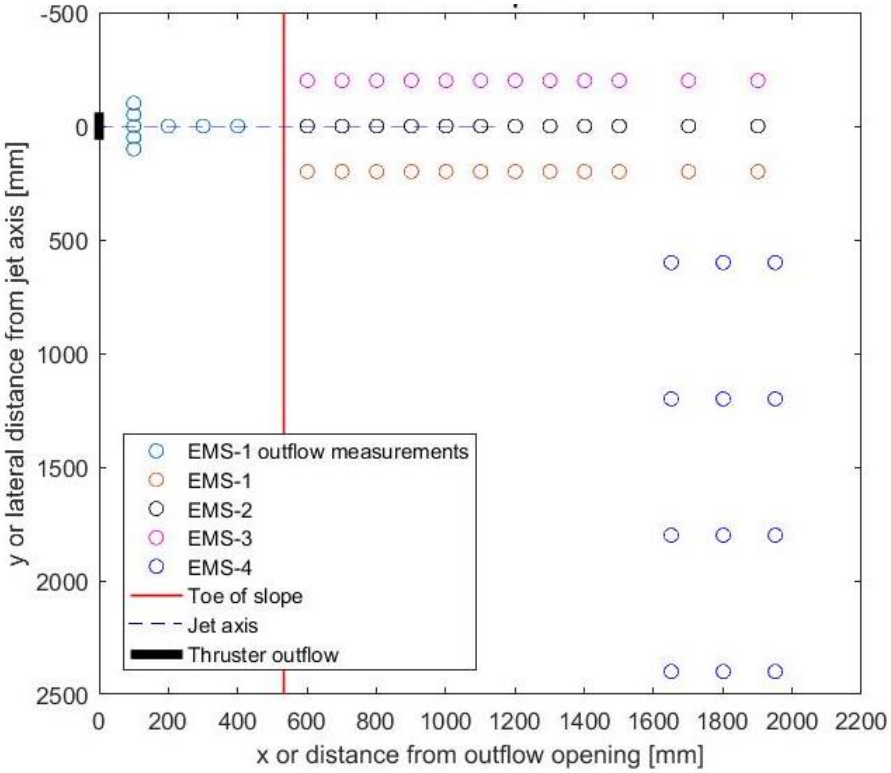

Figure 19 - Measurement locations for all scenarios, horizontal plane

An overview of the measuring locations in the horizontal plane and the vertical plane are shown in Figure 19 and Figure 20. The situation shown in Figure 19 and Figure 20 is a modification of test scenario T1. A larger distance (533 mm) between the point of outflow and the toe of the slope is created in order to measure the efflux velocities correctly and to have no influence of the slope. Distance between measurement locations for outflow velocity and outflow point are equal to measurement points of the researches of Schokking (2002) and Van Doorn (2012). The efflux velocity distribution is investigated to see if the bow thruster is correctly mounted and to check the thrust coefficient and therefore the relation between rotational speed of the propeller and efflux velocity correctly.

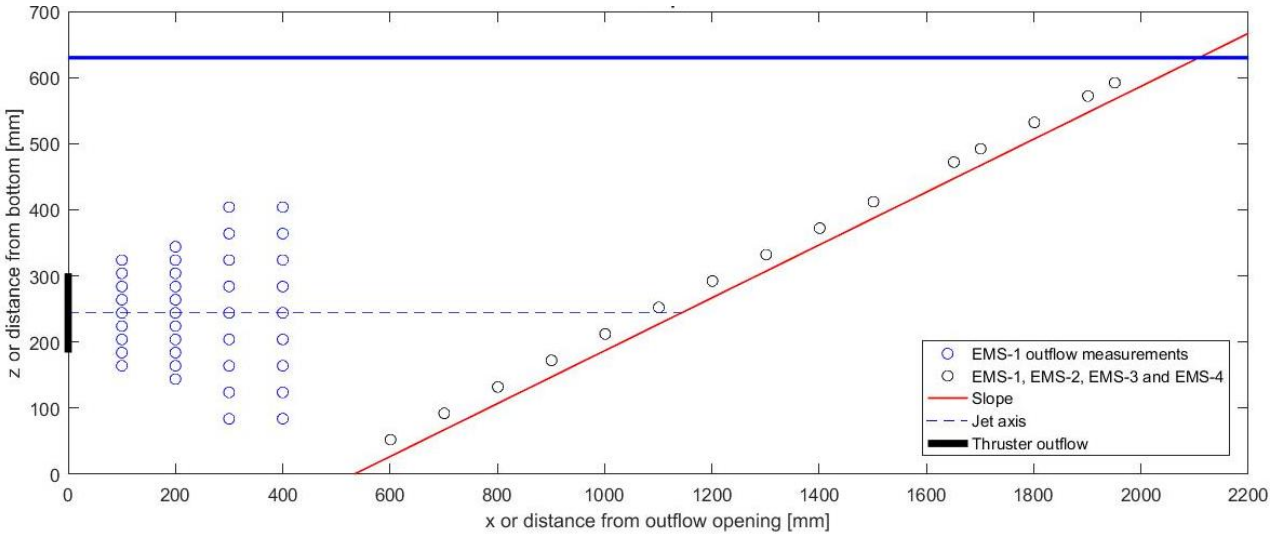

Figure 20 - Measurement locations, vertical plane

Sideward flow velocities are measured on only one side of the slope. The choice to do it only on one side is because of the restricted time and no construction is available to easily replace the sensors after each measurement. The sideward flow is measured until 2.4 m in scale model to the right of the jet axis. It is checked that the highest sideward flow velocities occur at the top of the slope. In order to prove this and also to get to know where the sideward flow at the top bends towards the toe, three rows in y-direction of four measuring points are set up.

For the last four test scenarios T7, T8, T9 and T10 partially different measurement locations are used. In order to get insight in the flow around the pile and the effect of the piles on the velocities and turbulences just above the slope several locations have different coordinates. Also some original locations are still used for these test scenarios so that comparisons are possible with the other scenarios. The points close to the piles are still 30 mm removed from the pile due to the size of the EMS and the size of the measurement volume which should not be disturbed.

Stability measurements for type III tests

One of the methods used to see where the stones are moving to, where the stones come from and how many stones are moved is used by Van Veldhoven (2002) and Schokking (2002). They performed tests by increasing the rotations of the propeller per minute with several small steps. At each step they counted the stones moved out of a colored square and reported the direction of the movement. Each square has dimensions of 50 by 50 mm. When a stone is moved out of a square it can be classified as damage. The total area with colored stones in their test setup was 0.6 m wide and at least 0.5 m long, this is dependent on the zone of possible impact of the propeller jet.

Because of a strict deadline for the tests performed within this research the stones will not be colored. The placement and replacement of these colored stones in each colored square will take a lot of time. Therefore an underwater camera will record the movement of the uncolored stones during the increasing of the propeller rotation speed. With a high enough accuracy of the view, clear water and not too many stones moving it was possible to record all the paths of the moved stones. Within the display of the record a raster will be created with squares of 50 mm wide and 60 mm long as is shown in Figure 21. This way it can be seen over what distance a stone moves. A stone movement is classified as damage when it is moved one time with a distance of $2d_{50}$ which is 0.030 m in the scale model and 0.75 m in prototype situation.

For riprap protection layers it is not desirable to have more than 5 to 10 stones moved out of the protection layer for practical purposes and this also gives a less chaotic record of the moved stones. When increasing the propeller rotational speed it is performed in steps as presented in Table 9. The duration of each step is set at 10 minutes (scale model time) which is in a prototype situation much larger than a bow thruster generally

operates. This way the bed situation can go to a stable situation for the lower rotational speeds. For the higher rotational speeds it will take a lot of time to become stable again and for the reason that time is restricted and the counting duration should be equal for each step it will have the same duration for each step. This entire program with all steps is repeated 5 times in order to get a reliable average.

When counting the amount of moved stones the focus area is limited to a damage area which is selected after a trial measurement. The damage area is selected based on the area where most of the stones move out during the trial measurement.

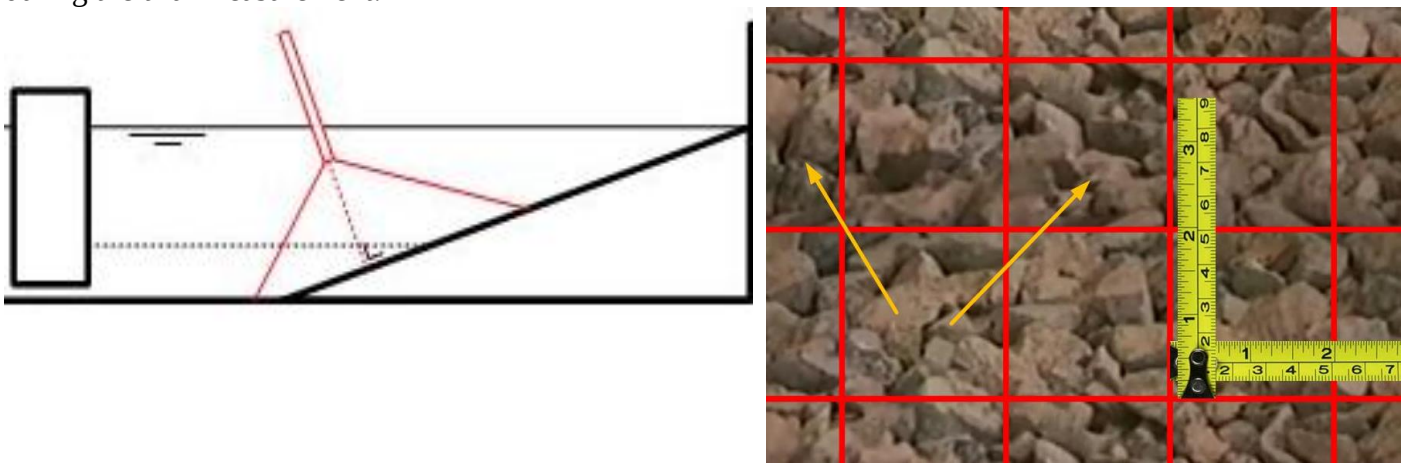

Figure 21 - Position underwater camera (left) and tracking the movements of the stones with a raster (right) of type III test

The definition of initiation of motion is unclear. It is recommended to consider practical applications for this definition. In most situations the strength of the design is highly dependent on the balance between initial construction (costs) and the maintenance (costs). When no movement of armor stones is allowed the strength and therefore the size of the stones is very high. If some movement of armor stones is allowed the strength and therefore the size of the stones is somewhat smaller however in this situation maintenance is needed. A distinction will be made between the allowance of no movement, the movement of 1 stone or the movement of multiple stones.

3.6.2 Settings

In this paragraph first the settings of the frequency regulator for the type I, type II and type III tests and secondly the settings of the measuring equipment for the type I and type II tests are discussed. The frequency regulator was used to vary the rotational speed of the propeller.

Propeller rotational speed and frequency regulator

Three different types of tests were conducted. First, the type I tests to measure the outflow velocity from the bow thruster, after that the type II tests to measure velocities at the slope and at the end the type III test that contains a stability test was performed. For the type I test with outflow velocity measurements the rotations per minute are set on 607, 900 and 1091 RPM. For these rotations per minute the frequency regulator is set on respectively 20.29 Hz, 30.06 Hz and 36.46 Hz. During the type II tests with the bed load measurements at the slope a constant amount of 1091 rotations per minute is applied. This is equal to the rotational speed applied by Van Doorn (2012), although Van Doorn wrongly reported 1021 RPM. And for this the frequency regulator is set on 36.46 Hz. For the last test scenario of the type III test a stability test is performed to find the initiation of motion and the rotational speeds were varied as presented in Table 9.

For the type III tests with the initiation of motion measurements the amount of rotations per minute is increased with steps. On beforehand a trial measurement is performed in order to get an idea at which rotational speed the first stones start to move. This way the focus comes more on the rotational speeds around the critical velocity. Therefore the amount of steps is not too large and a lot of time can be spared during the tests.

#	Frequency [Hz]	Rotations per minute [RPM][1)]	Efflux velocity[2), 3)] [m/s]
1	24	718	0.99
2	28	837	1.15
3	32	957	1.32
4	36	1077	1.48
5	40	1196	1.65
6	44	1316	1.81

Table 9 - Steps of rotational speed for measuring initiation of motion of type III test

Remark:

1) The rotations per minute shown are based on two separate calibration measurements with a stroboscope, which determines the amount rotations per minute when the frequency regulator is set on a specific frequency.
2) This efflux velocity is calculated with a thrust coefficient of 0.22. The K_T value provided by the manufacturer is corrected based on measurements, described in section 5.1 Type I tests - Efflux velocities. The relation between rotational speed and efflux velocity is presented in (Eq. 3-7).
3) Viscosity effects can be neglected for these efflux velocities following the criterion that the Reynolds number for jet-flow > 3,000 and (Eq. 3-4).

$$U_0 = 1.6 * \frac{RPM}{60} * D_0\sqrt{K_T} \qquad \textit{(Eq. 3-7)}$$

With: K_T: $Thrust\ coefficient$ $[-]$
RPM: $Rotations\ per\ minute$ $[min^{-1}]$

Sampling frequency and measuring duration

It is important to select a sampling frequency so that turbulent vortices which affect the stability of the stone the most are recorded. This means vortices in the scale model with a minimum size of approximately the stone diameter which is around 0.015 m and all vortices which have larger dimensions. A larger vortex contains more energy and therefore affects the stability of a stone more. There is a relation between the length scale of the vortex and the timescale of it. This is dependent on the flow velocity. For example when the flow velocity is around 1 m/s the timescale of a vortex of approximately 0.015 m is around the 0.015 s. This is just an estimation. Results of the experiments show that average velocities just above the bed occur around the 0.7 m/s. It can be concluded that with an effective measuring frequency of 7 Hz, and therefore a minimum measurable vortex period of 0.15 s, the vortices smaller than approximately 0.10 m in the scale model can not be detected well. Again this is just an estimation. Nevertheless it shows that a lot of the smaller vortices are not measured properly and therefore this leads to results with smaller turbulence intensities. The sampling frequency is set at 60 Hz. The effective measuring frequency of the device is 7 Hz, however it is advised to sample at much higher frequencies.

In order to obtain a proper average velocity the measuring duration is of importance. This should not be too short because then it can be the case that the velocity fluctuations are not fully averaged out. The measurement duration is optimized after the first measurement results are checked. The first measurements have a duration of 30 minutes after which it is shortened to 10 minutes because there was no considerable difference between the velocity pattern in time, the time-average velocities and the standard deviation of the velocities.

3.6.3 Data processing

Some important characteristics of the flow field should be determined and this means the data achieved should be processed. The data processing for the measurements conducted for the type I and type II tests are described.

Velocity measurements

The measuring devices perform several velocity measurements within the basin and these have to be transformed to the important characteristics and parameters that give insight in the occurring processes. The velocities measured in x-, x'- and y-direction are transformed into average velocities (Eq. 3-8) and velocity fluctuations for each direction. From these the absolute turbulence intensities (Eq. 3-9) and the relative turbulence intensities (Eq. 3-10) are determined. The turbulence intensities are the main factor that cause instabilities of the grains at the sloping bed.

$$\bar{U}_i = \frac{1}{N}\sum_{n=1}^{N} U_{n,i} \qquad \textit{(Eq. 3-8)}$$

With: $\bar{U}_i$: $Average\ velocity\ in\ i-direction\ [m/s]$
$U_{n,i}$: $Measured\ velocity\ of\ sample\ n\ in\ i-direction\ [m/s]$
N: $Number\ of\ samples$ [-]

$$\sigma_i = \sqrt{\frac{1}{N}\sum_{n=1}^{N}\left(U_{n,i} - \bar{U}_i\right)^2} \qquad \textit{(Eq. 3-9)}$$

With: σ_i: $Standard\ deviation\ (absolute\ turbulence\ intensity)\ [m/s]$

$$r_i = \frac{\sigma_i}{\bar{U}_i} \qquad \textit{(Eq. 3-10)}$$

With: r_i: $Relative\ turbulence\ intensity\ in\ i-direction\ [-]$

4. Test Results

This chapter includes the most important results that are achieved by performing measurements during all test scenarios. A distinction can be made between the type I test with the outflow measurements of test scenario T0, the type II tests with the slope velocity measurements of test scenario T1 until T10 except for T6 which is part of the type III test with stability measurements. These three different type of measurements are discussed in separate paragraphs. Part of the type II tests are extra measurements to obtain sideward flow velocities at the top of the slope which are conducted as well. First the test results of the type I measurements are described. Secondly, the test results of the type II tests. Finally, the test results of the type III tests.

4.1 Type I tests - Outflow velocities

In order to determine the representative efflux velocity U_0, the outflow velocity distribution and the thrust coefficient are investigated. All outflow measurements are performed when the model vessel is located at an axial distance to the slope of x/D_0=11.5. This means that the measurement points are located above a horizontal bed. For three different rotational speeds the outflow velocity distribution is investigated at 100mm distance from the outflow point in the vertical plane at y=0 mm. These rotational speeds are 607, 900 and 1091 rotations per minute. The time-averaged flow velocities in x-direction are shown in Figure 22. At each measurement point an error bar is plotted which shows the measured time-averaged velocity plus and minus one time the standard deviation to give an indication of the turbulence intensity at that point. As can be seen in Figure 22, is that the shape of the velocity distribution is similar, independent of the rotational speed and that it gives a two-peak profile. Besides the efflux velocity U_0 for each rotational speed is presented that is calculated with the axial momentum theory (Eq. 2-7) from the measured U_x velocities. The U_0 is presented over the height of the initial propeller diameter D_0.

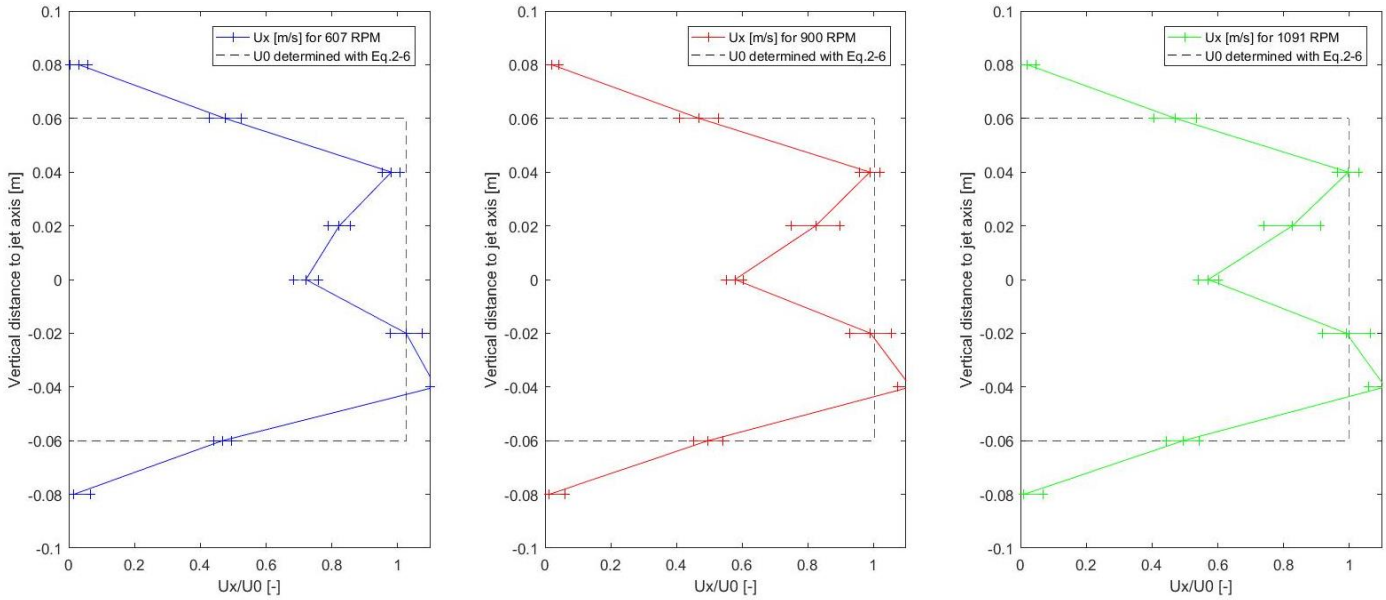

Figure 22 - Efflux velocities at 100mm from the outflow point in the vertical plane at y=0 mm for three rotational speeds

The rotational speed of 1091 rotations per minute (right plot, Figure 22) is used for the velocity measurements above the slope for all test scenarios. Therefore the velocity distribution of this rotational speed is investigated at multiple distances behind the outflow opening, respectively 100, 200, 300 and 450 mm. The measurements are conducted in the vertical plane at y=0 mm. Time-averaged flow velocities in x-direction are shown in Figure 23. In order to get an idea of what the Dutch and German calculation methods predict in the establishment zone, the predictions by these methods are shown as well. The measurements show a reduction in velocities, a wider distribution and a velocity profile with one peak instead of two peaks when at a distance of 4 times the jet diameter to the outflow point.

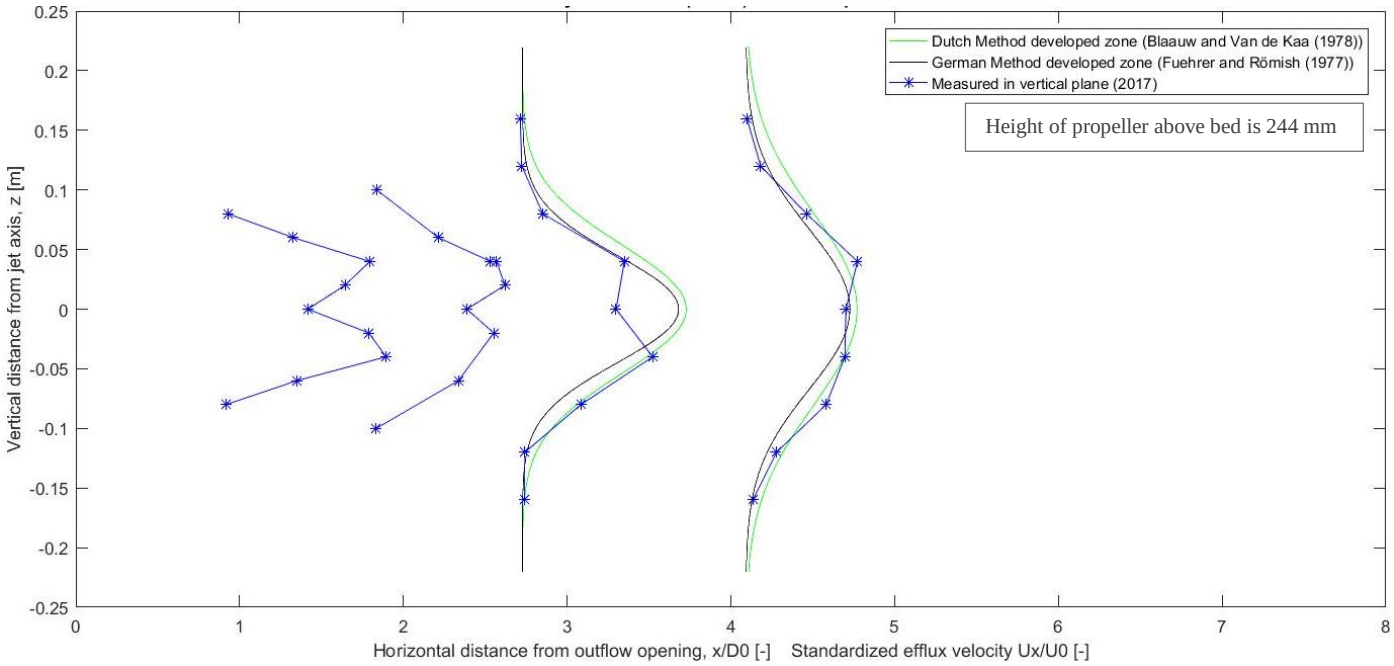

Figure 23 - Outflow velocity distribution for 1091 RPM. Measured in vertical plane at multiple distances behind the outflow point

For the same rotational speed the absolute and relative turbulence intensities are presented in Figure 24. The (relative) turbulence intensities are given for multiple z-coordinates and in order to give an overview that is not too chaotic some less important points are not plotted. From the figures it can be concluded that the turbulence increases for larger distances to the outflow point. Absolute and relative turbulence intensities have larger values for larger vertical distances to the jet axis as well. However the values are smaller than expected and are discussed in the next chapter.

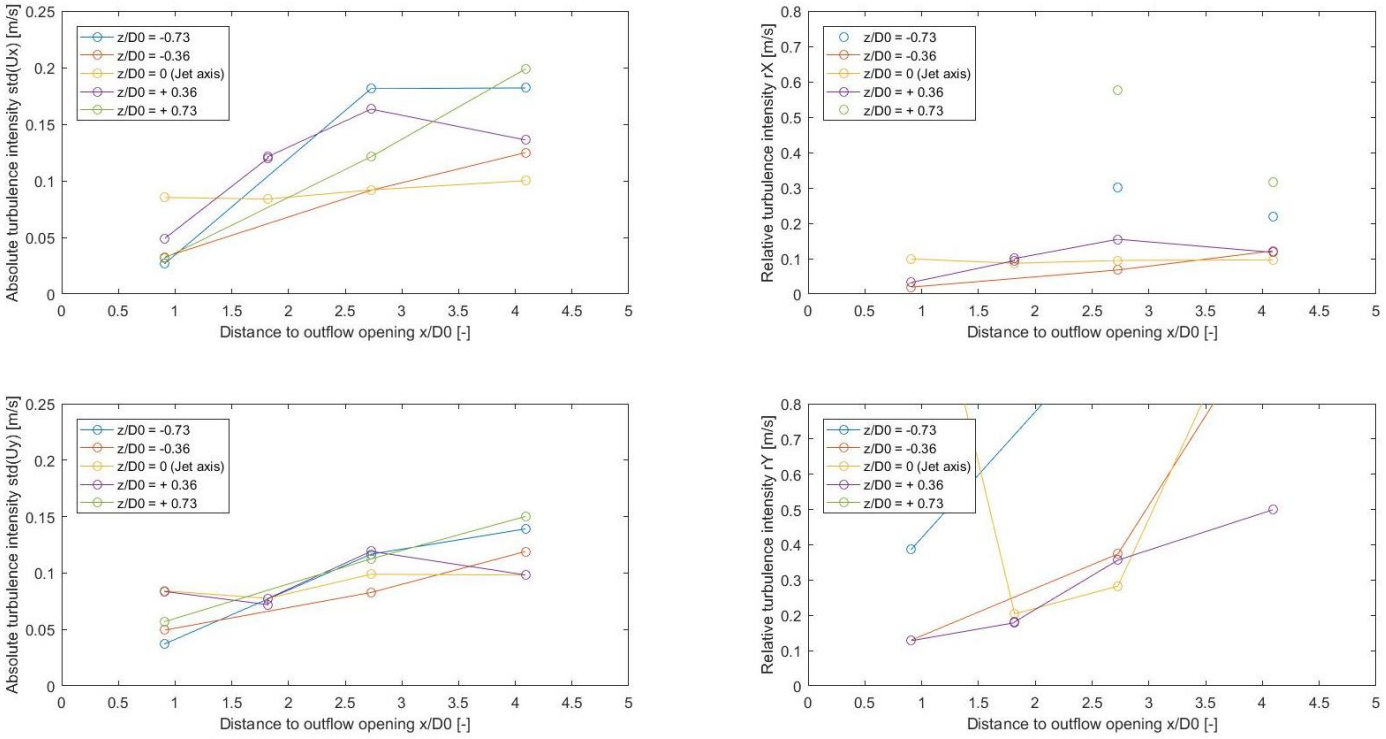

Figure 24 - Absolute (left) and relative (right) turbulence intensities in the propeller jet for 1091 RPM

4.2 Type II tests - Slope velocities

A distinction is made between the measured centre slope velocities and the sideward slope velocities. These are discussed subsequently in the first and second paragraph.

4.2.1 Centre slope velocities

For all test scenarios, except test scenario T6, slope velocity measurements are performed at 25 mm above the sloping bed at multiple locations at y = 0 mm, y = 155 mm and y = -155 mm. For this 3 EMSs were positioned next to each other. The rotational speed was set at 1091 rotations per minute. For some test scenarios extra measurement locations were added to the measurement program in order to achieve more information about the behaviour of the flow on the slope. The test scenarios differ in slope angle, axial distance, roughness and the addition of piles on the slope. An overview of the measured time-averaged velocities of the x'- and y-direction combined for test scenario T1 is presented in Figure 25. In this figure the velocity vectors are added in order to show the velocity direction. As can be observed is that a large resolution is used between the measurement locations and therefore the linearly interpolated velocities in between the measurement points might deviate from the actual velocities. All velocities and turbulence intensities measured for each scenario are presented in Appendix F - Test results.

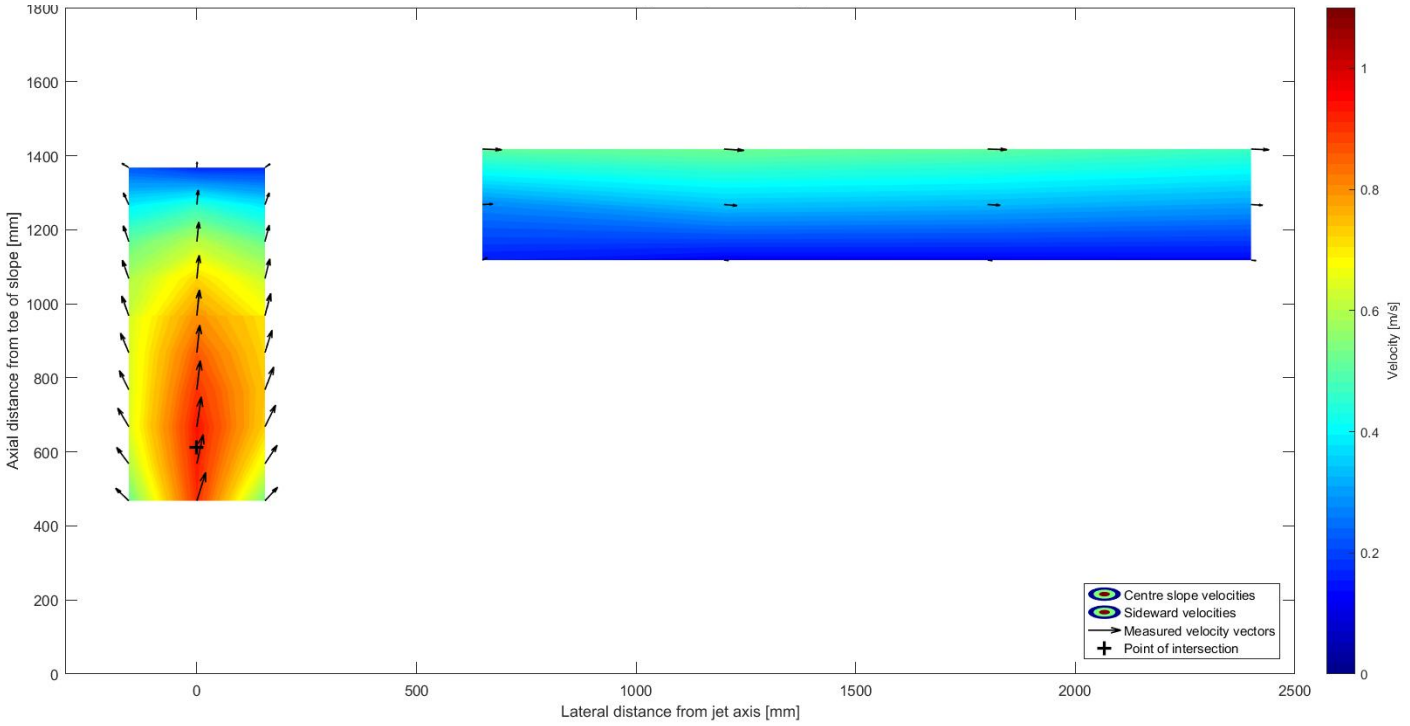

Figure 25 - Top view of all measured velocities (Ux' and Uy combined) for test scenario T1

It was assumed that the highest slope velocities occurred at y = 0 mm and are in x-direction. This is why in this paragraph only the $U_{x'}$-velocities and relative turbulence intensities in x'-direction at the y-location of the jet axis are presented for each test scenario. A distinction is made between the different variations in the model set ups. In addition a velocity profile according to (Eq. 2-10) is added to the plots. The derivation of this equation is presented in Appendix H – . The influence of the slope is partly taken into account in this equation. All the presented results are analyzed in the next chapter.

Variation in roughness

A smooth slope and a rough slope were applied during respectively test scenario T1 and test scenario T2. The measured $U_{x'}$ velocities are shown in Figure 26. There are no measurements performed closer to the toe because this was not possible with the construction build for the scale model. The x-axis presents the distance in x-direction to the point where the jet axis intersects with the slope. A higher negative value means closer to the toe of the slope. A velocity profile according to the unconfined jet calculation method (Eq. 2-10) is included to give an indication of what the slope velocities are. The graphs show that the maximum flow velocities occur around the point of intersection and that the velocities higher on the slope also are larger than according to this method.

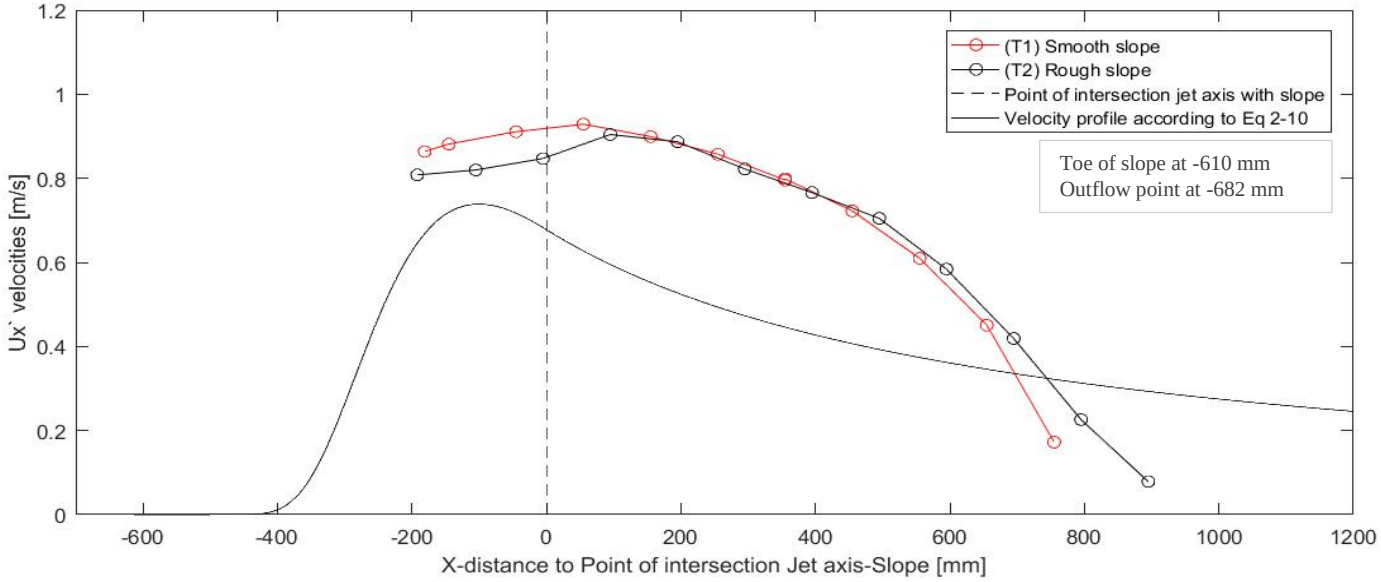

Figure 26 – Ux' slope velocities for T1 and T2, variation in roughness

The relative turbulence intensities in x'-direction for test scenario T1 and T2 are plotted in Figure 27. The very high relative turbulence intensities at the top of the slope are caused by the time-averaged x'-velocities that approach zero. The curves for the relative turbulence intensities are of a similar order and have a similar shape for both test scenarios. The values of the relative turbulence intensities around the location of maximum velocity are around the 0.10 to 0.15.

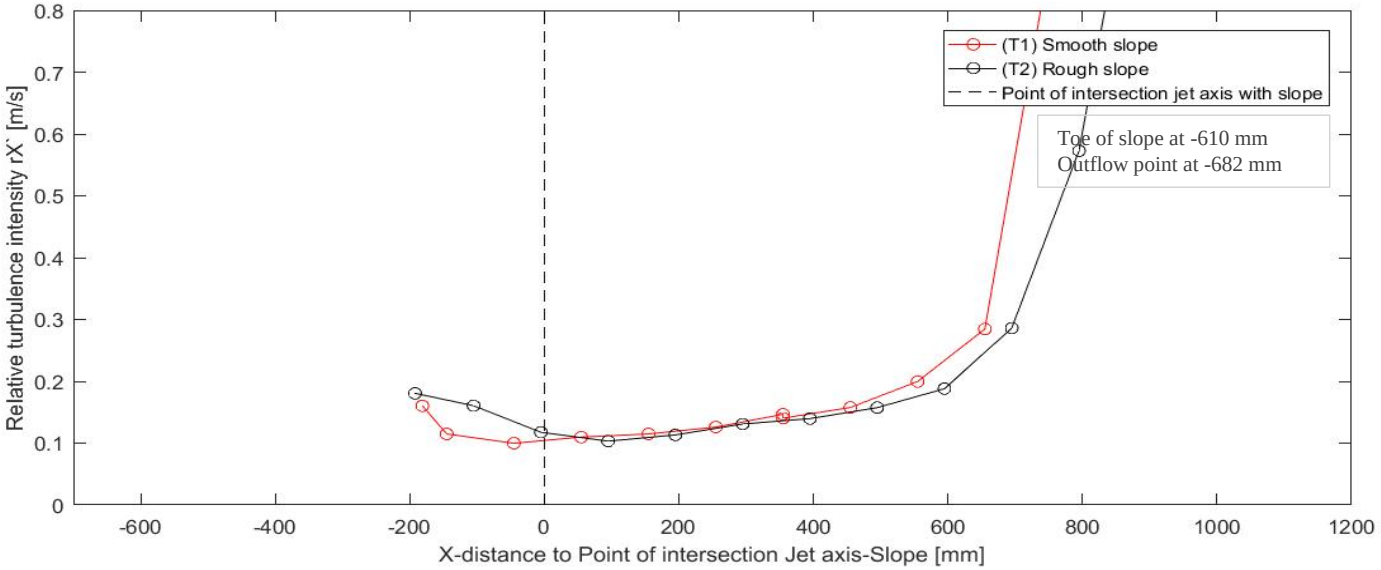

Figure 27 - Relative turbulence intensities rX' for T1 and T2, variation in roughness

Variation in slope angle

A slope of 1 in 2.5 and a slope of 1 in 3.0 are applied during respectively test scenario T2 and test scenario T3. Both model set ups contain a rough surface. The measured $U_{x'}$ velocities along the slope are plotted in Figure 28 together with the expected velocity profiles according to equation (Eq. 2-10). Again the construction allowed no measurements closer to the toe and therefore it is questionable if the maximum slope velocity might not be located lower on the slope. On the other hand the reliability of the most left measuring point of T3 is disputable, because in no of the other tests the maximum of the measured slope velocities was left (or more downwards on the slope) of the maximum according to the unconfined jet method.

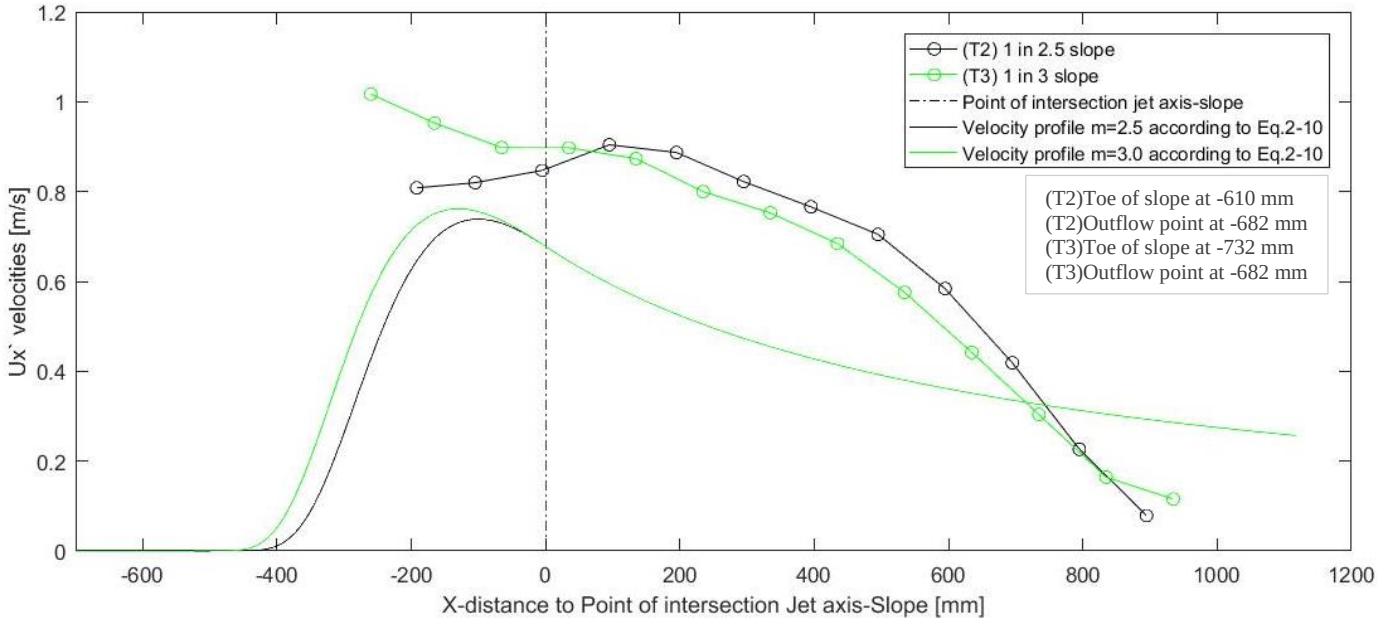

Figure 28 - Ux' slope velocities for T2 and T3, variation in slope angle

Relative turbulence intensities in x'-direction for test scenarios T2 and T3 are plotted in Figure 29. Some measurement points at the top of the slope have very large relative turbulence intensities as a result of the $U_{x'}$ velocities that approach zero. Again the shape of both curves are the same and only small differences can be observed below the point of intersection. The relative turbulence intensities around the location of maximum shows values of around 0.10 to 0.15.

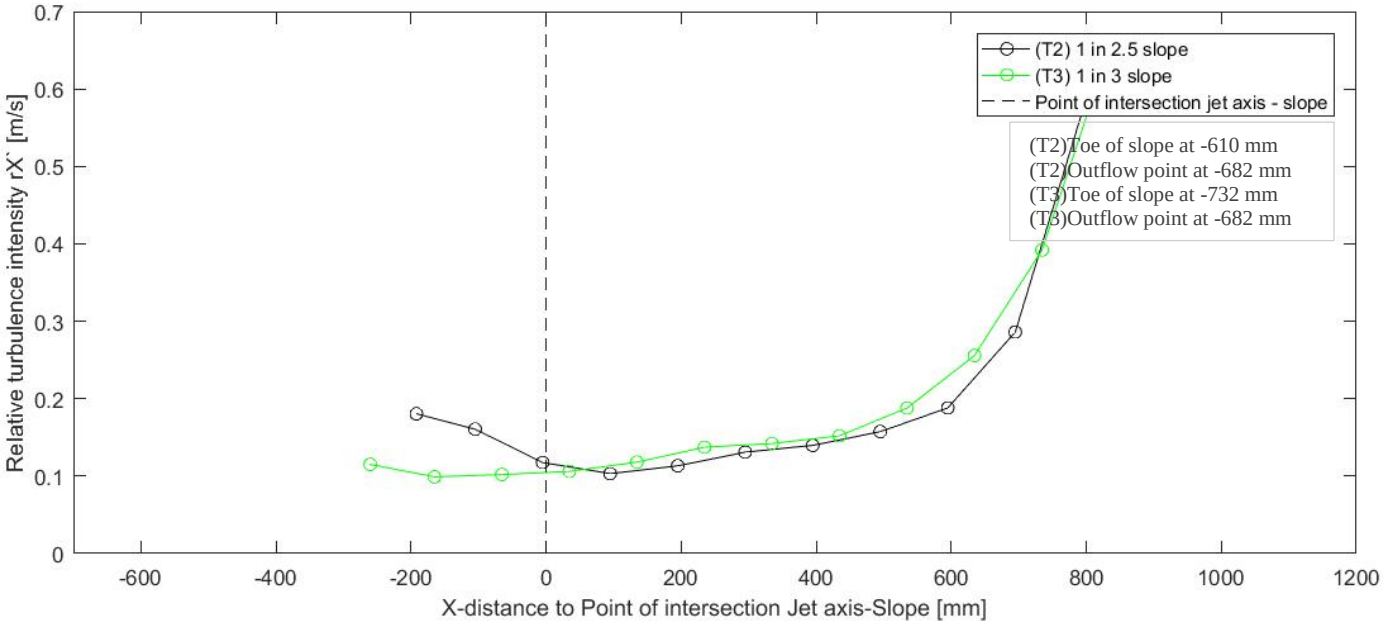

Figure 29 - Relative turbulence intensities rX' along the slope for T2 and T3, variation in slope angle

Variation in axial distance

For test scenario T3, T4 and T5 different axial distances are applied. Where the axial distance for T3 is the smallest and for T4 the largest. The slope applied is a 1 in 3 slope with a rough surface. The measured time-averaged velocities in x'-direction along the slope are presented in Figure 30 and a decrease in slope velocities can be observed for larger axial distances.

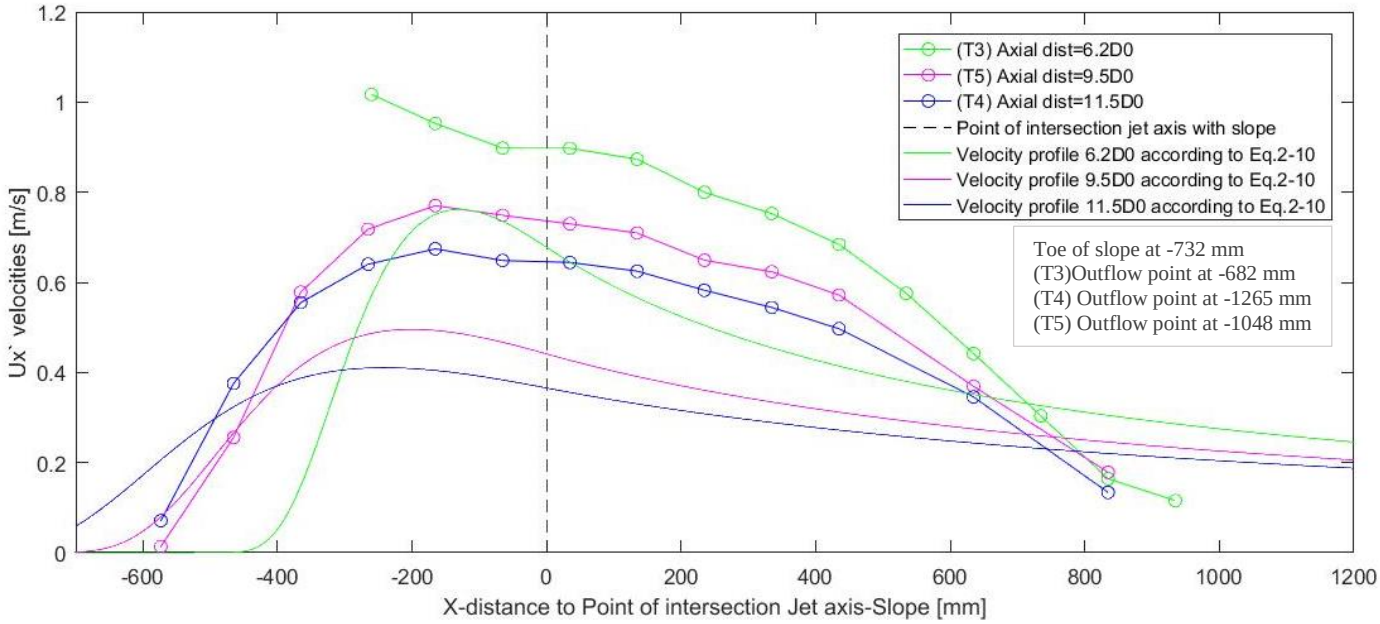

Figure 30 - Ux' slope velocities for T3, T4 and T5, variation in axial distance

The relative turbulence intensities along the slope in x'-direction for T3, T4 and T5 are shown in Figure 31. The first measurement point that is nearest to the toe of the slope and the last measurement point that is nearest to the top of the slope are doubtable due to the time averaged velocity in x'-direction which approaches zero and leads to very large relative turbulence intensities. The relative turbulence intensities around the location of maximum slope velocity is approximately between 0.10 and 0.20.

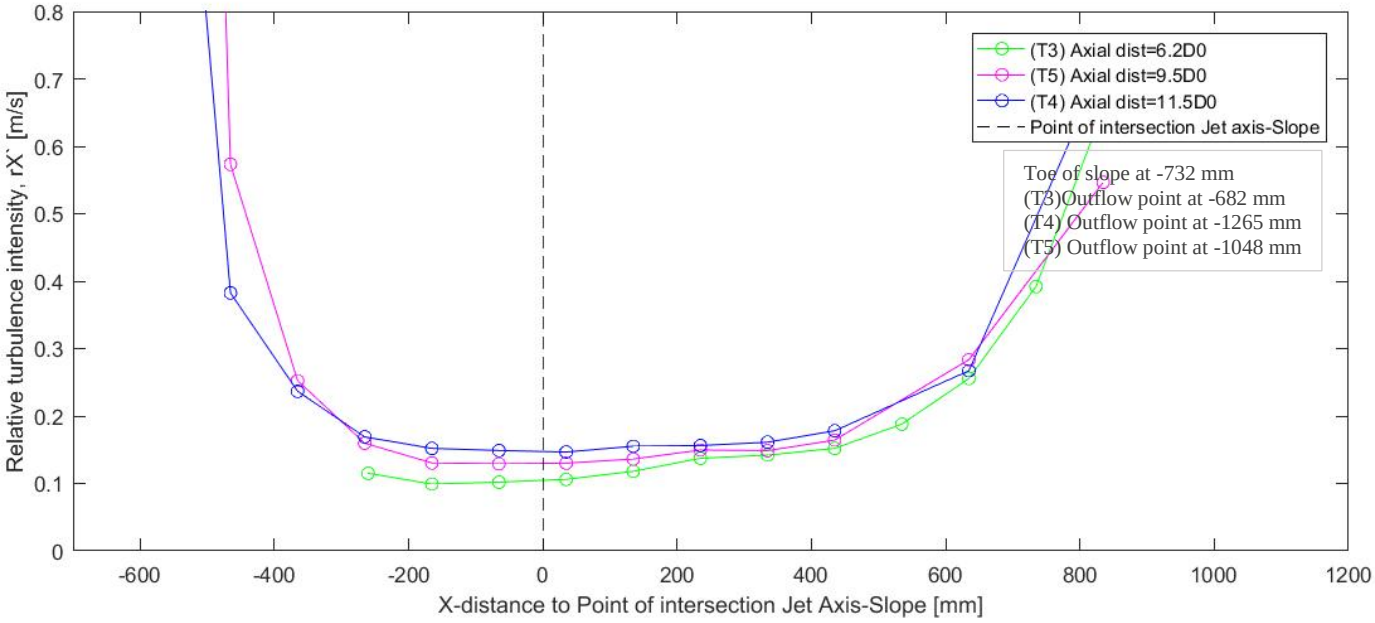

Figure 31 - Relative turbulence intensities rX' for T3, T4 and T5, variation in axial distance

Variation in the configuration of the piles

Two types of pile systems were tested, one pile system that represents a part of a jetty (T7 and T8) and one pile system that represents a part of an open quay wall (T9 and T10). During test scenarios T7 and T10 the jet axis was in line with the piles in the middle (y=0mm). During the other two test scenarios, T8 and T9, the jet axis was shifted 90 mm in positive y-direction. Due to the shift the velocities could be measured at the jet axis and therefore are compared to the time-averaged x'-velocities at the jet axis of test scenario T5. Test scenario T5 has the same set up however without piles. In addition the highest velocities occurred during the scenarios with an eccentric propeller jet. Figure 32 presents the axial $U_{x'}$ velocities. The locations of the piles are shown as well.

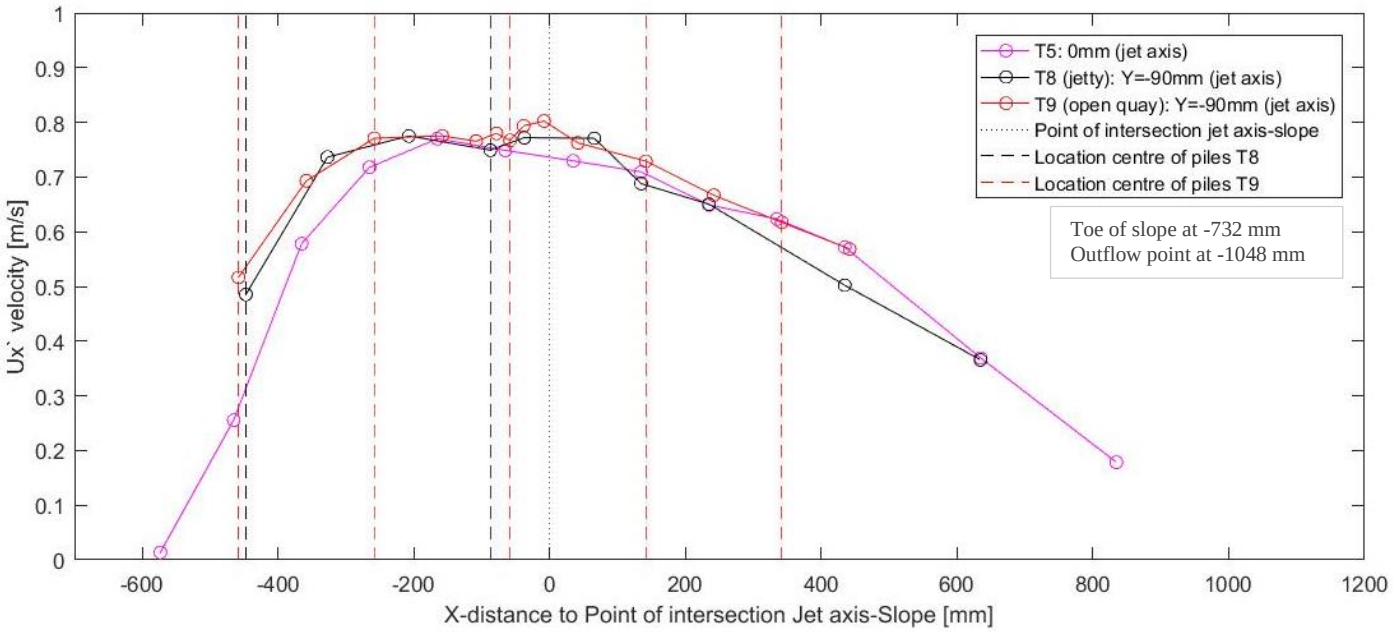

Figure 32 - Ux' slope velocities for T5, T8 and T9, variation in pile configuration

For the same test scenarios the relative turbulence intensities in x'-direction are plotted in Figure 33. Again the locations of the piles are shown in the plot. Again there can be no large differences observed and around the location of maximum velocity the relative turbulence intensities are around the 0.10 to 0.15.

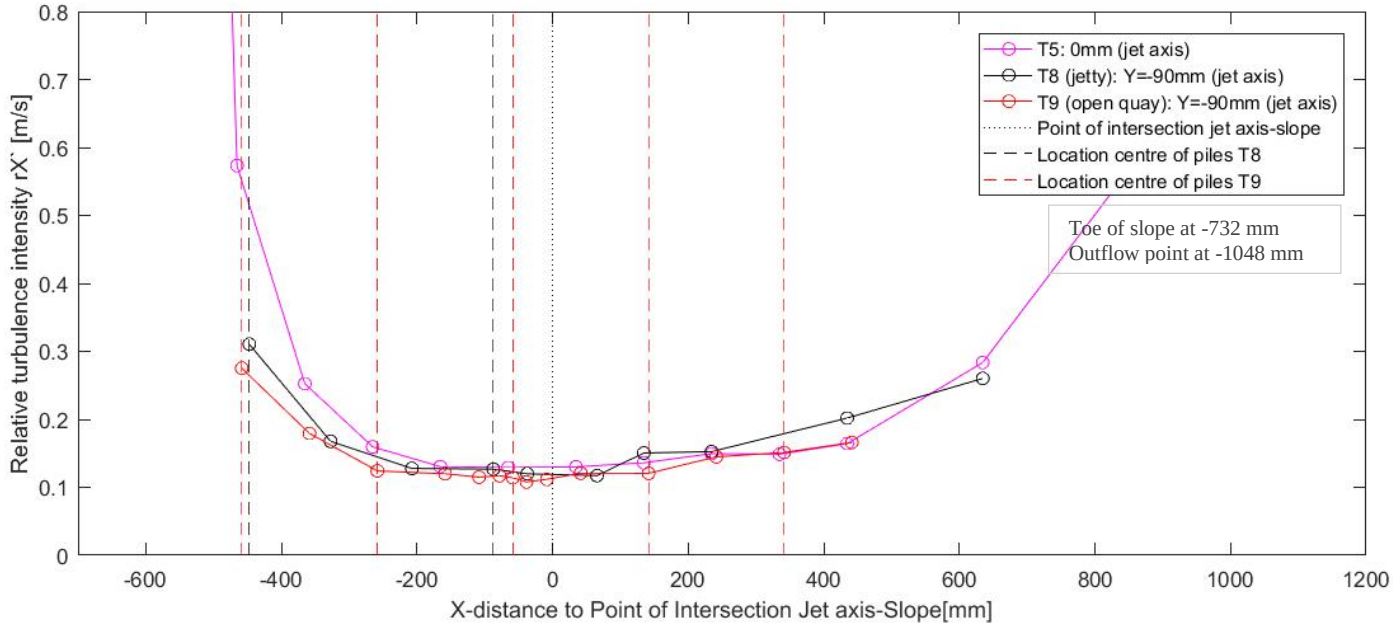

Figure 33 - Relative turbulence intensities rX' for T5, T8 and T9, variation in pile configuration

4.2.2 Sideward velocities

A fourth EMS is used to measure sideward velocities on the side with negative y-coordinates at the top of the slope. The measurements are performed in three rows in y-direction, each row presented in a different figure. As mentioned in the paragraph before, the rotational speed of the propeller is set at 1091 rotations per minute. The height of the EMS above the bottom is 25 mm. During all test scenarios except test scenario T6, T8 and T9, sideward velocity measurements are conducted. The time-averaged velocities in y-direction and the relative turbulence intensities in y-direction are presented. Besides the jet axis is located at y = 0 mm to have an indication of where the bow thruster is located.

Variation in roughness

Sideward velocities for test scenario T1 and T2 are plotted in Figure 34 and the relative turbulence intensities of these scenarios are plotted in Figure 35. The model set up of T1 contains a smooth slope and the model set up of T2 contains a rough slope. That is the only difference between the two scenarios. The distances of the measurement locations to the toe of the slope in x-direction are mentioned in the figures.

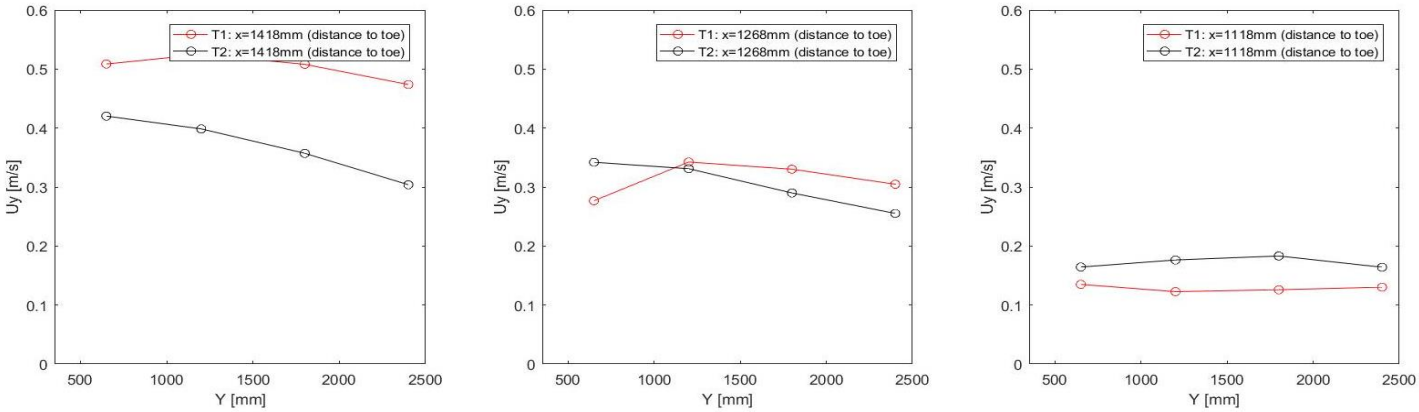

Figure 34 - Sideward velocities for T1 and T2, variation in roughness. Left: row highest on slope, Right: row lowest on slope.

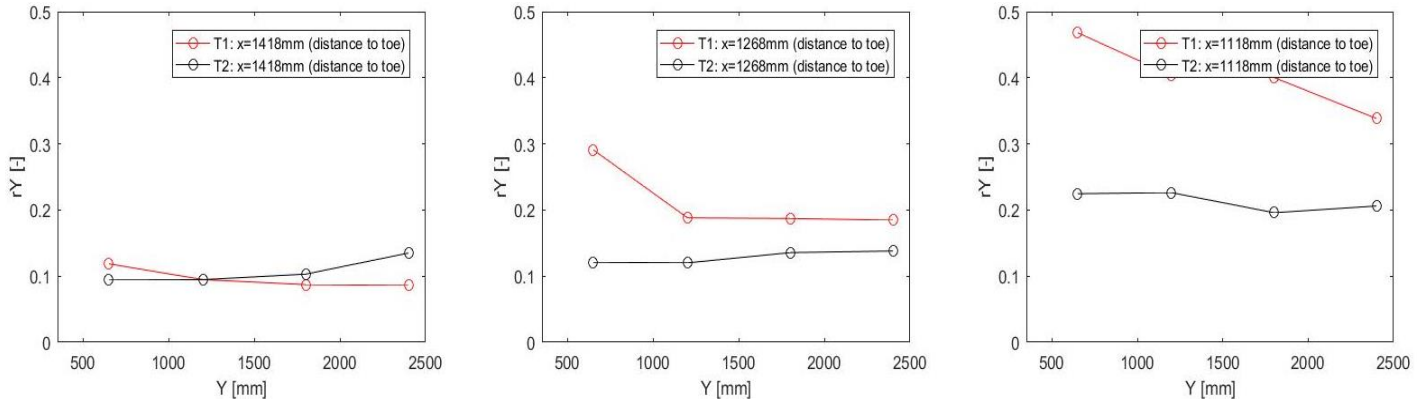

Figure 35 - Relative turbulence intensities sideward for T1 and T2, variation in roughness. Left: row highest on slope, Right: row lowest on slope.

Variation in slope angle

The difference between test scenario T2 and T3 is the slope angle, which is respectively 1 in 2.5 and 1 in 3. The sideward velocities for both scenarios are shown in Figure 36 and the relative turbulence intensities for both scenarios are presented in Figure 37. The measurement locations with the largest y-coordinate is different for both scenarios due to a differently applied lay out of the plates with glued stones on the slope. This inequality in lay out has however no consequences to the measured velocities as this is investigated during the tests. Furthermore, the difference in distance to the toe is due to the fact that the distance from the toe to the point that the water level intersects with the slope is larger for gentler slopes.

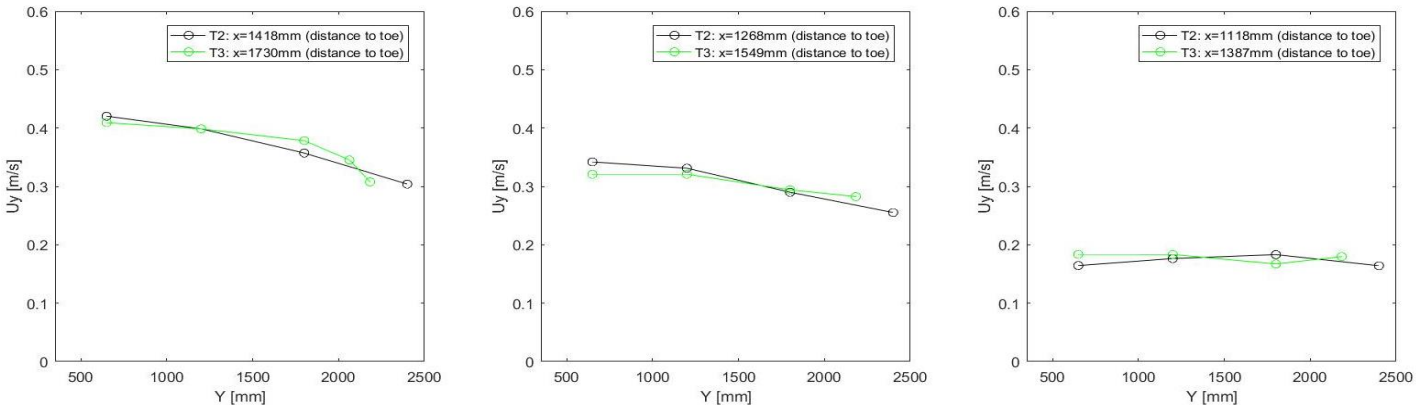

Figure 36 - Sideward velocities for T2 and T3, variation in slope angle. Left: row highest on slope, Right: row lowest on slope.

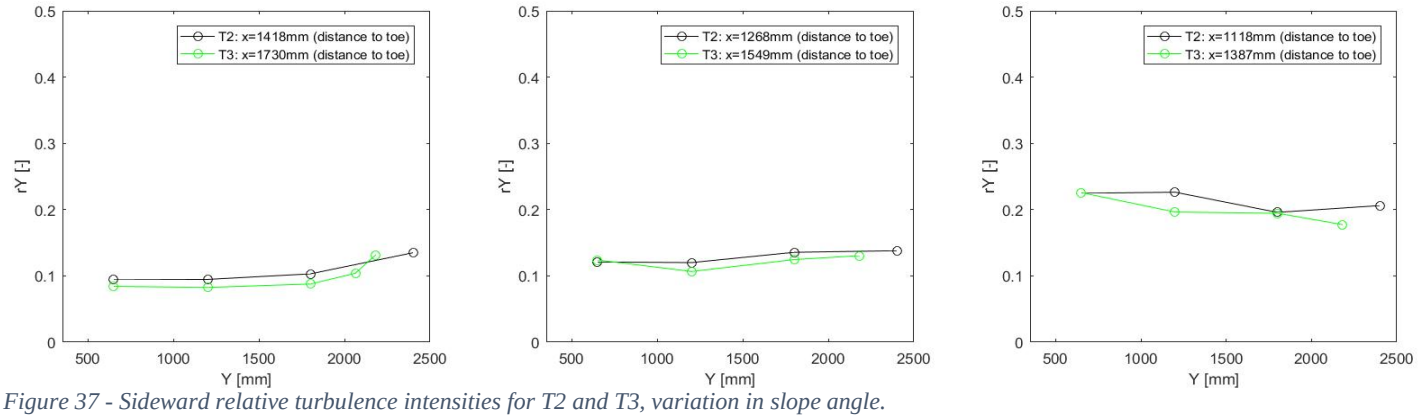

Figure 37 - Sideward relative turbulence intensities for T2 and T3, variation in slope angle.

Variation in axial distance

For test scenarios T3, T4 and T5 the axial distance is varied. The U_y velocities at the top of the slope are presented in Figure 38 and the relative turbulence intensities for these scenarios are plotted in Figure 39. Some extra measurement points are added closer to the jet axis.

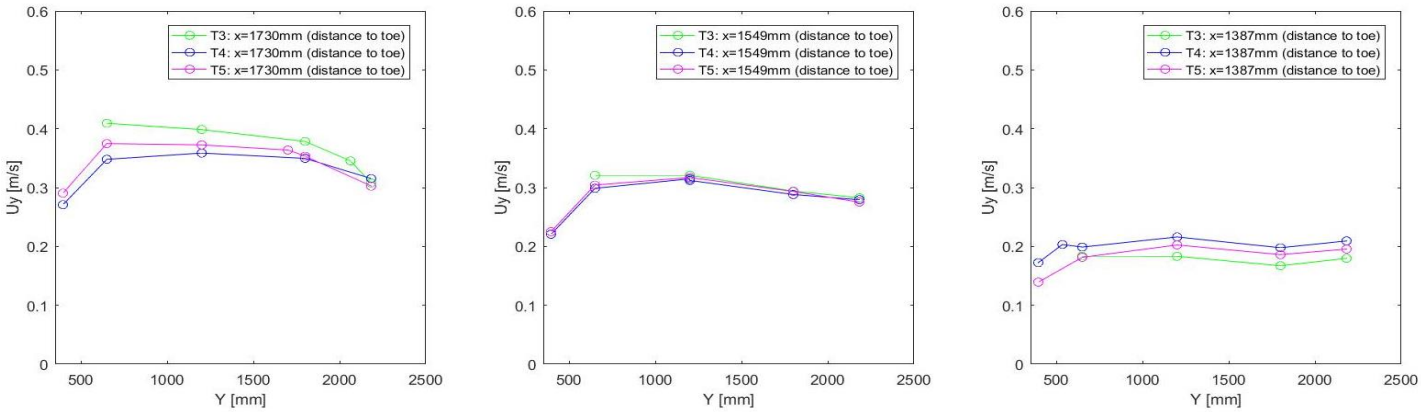

Figure 38 - Sideward velocities for T3, T4 and T5, variation in axial distance.. Left: row highest on slope, Right: row lowest on slope.

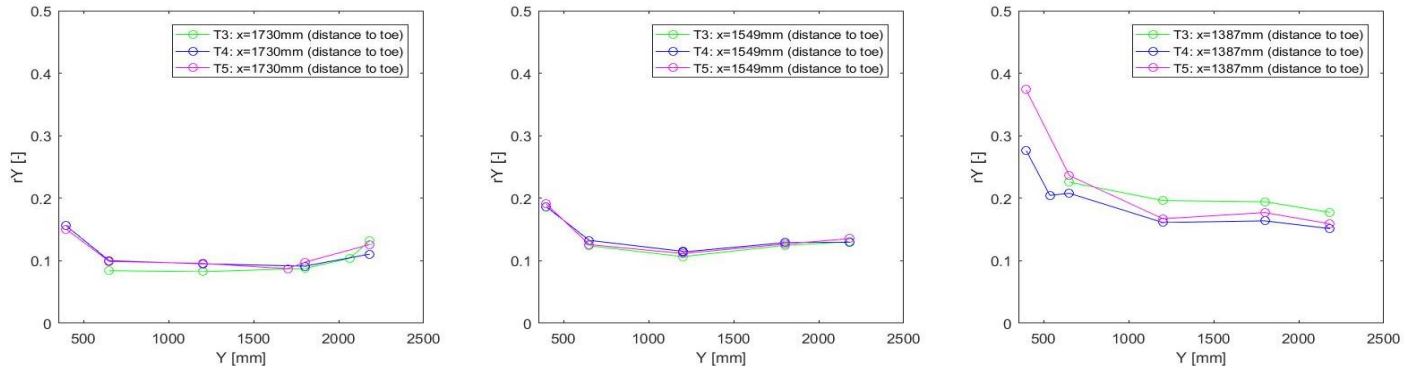

Figure 39 - Relative turbulence intensities sideward for T3, T4 and T5, variation in axial distance

Variation in the configuration of the piles

The results of test scenario T5, T7 and T10 present the influence of the piles on the sideward velocities and turbulence intensities. Test scenario T5 is without piles, test scenario T7 with a jetty configuration and test scenario T10 with an open quay configuration. For all scenarios the jet axis is located at y = 0mm. Sideward velocities for test scenarios T5, T7 and T10 are plotted in Figure 40. The measured relative turbulence intensities are plotted in Figure 41.

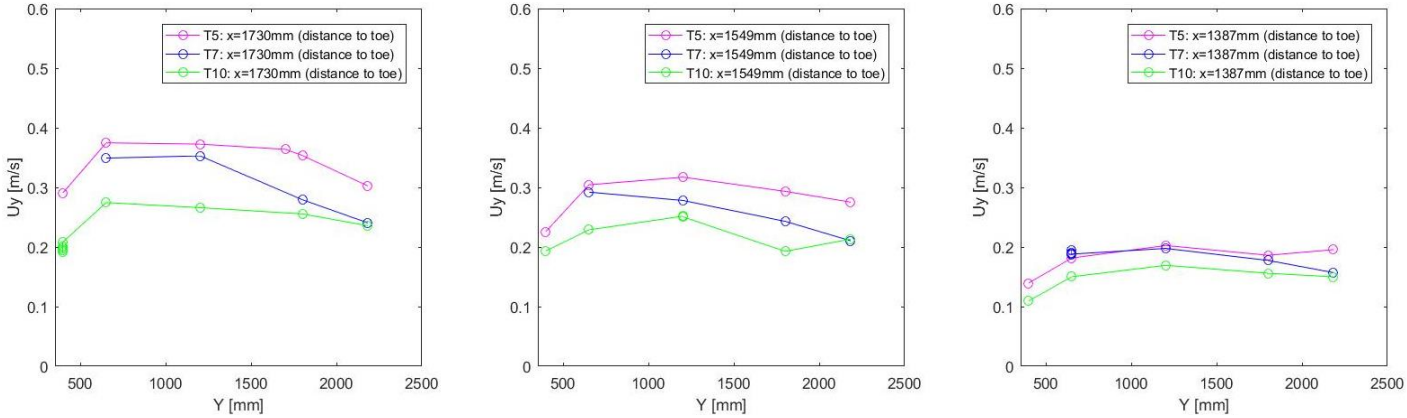

Figure 40 - Sideward velocities for T5, T7 and T10, variation in pile system. Left: row highest on slope, Right: row lowest on slope.

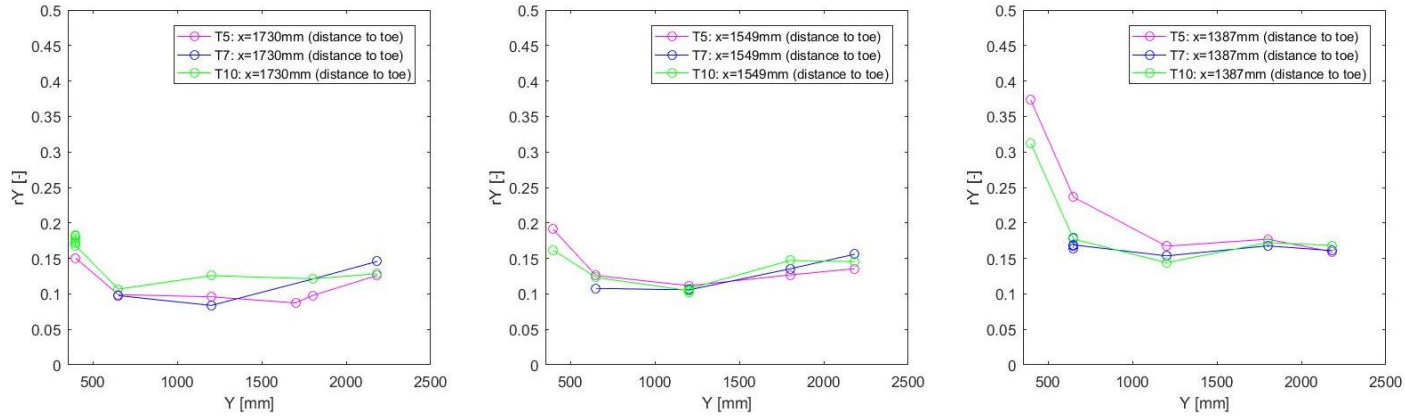

Figure 41 - Sideward relative turbulence intensities for T5, T7 and T10, variation in pile configuration

4.3 Type III tests - Stability

The test scenario for the stability measurements is T6 and has a similar model set up as test scenario T5 except that there is an extra layer of loose stones with a thickness of $2d_{n50}$ placed on top of the glued stones. The axial distance is equal for both test set ups. Furthermore the slope is an 1 in 3 slope and there are no piles located on the slope. Specifications and set-up for this scenario are discussed in section 3.6.1 Measurement set up.

During the measurements movements of the loose stones are recorded with a Nikkei Action Cam which was placed with its lens located just below the water level. A damage location was selected based on a trial measurement which gave an indication of the area where most of the stones start to move as is indicated in Figure 42. This is done in order to limit the focus area. All the movements, the movement intensity per square meter and the movement direction are recorded in this area for each run. In total 5 runs were conducted.

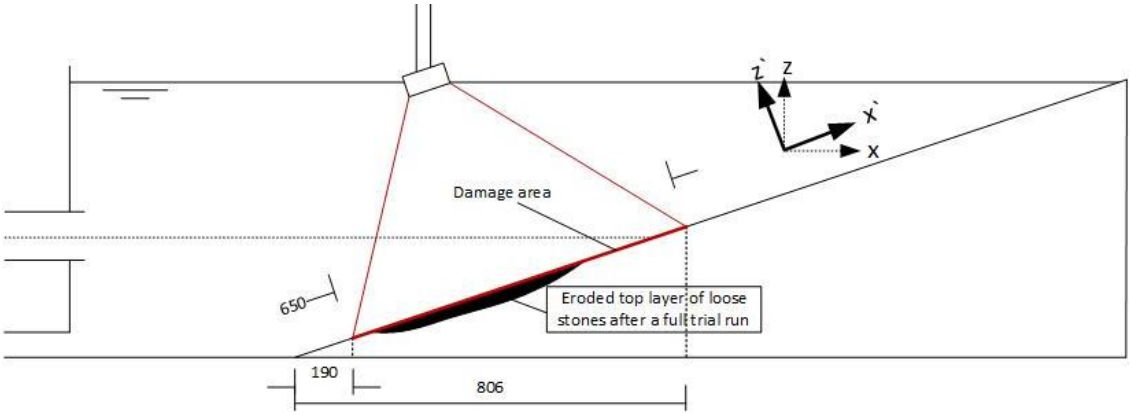

Figure 42 - Damage area where the moved stones are recorded and counted, dimensions in mm

For each step of every run the amount of moved stones are counted for 10 minutes. This gave results as shown in Figure 43. The influence of this counting duration on the results is analyzed in chapter 6. Stability analysis. In addition more analyzed results are presented in this chapter as well.

The plot in Figure 43 shows that there is a critical rotational speed of the bow thruster at which the stones start to move. For rotational speeds higher than this speed the amount of moved stones is increasing fast. Besides the variation between the runs seems to be small.

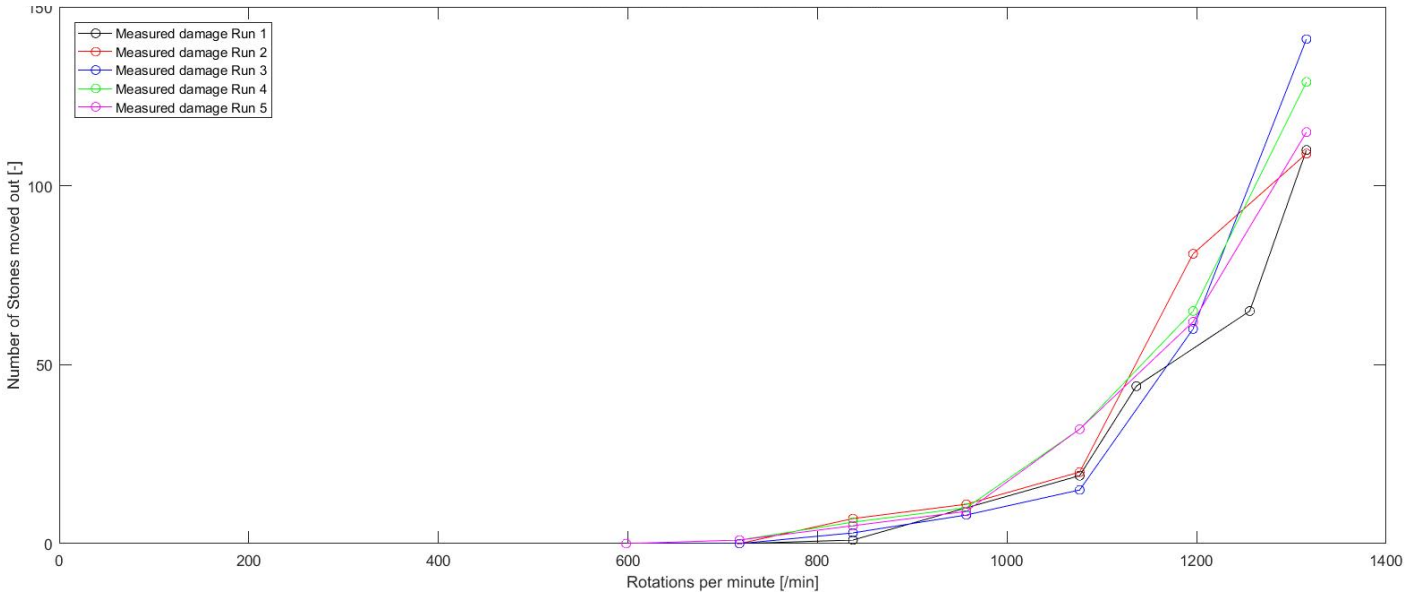

Figure 43 - Number of stone movements per rotational speed for each run and for a counting duration of 10 minutes.

5. Velocity Analysis

The test results of the velocity measurements for the type I and type II tests presented in the chapter before are analyzed in this chapter. A distinction is made between the type I tests which are the efflux velocities and the type II test which are the near bed velocities at the slope.

5.1 Type I tests - Efflux velocities

The main purpose of this analysis is to determine the efflux velocity U_0 which is an input parameter in the design methods for the hydraulic bed loads on the slope. Furthermore it is important to check if the outflow velocities and velocity fluctuations are comparable to the theory, to check if there are any inaccuracies in the scale model and to get an overview of what processes take place behind the outflow opening of the bow thruster. This can be useful when analyzing the near bed velocities and the slope stability of the stones in respectively the following paragraph and the following chapter.

5.1.1 Distribution of the velocities

When analyzing the outflow velocity distribution in the horizontal or the vertical plane comparisons are made with the German and the Dutch method. It is already mentioned that when designing a slope protection only one of the two methods should be used for both the velocity calculations as the stability calculations. This is due to the fact that the German method leads to higher near bed velocities and this is partly compensated with a smaller stability parameter. Whereas the Dutch method uses a higher stability parameter to partly compensate for lower calculated velocities and generally leads to smaller stones.

In Figure 44 the measured time-averaged outflow velocities in x-direction are shown together with the distributions according to the Dutch and German calculation method. In order to make a reliable comparison also the measured outflow velocities conducted by Van Doorn (2012) with a similar bow thruster are presented. Unlike the measurements of this research, the measurements by Van Doorn are performed in the horizontal plane. The rotational speed presented in the figure is assumed to be the correct rotational speed as it has been checked during the tests with a stroboscope. This means that the rotational speed as reported by Van Doorn is assumed to be incorrect and is corrected in this report.

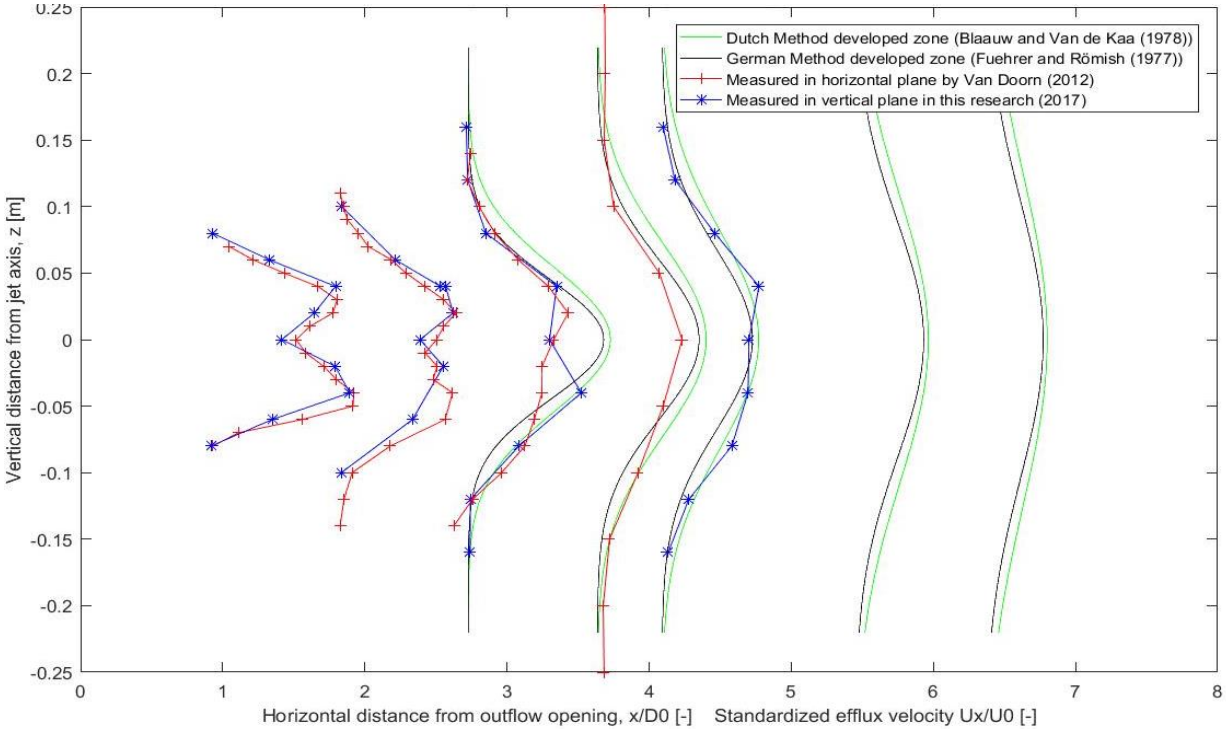

Figure 44 - Vertical velocity distribution at multiple distances from the outflow as has been measured.

Figure 44 shows that at x/D0=0.9 the measured velocity distribution is nearly similar to the distribution measured by Van Doorn in 2012. At larger distances to the outflow opening the measured profile shows larger differences, this might be caused by the difference in resolution of the measurements. As can be seen at x/D0=1.8 is that a velocity peak is missing because there is no measurement performed at the location of the peak. Therefore a higher resolution of measurement points might lead to a more comparable velocity profile. It is also observed that the measured velocities of both researches below the jet axis are higher than the measured velocities above the jet axis at x/D0>0.9 which indicates that the propeller jet is slightly directed towards the bottom. This can be explained by the fact that the jet axis is located closer to the bottom than to the water level.

The velocity distribution according to the Dutch and German method at $x/D_0=2.7$ shows some differences compared to the measured velocities. This probably is because the transition between the non-established zone and the established zone is located at $x/D_0=2.8$ according to the Dutch method and at $x/D_0=2.6$ according to the German method. Therefore also only the curve of the German method is shown. The measured velocities are smaller than the theory and it seems like it is still a non-established two peak velocity distribution however there are not enough measurements performed to make this conclusion.

5.1.2 Turbulence intensities

The turbulence induced by the propeller has a considerable influence on the stability of the slope protection which will be discussed in the chapter hereafter. Therefore it is important to have a look at the relative and absolute turbulence intensities that arise in the jet. In 1978 Blaauw and Van de Kaa measured maximum relative turbulence intensities of 0.25 to 0.30 within the axis of the bow thruster jet. In addition, Van Doorn (2012) measured absolute turbulence intensities up to 0.50 in the propeller jet.

As is shown in Figure 24 the relative turbulence intensities in the jet axis are in the order of 0.10 and therefore small compared to values according to other researches. Only at larger distances to the outflow point and at larger radial distances to the jet axis the relative turbulence intensity is in the order of 0.3 to 0.6. An explanation for this is the measuring frequency and measurement volume of the measurement equipment used. As is discussed in Appendix G - Comparison to test results by Van Doorn (2012) there are considerable differences between the measured absolute turbulence intensities between test scenario 1 of Van Doorn (2012) and test scenario T1 of this research and this can be explained with the different measurement equipment used. However, the data by Van Doorn is not reliable enough to conclude this as the variation between the values of sequential data points is too large. It is not clear what causes this scattered pattern of data points that can be observed in Figure 103. It should be investigated if the measurement duration is too short or the measurement equipment did not work properly.

5.1.3 Thrust coefficient

A thrust coefficient is a propeller characteristic and is an indication for the relation between the produced outflow velocities or thrust by the propeller and the propeller rotational speed. According to the manufacturer the thrust coefficient (K_T) of the bow thruster from the scale model should be 0.28 as stated by Van Doorn (2012). This is in the range that is provided by Römish (1993), he gives 0.25 – 0.50 for possible thrust coefficients for different propellers. Also Blokland (1997) indicated that a thrust coefficient for a proper designed propeller should be between 0.25 and 0.45.

In order to check if this provided coefficient matches the measured outflow velocities a few theories could be applied. Normally when designing a hydraulic structure that is subjected to a propeller jet only the axial momentum theory is applied and therefore only this theory will be used when determining the thrust coefficient.

First the representative outflow velocity U_0 is determined for three different rotational speeds with the axial momentum theory (Eq. 2-7). Using this equation it is assumed that the U_x velocities are uniformly distributed in tangential direction and the U_x velocities are integrated in radial direction. Then a curve is

plotted through the determined values of U_0. After that the equation by Blaauw and Van de Kaa (1978) (Eq. 2-4) is used to determine the thrust coefficient of the propeller. In Figure 45 the expected curve is plotted for a thrust coefficient of 0.28 according to the manufacturer Vetus. Furthermore, the determined efflux velocity U_0 from the outflow measurements by Van Doorn (2012) is added to this plot. In that research the same type of propeller is used and the outflow velocities are measured in the vertical and horizontal plane at 100 mm from the outflow opening. As already mentioned in section 2.2.1 Unconfined jet method for slopes the reported rotational speed in the report by Van Doorn (2012) is assumed to be incorrect. The presented determined efflux velocity by Van Doorn is for the correct rotational speed of 1091 rpm and shows an equal measured efflux velocity as determined during this research.

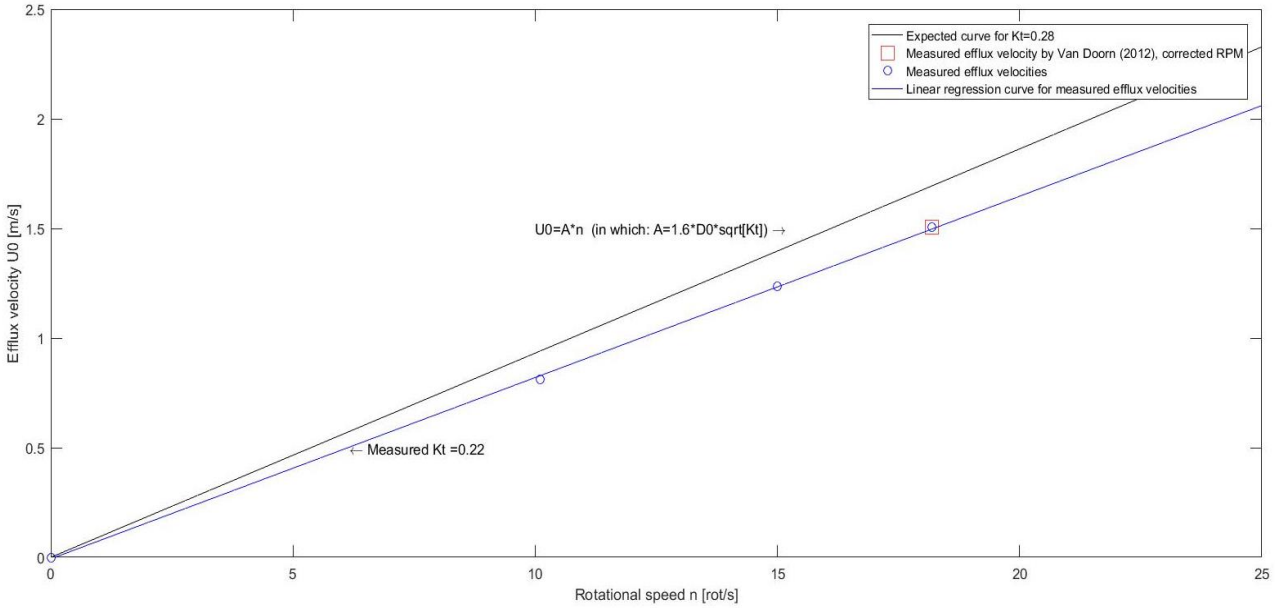

Figure 45 – Relation efflux velocity to rotational speed of the used bow thruster to determine the thrust coefficient

After the U_0 is determined for the four data points and a curve is fitted through these efflux velocities, a thrust coefficient of 0.22 is found. This is smaller than the thrust coefficient provided by the manufacturer. A possible explanation for this is that the thrust coefficient provided is based on different conditions. In this scale model probably a different nozzle is used than for the conditions where the provided thrust coefficient is based on.

The efflux velocity U_0 is also computed with measurements performed at multiple distances from the outflow opening (Figure 23) for a rotational speed of 1091 rpm and the results are shown in Figure 46. As can be seen the distance to the outflow opening is not of significant influence on the determination of U_0. This is conform the axial momentum theory which assumes that momentum is conserved. In Figure 46 small differences can be observed which are assumed to be the effect of a low resolution of the measurement locations, differences in the bin width used for the axial momentum calculation method and the inaccuracies in the measured time-averaged velocities.

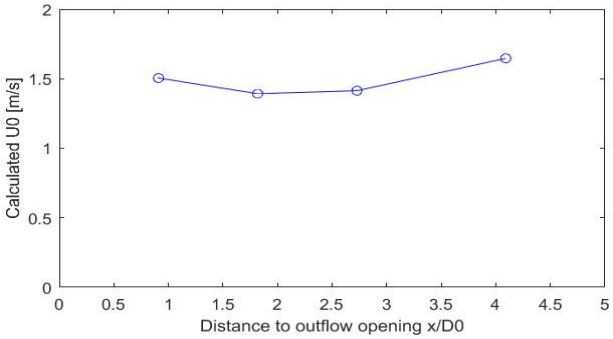

Figure 46 - Efflux velocity U0 calculated at multiple distances to outflow opening with axial momentum theory

A corrected thrust coefficient of 0.22 is used for the calculations in this research. The axial momentum theory is a reliable method to determine the efflux velocity as already stated in section 2.1.2 Efflux velocity. Next to that, it can also be concluded that the distance to the outflow opening of the measurements used for the calculation is not of significant influence on the value of the efflux velocity.

5.2 Type II tests - Slope velocities

In this paragraph first a vertical profile with measured velocities and relative turbulence intensities is discussed and also the presence of a circulation in the basin during the measurements is analyzed. Besides a comparison with the measurements by Van Doorn (2012) is made for test scenario T1. After that, the possible influence of the changing roughness, slope angle, axial distance and the changing pile configuration on the slope is analyzed. Specifically the effects on the height and location of the maximum velocity and the turbulence intensity are investigated. In addition comparison of the measurements with existing calculation methods are done for all test scenarios. For both the value and the location of the maximum slope velocity.

Furthermore the velocities directed sideways at the top of the slope are investigated. Sideward flow velocities determine the sideward extension of the flow field and therefore the width of a slope protection. It is analyzed until which extend the velocities are to be considered for a stable design and what the turbulence intensities are.

Finally, also the consequence of the difference between measured and slope velocities according to the unconfined jet method for the design of a slope protection is determined. This section includes a summary of the differences between measured and slope velocities according to equation (Eq. 2-10)(Table 19) and of the locations of maximum bed load of all test scenarios (Figure 58).

5.2.1 Velocity profile in vertical plane above slope

Next to the outflow measurements and the near bed velocity measurements also some measurements of the horizontal flow velocity in the vertical plane are conducted. The velocities and relative turbulence intensities measured together with the jet axis presented as a dashed line are shown in Figure 47. The measurement locations and therefore the positions of the EMS are shown in Figure 48. All measurement points are located at y = 0 mm and at an x-distance to the point of intersection of - 312 mm.

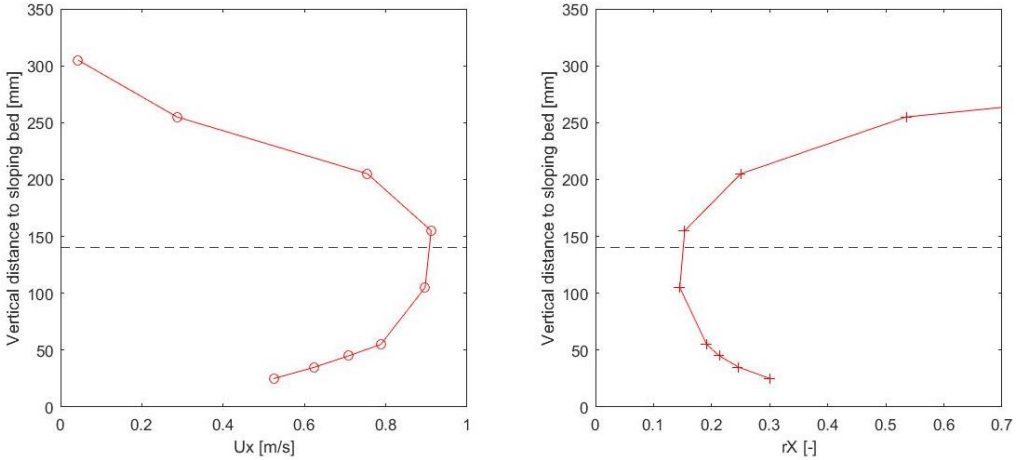

Figure 47 - Velocities and relative turbulence intensities measured in vertical plane above slope

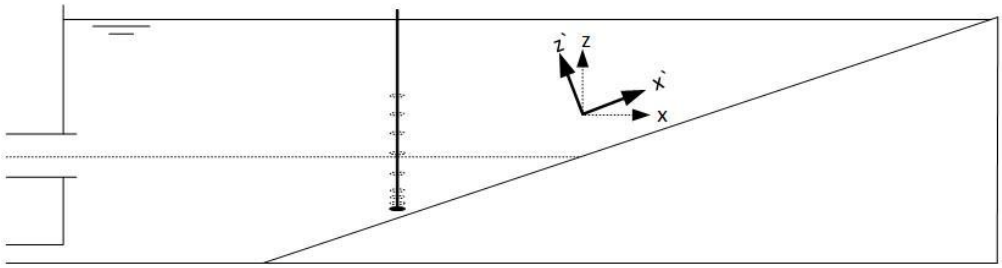

Figure 48 - Position EMS during the measurements in vertical plane above slope

Results show an increase of the time-averaged velocities and a decrease of the relative turbulence intensities nearby the jet axis. The increase is caused by the propeller jet and the fact that in the jet axis the time-averaged U_x velocities are largest. Due to this increase of the time-averaged velocities the relative turbulence intensities in x-direction decrease nearby the jet axis. At a height of 25 mm in z-direction above the bed (in the vertical plane) a relative turbulence intensity of 0.30 is observed. At larger heights until 50 mm above the bed in the vertical plane the absolute turbulence intensities decrease slightly, the time-averaged velocity increases and therefore the relative turbulence intensity decreases as well.

5.2.2 Circulation within the basin

During the scale model tests it was checked if there might be any influence of a basin circulation on the measured velocities. This was checked by continuing with the velocity measurements after the bow thruster stopped rotating. The bow thruster rotated for 30 minutes and 102 seconds before it was stopped. The measured velocity for three EMSs is presented in Figure 49 for the time before and after the rotation of the propeller stopped. EMS 4 is not included in the plot because it gave no signal during the measurement. All three EMSs that are presented are located above the slope around the point of intersection.

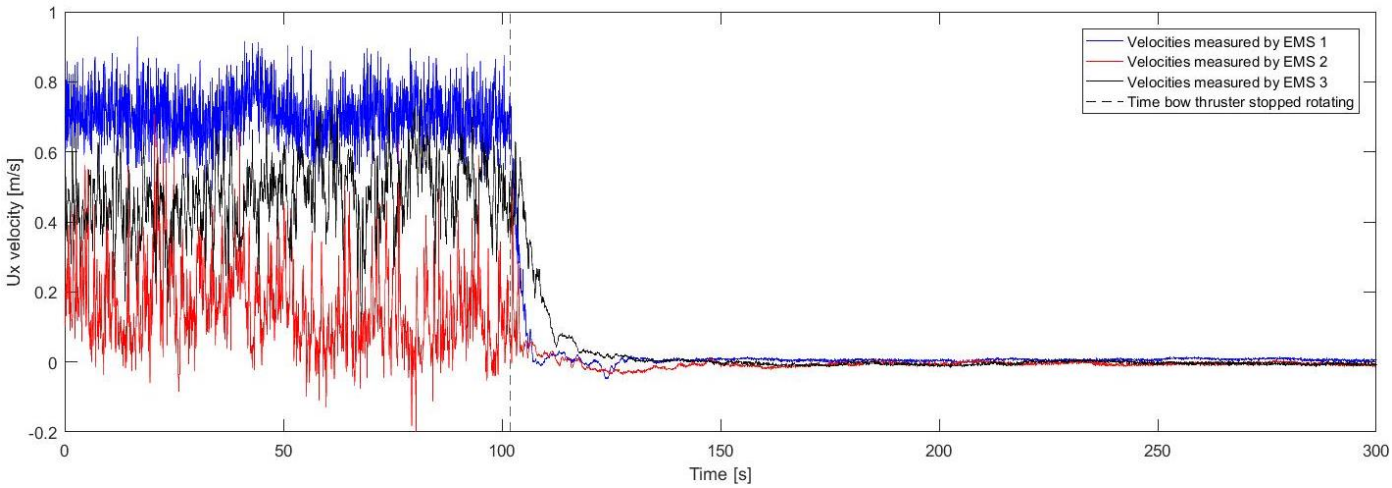

Figure 49 – Measured velocities in time after bow thruster stopped rotating

The plots show that the velocities above the slope are nearly zero within 50 seconds after the propeller stopped rotating. If a circulation occurred in the basin it would have a relatively large period due to the large basin dimensions and it would result in slope velocities after the bow thruster stopped rotating. Nevertheless this is not the case as is shown in Figure 49. Therefore it is assumed that no basin circulation is present during the measurements.

5.2.3 Results test scenario T1 compared to results by Van Doorn (2012)

The first test scenario T1 has a similar model set up as the first test scenario tested by Van Doorn in 2012. The reason for this is that the model set ups tested in this research are an extension to the model set ups tested by Van Doorn (2012). It is therefore important to make a comparison between the data obtained by both researches for the same model set up in order to check if similar test results are obtained. The results are presented and discussed in Appendix G - Comparison to test results by Van Doorn (2012).

It can be concluded that maximum time-averaged slope velocities have a value that is nearly equal for both researches however that the absolute turbulence intensities show differences. Measured absolute turbulence intensities for this research are in the order of 0.10 to 0.20 m/s where for the other research these are in the order of 0.20 to 0.40 m/s. This difference can be explained with the difference in measurement volume and measuring frequency of the measurement equipment used. The ADV used by Van Doorn makes use of a smaller measurement volume and larger measuring frequency than the EMSs used in this research. Therefore the smaller vortices are not measured by the EMS and this can lead to smaller absolute turbulence intensities. This also explains the small relative turbulence intensities presented in this research. Moreover, the data

points of both the velocities and the turbulence intensities show a large variation in sequential points. This makes the data less reliable and it should be investigated what the cause for this is. An explanation for this can be a too short measurement duration or the measurement equipment did not work properly.

5.2.4 Variation in roughness

The unconfined jet method to calculate the hydraulic bed load, (Eq. 2-10), does not include a parameter for the roughness. This however does not mean that there is no difference in slope velocities for varying roughness. It is expected that slopes with higher roughness induce more resistance on the flowing jet and contributes to the arise of more small turbulent vortices.

The plots of the time-averaged slope velocities in x'-direction presented in Figure 26 show higher measured velocities than the calculated velocities according to equation (Eq. 2-10). The presented curve of the unconfined jet method (Eq. 2-10) is deviating from the measurement results, especially higher on the slope. This is probably caused by the fact that the presented curve is derived from the equation (Eq. 2-3) for an unconfined propeller jet with a few corrections that might not take into account all the effects when the jet hits the slope. Also after the point of intersection only the upper half of the propeller jet is considered. The corrections applied include a derivation for the input parameter 'r' in (Eq. 2-3) to translate it to a location on the slope and a derivation for slope velocities after the point of intersection of the jet axis with the slope. These corrections and derivations are presented in Appendix H – .

Effect on maximum slope velocity

It is expected that the variation in roughness has some influence on the maximum measured slope velocity $U_{slope,max}$. As can be observed in Figure 26 is that the smooth slope gives a slightly higher maximum slope velocity than the rough slope. This is not remarkable because when the jet hits the slope and flows upwards along the slope it will be affected by the resistance caused by the roughness. This might cause a smaller maximum slope velocity compared to the smooth situation where there is less resistance.

		Factor difference w.r.t. $U_{slope,max,theo}$	**Factor difference w.r.t. $U_{slope,max}$ for smooth slope**
$U_{slope,max,theo}$	0.74 m/s	1.00	-
$U_{slope,max}$ for smooth slope	0.92 m/s	1.24	1.00
$U_{slope,max}$ for rough slope	0.90 m/s	1.22	0.98

Table 10 - Measured and maximum velocity according to equation (Eq. 2-10) for variation in roughness

There is a factor difference of 0.98 between the maximum time-averaged slope velocity of the rough slope compared to the maximum time-averaged slope velocity of the smooth slope. This difference is relatively small and therefore it is assumed that the roughness only has a small influence on the decrease of the maximum time-averaged slope velocity.

In Table 10 the values according to the unconfined jet method (Eq. 2-10) and the measured values for the smooth and rough bed are presented. It shows that the measured maximum time-averaged slope velocity for the smooth bed is a factor 1.24 higher. It is already mentioned that the roughness has a relatively small influence on the value of the maximum slope velocity and therefore this difference can not be ascribed to the difference in roughness. Furthermore the table also shows that the maximum time-averaged measured slope velocity for a rough bed is a factor 1.22 higher than $U_{slope,max,theo}$ which is the value according to equation (Eq. 2-10).

Effect on location of maximum slope velocity

The measured location of the maximum velocity $X_{u,max}$ is expected to be around the point of intersection of the jet axis with the slope. However the variation in roughness influences the exact location of the maximum velocity. Figure 26 shows this difference in the location of the maximum velocity. Nevertheless both

locations for the smooth and rough situation are located relatively close to each other at the upper side of the point of intersection and therefore the difference is small.

	X-distance w.r.t. point of intersection	Y-location
$X_{u,max,theo}$ in [m]	- 0.100	0.000
$X_{u,max}$ smooth slope in [m]	0.055	0.000
$X_{u,max}$ rough slope in [m]	0.095	0.000
$X_{u,max}$ / $X_{u,max,theo}$ smooth slope [-]	- 0.55	-
$X_{u,max}$ / $X_{u,max,theo}$ rough slope [-]	- 0.95	-

Table 11 - Measured and location of maximum velocity according to equation (Eq. 2-10) for variation in roughness

The exact locations are mentioned in Table 11. The values given are the locations in x-direction of the maximum velocities with respect to the point of intersection of the jet axis with the slope. A negative value means that the location is lower on the slope than the point of intersection and a positive value means that the location is higher on the slope than the point of intersection.

It is remarkable that both locations of the maximum velocity are located at the upper side of the point of intersection because the location according to the unconfined jet method $X_{u,max,theo}$ predicts that it is located at the lower side of this point. This is remarkable because it is expected that the maximum velocity occurs lower on the slope than the point of intersection because that part of the slope is closer to the outflow point and therefore higher velocities in the jet are expected. An explanation for this is not found yet.

Effect on turbulence intensity

The relative turbulence intensities are shown in Figure 27. The plots of both test scenarios show that the relative turbulence intensities are higher closer to the toe and closer to the top of the slope than in the middle of the slope. The reason for the larger relative turbulence intensities can also be that the time-averaged flow velocity is very small. Therefore another plot is presented in Figure 50 of the absolute turbulence intensities in order to observe where the largest velocity fluctuations occur.

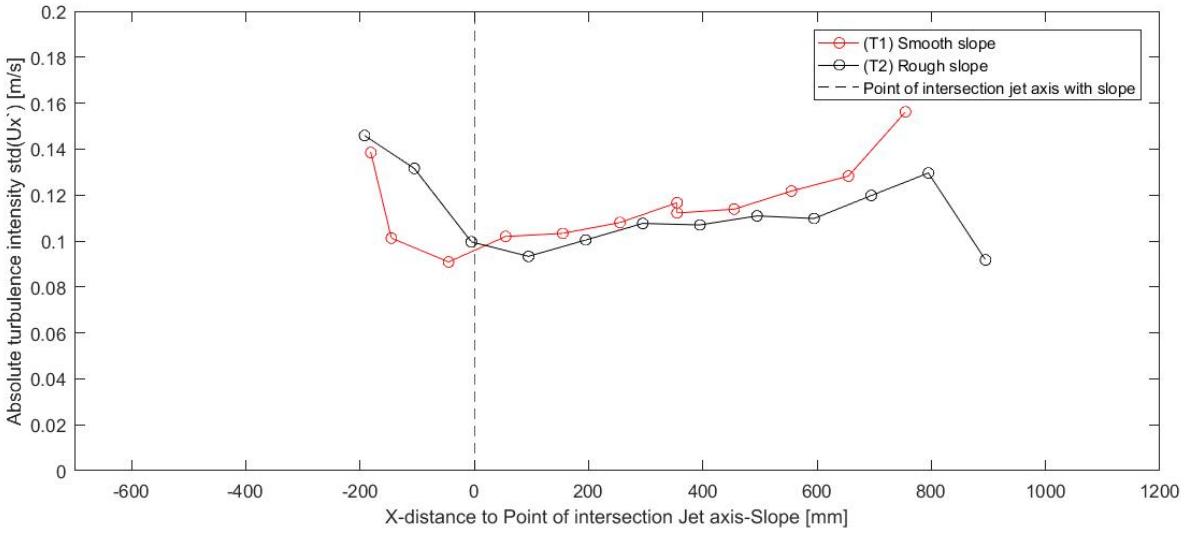

Figure 50 - Absolute turbulence intensities for variable roughness

It shows that the absolute turbulence intensity increases from the point of intersection towards the toe for both scenarios. However the rough slope shows larger intensities closer to the point of intersection and the smooth slope shows large absolute turbulence intensities closer to the top of the slope. The larger turbulence intensities at the top of the slope for the smooth bed is probably because the turbulent vortices can develop more and therefore become larger.

5.2.5 Variation in slope angle

As can be concluded from (Eq. 2-10) is that the slope angle is an important parameter in order to determine the maximum slope velocity and the location of that velocity. The test results of a slope of 1 in 2.5 and a slope of 1 in 3 are shown in Figure 28. As can be observed is that the shape of both plots is similar and the differences are small.

Effect on maximum slope velocity

According to the theory and to the measurements the variation in slope angle gives different maximum slope velocities. This is presented in Figure 28. The differences between the measurements and the theory is determined as well as the factor differences due to the influence of the different slope angle.

		Factor difference w.r.t. $U_{slope,max,theo}$	**Factor difference $U_{slope,max,theo}$ (w.r.t. $U_{slope,max,theo}$ 1 : 2.5 slope)**	**Factor difference $U_{slope,max}$ (w.r.t. $U_{slope,max}$ 1 : 2.5 slope)**
$U_{slope,max,theo}$ 1 : 2.5 slope	0.74 m/s	1.00	1.00	-
$U_{slope,max}$ 1 : 2.5 slope	0.90 m/s	1.22	-	1.00
$U_{slope,max,theo}$ 1 : 3.0 slope	0.76 m/s	1.00	1.03	-
$U_{slope,max}$ 1 : 3.0 slope	1.02 m/s	1.34	-	1.13

Table 12 - Measured and maximum velocity according to equation (Eq. 2-10) for variation in slope angle

As given in Table 12 a slope of 1 in 3.0 gives a factor 1.13 higher maximum slope velocities compared to a slope of 1 in 2.5. This is larger than the difference between the values according to equation (Eq. 2-10) for both slopes. In line with the theory the maximum velocity of the 1 in 3.0 slope should be a factor 1.03 higher. That this maximum velocity is larger can be explained by the fact that for an 1 in 3.0 slope the lower part of the propeller jet hits the slope closer to the outflow opening. Besides when considering the measurements of test scenario T3, larger slope velocities might occur lower on the slope. Nevertheless this is unlikely because the location of the measured maximum velocity is already lower on the slope than expected.

The measured values again are larger than the values according to equation (Eq. 2-10). The measured velocity for the 1 in 3.0 slope is a factor 1.34 higher and the measured velocity for the 1 in 2.5 slope is a factor 1.22 higher.

Effect on location of maximum slope velocity

The influence of the variation in slope angle on the location of the maximum time-averaged velocity is investigated. The locations according to the theory and to the measurements are determined and presented in Table 13.

	X-distance to point of intersection	**Y-location**
$X_{u,max,theo}$ for 1 : 2.5 slope in [m]	- 0.100	0.000
$X_{u,max,theo}$ for 1 : 3.0 slope in [m]	- 0.130	0.000
$X_{u,max}$ for 1 : 2.5 slope in [m]	0.095	0.000
$X_{u,max}$ for 1 : 3.0 slope in [m]	- 0.261	0.000
$X_{u,max}$ / $X_{u,max,theo}$ for 1 : 2.5 slope in [-]	- 0.95	-
$X_{u,max}$ / $X_{u,max,theo}$ for 1 : 3.0 slope in [-]	2.01	-

Table 13 - Measured and location according to equation (Eq. 2-10) of maximum velocity for variation in slope angle

The location of the maximum velocity shifts towards the toe of the slope for gentler slopes according to the unconfined jet method (Eq. 2-10). This is also what happens when looking at the results presented in Table 13. However this shift towards the toe is larger according to the measured values instead of the values according to equation (Eq. 2-10).

Also another difference is that the location of the measured maximum velocity of the 1 in 2.5 slope is higher on the slope (after the point of intersection) than according to equation (Eq. 2-10) which states that it should be located lower on the slope than the point of intersection. This is remarkable because it is expected that the maximum velocity occurs lower on the slope than the point of intersection because that part of the slope is closer to the outflow point and therefore higher velocities in the jet are expected. An explanation for this is not found yet.

Effect on turbulence intensity

The relative turbulence intensities of test scenario T2 and T3 are shown in Figure 29. This plot shows similar relative turbulence intensities for both slopes except for the locations lower on the slope than the point of intersection. There the 1 in 2.5 slope shows larger relative turbulence intensities. A plot of the absolute turbulence intensities is included in Figure 51 in order to see if the larger time-averaged slope velocities are the cause of this or that it is caused due to the larger absolute turbulence intensities.

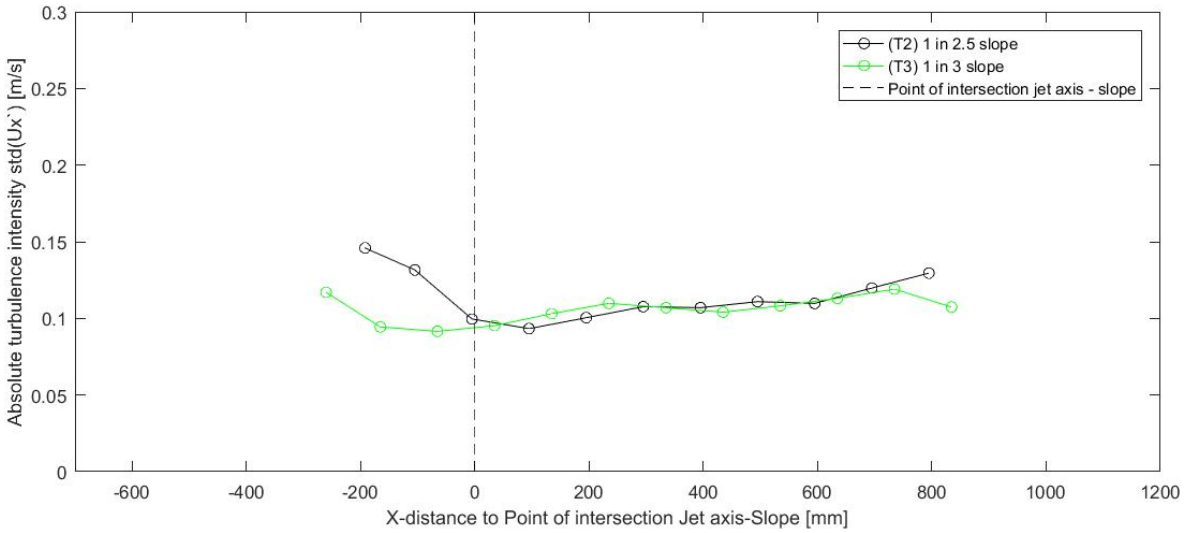

Figure 51 - Absolute turbulence intensities of test scenario T2 and T3

This plot shows that the larger relative turbulence intensities for T2 beneath the point of intersection compared to T3 are caused by a combination of larger time-averaged velocities in T3 and larger absolute turbulence intensities in T2.

5.2.6 Variation in axial distance

The results for the variable axial distance are plotted in Figure 30 and present the slope velocities for axial distances of $x/D_0 = 6.2$, $x/D_0 = 9.5$ and $x/D_0 = 11.5$. The slope used for these variations is an 1 to 3 slope. All measured velocities show relatively large deviations with the velocity curve according to the unconfined jet method (Eq. 2-10). The differences between the measured and calculated velocities after the point of intersection and higher on the slope can be explained by the fact that the equation for the unconfined jet method for slopes equations ((Eq. H-4) and ((Eq. H-5) takes only the upper half of the jet into account on the slope after the point of intersection of the jet axis with the slope. This leads to smaller slope velocities.

Effect on maximum slope velocity

According to the unconfined jet method for slopes (Eq. 2-10) it is expected that for larger axial distances the maximum slope velocities are smaller than for smaller axial distances. The maximum measured and maximum calculated slope velocities together with the factor differences are presented in Table 14.

The reduction of the maximum slope velocity due to a larger axial distance is larger according to equation (Eq. 2-10) than according to the measurements. The measurements show a reduction of the velocity with a

factor difference of 0.66 for an increase of axial distance from x/D_0=6.2 to x/D_0=11.5. However equation (Eq. 2-10) shows a reduction of the velocity with a factor difference of 0.54 for a similar increase of axial distance.

The measured velocity for an axial distance of x/D_0=6.2 is a factor 1.34 higher than the calculated value for that distance. Whereas the measured values for the two larger axial distances deviate even more from the calculated values. For an axial distance of x/D_0=9.5 the measured velocity is a factor 1.54 higher compared to the determined velocity with equation (Eq. 2-10) and for an axial distance of x/D_0=11.5 the measured velocity is even a factor 1.63 higher.

		Factor difference w.r.t. $U_{slope,max,theo}$	Factor difference w.r.t. $U_{slope,max,theo}$ for x/D_0=6.2	Factor difference w.r.t. $U_{slope,max}$ for x/D_0=6.2
$U_{slope,max,theo}$ for x/D_0=6.2	0.76 m/s	1.00	1.00	-
$U_{slope,max}$ for x/D_0=6.2	1.02 m/s	1.34	-	1.00
$U_{slope,max,theo}$ for x/D_0=9.5	0.50 m/s	1.00	0.66	-
$U_{slope,max}$ for x/D_0=9.5	0.77 m/s	1.54	-	0.75
$U_{slope,max,theo}$ for x/D_0=11.5	0.41 m/s	1.00	0.54	-
$U_{slope,max}$ for x/D_0=11.5	0.67 m/s	1.63	-	0.66

Table 14 - Measured and maximum velocity according to equation (Eq. 2-10) for variation in axial distance

The values of the factor 'f' resulting from Table 14 are rather large (larger than 1.5) for larger axial distances of $x/D_0 \geq 9.5$. The increase of 'f' with increasing axial distance is remarkable. At the location $X_{u,max,theo}$ where the maximum flow velocity according to the unconfined jet method occurs, the ratio $U_{axis,theo}$ / $U_{slope,max,theo}$ has a constant value independent of the axial distance between outflow point and slope. This constant value is 1.10 for an 1 : 3 slope. Although $U_{axis,theo}$ / $U_{slope,max,theo}$ has a constant value, the value of 'f' is not constant with increasing lateral distance. The measured values of 'f' are significantly larger than $U_{axis,theo}$ / $U_{slope,max,theo}$, which means that the actual U_{axis} must be significant larger than $U_{axis,theo}$ due to jet confinement by the slope. A certain increase of U_{axis} due to the jet confinement corresponds to what is expected.

Effect on location of maximum slope velocity

It is expected that the axial distance of the propeller to the slope has an influence on the location of the maximum velocity because the locations for maximum velocities according to equation (Eq. 2-10) show a shift towards the toe of the slope for larger axial distances. This is also shown in Figure 30. The locations of the maximum measured and calculated velocities are given in Table 15.

	X-distance to point of intersection	Y-location
$X_{u,max,theo}$ for x/D_0=6.2 in [m]	-0.130	0.000
$X_{u,max,theo}$ for x/D_0=9.5 in [m]	-0.200	0.000
$X_{u,max,theo}$ for x/D_0=11.5 in [m]	-0.242	0.000
$X_{u,max}$ for x/D_0=6.2 in [m]	-0.261	0.000
$X_{u,max}$ for x/D_0=9.5 in [m]	-0.166	0.000
$X_{u,max}$ for x/D_0=11.5 in [m]	-0.166	0.000
$X_{u,max}$ / $X_{u,max,theo}$ for x/D_0=6.2 [-]	2.01	-
$X_{u,max}$ / $X_{u,max,theo}$ for x/D_0=9.5 [-]	0.83	-
$X_{u,max}$ / $X_{u,max,theo}$ for x/D_0=11.5 [-]	0.69	-

Table 15 - Measured and location of maximum velocity according to equation (Eq. 2-10) for variation in axial distance

For the two largest axial distances the location of the maximum velocity seems to be located on the same horizontal distance to the point of intersection. However the real position of the maximum velocity might

slightly deviate from the measured location because the resolution of the measurement points is relatively large (100 mm) and that is why the exact location could also be located several millimetres lower or higher on the slope. Furthermore for all axial distances the location of the maximum slope velocity is located before the point of intersection.

The location of the maximum velocity on the slope has no large shift towards the toe of the slope for larger axial distances according to the measurements that are presented in Figure 30. The measurements show no shift however there might be a small shift as discussed before. Nevertheless this indicates that there is no significant branching off of the propeller jet towards the slope for the tested axial distances.

It is remarkable that the location of maximum velocity of the smallest axial distance is located lower on the slope than the locations of maximum velocity of the two larger axial distances. It is therefore questionable if the measured maximum velocity for x/D_0=6.2 is reliable as already discussed before.

Effect on turbulence intensity

The relative turbulence intensities plotted in Figure 31 and the absolute turbulence intensities plotted in Figure 52 show a similar shape of the curve for all axial distances. The only difference is that the relative turbulence intensities are smaller for smaller axial distances caused by the larger slope velocities. As also is observed in the measurement results of the other test scenarios is that the absolute and relative turbulence intensities increase towards to the toe of the slope. This will have influence on the stability of the slope protection as these are most responsible for instabilities of the stones on the slope. The largest turbulence intensities in combination with the time-average velocity cause the largest peak velocities and these will affect the stability. The test results of test scenario T5 become important for the stability analysis performed in the next chapter.

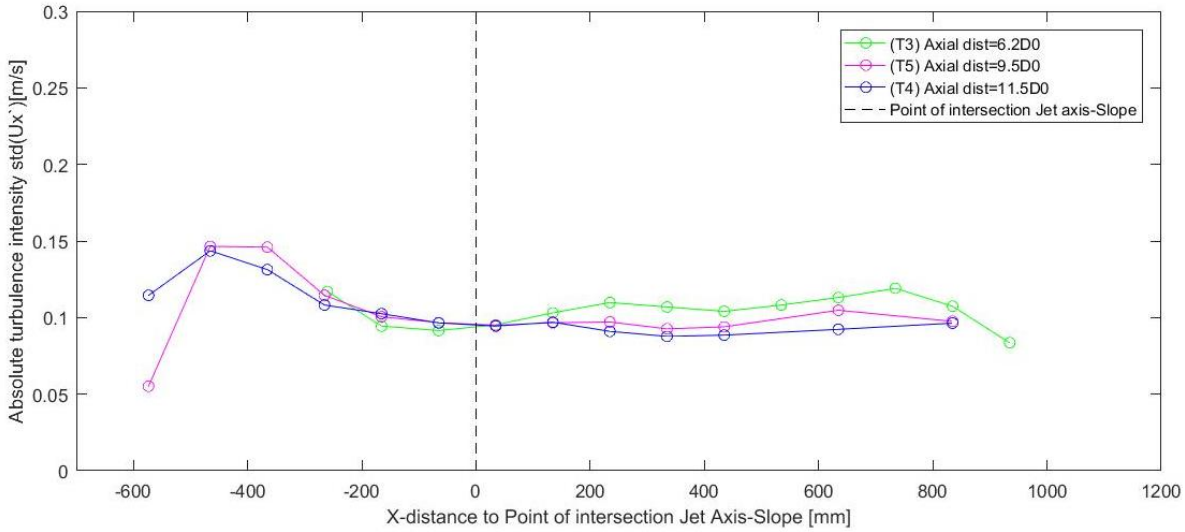

Figure 52 - Absolute turbulence intensities T3, T4 and T5

5.2.7 Variation in pile configuration

The equation of the Dutch design method for hydraulic bed loads (Eq. 2-10) does not include influence of any piles on the slope. Nevertheless when considering jetties or quay walls on piles, and therefore situations where piles are located on the slope, it can be assumed that the obstructions influence the flow pattern and the hydraulic bed loads on the slope.

The test scenarios where the jet axis is located eccentric w.r.t. to the piles show the largest velocities and therefore these are plotted in a figure together with the situation without piles in Figure 32. In this figure the slope velocities at the jet axis are presented for the configuration without piles, a configuration with piles of a jetty system and a configuration with piles of an open quay system. Both scenarios that are presented are with an eccentricity of the jet axis with respect to the axis of the pile. It shows only small differences.

Locations on the slope at x-locations of the first row of piles show that the slope velocities are larger, probably due to the contraction caused by the piles. At this location no differences are observed between the larger diameter piles and smaller diameter piles. Furthermore, around the point of intersection of the jet axis with the slope the slope velocities increase even more and become larger for the configurations with piles than for the configuration without piles. It is assumed that this is caused due to the combination of flow contraction caused by the piles and the fact that the highest slope velocities occur around the point of intersection.

The effect of the piles on the maximum velocity, location of the maximum velocity and the turbulence intensity are discussed hereafter. Also the velocities around the piles are investigated in more detail because for some test scenarios the highest velocities occur next to the pile and not in the jet axis.

As already discussed in section 2.1.5 Flow field around vertical piles, the vertical piles situated on the slope create a flow contraction between the piles. This flow contraction leads to higher flow velocities in between the piles and roughly this can be estimated as twice the approach velocity (Eq. 2-9) according to Breusers, et al. (1997). When the flow approaches a pile it will deflect and create vortices. This will result in higher near bed velocities around the pile. This equation is not valid for the pile configurations tested in this research as the maximum observed slope velocities are much smaller than 2 times the approach velocity. This is shown in the paragraphs hereafter.

Another empirical relation (Eq. 5-1) states that the velocity in between two piles is dependent on the centre-to-centre distance between the piles, the pile diameter and some empirical coefficient. During the scale model tests this pile diameter and centre to centre distance is varied and the influence of this variation on the velocity U_1 can be analyzed and compared to this empirical relation.

$$\frac{U_1}{U_2} = \left(\frac{G + \alpha_p * D_{pile}}{G}\right) \qquad \textit{(Eq. 5-1)}$$

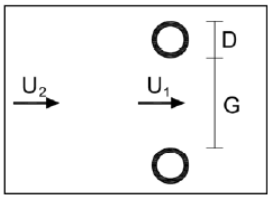

Figure 53 - Definition of the parameters of the velocity equation with piles

Centre to centre distance

The centre-to-centre distance between the piles in the two pile systems is different. The jetty system has a centre-to-centre distance of $5.71D_{pile,jetty}$ and the open quay wall system has a centre-to-centre distance of $6.25D_{pile,openquay}$. However the pile diameter of the jetty system is 2 times the pile diameter of the open quay wall system.

It can be observed from Figure 54 that there is a gradient in the measured velocities for the jetty situation between the pile in the middle and the pile on the right. Shown in two top plots of the figure. This velocity gradient is not observed in the results of the of the open quay wall situation. This is probably caused by the fact that the axis of the propeller jet is located nearly in the middle between the centre pile and the right pile for the open quay wall system. Therefore the contraction of the flow due to the piles increases velocities on both sides of the jet axis. For the jetty system the jet axis is closer to the centre pile than to the right pile and therefore probably the contraction around the centre pile increases the velocity more than the contraction around the right pile.

The theory for the effects of the centre to centre distance between the piles (Eq. 5-1) states that a smaller centre-to-centre distance will increase the near bed velocities around the piles. This can not be observed from the test results.

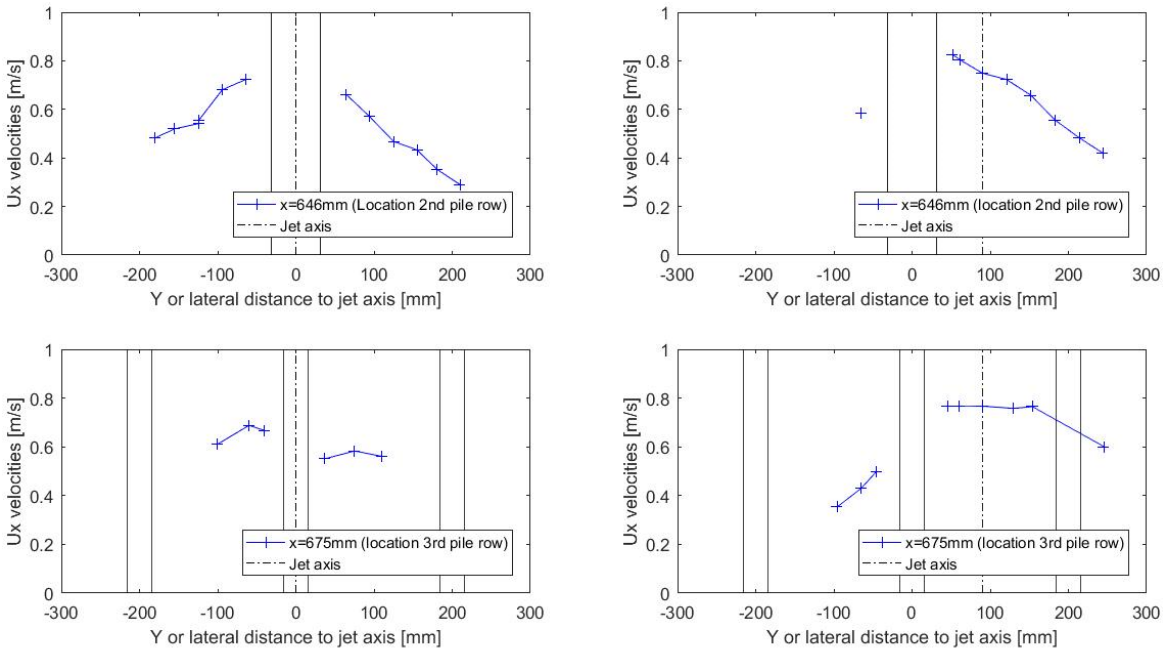

Figure 54 - Slope velocities in x-direction next to piles for the four test scenarios

Pile diameter

For the test scenarios with the jetty system a pile diameter of $0.57D_0$ is applied where for the scenarios with the open quay wall system a pile diameter of $0.29D_0$ is applied. This difference in pile diameter influences the flow pattern and therefore also the hydraulic bed loads on the slope.

The plots in Figure 54 show that the velocity close next to the pile is larger for the larger pile diameter than for the smaller pile diameter. The near bed velocity closest to the pile at the right side is 7% larger for the larger pile diameter.

From Figure 55 it can also be observed that the bigger pile diameter influences the flow direction just next to a pile and in between the piles. The two top plots show that for a larger pile diameter the y-component of the velocities is larger than for the smaller pile diameter.

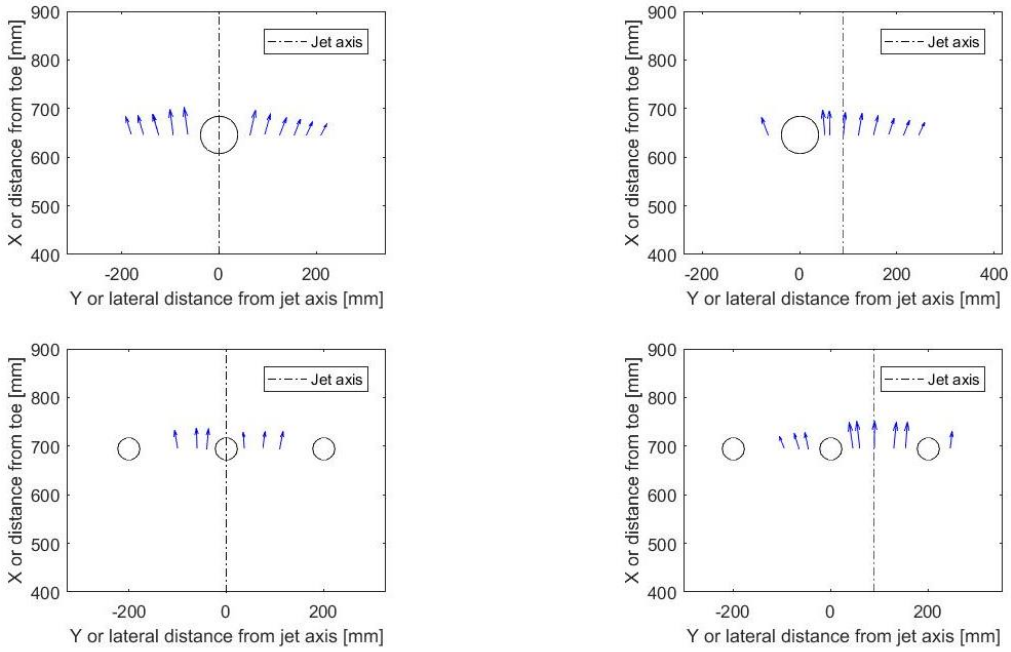

Figure 55 – Direction of slope velocities next to piles for T7 (top left), T8 (top right), T9 (bottom right) and T10 (bottom left)

Jet axis location with respect to pile location

The location of the jet axis is shifted in positive y-direction for both pile configurations as presented in Figure 15. This shift has influence on the flow pattern on the slope and therefore on the maximum slope velocity as well. In Figure 54 the slope velocities in x'-direction are presented for measuring points located next to the row of piles that is closest to the point of intersection. This location is chosen because the maximum slope velocity occurs nearby the point of intersection.

As can be observed from the plots slope velocities are larger when the jet axis is positioned eccentrically with respect to the pile. Especially the velocities measured closest to the piles are larger for an eccentric propeller jet. That the slope velocities are smaller for the scenarios without eccentricity is due to that generally the largest velocities occur in the axis of the propeller jet and when these large velocities 'collide' against a pile these velocities are reduced and redirected. If these largest axial velocities are not obstructed and the propeller jet is contracted instead of diverted it will lead to an increase of slope velocities. So the slope velocities for the eccentric situation are larger due to contraction and less obstruction. The slope velocities for the situation without eccentricity are reduced due to the separation of the jet caused by the centre piles.

Effect on maximum slope velocity

The maximum measured slope velocity for three configurations are compared. The three configurations contain the configuration without piles, the configuration of the jetty system and the configuration of the open quay wall system. Together with the theoretical velocity calculated with (Eq. 2-10) the maximum measured slope velocities are given in Table 16. The factor differences of the maximum measured velocities with respect to the calculated theoretical maximum velocity and the factor differences of the maximum measured velocity for the scenarios with piles with respect to the scenario without piles are presented as well.

		Factor difference w.r.t. theoretical value	Factor difference w.r.t. measured value without piles	Factor difference w.r.t. open quay y=0mm (T7)	Factor difference w.r.t. open quay y=90mm (T8)	Factor difference w.r.t. y=0mm for jetty (T7)	Factor difference w.r.t. y=0mm for open quay (T10)
$U_{slope,max,theo}$ no piles, y=0mm	0.50 m/s	1.00	-	-	-	-	-
$U_{slope,max}$ no piles,y=0mm (T5)	0.77 m/s	1.54	1.00	-	-	-	-
$U_{slope,max}$ jetty,y=0mm (T7)	0.72 m/s	1.44	0.94	1.00	-	1.00	-
$U_{slope,max}$ jetty,y=90mm (T8)	0.83 m/s	1.66	1.08	-	1.00	1.15	-
$U_{slope,max}$ open quay,y=90mm (T9)	0.80 m/s	1.60	1.04	-	0.96	-	1.14
$U_{slope,max}$ open quay,y=0mm (T10)	0.70 m/s	1.40	0.91	0.97	-	-	1.00

Table 16 - Measured and maximum velocity according to equation (Eq. 2-10) for variation in pile configuration. Velocities are at the location of the jet axis.

It is determined that all measured velocities are larger than the calculated velocities according to the theory. This factor difference with the theory varies between 1.40 for the open quay wall situation where the jet axis is in line with the centre pile and 1.66 for the jetty situation with an eccentric propeller jet.

The differences of the maximum measured slope velocity between the situation without piles and the situation with piles are smaller than the differences with the theoretical value. The maximum measured slope velocity for the situation with piles and without eccentricity is smaller with a factor difference of 0.91 to 0.94 than for the situation without piles. For the situations with piles and with eccentricity this velocity is a factor difference 1.04 to 1.08 larger than for the situation without piles. These differences can be explained with the explanation given in the section about the influence of the jet axis location with respect to the pile location.

From Table 16 can be concluded that the larger pile diameter leads to a larger maximum slope velocity. The slope velocity for the open quay system is a factor difference 0.97 smaller than for the jetty system for the situation without eccentricity. For the situation with eccentricity the maximum slope velocity is a factor difference 0.96 smaller for the open quay system as well. It can be assumed that this is due to the larger pile diameter of the jetty system because normally an increase of the centre-to-centre distance does not lead to an increase in the slope velocity.

Furthermore the eccentricity leads to larger slope velocities as well. For both the jetty situation and the open quay situation the velocity is respectively a factor difference of 1.15 and 1.14 larger compared to the situations without eccentricity. A possible explanation for this is already discussed in the section about the influence of the jet axis location with respect to the pile location.

Effect on location of maximum slope velocity

For the three different pile configurations the location of the maximum slope velocity is compared. Together with the location according to the theoretical calculation method these are presented in Table 17.

The results show that for all configurations the location of maximum velocity is located closer to the point of intersection than the location according to the theory. All points of maximum velocity are still located lower on the slope than the point of intersection of the jet axis with the slope.

	Location	X-distance w.r.t. point of intersection	Y-location
$X_{u,max,theo}$ in [m]	Jet axis	- 0.200	0.000
$X_{u,max}$ without piles in [m]	Jet axis	- 0.166	0.000
$X_{u,max}$ jetty, y=0mm in [m]	Next to pile	- 0.086	- 0.064
$X_{u,max}$ jetty, y=90mm in [m]	Next to pile	- 0.086	0.052
$X_{u,max}$ open quay, y=90mm in [m]	Jet axis	- 0.007	0.000
$X_{u,max}$ open quay, y=0mm in [m]	Next to pile	-0.037	- 0.060

Table 17 - Measured and location of maximum velocity according to equation (Eq. 2-10) for variation in pile configuration. Velocities are at the location of the jet axis.

It seems that the eccentricity of the propeller jet with respect to the centre pile has influence on the location of the maximum velocity. The eccentricity in the jetty system causes the maximum velocity to occur next to the centre pile that is closest to the point of intersection. The eccentricity in the open quay wall system causes the maximum velocity to occur higher on the slope and therefore closer to the point of intersection but still lower than the point of intersection.

Furthermore, for the open quay wall system the maximum slope velocity occurs higher on the slope and therefore closer to the point of intersection than the maximum slope velocity measured at the jetty system. It can be assumed that this is caused by the higher pile density higher on the slope and the smaller centre-to-centre distance. Which factor of these two factors has the most influence on this shift in location of maximum velocity can not be determined from the results.

Effect on turbulence intensity

In the chapter before the relative turbulence intensities in the jet axis are presented in Figure 33 for the test scenarios T5, T8 and T9. The curves have a similar shape as the curves of the relative turbulence intensities of the other test scenarios. At locations close to the toe of the slope and in the line of the jet axis the relative turbulence intensities are smaller for the scenarios with piles and an eccentricity than for the scenario without piles.

In Appendix F - Test results the all measured turbulence intensities are shown for test scenario T7, T8, T9 and T10. From these figures it can be concluded that again the highest absolute turbulence intensities occur at the lower part of the slope and around the y-location of the jet axis as also is the case for the other test scenarios.

5.2.8 Sideward flow velocities

In order to have an indication until which location considerable near bed velocities occur the measured sideward velocities and relative turbulence intensities are analyzed. The test results of all measured sideward velocities are presented in Figure 34, Figure 36, Figure 38, and Figure 40 for respectively the variation in roughness, the variation in slope angle, the variation in axial distance and the variation in pile configuration. Also the relative turbulence intensities are plotted for these variations in Figure 35, Figure 37, Figure 39 and Figure 41. The sideward velocities and sideward relative turbulence intensities of the row of measurement locations located highest on the slope and for all scenarios are also presented in Figure 56 because the highest velocities occur at locations highest on the slope.

Extent of flow field

In order to know to what extent the flow field is of any influence on the slope protection the decrease in sideward flow velocity has to be known. Therefore this factor of decrease is determined for each test scenario where these flow velocities are measured and are presented in Table 18. The minimum and maximum time-averaged velocities in y-direction are presented as well. Only the results of the measurement locations of the row that is highest on the slope are analyzed because these gave the largest flow velocities

and are therefore the normative slope velocities. The maximum sideward slope velocity is measured at y/D_0 = + 5.9. Except for test scenario T1, where the maximum is located at y/D_0 = +10.9. The minimum sideward slope velocity is measured at y/D_0 = + 19.9.

	T1	T2	T3	T4	T5	T7	T10
Min sideward velocity [m/s]	0.47	0.30	0.31	0.32	0.30	0.24	0.24
Max sideward velocity [m/s]	0.52	0.42	0.41	0.36	0.37	0.35	0.27
Factor decrease in sideward velocity [-]	1.11	1.40	1.32	1.13	1.23	1.46	1.13

Table 18 - Maximum decrease in sideward velocities at top row measurement points for each test scenario

The sideward velocity decreases on average with a factor 1.25. If it is assumed that the decrease in y-velocities at the top of the slope is linear then this velocity decreases on average with a factor 1.02 per y/D_0 sideward. This assumption of linear decrease is a conservative approach because the sideward slope velocities decrease faster for larger sideward distances as also can be observed in the left plot of Figure 56.

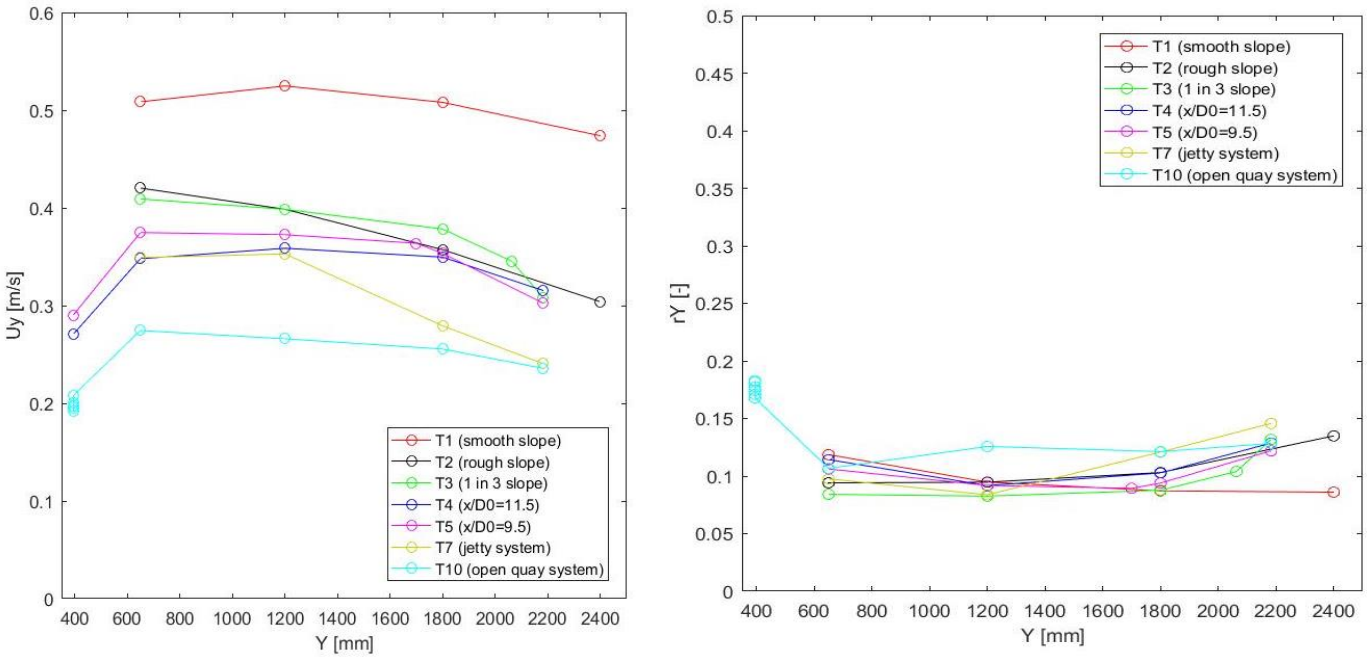

Figure 56 – Sideward flow velocities top row (left) and sideward relative turbulence intensities (right) for each test scenario

As can be observed from the left plot is that the roughness has a considerable influence on the time-averaged sideward flow velocities at the top of the slope. The time-averaged sideward flow velocities are larger for T1 than for T2.

The relative turbulence intensities in y-direction as shown in the right plot of Figure 56 are very small for all test scenarios. That there is a small difference in relative turbulence intensity between for example test scenario T1 with the smooth slope and test scenario T10 with a rough slope with several piles indicates that the absolute turbulence intensities in y-direction are somewhat higher for test scenario T1 compared to test scenario T10.

Influence of variations on sideward flow

The variations in model set ups applied during the scale model tests have influence on the sideway flow velocities. The influences on these velocities due to variations in roughness, slope angle, axial distance and pile configuration are discussed in this sub-paragraph. To determine the influence of the variation the

maximum sideward velocity of each test scenario is considered. The influence of the roughness is presented as the decrease in maximum y-velocity at the top of the slope with respect to the smooth situation. The influence of the slope angle is with respect to the 1 in 2.5 slope. The influence of the axial distance is with respect to the smallest axial distance of x/D_0 of 6.2. The influence of the jetty system and the open quay wall system is with respect to test scenario T5 without piles. The decrease in sideward velocities for each variation is presented in Figure 57.

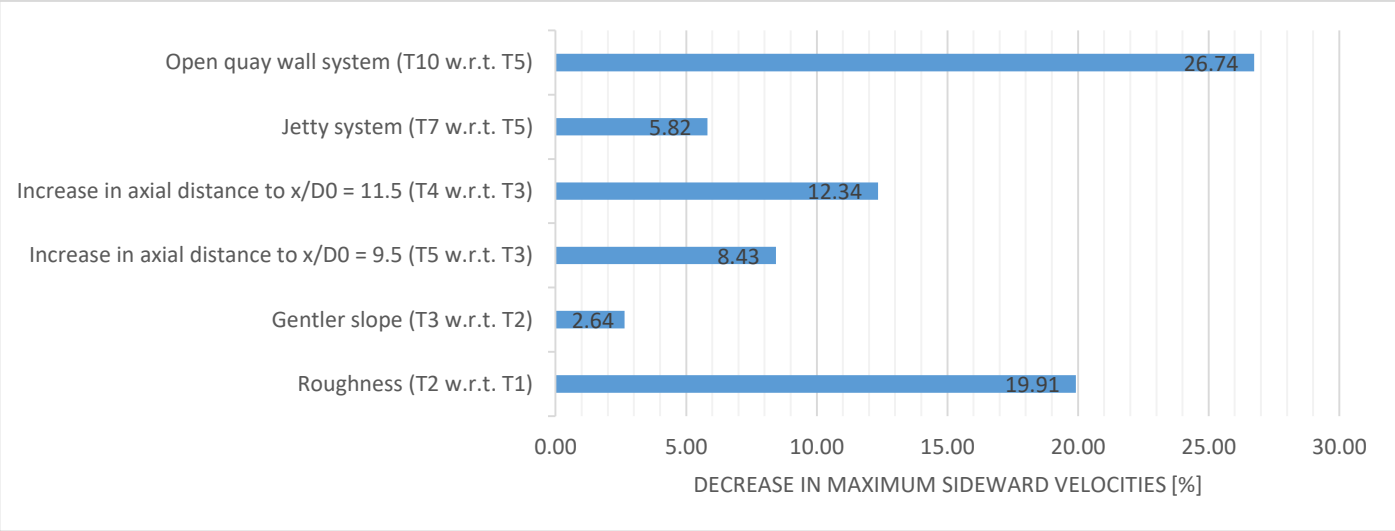

Figure 57 - Decrease in sideward velocities for multiple variations

In Figure 57 it is shown that the open quay wall system leads to a large decrease in maximum sideward flow velocity of roughly 27 %. Which is not remarkable because of the large amount of piles that obstruct the propeller jet flow on the slope. Also the roughness of the slope causes the maximum sideward flow velocities to decrease with roughly 20%. After all the change in slope from an 1 in 2.5 to an 1 in 3 slope shows no significant decrease.

5.2.9 Influence on the design of a slope protection

For each test scenario a correction factor is found which is the difference between the measured and maximum slope velocity according to (Eq. 2-10) as discussed in the sections before. The calculation with this equation uses no correction factor ‘f’ for the scenarios discussed in this research, in other words ‘f’ is equal to 1, because a correction factor ‘f’ was not yet available for these scenarios and are therefore determined in this research. The differences determined in the sections before are translated to correction factors ‘f’ that are suggested to use from now on for the scenarios presented. These correction factors are presented in Table 19 and are actually an extension of the proposed correction factors presented in Table 1 for different scenarios with steeper slopes.

	Slope	Bed	Axial distance in x/D_0	Piles	Correction factor 'f' or factor difference measured time-averaged max velocity w.r.t. max velocity by (Eq. 2-10) [-]
T1	1 : 2.5	Smooth	6.2	No	1.26
T2	1 : 2.5	Rough	6.2	No	1.22
T3[1]	1 : 3.0	Rough	6.2	No	1.34
T4	1 : 3.0	Rough	11.5	No	1.64
T5	1 : 3.0	Rough	9.5	No	1.55
T7	1 : 3.0	Rough	9.5	Jetty	1.46
T8	1 : 3.0	Rough	9.5	Jetty	1.67
T9	1 : 3.0	Rough	9.5	Open quay	1.62
T10	1 : 3.0	Rough	9.5	Open quay	1.50

Table 19 - Correction factors 'f' suggested for each tested scenario

When using these correction factors to correct the slope velocities calculated with equation (Eq. 2-10) will have an influence on the design of a slope protection. To investigate this influence two stability relations are used to determine the median stone diameter of a slope protection design. First the original Izbash type stability relation is discussed and secondly the modified Izbash type stability relation.
The locations of the measured maximum time-averaged slope velocities $U_{max,meas}$ and of the measured peak velocities U_{peak} are presented in the left panel of Figure 58. The locations of the measured maximum time-averaged slope velocities $U_{max,meas}$ and the locations of the maximum slope velocity according to equation (Eq. 2-10) $U_{max,theo}$ are presented in the right panel of Figure 58. This figure is a summary of the sections before and also gives the locations of the maximum time-averaged slope velocities and of the measured peak velocities which are used for the determining of the median stone diameters in the sub-sections hereafter. From the plots it can also be observed that the locations of the measured peak velocities are equal to the locations of the measured maximum time-averaged slope velocities.

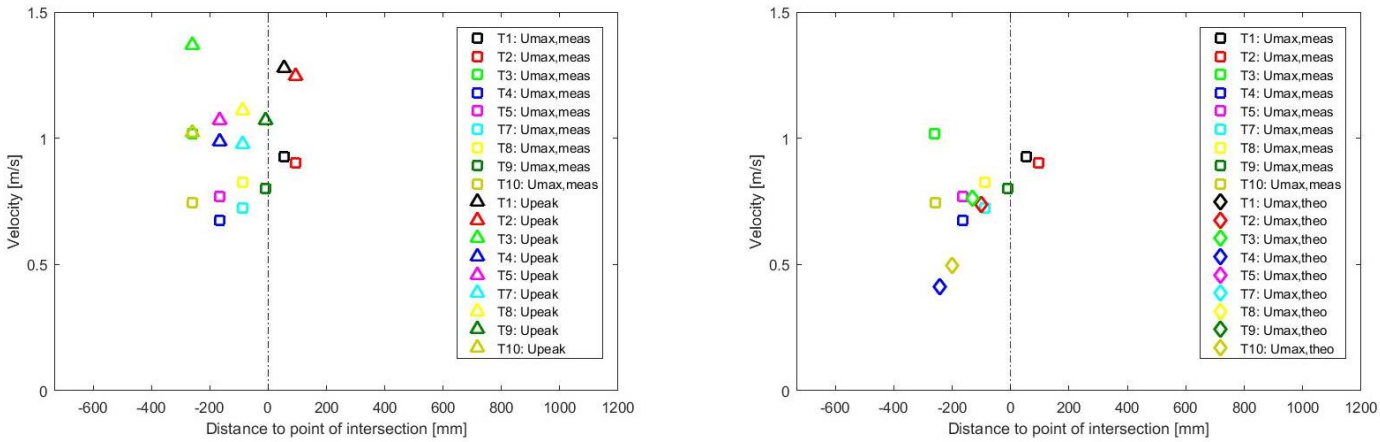

Figure 58 – Locations of peak slope velocities and measured maximum time-averaged slope velocities compared (left) and the locations of the maximum slope velocities according to (Eq. 2-10) and measured maximum time-averaged slope velocities compared (right).

[1] For T3 the value of the correction factor 'f' becomes 1.25 if the most left (and disputable) measuring point is left out of consideration (see section 4.2.1, Figure 28).

Original Izbash type stability relation (Eq. 2-11)
According to the original Izbash type stability relation (Eq. 2-11) the stone diameter will increase with the increase in velocity squared. In this subsection first the d_{50} is determined for each scenario according to equation (Eq. 2-11) with the maximum slope velocity calculated with equation (Eq. 2-10) and the results are presented in the first column of Table 20. For the calculation of the maximum slope velocity again the correction factor 'f' is set equal to 1 because before this research the factor 'f' was not yet available. For the slope coefficient it is assumed that the angle of internal friction is 40 degrees[2] and the slope velocity is directed upward the slope. Also the relative density is 1.65 and a stability parameter $\beta_{Iz,cr}$ of 2.5 is applied which means that little movement is allowed. Secondly the d_{50} is determined according to equation (Eq. 2-11) with the measured maximum time-averaged slope velocity. Again similar input parameters as for the calculation just before are used for this calculation and results are shown in the second column of Table 20. Finally the factor difference is determined and presented in the third column.

	d_{50} with maximum slope velocity according to equation (Eq. 2-10) with f = 1 [m]	d_{50} with measured max time-averaged slope velocity in [m]	Factor difference d_{50} of the second column w.r.t. d_{50} of first column [-]
T1	0.031	0.049	1.58
T2	0.031	0.046	1.50
T3	0.034	0.060	1.78
T4	0.010	0.026	2.70
T5	0.014	0.035	1.42
T7	0.014	0.030	2.13
T8	0.014	0.040	2.78
T9	0.014	0.038	2.62
T10	0.014	0.032	2.26

Table 20 - Calculated d_{50} with max slope velocity according to equation (Eq. 2-10) and with measured max time-averaged slope velocity and the factor difference

The third column gives the differences between the median stone diameters for both maximum slope velocities. In fact this is the difference presented in Table 19 squared. It shows the largest differences for test scenarios T4, T7 and T8. As mentioned earlier is that the maximum slope velocity according to the unconfined jet method for slopes (Eq. 2-10) is underestimated largely for test scenario T4 with a large axial distance of x/D_0=11.5. Next to that the piles on the slope in combination with an eccentricity for test scenarios T7 and T8 lead to larger maximum slope velocities than according to the theory and this is already explained in the section about piles.

To sum things up, the results from the third column show that the median stone diameters should be 1.5 to 2.8 times larger according to the measurements. However it is questionable if this is really necessary. It was stated before that when using the Dutch calculation method (which is actually the unconfined jet method for slopes in this report) for the hydraulic bed load also the stability parameters recommended by Blokland (1997) and presented in Table 2 should be used. This is probably because the unconfined jet method for hydraulic bed load underestimates the load as already shown in this analysis and when the Dutch stability design calculation is performed this underestimation is compensated with a larger stability parameter. Therefore when the measured maximum time-averaged slope velocities are used in the second column this leads to much larger median stone diameters which are probably larger than really needed.

[2] For stones with a d_{50} larger than 10 cm the internal friction angle can be estimated as 42° and stones with a smaller d_{50} and that are less angular the internal friction angle can be estimated as 40° (Blokland, personal communication). According to CUR (1999) the internal friction angle is between 25° and 55°. According to RWS (1990) the internal friction angle of coarse stones is approximately 40°.

Modified Izbash type stability relation (Eq. 2-17)
After that also the d_{50} is determined with the modified Izbash type stability relation (Eq. 2-17) where the turbulence is not included in the stability parameter $\beta_{Iz,cr}$ but in the relative turbulence intensity that is an input parameter within the equation. The measured maximum time-averaged slope velocity in combination with the measured relative turbulence intensity are used for the determination. It is important to use the peak velocities on the slope because these cause the instabilities on the stones. Therefore the maximum of the combination of the time-averaged slope velocity and three times the absolute turbulence intensity (Eq. 6-7) is used for the calculation. It is important to use the slope velocity and the relative turbulence intensity at the same location. This location and therefore the locations of the measured peak velocities are presented in Figure 58 for each scenario. Now that the measured maximum time-averaged slope velocity and the measured relative turbulence intensity are known at the location of the highest measured peak velocity for each test scenario, the median stone diameter d_{50} is determined. Results together with the relative turbulence intensity, the measured maximum time-averaged slope velocity and the $\beta_{Iz,mod,cr}$ calculated with equation (Eq. 2-20) are presented in the second column of Table 21. The first column includes the d_{50} that is calculated in the subsection before with the original Izbash type stability relation (Eq. 2-11) and for the maximum slope velocity calculated with equation (Eq. 2-10) and again the correction factor 'f' is set equal to 1 because before this research the factor 'f' was not yet available.

	d_{50} according to (Eq. 2-11) with maximum slope velocity according to equation (Eq. 2-10) with f = 1 [m]	**d_{50} with measured maximum time-averaged slope velocity and measured relative turbulence intensity [m]**				**Factor difference d_{50} of first column w.r.t. d_{50} of second column [-]**
		$r_{x'}$ [-]	U_{slope} [m/s]	$\beta_{Iz,cr}$ [-]	d_{50} [m]	
T1	0.031	0.160	0.864	0.900	0.015	0.49
T2	0.031	0.181	0.808	0.974	0.014	0.47
T3	0.034	0.115	1.017	0.742	0.018	0.53
T4	0.010	0.152	0.674	0.870	0.009	0.94
T5	0.014	0.131	0.770	0.794	0.011	0.77
T7	0.014	0.117	0.723	0.747	0.009	0.64
T8	0.014	0.114	0.826	0.740	0.012	0.82
T9	0.014	0.112	0.802	0.732	0.011	0.77
T10	0.014	0.125	0.745	0.774	0.010	0.70

Table 21 - Calculated d_{50} with velocities according to equation (Eq. 2-10), measured velocities and measured velocities including turbulence intensities

The third column shows that the stone diameters for the method with the combination of measured maximum time-averaged slope velocity and measured relative turbulence intensity are smaller than the stone diameters according to the original Izbash type stability relation with maximum slope velocities according to equation (Eq. 2-10). The main reason for this is that the relative turbulence intensities at the location of the peak velocities are in the order of 0.10 to 0.20 and therefore small compared to relative turbulence intensities measured during researches in the past. During researches performed before relative turbulence intensities of 0.25 to 0.80 were found. For example Van Doorn (2012) measured relative turbulence intensities of 0.30 to 0.50 and Blaauw and Van de Kaa (1978) found values up to 0.60 for near bed situations. The associated stability parameters $\beta_{Iz,cr}$ are also smaller than the recommended value for little movement ($\beta_{Iz,cr}$ = 2.5). This is due to the small relative turbulence intensities as well because in order to have a value of $\beta_{Iz,cr}$ of 2.5 the relative turbulence intensity should be 0.49 as also can be derived with equation (Eq. 2-18).

The results in Table 21 show smaller median stone diameters due to the very small relative turbulence intensities. In order to make an adequate comparison the median stone diameters are determined again with a

recommended relative turbulence intensity of 0.30 by Schiereck (2012). The results are presented in Table 22.

	d_{50} with maximum slope velocity according to equation (Eq. 2-10) with f = 1 [m]	**d_{50} with measured time-averaged velocity and recommended turbulent fluctuations [m]**				**Factor difference d_{50} of first column w.r.t. d_{50} of second column [-]**
		$r_{x'}$ [-]	U_{slope} [m/s]	$\beta_{lz,cr}$ [-]	d_{50} [m]	
T1	0.031	0.300	0.864	1.480	0.025	0.81
T2	0.031	0.300	0.808	1.480	0.022	0.71
T3	0.034	0.300	1.017	1.480	0.034	1.02
T4	0.010	0.300	0.674	1.480	0.015	1.54
T5	0.014	0.300	0.770	1.480	0.020	1.38
T7	0.014	0.300	0.723	1.480	0.017	1.22
T8	0.014	0.300	0.826	1.480	0.023	1.59
T9	0.014	0.300	0.802	1.480	0.021	1.50
T10	0.014	0.300	0.745	1.480	0.018	1.29

Table 22 - Calculated d_{50} with velocities according to equation (Eq. 2-10), measured velocities and measured velocities including adjusted turbulence intensities assumed to be 0.30

From the table it can be observed that this leads to larger values for d_{50} for nearly all test scenarios however the differences are smaller than the results of Table 20. Compared to the differences shown in the third column of Table 21 it shows that the median stone diameters are increased for larger relative turbulence intensities.

It can be concluded from this table with the currently used design method that includes the relative turbulence intensity, that the corrections for the maximum velocities lead for nearly all scenarios to larger values for the median stone diameter.

6. Stability Analysis

The results of the stability tests of the type III tests are shown in chapter 4. Test results. These results are analyzed by determining the initiation of motion and the locations of the first stone movements and of the maximum damage.

6.1 Type III tests - Initiation of motion

By definition the moment of initiation of motion is unclear. When a slope protection is considered it is not allowable that a lot of stones are moving away by the current. This means that the stability criterion should be defined in such a way that only a few or no stones at all are relocated or removed from the slope. This criterion therefore depends on the amount of maintenance that is acceptable during the life time of the structure.

6.1.1 Amount of movements in time

During the analysis of the recordings of the stability tests it was observed that the amount of stones that move varies in time. Therefore the cumulative amount of movements in time for one run is determined. This is important in order to define the counting duration of the amount of movements and to see what the influence of this duration would be on the total amount of movements per step. The cumulative amount of movements per step in time for the first run is presented in Figure 59 and Figure 60 for respectively all steps and for the first steps. A step is the increase in rotational speed and a step lasts 10 minutes in scale model time.

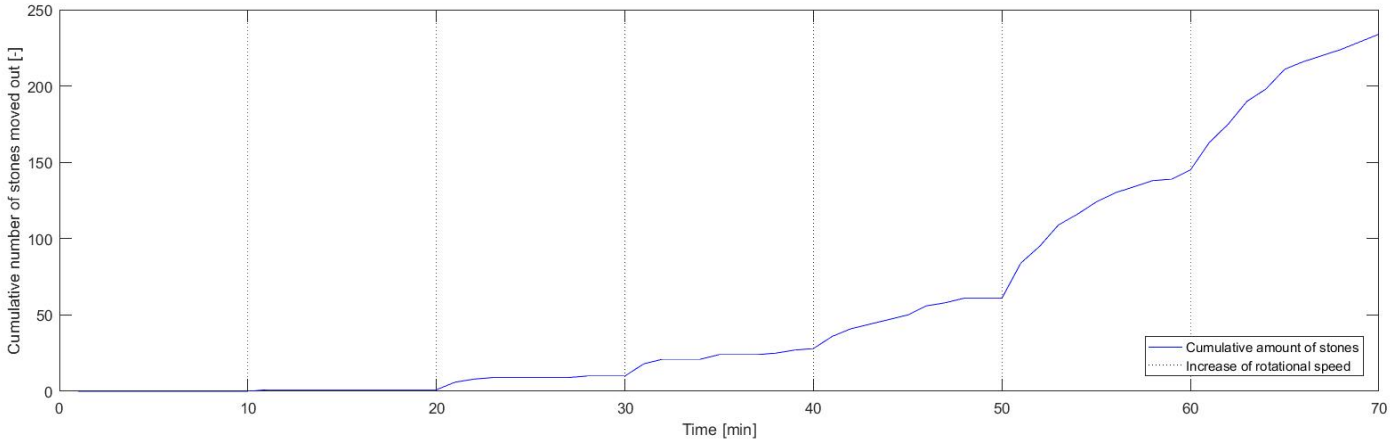

Figure 59 - Cumulative amount of movements in time per step for the first run (all steps)

It is shown that between a time of 10 minutes and 40 minutes, or for step 2 until step 4, approximately 70 to 100 % of all the movements take place in the first two minutes. Where for step 5 until step 7 and therefore the larger rotational speeds the movements are wider spread in time. A better overview of the first four steps is given in Figure 60.

The goal of the first part of the analysis is to determine the critical slope velocity at the moment of initiation of motion. Therefore only the first four steps are considered because for the steps thereafter the amount of movements becomes too large to assign it as initiation of motion (>25 movements).

Only the first four steps are important for the determination of the critical slope velocity and therefore the counting duration (if larger than 2 minutes) will not be of considerable influence on the calculations performed hereafter.

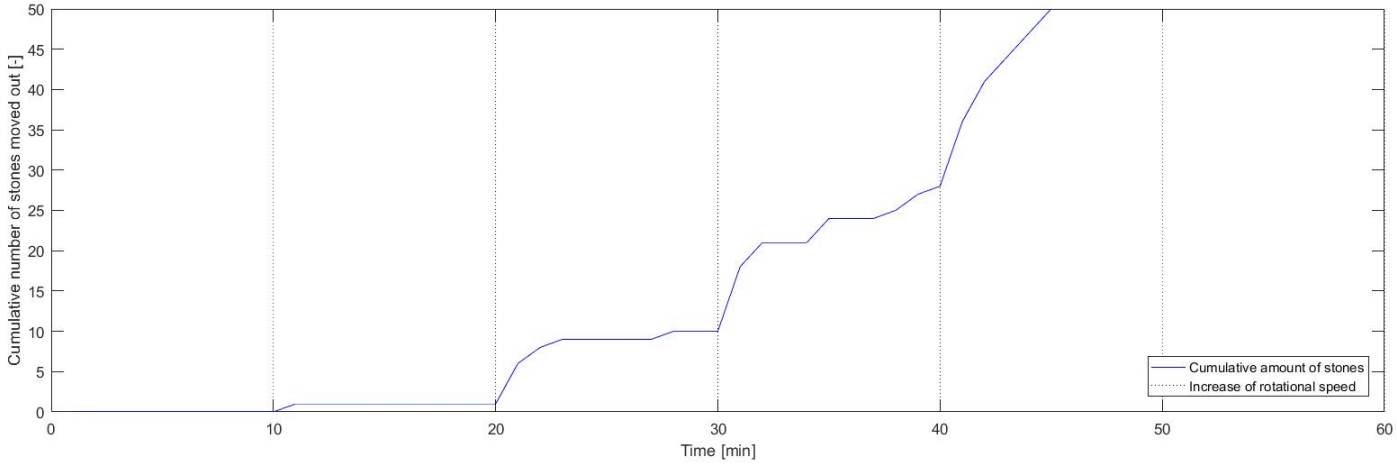

Figure 60 - Cumulative amount of movements in time per step for the first run (only the first steps)

6.1.2 Critical slope velocity

In order to determine the critical slope velocity first the critical rotational speed of the ducted propeller has to be determined. This is achieved by calculating the average movements of all runs per rotational speed and after that it is determined what the critical amount of rotations per minute is for different considerations of initiation of motion.

The amount of stones that is moved away per rotational speed of all the runs is presented in Figure 43. Because the stones are counted for 10 minutes the amount of movements for the higher steps are very large. First the average number of movements per measured rotation speed is determined. Next to that also a lower and upper bound of the 95% confidence interval is determined with a student t-distribution (Eq. 6-1) in order to present with a certainty of 95 % between which values the average amount of stone movements will be for an infinite number of runs. This is shown in Figure 61, the left plot is of all steps and the right plot is zoomed in on the first four steps for a better overview.

$$x_{min,max} = x_{avg} \pm t_{\frac{\alpha}{2},n-1} * \frac{\sigma}{\sqrt{n}} \qquad \textit{(Eq. 6-1)}$$

$$\alpha = 0.05; For\ 95\%\ confidence\ interval$$

$$n = 5; Number\ of\ freedoms$$

$$\sigma = \sqrt{\frac{\sum(x_i - x_{gem})^2}{n-1}}; Standard\ deviation$$

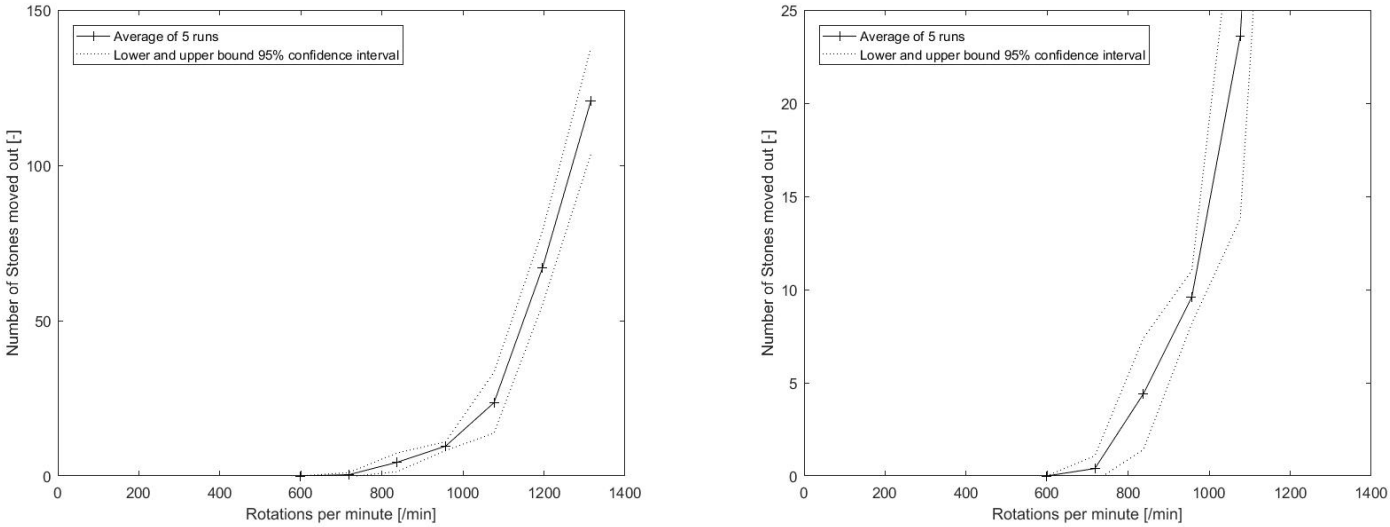

Figure 61 - Average and lower and upper bound of 95% confidence interval of the amount of movements per step of all runs

Now the critical rotational speed can be determined. The criterion for initiation of motion is dependent on the situation and on the amount of maintenance that is desirable. For a very conservative approach the criterion of initiation of motion can be set on only 1 stone movement. However for a situation where no frequent propeller jets at the same location against the slope are expected the initiation of motion can be set on for example 10 stone movements. When the criterion for initiation of motion is set at more stones the stability parameter will be lower and this leads to a smaller stone diameter. For both criteria of initiation of motion the critical rotational speed is defined. This is performed with two methods as shown in Figure 62. The results are presented in Table 23.

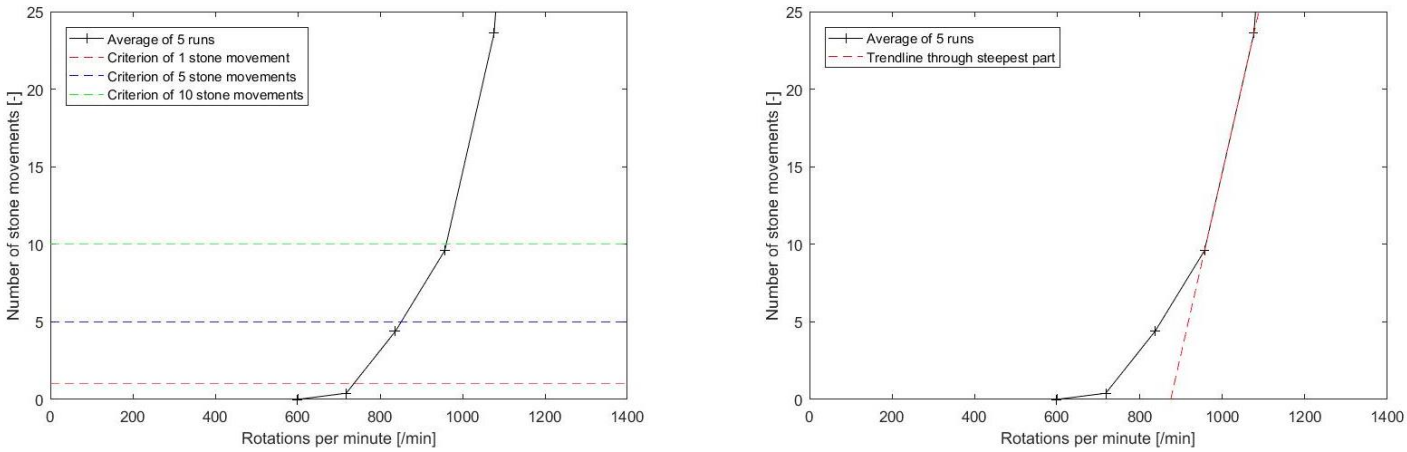

Figure 62 - Determination of critical rotational speed

The first method is by defining a criterion for the initiation of motion. For this case it is set at 1, 5 and 10 stone movements. Three criteria are chosen because the influence of the difference between the criteria is analyzed as well. Then the rotations per minute is determined from the curve of the average of all runs at these three criteria.

Another method to determine the critical velocity is with a trend line through the data points of the steepest part of the curve (referred to in Van Veldhoven, 2002). Then the crossing of this trend line with the horizontal axis represents the critical velocity for that specific case. The idea of this method is to find the velocity after which the damage increases very fast and that is why the trend line through the steepest part is considered. For this method only the first four steps are taken into account because the bed during the steps hereafter had already a cumulative amount of damage and this probably influences the amount of stone movements in these steps.

	1 movement	5 movements	10 movements	Trend line
RPM_{crit} [min^{-1}]	736	851	960	875
$U_{0,crit}$ [m/s]	1.013	1.171	1.321	1.204
$U_{slope,crit,calc}$ [m/s]	0.334	0.387	0.436	0.397
$U_{slope,crit,corr}$ [m/s]	0.518	0.600	0.676	0.616
Factor increase in $U_{slope,crit}$ w.r.t. criterion of 1 movement [-]	1.00	1.16	1.30	1.19

Table 23 - Critical rotational speeds for multiple criteria of initiation of motion

Next step is to determine the critical slope velocities from the critical rotational speeds. First the associated efflux velocities are calculated with (Eq. 3-7) for a thrust coefficient of 0.22 that is derived in the efflux velocity analysis. After that the slope velocities are calculated with (Eq. 2-10). Finally these calculated slope velocities are corrected with a correction factor 'f' of 1.55 based on the results from the velocity analysis, see Table 19. This means that it is the maximum time-averaged slope velocity and not a peak velocity. This corrected critical maximum time-averaged slope velocity is used in the calculations of the paragraphs hereafter. The results are given in Table 23.

As can be concluded from this table is that the critical slope velocity is 0.52 m/s for the criterion of 1 movement. This critical slope velocity increases with a factor 1.19 when it is determined with the trend line method. When the criterion for the amount of movements is increased to 5 movements and 10 movements the critical slope velocity increases respectively with a factor of 1.16 and 1.30. For practical considerations this means that a 30 % higher rotational speed of the bow thruster can be applied at slopes where a criterion for initiation of motion of 10 movements is acceptable. This however might lead to more maintenance when this occurs frequently at the same spot at a slope protection.

6.1.3 Stability parameter

Now that the critical slope velocities are known for multiple criteria it is important to determine the stability parameter with the existing and proposed design calculations. This way it is possible to check if the found stability conditions and calculated stability parameters are similar to the recommended parameters. Furthermore it is also determined what the influence of the different criteria is on the stability parameter. This is done for the original Izbash type stability relation (Eq. 2-11), for the modified Izbash type stability relation (Eq. 2-17) and for the proposed stability equation derived from the method by Roelse (2014) (Eq. 2-25) that is based on the method by Pilarczyk (1995) and therefore named as the Pilarczyk type stability relation in this report.

Original Izbash type stability relation (Eq. 2-11)

As already discussed in section 2.3 Slope material stability, is that most design methods for riprap slope protections are an Izbash-type equation. These include an Izbash type stability parameter. For each specific situation this stability parameter might be different and should therefore be tested for each different case.

First the original Izbash type stability relation is discussed. The critical Izbash type stability parameter $\beta_{Iz,cr,calc}$ is calculated for the test scenario considered. Four different criteria are applied to this calculation which are similar to the criteria of the section before. The criteria for the initiation of motion are respectively 1 stone movement, 5 stone movements, 10 stone movements and the moment the damage increases fast which is defined as the trend line method. Equation (Eq. 6-2) is used for the determination of the stability parameter. Also a relative density of 1.65, a d_{50} of 0.015 m and a slope factor m_h of 0.754 is used. This slope factor is based on an internal friction angle of 40 degrees, the direction of the velocity vector upwards the slope and a slope angle of 18.43 degrees. For stones with a d_{50} larger than 10 cm the internal friction angle is usually up to 42° and stones with a smaller d_{50} and that are less angular the internal friction angle can be estimated as 40°. For the critical slope velocity the corrected critical maximum slope velocity mentioned in Table 23 is used. Furthermore, the factor difference of $\beta_{Iz,cr,calc}$ between the different criteria is determined. The results are presented in Table 24.

$$\beta_{Iz,cr,calc} = \frac{2 * g * \Delta * d_{50}}{m_h U^2_{slope,crit}} \qquad \textit{(Eq. 6-2)}$$

	1 movement	5 movements	10 movements	Trend line
$U_{slope,crit,corr}$ [m/s]	0.518	0.600	0.676	0.616
$\beta_{Iz,cr,calc}$ [-]	2.398	1.794	1.410	1.697
Factor difference in $\beta_{Iz,cr,calc}$ w.r.t. the criterion of 1 movement [-]	1.00	0.75	0.59	0.71

Table 24 - Calculation of stability parameter for the original Izbash type stability relation

It is given that the differences between the criteria are relatively large and therefore when designing a situation that is similar to the scenario tested in this research the criterion of initiation of motion should be defined carefully. For such a situation it is very important to consider the frequency of the hydraulic bed loads acting on the slope and the location where these loads are acting.

For example the results show that for this situation a smaller stability parameter with a factor difference of 0.59 is found for the criterion of 10 movements compared to the criterion of no movement. This means that the applied stone diameter for a slope protection can be a factor 0.59 smaller when 10 stone movements are allowed instead of 1 stone movement. This will save a lot of initial construction costs. Nevertheless the maintenance and therefore the maintenance costs will become higher.

Modified Izbash type stability relation (Eq. 2-17)
Secondly the modified Izbash type stability relation is discussed. The recommended value for the modified Izbash stability parameter $\beta_{Iz,cr,mod}$ is equal to 0.414 (see section 2.3.4).

According to equation (Eq. 2-19) and assuming p = 3 the values of $\beta_{Iz,cr}$ of 3.0 and $\beta_{Iz,cr}$ of 2.5 correspond to respectively values of 'r' of 0.57 and 0.49 which are in the range of measured relative turbulence intensities by researches in the past.

The difference with the stability relation of the subsection before is that this relation contains a modified Izbash type stability parameter which does not indirectly include the influence of the turbulence intensity. For this case the critical stability parameter for is determined with equation (Eq. 6-3) and the relative turbulence intensity is included as an input parameter in the equation.

$$\beta_{Iz,cr,mod,calc} = \frac{2 * g * \Delta * d_{50}}{m_h U_{slope,crit}^2 (1 + p * r)^2} \qquad \textit{(Eq. 6-3)}$$

For the calculation the corrected critical maximum slope velocity found and presented in Table 23 that is corrected according to the measurements is used. Also the measured relative turbulence intensity 'r' and a p=3 are used for the calculation. The median stone diameter from the scale model tests is used for the parameter d_{50} (=0.015m). The relative density is 1.65 and the slope factor m_h is determined with (Eq. 2-9) for a slope angle of 18.43° because an 1 to 3 slope is applied, an angle of internal friction of the stones of 40° and an angle of the velocity factor Θ_u that is zero. The slope factor m_h is equal to 0.754 for this case.

Measurements conducted during the scale model tests of this research for test scenario T5 resulted in a relative turbulence intensity of 0.13 at the location where the peak velocity is maximum. The measured peak velocity is a combination of the measured maximum time-averaged slope velocity and three times the measured absolute turbulence intensity as presented in equation (Eq. 6-7). However this value for the measured relative turbulence intensity is very small and according to Blokland (personal communication) the relative turbulence intensities that are measured during several other researches ranges between 0.25 and 0.80.

In this paragraph only the differences between the multiple criteria are discussed and the comparison with other stability parameters is discussed in next paragraph. The results of the calculation of the stability parameter for the four criteria are presented in Table 25.

	1 movement	5 movements	10 movements	Trend line
$U_{slope,crit,corr}$ [m/s]	0.518	0.600	0.676	0.616
$\beta_{Iz,cr,mod,calc}$ [-]	1.241	0.928	0.730	0.878
Factor difference in $\beta_{Iz,cr,mod,calc}$ w.r.t. the criterion of 1 movement [-]	1.00	0.75	0.59	0.71

Table 25 - Calculation of stability parameter for the modified Izbash type stability relation

It is given that the differences between the criteria are relatively large and similar to the differences between the $\beta_{Iz,cr,calc}$ of Table 24. Therefore again it can be concluded that when designing a situation that is similar to the scenario tested in this research the criterion of initiation of motion should be defined carefully. For such a

situation it is very important to consider the frequency of the hydraulic bed loads acting on the slope and the location where these loads are acting.

Pilarczyk type stability relation (Eq. 2-25)

In section

2.3.6 Stability relation derived from the method by Roelse a stability relation is proposed which is based on the method by Pilarczyk (1995). This is a Shields type equation with extra parameters to include turbulence effects, the influence of the slope, the mobility of the slope material and the location where the velocity is determined. Roelse (2014) made a distinction between a situation with and without piles on a slope when formulating his new proposed equation. The equations for these situations are assigned as respectively the pile obstruction mechanism and the jet diffusion mechanism and are discussed in Appendix C - Equilibrium scour depth. Because the model set-up of the stability test performed was a situation where the equation of the jet diffusion mechanism can be applied, only this part of the proposed stability relation is used for the comparison. This equation is reformulated and the critical mobility parameter is determined with equation (Eq. 6-4).

$$\Psi_{cr,calculated} = \frac{m_h * 0.035 * U^2_{slope,crit} * k_t^2}{\Delta * d_{n50} * 2 * g} \qquad \textit{(Eq. 6-4)}$$

In this equation the same slope coefficient m_h and relative density Δ as for the Izbash type equation is used. The d_{n50} is 0.013 m for this case and the measured relative turbulence intensity is taken as r = 0.13. This relative turbulence intensity is very small however it is determined at the location where the maximum of the time-averaged velocity and three times the absolute turbulence intensity combined is a maximum. Again multiple criteria for the initiation of motion are considered and the results of the calculations are presented in Table 26. The differences between outcomes for each criterion are determined as well. Comparisons with recommended mobility parameter are discussed in the next sub-paragraph.

	1 Movement	5 Movements	10 Movements	Trend line
$U_{slope,crit,corr}$ [m/s]	0.518	0.600	0.676	0.616
$\Psi_{cr,calc}$ [-]	0.020	0.027	0.034	0.028
Factor difference in $\Psi_{cr,calc}$ w.r.t. the criterion of 1 movement [-]	1.00	1.34	1.70	1.41

Table 26 - Calculation of mobility parameter for Pilarczyk type stability relation

It is already mentioned before that when designing a slope protection the criterion of initiation of motion should be defined carefully and based on the specific practical situation where it is aimed for. This again is proven by the large differences in resulting stone diameters. The differences shown are larger for the mobility parameter compared to the differences presented in Table 25. However because in this case it is a mobility parameter and not a stability parameter the differences presented lead to a similar decrease in stone diameter as for the Izbash type equation.

Comparison with recommended stability and mobility parameters

The determined stability and mobility parameters for the test scenario considered in this research are compared to the recommended stability and mobility parameters from the literature in order to get an idea what the differences are and how much they differ. Especially for the modified stability equation by Roelse (2014) this might lead to recommendations for improvement or the validation of the proposed equation. First the original Izbash type stability relation (Eq. 2-11) is discussed, secondly the modified Izbash type stability relation (Eq. 2-17) is discussed and finally also the proposed stability equation derived from the method by Roelse (2014) (Eq. 2-25) is discussed. This relation is based on the method by Pilarczyk (1995) and therefore named as the Pilarczyk type stability relation in this report.

Original Izbash type stability relation (Eq. 2-11)
First the original Izbash type stability relation is discussed, the Izbash type stability parameter is determined with equation (Eq. 6-2). A research by Blokland (1997) recommends a stability parameter $\beta_{Iz,cr}$ of 3.0 for situations where no movement is allowed and a stability parameter $\beta_{Iz,cr}$ of 2.5 for situations where little movement is allowed. In these stability parameters the turbulence is indirectly included in this stability parameter.

The determined $\beta_{Iz\ ,cr,calc}$ is compared to the recommended $\beta_{Iz,cr}$ and the factor difference for each criterion is presented in Table 27.

	1 Movement	5 Movements	10 Movements	Trend line
$\beta_{Iz,cr}$ [-]	3.0	2.5	2.5	2.5
$\beta_{Iz,cr,calc}$ [-]	2.398	1.794	1.410	1.697
Factor difference [-]	0.80	0.72	0.56	0.68

Table 27 - Comparison of calculated with recommended stability parameters for original Izbash type stability relation

As can be observed from the table is that the determined values for $\beta_{Iz,cr,calc}$ are smaller than the recommended values by Blokland (1997). This means that the median stone diameter could be designed smaller when the recommended Izbash stability parameter $\beta_{Iz,cr}$ is used for a design for this test scenario. For the criterion of 1 movement the factor difference is 0.80 and for the criterion of 5 movements the factor difference is 0.72. It is also shown that the difference for the trend line criterion is smaller than for the criterion of 10 movements which implies that when applying the criterion of 10 movements the damage can increase fast even before the criterion of 10 stone movements is reached.

Modified Izbash type stability relation (Eq. 2-17)
Secondly the modified Izbash type stability relation is discussed. The recommended value for the modified Izbash stability parameter $\beta_{Iz,cr,mod}$ is equal to 0.414 according to Blokland (personal communication). The difference with the Izbash stability parameter $\beta_{Iz,cr}$ is that it does not indirectly include the influence of the turbulent fluctuations in it. Instead of that, the relative turbulence intensity is included in the calculation as an input parameter. The relation to determine the modified stability parameter is formulated in equation (Eq. 6-5) which is similar to equation (Eq. 2-20). When it is assumed that the stability parameter for uniform flow as formulated by Izbash is 0.7 and a value for p = 3 as is discussed in section 2.3.3 Turbulence and a relative turbulence intensity for uniform flow of 0.1 then this leads to a $\beta_{Iz,cr,mod}$ of 0.414. This is the recommended modified Izbash stability parameter to which the calculated modified Izbash stability parameters are compared. There is however no criterion of initiation of motion assigned to this parameter and therefore all criteria are compared to this recommended parameter. According to (Eq. 2-21) the values $\beta_{Iz,cr}$ of 3.0 and $\beta_{Iz,cr}$ of 2.5 correspond to respectively values for ‘r’ of 0.57 and ‘r’ of 0.49 which are in the range of measured relative turbulence intensities by researches in the past.

$$\beta_{Iz,cr,mod} = \beta_{Iz,cr,uniform} * \left(\frac{1}{1 + pr_{uniform}}\right)^2 \qquad \textit{(Eq. 6-5)}$$

The results of the calculation of $\beta_{Iz,cr,mod,calc}$ presented in Table 25 are compared to the recommended values. The values of both parameters together with the difference are presented in Table 28.

	1 Movement	5 Movements	10 Movements	Trend line
$\beta_{Iz,cr,mod}$ [-]	0.414	0.414	0.414	0.414
$\beta_{Iz,cr,mod,calc}$ [-]	1.241	0.928	0.730	0.878

Factor difference [-]	3.00	2.24	1.76	2.12

Table 28 - Comparison of calculated with recommended stability parameters for modified Izbash type stability relation

The results show that all calculated stability parameters are much larger than the recommended stability parameters. A larger stability parameter for this equation means that a larger stone diameter should be applied for practical situations like the test scenario tested here.

A reason for the high values for $\beta_{Iz,cr,mod,calc}$ is possibly the low value for the measured relative turbulence intensity 'r'. The relative turbulence intensity has a large influence on the value of the modified stability parameter. Generally this is much larger for situations with propeller jets and it was expected to be in the range of 0.25 to 0.8. As is discussed in Appendix G - Comparison to test results by Van Doorn (2012) this small value can be explained with the effective measuring frequency and the size of the measurement volume of the measurement equipment. Due to this the absolute turbulence intensities are smaller than expected which lead to smaller relative turbulence intensities.

The slope factor m_h is also a parameter that influences the value for the stability parameter. Nevertheless this influence is small. This factor is calculated with a velocity direction which is directed upwards the slope ($\Theta_u = 0$). However actually this angle is changing in time and as concluded in an earlier research by Van Doorn (2012) it has an average value of 15 degrees. This leads to a reduction of the stability parameter of only 1 % and therefore this is not the cause of the large difference. However it is important to consider this angle of the velocity factor.

In addition, the stability parameter is calculated again and now with a larger relative turbulence intensity so that an adequate comparison can be made with the recommended parameters. A value of r = 0.30 is used which is as recommended by Schiereck (2012). The corrected stability parameters are presented in Table 29.

	1 Movement	5 Movements	10 Movements	Trend line
$\beta_{Iz,cr,mod}$ [-]	0.414	0.414	0.414	0.414
$\beta_{Iz,cr,mod,new}$ [-]	0.664	0.497	0.390	0.470
Factor difference [-]	1.60	1.20	0.94	1.14

Table 29 - Comparison of recommended and corrected calculated stability parameters for modified Izbash type stability relation

The determined modified Izbash stability parameters with a different relative turbulence intensity show again differences with the recommended value. For the criterion of 1 movement it shows that the calculated value is a factor 1.60 higher and this means that according to the test results when using the recommended parameter for this scenario it underestimates the median stone diameter with a factor 0.63. In addition when the criterion of 5 movements is applied it shows an underestimation of with a factor 0.83 when the recommended parameter was used for this scenario. For the criterion of 10 movements it shows an overestimation when the recommended parameter was used for this scenario.

It can be concluded that for 1 movement and 5 movements the stability parameters determined for this scenario are larger than the recommended stability parameters when a relative turbulence intensity of 0.30 is assumed. This implies that when the recommended stability parameter was used for this situation it underestimated the median stone diameter if the criterion of initiation of motion is set at 1 movement or 5 movements.

Pilarczyk type stability relation (Eq. 2-25)

Finally, the stability equation based on the equation by Pilarczyk (1995) and modified by Roelse (Eq. 6-4) is discussed. The mobility parameter $\Psi_{cr,calc}$ is calculated for the four selected criteria in the paragraph before and presented in Table 26. These values are compared to the recommended mobility parameter. According to (CIRIA, 2007) the mobility parameter $\Psi_{cr,pilarczyk}$ for rip-rap and armourstone is 0.035 and therefore this value is used for the comparison. This recommended value is according to Shields for the criterion of little movement. The results are given in Table 30.

	1 Movement	5 Movements	10 Movements	Trend line
$\Psi_{cr,pilarczyk}$ [-]	0.035	0.035	0.035	0.035
$\Psi_{cr,calc}$ [-]	0.020	0.027	0.034	0.028
Factor difference [-]	0.57	0.76	0.97	0.80

Table 30 - Comparison of calculated and recommended mobility parameters for Pilarczyk type stability relation

It can be observed from the results that the difference for the criterion of 1 movement is the largest and the difference for the criterion of 10 movements the smallest. Next to that the calculated mobility parameters for all criteria are smaller than the recommended parameter of 0.035. This means that for all criteria a larger stone diameter should be applied for situations in practice that are like test scenario T6 tested in this research.

The large differences might be ascribed to the low relative turbulence intensity that is measured and applied during the calculation. As discussed in section 2.3.5 Stability relation by Pilarczyk the relative turbulence intensities are proposed to be between 0.4 and 0.53 for propeller jets and therefore the turbulence factor k_t should then be between 2.9 and 4.0. The relation between the turbulence factor and the relative turbulence intensity is given in equation (Eq. 2-23).

Another remark should be made on the proposed equation. In the proposed equation by Roelse (2014) the stability correction factor Φ_{sc} was assumed to be equal to 1. However this correction factor is also part of the equation by Pilarczyk (1995) and according to (CIRIA, 2007) this factor should be 0.75 for continuous rock protection. When including this factor in the calculation the mobility parameters become 75% smaller and therefore this does not explain the difference observed in the table before because it makes the differences even larger.

The corrected equation (Eq. 6-6) for this situation is the correct stability relation and therefore the results of Table 31 are used for the discussion, conclusion and recommendations.

$$\Psi_{cr,calc} = \frac{\Phi_{sc} * m_h * 0.035 * U_{slope,crit}^2 * k_t^2}{\Delta * d_{n50} * 2 * g} \qquad \textit{(Eq. 6-6)}$$

This is the corrected stability relation that is based on the equation by Pilarczyk (1995) and that should be used for further research.

	1 Movement	5 Movements	10 Movements	Trend line
$\Psi_{cr,pilarczyk}$ [-]	0.035	0.035	0.035	0.035
$\Psi_{cr,calc,corr}$ [-]	0.015	0.020	0.025	0.021
Factor difference [-]	0.43	0.57	0.72	0.60

Table 31 - Comparison of recommended and corrected calculated mobility parameters for corrected Pilarczyk type stability relation

The results in Table 32 again show large differences with the recommended mobility parameter $\Psi_{cr,pilarczyk}$. This is not remarkable as the turbulence factor (k_t^2 equal to 1.14) used for this calculation is much lower than recommended turbulence factor k_t^2 of 2.9 to 4.0 by Pilarczyk (1995). This small turbulence factor is caused by the small measured relative turbulence intensity.

Furthermore, for the same reason as for the Izbash type stability relation a corrected relative turbulence intensity is used for an adequate comparison with the recommended mobility parameter. Again the relative turbulence intensity is set at 0.30 as recommended by Schiereck (2012). This means that the turbulence factor k_t becomes equal to 2.14 which is still smaller than recommended by Pilarczyk (1995). The determined values for the mobility parameter for the corrected relation are presented in Table 32.

	1 Movement	5 Movements	10 Movements	Trend line
$\Psi_{cr,pilarczyk}$ [-]	0.035	0.035	0.035	0.035
$\Psi_{cr,calc,new}$ [-]	0.028	0.037	0.047	0.039
Factor difference [-]	0.80	1.06	1.35	1.12

Table 32 - Comparison of recommended and new corrected calculated mobility parameters for corrected Pilarczyk type stability relation

It can be observed from the results that for the criterion of 1 stone movement the mobility parameter $\Psi_{cr,calc,new}$ is smaller than the recommended mobility parameter $\Psi_{cr,pilarczyk}$. This means that the median stone diameter is underestimated when using the recommended mobility parameter for this situation according to the results for the criterion of initiation of motion of 1 movement. Similar to the results of the Izbash type relation is that again the mobility parameter for the criterion of 10 stone movements is higher than for the criterion with the trend line. That means that it might lead to a risky situation when the criterion of 10 stone movements is applied.

Summary of the comparisons for all stability relations

The original Izbash type stability relation (Eq. 2-11) leads for all criteria to a smaller calculated Izbash stability parameter $\beta_{Iz,cr,calc}$ compared to the recommended Izbash stability parameter $\beta_{Iz,cr}$. This means that the recommended Izbash stability parameter overestimates the median stone diameter d_{50} for the test scenario tested.

The modified Izbash type stability relation (Eq. 2-17) leads for the criteria of 1 stone movement and 5 stone movements to a larger calculated modified Izbash stability parameter $\beta_{Iz,cr,mod,new}$ compared to the recommended modified Izbash stability parameter $\beta_{Iz,cr,mod}$. This means that the recommended modified Izbash stability parameter underestimates the median stone diameter d_{50} for the criteria of 1 and 5 stone movements for the scenario tested. It should be noted that a relative turbulence intensity of 0.30 is assumed as recommended by Schiereck (2012) because the measured relative turbulence intensity was considered to be too small.

The Pilarczyk type stability relation (Eq. 2-25) corrected to equation (Eq. 6-6) leads for the criterion of 1 stone movement to a smaller calculated corrected Pilarczyk type mobility parameter $\Psi_{cr,calc,new}$ compared to the recommended Pilarczyk type mobility parameter $\Psi_{cr,pilarczyk}$. For the criterion of 5 and 10 stone movements the corrected Pilarczyk type mobility parameter is larger than the recommended Pilarczyk type mobility parameter. This means that the recommended Pilarczyk type mobility parameter underestimates the median stone diameter d_{n50} for the criterion of 1 stone movement for the scenario tested. Also the recommended Pilarczyk type mobility parameter overestimates the median stone diameter d_{n50} for the criterion of 5 and 10 stone movements. It should be noted that again a relative turbulence intensity of 0.30 is assumed for the same reason as mentioned before.

6.2 Type III tests - Location of damage

Next to the determination and analysis of the critical slope velocity and the associated stability parameter, it is important to determine and analyse the location of damage as well. It is important to know at what location the first stones move out. Furthermore the movement intensity and thereby the location of maximum damage are also important. When this is all determined it is compared to the results of the velocity analysis.

6.2.1 Location of start of motion

For practical considerations and for planning of the maintenance it is important to know where the first damage occurs on the slope. Therefore the location of the first movements is determined from the recordings of the stability tests. What can be classified as the first movements depends on the criterion of initiation of motion and the practical situation that is considered. For this case the first movements are the movements that occur during step 1, step 2 and step 3 because as is shown in Figure 62 is that the initiation of motion occurs in the range of rotational speeds of these three steps, when a criterion of no more than 10 stones is considered. For all 5 runs the locations of the first movements are given in Figure 63. In the figure the point of intersection of jet axis with slope is marked with a red '+' sign. The toe of the slope is at an x-distance to the point of intersection of -732 mm.

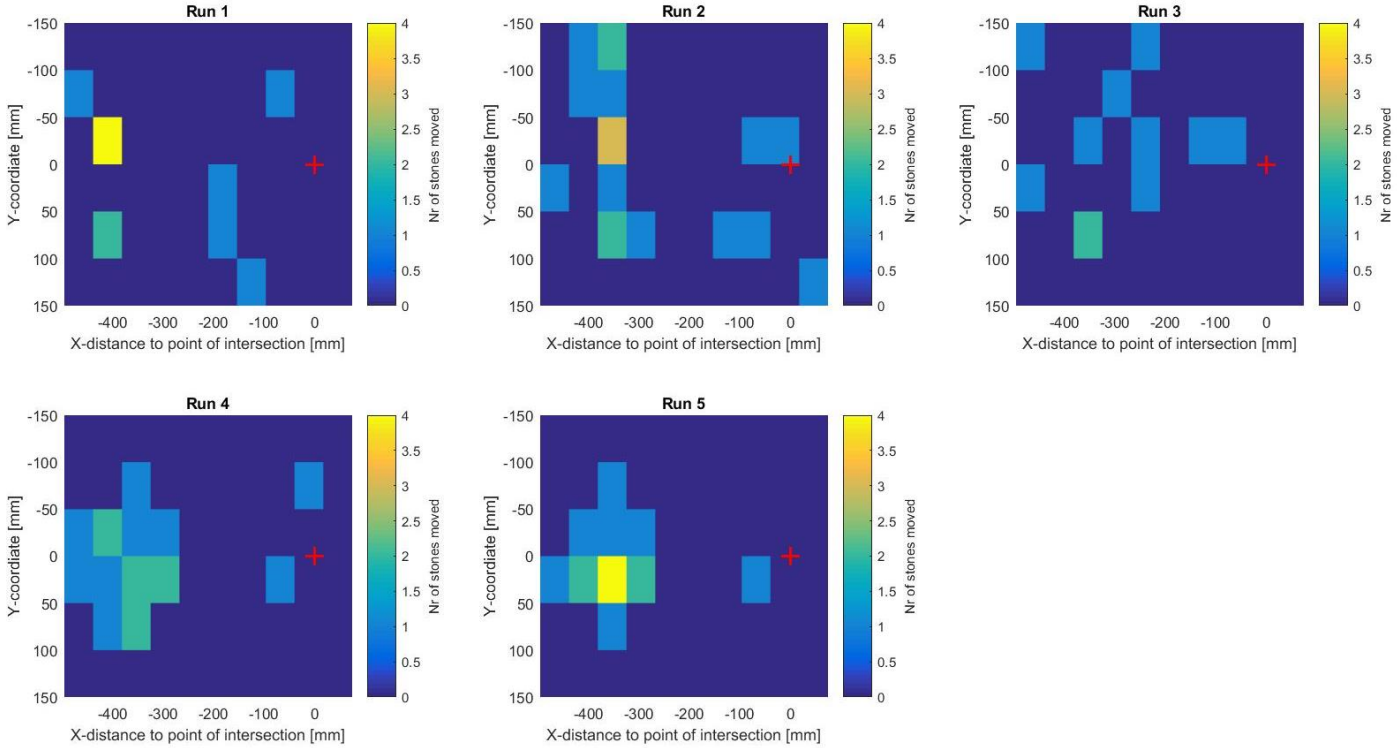

Figure 63 - Locations of start of motion for all runs

Most of the movements during the first steps occur close to the toe in line with the jet axis at y = 0 mm. However some movements of stones are randomly distributed in the damage area. This can be due to the fact that before a run starts some stones might be positioned unstable and more exposed than the other stones. Therefore a lower force is needed to move such a stone than for other stones. The squares between y = - 50 mm, y = + 50 mm and between x-distance to point of intersection of -270 mm and -450 mm are most likely to be the locations of the start of motion.

6.2.2 Movement intensity

In order to determine how the damage is distributed on the slope it is important to investigate the intensity of the stone movements within the selected damage area. The location on the slope of this selected damage area is shown in Figure 42. All five runs of the stability tests are considered.

The recordings of all stability tests are analyzed and the amount of movements at the selected damage area are counted at each square of 5 by 6 cm. Every moved stone is counted one time and only the outgoing movements at each square are taken into account. So when a stone moves more than one time it is only counted as one movement. The damage area is partitioned in 60 squares and the counting is continued for 10 minutes for each step. Finally all the movements per step are summed up for each square and the results are shown in Figure 64. In this figure also the point of intersection of the jet axis with the slope is marked with a red '+'. The toe of the slope is at -732 mm.

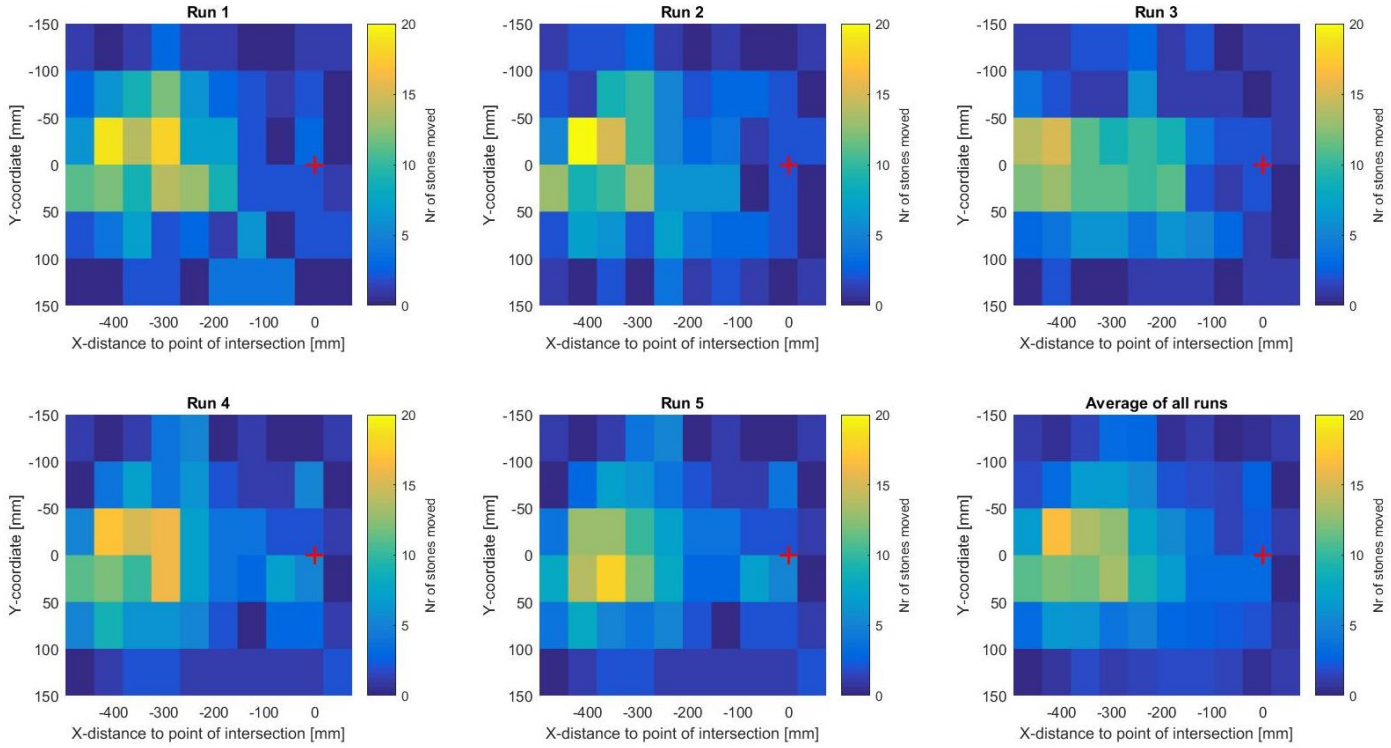

Figure 64 - Movement intensity for run 1 until run 5 and the average of all runs

The results show that most movements take place at locations below the point of intersection of the jet axis with the slope, between an x-distance to point of intersection of approximately - 200 mm until - 500 mm and between the y-coordinates - 50 mm and + 50 mm. For locations higher on the slope and therefore higher x-distance to toe values only a few movements take place. Also it is observed from the plot of the average of all runs that the distribution of the movements is nearly symmetrical around the jet axis (y = 0 mm). It can be concluded that the highest amount of movements are originated from the squares located at an x-distance to toe of -270 mm to -450 mm and between y = - 50 mm and y = + 50 mm.

6.2.3 Location of maximum damage

In the sub-paragraph before the intensity of the movements within the selected damage area is analyzed. From this part of the analysis follow the coordinates of the location where the highest amount of stones are moving out. Therefore this can be assigned as the location of maximum damage.

This maximum damage location has also been observed during the scale model tests. A picture of it together with the measured dimensions of the eroded top layer are shown in Figure 65. This eroded top layer and therefore the location of maximum damage was achieved after completing all runs of the stability tests. However only during the first run the dimensions were measured. Besides the results in Figure 59 already showed that the cumulative amount of movements is very large during the last two steps and that implied already that there had to be a lot of damage at the slope.

The small eroded hole in the top layer of loose stones had a width of 310 mm, a length of 430 mm, a depth of roughly 30 mm (which is equal to $2d_{n50}$) and the centre of the hole is located at approximately 445 mm in

x’ direction from the toe. These dimensions are larger than the dimensions found with the movement intensity analysis. This can be explained by the reason that the dimensions were measured during the first run and that run consisted of one step more than the other runs. The results of run 1 in Figure 64 also show that there are more movements than the other runs in the squares assigned for maximum damage and also the movements are wider spread. Another reason is that the measured dimensions of the erosion hole are measured just outside the actual real eroded layer because a lot of stones are deposited next to the erosion hole and therefore the erosion hole looks wider and longer than it actually is.

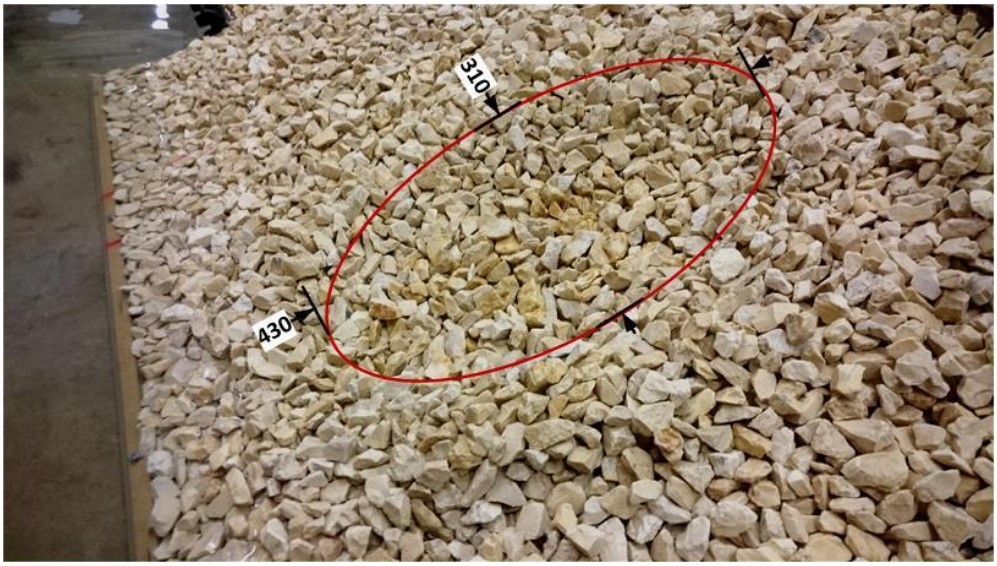

Figure 65 - Location of maximum damage observed during the scale model tests

This result is in accordance with results from researches performed in the past. As stated by Van Veldhoven (2002) the location of maximum damage is close to the toe as well. Besides in the theory it was also stated that most damage is expected to occur at locations where the turbulence intensity is highest and therefore below the point of intersection and close to the toe of the slope. More about the relation with the velocities and turbulence intensities in the next sub-paragraph.

6.2.4 Comparison with velocity field and turbulence intensity field

Now that the location of maximum damage is determined from the data obtained during the stability tests it is compared to the velocity measurements and the velocity analysis of the chapter before. This way it is possible to explain the results of the stability tests. The test scenario with velocity measurements that has an equal model set up as the stability test is test scenario T5. Therefore the measurements of the velocity and turbulence intensity of this test scenario are used. The measurement results of both the stability and the velocity are presented in Figure 66.

In the top left plot the stone movements are compared with the time-averaged $U_{slope,max}$. In the top right plot the stone movements are compared with the absolute turbulence intensities in x’-direction or the standard deviation of $U_{slope,max}$. In the bottom left plot the relative turbulence intensity of $U_{slope,max}$ is shown together with the stone movements and in the bottom right plot the peak velocities in x’-direction U_{peak} (Eq. 6-7) is presented with the stone movements. The amount of stone movements in the plot is divided by the maximum amount of stone movements. This presented value for the movements is the average of the movements per square left and right of the jet axis at y = 0 mm. The x-location of the middle of each square is used.

$$U_{peak} = \overline{U_{slope,max}} + 3 * \sigma(U_{slope,max}) \qquad \textit{(Eq. 6-7)}$$

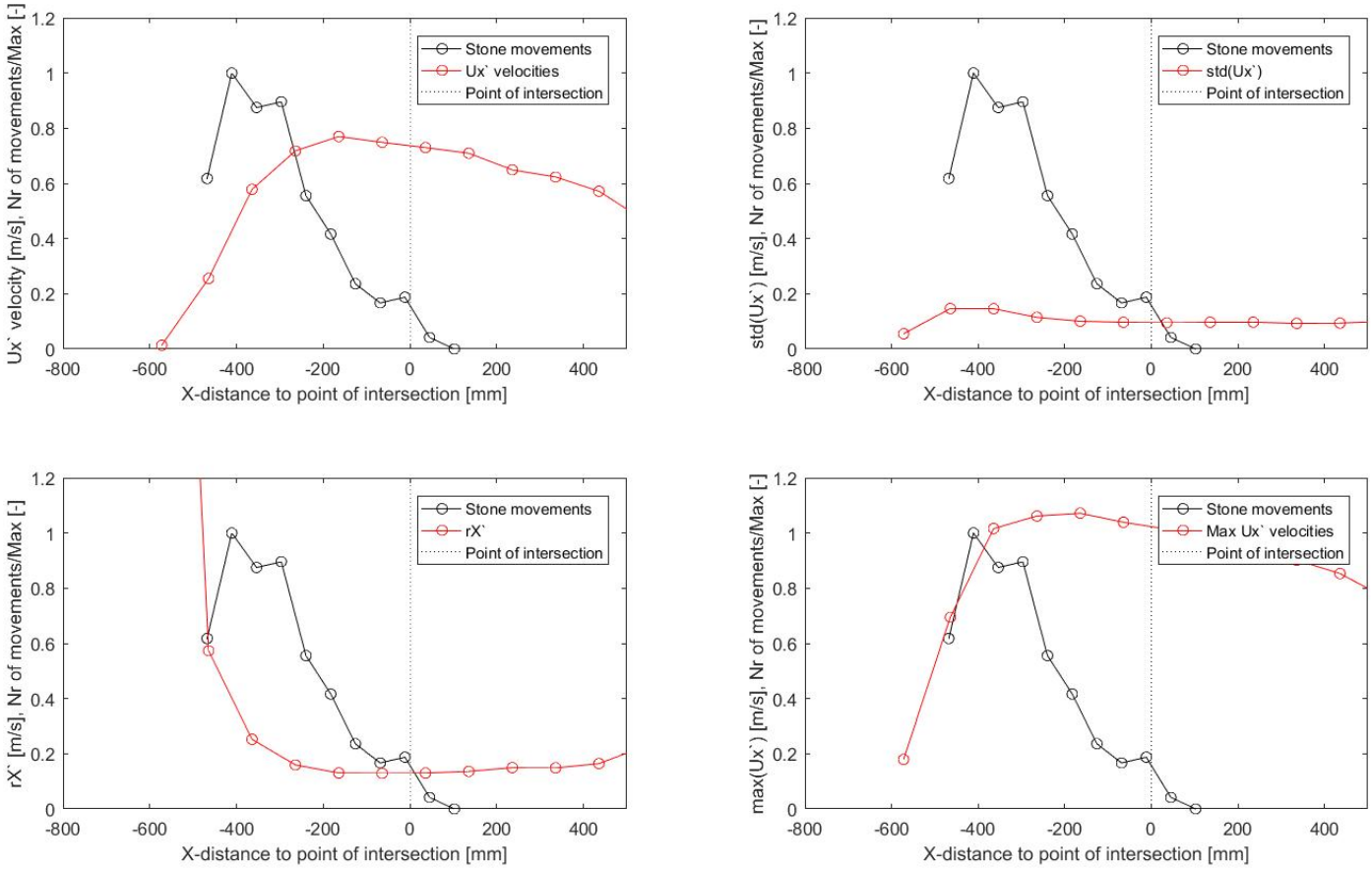

Figure 66 - Velocity measurements compared with stability measurements

As can be observed from the top left plot is that the time-averaged velocity on its own is not the main reason for the stone movements, because the stones already start to move where the time averaged velocity is very small. From the top right plot and the bottom left plot it can be seen that at the location the absolute and the relative turbulence intensity (the first data point is not considered because the time-averaged velocity is nearly zero) are largest the first damage that is observed starts. Therefore this can be assigned as a possible reason for the stone movements. The bottom right figure shows the maximum velocities including the fluctuations and it is shown that where the first peak velocities are increasing fast the first damage starts. At the location of the peak of the damage curve the first peak velocities are observed. However the peak velocities stay at an equal height while the curve of the stone movements reduces towards zero. A large part of the peak velocities at the locations where most of the damage occurs consists of the turbulence intensities. Where higher on the slope the turbulence intensities become lower and the time-averaged velocities are the largest part of the peak velocities.

When considering all this it is probably the turbulence intensities that are most responsible for the stone movements. Nevertheless this analysis is not comprehensive enough to conclude that the turbulence intensities are the main reason for the stone movements.

7. Discussion

Now that the test results are presented and analyzed in the chapters before it is important to evaluate the findings from these sections. In this chapter these findings are discussed and it is important to argue if these findings are valuable and can contribute to existing design methods. A distinction is made between the hydraulic bed loads and the stability relations.

7.1 Hydraulic bed loads

From the efflux velocity measurements the representative outflow velocity U_0 and the thrust coefficient K_T for this propeller are determined and this is important for the determination of a correction factor for the maximum slope velocities. It is shown that the calculated value of K_T with the axial momentum theory is smaller than the provided thrust coefficient by the manufacturer and as stated by Van Doorn (2012). The determined value of K_T is 0.22 and the provided value is 0.28. The thrust coefficient K_T of 0.22 is a proper estimate for the relation between rotational speed of the propeller and the efflux velocity. This is because the axial momentum theory is a reliable method to determine the efflux velocity U_0 from measured U_x velocities according to PIANC (2015) and also because of the fact that more than one rotational speed is taken into account. An explanation for the difference between provided and calculated K_T value is probably the different conditions it is tested in. Such a condition can be a different nozzle used.

The relative turbulence intensities measured in the propeller jet at a distance to the outflow opening of x/D_0 equal to 4 are comparable to the relative turbulence intensities measured on the slope around the location of maximum time-averaged flow velocity and have a value of 0.1 to 0.15. However these values are not comparable to values found by several other researches. Van Doorn (2012) measured values between 0.30 and 0.55. In addition Blaauw and Van de Kaa (1978) measured relative turbulence intensities of 0.25 to 0.30 within the propeller jet and for points further away from the outflow opening and therefore closer to the bed the measured values are up to 0.60. An explanation for the small measured turbulence intensities is that the measurement equipment used is not able to measure the smaller vortices that are important for this research because of the relatively low effective measuring frequency and large measurement volume. Therefore values for the relative turbulence intensities of 0.30 as recommended by Schiereck (2012) are used for the comparison with existing guidelines.

All measurements show an underestimation of the slope velocities by the unconfined jet calculation method (Eq. 2-10). Correction factors ‘f’ up to 1.67 are determined for the maximum slope velocity. The scenario with piles and with an eccentric propeller jet leads to the largest correction factor ‘f ‘. It should be noted that the curve through the data points of the measured time-averaged velocities along the slope shows a fluent line and no salient outliers are observed. There is a clear maximum in the curve as well and this makes the measured maximum slope velocity that is used to derive these correction factors ‘f’ is more likely to be the actual maximum velocity.

When the measured maximum time-averaged slope velocity is used to determine d_{50} for a riprap or an armourstone revetment with the original Izbash type stability relation (Eq. 2-11) it leads to larger stone diameters of the order of the correction factor ‘f’ squared compared to when the maximum slope velocity according to the unconfined jet method (Eq. 2-10) is used. When at the location of the largest peak velocity the measured time-averaged slope velocity and the measured relative turbulence intensity are used to determine d_{50} for a riprap or an armourstone revetment with the modified Izbash type stability relation (Eq. 2-17) it leads to smaller stone diameters with a factor between 1.07 to 2.14. An explanation for this is that the measured relative turbulence intensities are small. When for the same stability relation (Eq. 2-17) a recommended relative turbulence intensity of 0.30 by Schiereck (2012) is used the derived value for d_{50} becomes again a factor 1.02 to 1.59 larger compared to the d_{50} determined with the maximum slope velocity according to equation (Eq. 2-10) and the original Izbash type stability relation (Eq. 2-11).

7.2 Stability of slope material

During the design process of a riprap slope protection it is very important to define a clear criterion for the initiation of motion that is acceptable for that situation. From the obtained test results of test scenario T6 the critical slope velocity is determined for four different criteria. The first criterion was an initiation of motion set at 1 stone movement which is very conservative, the second criterion was an initiation of motion set at 5 stone movements and the third criterion was set at 10 movements. The fourth criterion of initiation of motion was set at the moment that the damage increases fast or mentioned as the trend line method. The choice which criterion will be used is of significant influence on the critical slope velocity and therefore also on the median stone diameter that is used for the design.

The critical slope velocity is calculated from the critical rotational speed of the propeller using a correction factor 'f' (f = 1.55, Table 19) that is determined during the velocity analysis. This correction factor is determined only for a propeller rotational speed of 1091 RPM and not for other rotational speeds that are used during the stability tests. After all the correction factor is assumed to be applicable to other rotational speeds of the propeller as well. This is because the relation between the rotational speed and the outflow velocity is linear and the relation between outflow velocity and slope velocity is also linear according to the unconfined jet method (Eq. 2-10). The relation between the rotation frequency and the rotational speed is linear as well as this is checked during the scale model tests with a stroboscope for multiple frequencies.

The Izbash type stability parameters $\beta_{Iz,cr,calc}$ that are determined with the determined critical slope velocities are smaller than the recommended values for all selected criteria of initiation of motion. For the calculation the corrected maximum slope velocity is used and this means that the recommended value of 3.0 by Blokland (1997) for $\beta_{Iz,cr}$ is a safe value for the design of a riprap or an armourstone slope protection. It can be concluded that the underestimation of the maximum slope velocity by the unconfined jet method (Eq. 2-10) is wholly or partly taken into account in the value of $\beta_{Iz,cr}$. The modified Izbash type stability parameters $\beta_{Iz,cr,mod,new}$ that are determined are larger than the recommended value of 0.41 (see section 2.3.4) for the criterion of initiation of motion of 1 stone movement and 5 stone movements. The mobility parameters $\Psi_{cr,calc,new}$ that are determined is smaller for the criterion of 1 stone movement and larger for the other criteria compared to the recommended value of 0.035 (CIRIA, 2007).

Just above the toe of the slope around y = 0 mm the maximum damage is observed. This location of maximum damage observed during this research is similar to the location of maximum damage of another research by Schokking (2002). In that research it was concluded that the location of maximum damage is just above the toe of the slope. The settings were different and an axial distance of L/D_0=11.3 and a slope of 1 : 3 were used.

8. Conclusions and recommendations

This research is performed in order to answer the main objective which is formulated as:

- Extend and validate methods to calculate (1) the hydraulic loads from a bow thruster on a slope proposed by Van Doorn (2012) and (2) the stability of slope material proposed by Roelse (2014) for multiple bank slope configurations with and without piles.

In order to answer this main objective the sub-research questions formulated have to be answered. The sub-research questions are:

- If there are any differences, what are the differences between the measured and the theoretical maximum hydraulic bed loads for lab test set ups:
  - With varying distances between outflow opening and the slope?
  - With varying slope angles?
  - With varying pile configurations on the slope?

- What are the effects of any differences between the measured and the theoretical maximum hydraulic bed loads on the design of a slope protection?

- How can the method to calculate equilibrium scour depth proposed by Roelse (2014) be changed into a stability formula for riprap revetments?

- Which values can be found for the stability and mobility parameters of the original Izbash type stability relation, the modified Izbash type stability relation and the stability relation derived from the method proposed by Roelse (2014) for the test scenario tested in this research?

The answers are obtained during the entire research and are summed up in this chapter. The research has been carried out by conducting small-scale laboratory experiments at the test facilities of Deltares.

8.1 Conclusions

First the conclusions for the hydraulic bed load and the available calculation methods are presented. Secondly, the conclusions for the stability of stones on a slope as well as the calculation methods are presented.

8.1.1 Conclusions for hydraulic bed load and the calculation method

A distinction is made between experimental results and results considering the calculation method.

Experimental results

- The measured slope velocities for a slope of 1 : 2.5 with a smooth bed are larger than the measured slope velocities by Van Doorn (2012).
- The measured relative turbulence intensities are too small because for the vortices interested in, the effective measuring frequency is too low and the measurement volume is too large of the EMS's used.
- The measured location of the maximum slope velocities for all test scenarios are located close to the point of intersection. For the 1 : 2.5 slopes these are located higher on the slope than the point of intersection of the jet axis with the slope and for the 1 : 3 slopes lower on the slope than the point of intersection.
- Piles on a slope together with an eccentric propeller jet increases the maximum slope velocity by a factor of 1.07 compared to a similar slope without piles.

Calculation method

- The measured maximum slope velocities are larger than the maximum slope velocities according to the unconfined jet method (Eq. 2-10) with an 'f' equal to 1 for all tested scenarios.
- The following correction factors 'f' are suggested for the unconfined jet method (Eq. 2-10):
    - For a slope of 1 : 2.5, a smooth bed and smaller axial distances a correction factor 'f' of 1.26.
    - For a slope of 1 : 2.5, a rough bed and smaller axial distances a correction factor 'f' of 1.22.
    - For a slope of 1 : 3, a rough bed and smaller axial distances a correction factor 'f ' of 1.2 to 1.34 (the measured value of 1.34 is possibly not reliable).
    - For a slope of 1 : 3, a rough bed and larger axial distances a correction factor 'f ' of 1.64.
    - For a slope of 1 : 3, with piles and a rough bed and larger axial distances a correction factor of 1.67.

  Smaller axial distance and larger axial distance are in this research specified as respectively x/D_0 of 6.2 and $x/D_0 \geq 9.5$.
- Applying these correction factors to the original Izbash type stability relation (Eq. 2-11) increases the median stone diameter d_{50} in the order of the correction factor 'f' squared.
- The correction factors proposed by Van Doorn (2012) and corrected by De Jong (2014) are improved by taking into account the correct propeller rotational speed and propeller thrust coefficient. The improved correction factors are presented in Table 1.
- Locations of the maximum time-averaged slope velocity for scenarios with and without piles are located higher on the slope and closer to the point of intersection than according to the unconfined jet method (Eq. 2-10).
- Higher on the slope the correction factors for the slope velocity are larger than the suggested correction factors 'f' for the maximum slope velocity.

8.1.2 Conclusions for stability of stones and the calculation methods

A distinction is made between experimental results and results considering the calculation method.

Experimental results

- For different criteria for the initiation of motion the critical slope velocity $U_{slope,crit,corr}$ is determined and presented in Table 33.

	1 movement	5 movements	10 movements	Trend line method
$U_{slope,crit,corr}$ [m/s]	0.52	0.60	0.68	0.62

Table 33 - Critical slope velocities corrected with a correction factor 'f' of 1.55 for the selected criteria of initiation of motion

- The location of maximum damage is just above the toe of the slope and the largest turbulence intensities that cause the largest peak velocities are most responsible for this damage.

Calculation methods

A recommended value for the relative turbulence intensity of 0.30 by Schiereck (2012) is used for the conclusions of the stability relations presented in this section because the measured relative turbulence intensity is too small as is concluded before.

In the following conclusions 'no movement' and 'little movement' match with respectively 1 stone movement and 5 stone movements in the test results.

For the original Izbash type stability relation (Eq. 2-11):

- For the criterion of no movement the determined stability parameter $\beta_{Iz,cr,calc}$ is smaller than the recommended value of 3.0 by Blokland (1997) and this means that for this scenario the d_{50} is overestimated with a factor 1.25 when using the recommended stability parameter $\beta_{Iz,cr}$.
- For the criterion of little movement the determined stability parameter $\beta_{Iz,cr,calc}$ is smaller than the recommended value of 2.5 by Blokland (1997) and this means that for this scenario the d_{50} is overestimated with a factor 1.39 when using the recommended stability parameter $\beta_{Iz,cr}$.

For the modified Izbash type stability relation (Eq. 2-17):

- For the criterion of no movement the determined stability parameter $\beta_{Iz,cr,mod,calc}$ is larger than the recommended value of 0.41 and this means that for this scenario the d_{50} is underestimated with a factor 1.60 when using the recommended stability parameter $\beta_{Iz,cr,mod}$.
- For the criterion of little movement the determined stability parameter $\beta_{Iz,cr,mod,calc}$ is larger than the recommended value of 0.41 and this means that for this scenario the d_{50} is underestimated with a factor 1.20 when using the recommended stability parameter $\beta_{Iz,cr,mod}$.

For the Pilarczyk type stability relation (Eq. 8-1):

- The following stability relation is proposed in this research for the design of riprap revetments without piles that are affected by propeller jets induced by bow thrusters:

$$\Delta d_{n50} = \frac{0.035 * \Phi_{sc} * U_{slope,crit}^2 * m_h * k_t^2}{2 * g * \Psi_{cr}} \qquad \textit{(Eq. 8-1)}$$

- For the criterion of no movement the determined mobility parameter $\Psi_{cr.calc,new}$ is smaller than the recommended value of 0.035 (CIRIA, 2007) and this means that for this scenario the d_{n50} is underestimated with a factor 1.26 when using the recommended mobility parameter Ψ_{cr}.
- For the criterion of little movement the determined mobility parameter $\Psi_{cr,calc,new}$ is larger than the recommended value of 0.035 (CIRIA, 2007) and this means that for this scenario the d_{n50} is overestimated with a factor 1.06 when using the recommended mobility parameter Ψ_{cr}.

8.2 Recommendations

As result of the analysis and discussion of the test results and the formulated conclusions some recommendations are presented. A distinction is made between recommendations for the designer based on the conclusions and recommendations for more research on this subject.

8.2.1 Recommendations for designer

- The original Izbash type stability relation (Eq. 2-11) is safe to use as a design method for a riprap or an armourstone slope protection according to test results of this research as it showed an overestimation of the d_{50} for the criteria of initiation of motion of no movement and little movement for the scenario tested.
- When the modified Izbash type stability relation (Eq. 2-17) is used as a design method for a riprap or an armourstone slope protection it should be used carefully as it is concluded that it underestimated the d_{50} for the criteria of initiation of motion of no movement and little movement for the scenario tested in this research.
- When the proposed Pilarczyk type stability relation (Eq. 8-1) is used as a design method for a riprap or an armourstone slope protection it should be used carefully as it is validated with only one lab experiment and showed an underestimation of the d_{n50} for the criterion of initiation of motion of no movement for the scenario tested in this research.

8.2.2 Recommendations for further research

- The factor ‘f’ resulting from the test results increases when the axial distance between thruster outflow point and the slope increases. The values of ‘f’ for larger axial distances are rather high (larger than 1.5), which has significant consequences for the design of a slope protection. For this reason, the large values of ‘f’ need more attention in further research.
- When considering smaller grain sizes on the slope also the smaller vortices near the slope bed become important. The EMS’s that are used to measure the velocities have a relatively small effective measuring frequency and make use of a relatively large measuring volume which make it impossible to measure the small vortices which are relevant for the stability of small grain sizes. Therefore it is recommended to do similar model tests with measurement equipment that are able to perform these measurements like an Acoustic Doppler Velocimeter. Or when it is still preferred to use an EMS to perform measurements it can also be a solution to conduct scale model tests with a smaller scale factor.

- Multiple correction factors ‘f’ are proposed for the scenarios tested. However these correction factors are just for these specific situations and it might be valuable to have a correction factor that is applicable to every situation. Therefore more scenarios should be investigated and a formula should be proposed for the correction factor ‘f’ that is a function of the parameters that are missing in the original unconfined jet formula for slopes (Eq. 2-10) and that are of a considerable influence.
- The correction factors ‘f’ proposed are based on the difference between the slope velocity according to the unconfined jet method (Eq. 2-10) and the maximum slope velocity according to the measurements. However, the measured slope velocities at other locations deviate with different factors from the slope velocities according to the unconfined jet method. When designing for example a riprap revetment it might save costs when the median stone diameter is smaller at locations with smaller hydraulic bed loads. For that reason it can be relevant to make the correction factor ‘f’ dependent on the location along the slope.
- During this research only the jet diffusion mechanism of the proposed stability relation by Roelse (2014) is considered and the results presented and analyzed are based on stability tests of only one scenario. Therefore it is important to investigate also other type of scenarios in order to get a relation that is more reliable and wider applicable.
- The combination of pile obstruction mechanism and jet diffusion mechanism of the proposed stability relation by Roelse (2014) should still be investigated. This means that stability tests including piles on a slope should be tested as well in order to validate this part of the stability relation.
- The original equation that is formulated in the research by Roelse (2014) is an equation for the equilibrium scour depth induced by the jet diffusion mechanism or a combination of the jet diffusion mechanism and pile obstruction mechanism. Lab tests should be performed so that this equation can be validated. Especially for the sand and gravel range because it is preferred to use slope material with smaller grain sizes around piles. During the lab experiments the coefficients α_2, β_2 and γ should be determined and therefore it is important to measure the bed location.
- Velocity measurements close to the piles on a slope and more measurements around the piles should be performed to get a better view of the flow pattern and the velocity gradient near a pile. As is concluded from the test results in this research is that the highest velocities occur most of the times near a pile for both an eccentric and a centric propeller jet. During the measurements in this research it was impossible to measure at locations close in front of a pile and close behind a pile due to the measurement set up.

References

Albertson, M., Dai, Y., Jensen, R., & Rouse, H. (1948). *Diffusion of submerged jets.* paper No. 2409: 639-644: ASCE Transactions.

BAW. (2010). *Principles bank and bottom protection of inland waterways.* Karlsruhe, Germany: BAW Codes of Practice and Guidelines.

Blaauw, H., & Van de Kaa, E. (1978). *Erosion of bottom and sloping banks caused by the screwrace of manoeuvring ships.* Delft, The Netherlands.

Blokland, T. (1997). *Bodembescherming belast door schroefstralen.* Rotterdam: Ingenieursbureau Gemeentewerken Rotterdam.

Booij, R. (1998). *Erosie onder een geometrisch open filter.* DUT.

CIRIA, C. C. (2007). *The Rock Manual (C683), The use of Rock in Hydraulic Engineering.* London: CIRIA.

CUR. (1999). *Natuurvriendelijke oevers. Oeverbeschermingsmaterialen.* Gouda.

De Jong, J. (2014). *Numerical Modelling of Bow Thrusters at Open Quay Structures.* Delft: Delft University of Technology.

Hamill, G., Johnston, H., & Stewart, D. (1996). Estimating the velocities in a ship's propeller wash. In *PIANC Bulletin No. 89* (pp. 46-54).

Hoan, N. (2008). *Stone stability under non-uniform flow (PhD Thesis).* Delft: Delft Technical University.

Hoffmans, G., & Verheij, H. (1997). *Scour manual.*

Hofland, B. (2001). *Report on measurements: Pressure and velocity fluctuations around a granular-bed element.* TU Delft, Department Hydraulic Engineering.

Hofland, B. (2005). *Rock & Roll, turbulence-induced damage to granular bed protection (PhD Thesis).* Delft: Delft University of Technology.

KPS Delft. (2016, November 9). *Grind en Split*. Retrieved from KPS Delft: http://shop.kpsdelft.nl/shop/tuinaccessoires/grind-en-split/bigbags/yellow-sun-split-11-22-mm-bigbag

MARIN. (2008). *New inventory of ship manoeuvring devices.* Wageningen: MARIN.

PIANC. (1997). *Guidelines for the design of armoured slopes under open piled quay walls.* Brussels, Belgium: PIANC.

PIANC. (2008). *Considerations to reduce environmental impacts of vessels, Report 99.* Brussels: PIANC.

PIANC. (2015). *Guidelines for protecting berthing structures from scour caused by ships.* Brussels, Belgium: PIANC.

Pilarczyk, K. (1995). *Simplified unification of stability formulae for revetments under current and wave attack.*

Roelse, F. (2014). *Stability of slope material affected by bow thrusters at open quay structures.* Delft: TU Delft.

Römish, K. (2006). *Erosion potential of bow thrusters on canal banks.* Binnenschiffahrt - ZfB 11.

Römish, K. a. (1977). Effects of modern ship traffic on inland- and ocean waterways and their structures. *24th Int. Navigation Congress*, (pp. p79-94). Leningrad.

Römish, K. a. (1981). Criteria for dimensioning the bottom and slope protections and for applying the new methods of protecting navigation channels. *PIANC 25th Int. Navigation Congress*, (pp. p. 29-37). Edinburgh.

Roubos, A. (2006). *Omgaan met onzekerheden bij het ontwerpen van bodembescherming nabij kademuren (MSc Thesis).* Delft: Delft Technical University.

Roulund, A. e. (2005). Numerical and experimental investigation of flow and scour around a circular pile. *Journal of Fluid Mechanics*, 351-401.

RWS. (1990). *Rekenregels voor waterbouwkundig ontwerpen.*

Schiereck, G. (2007). *Concise overview of scale rules in coastal engineering.* Hanoi, Vietnam.

Schiereck, G., & Verhagen, H. (2012). *Introduction to bed bank and shore protection.* Delft: VSSD.

Schokking, L. (2002). *Bow thruster induced damage.* Delft, The Netherlands: Delft Technical University.

Sievers, M. (2011). *Auswertung und statistische analyse von pilot cards zur emittlung von fahrtstufen bei an- und ablegemanövern.* Hamburg: Bachelorarbeit der Hafen City Universität Hamburg.

Van der Schriek, G. (2011). *Dredging Technology (Lecture Notes).* Delft: Delft Technical University.
Van Doorn, R. (2012). *Bow thruster currents at open quay constructions on piles (MSc thesis).* Delft: TU Delft.
Van Veldhoven, V. (2002). *Vooronderzoek schroefstraal op een talud met breuksteen.* Delft: Delft University.
van Velzen, G. (2012). *Flexible scour protection around cylindrical piles (MSc Thesis).* Delft: Delft University of Technology.
Verhagen, H. (2001). *Bowthrusters and the stability of a riprap revetment.* Delft: Delft University of Technology.
Verheij. (2010). *Nieuwe formules voor predictie schroefvermogens hoofdschroeven en boegschroeven van schepen in de binnenvaart.* Delft: Delft Technical University.
Verheij, H. (1983). The stability of bottom and banks subjected to the velocities in the propeller jet behind ships. *Proceedings 8th Int. Harbour Congress*, (pp. 1-11). Antwerp, Belgium.
Verheij, H. (1985). *Aantasting van dwarsprofielen in vaarwegen, schroefstralen en stabiliteit van bodem en oevers onder invloed van stroomsnelheden in de schroefstraal (M1115 - VII & Xa).* Delft, The Netherlands: WL Delft Hydraulics.
Vetus. (2016, October 29). *VETUS Boegschroef 25 kgf, 12 Volt*. Retrieved from Vetus: http://www.vetus.com/vetus-boegschroef-25-kgf-12-volt.html

Appendix A - Bow thrusters

A bow thruster has a propeller which usually consists of 4 or 5 blades that are symmetrically attached to the propeller hub. This propeller hub is rotating in a vertical plane around the shaft that is driven by an engine. In order to provide a force that is pushing the vessel forward the blades are 3-dimensional and have a wing-type profile. This also prevents cavitation to occur and meets with the Bernoulli theorem. Characterizations of a propeller are the power and thrust delivered at standard regime, the rotational speed and direction, the amount and angle of the blades and the external diameter.

A bow thruster is a ducted propeller. Especially for tugboats and bow thrusters on most other type of vessels the ducted propellers are very useful. The modified pipe around the propeller makes it a ducted propeller and this increases the efficiency at low navigation speeds and turning movements. Due to the fact that the centrifugal force of a propeller pushes the water to the outside of the edges of the blades, it loses energy and therefore reduces the efficiency. When this side effect of the centrifugal movement is improved by pushing the water only in the axial direction of the propeller the efficiency is increased.

Figure 67 - Ducted propellers (PIANC, 2015)

A transverse thruster is a type of ducted thruster that consists of a propeller in a tunnel. In the case of bow thrusters it is a tunnel that is going through the hull near the bow of the vessel. Therefore it has openings on both sides of the hull as shown in Figure 68 and depending on the rotation direction it takes water in at one side and expels it out of the other side. This provides a transverse thrust and makes the assistance of tugboats while manoeuvring unnecessary. It is mainly used for mooring and departing activities. If the sailing speed becomes above 2 knots the efficiency of a bow thruster decreases and the power of it can reach up to 4 MW according to PIANC (2015).

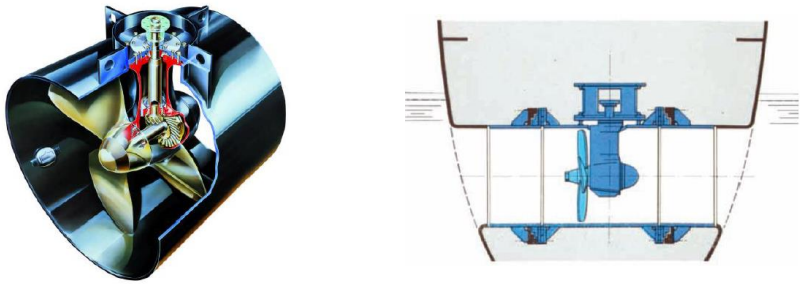

Figure 68 – Transverse tunnel thruster (PIANC, 2015)

A.1 Empirical relation size and bow thruster power

Several data about the size and propulsion systems were collected of vessels in the Bremerhaven port, the port of Hamburg and the port of Rotterdam. These data are presented by Roubos (2006) and Sievers (2011). From these data relationships between the beam of the vessel and respectively the power of the bow thruster and the diameter of the bow thruster, shown in (Eq. A-1) (PIANC, 2015). The relationships are for sea-going vessels.

$$P_{thruster} = 87.5 * B_{vessel} - 1350 \qquad \textit{(Eq. A-1)}$$

$$D_{thruster} = 0.05 * B_s + 0.5$$

With: $P_{thruster}$: $Power\ of\ bow\ thruster\ on\ the\ vessel\ [kW]$
$D_{thruster}$: $Diameter\ of\ bow\ thruster\ on\ the\ vessel\ [m]$
B_{vessel}: $Beam\ width\ of\ the\ vessel\ [m]$

For inland vessels relationships between bow thruster power and respectively the length and draught of the vessel and the diameter of the bow thruster are derived by Verheij (2010). These are shown in (Eq. A-2). A distinction is made for different type of vessels, which are container vessels, general cargo vessels, tankers and passenger vessels.

$$P_{container,thruster} = 2.0 * L_s * T_s - 250 \qquad \textit{(Eq. A-2)}$$
$$P_{general\ cargo,thruster} = 1.75 * L_s * T_s - 150$$
$$P_{tanker,thruster} = 0.8 * L_s * T_s - 100$$
$$P_{passengers,thruster} = 275$$

$$D_{thruster} = 0.1636 * P_{thruster}^{0.3656}$$

With: $P_{x,thruster}$: $Power\ of\ bow\ thruster\ on\ vessel\ type\ 'x'\ [kW]$
T_s: $Draught\ of\ vessel\ [m]$
L_s: $Length\ of\ vessel\ [m]$

A.2 Design bow thruster power

According to PIANC (2015) it is recommended to apply the conservative approach, which means use the full 100% of the engine power for the bow thruster, to design calculations. This is recommended for both the port situation and the inland waterway situation. Sometimes a vessel class is equipped with a more powerful engine than average and it can be more economical to apply only 60% of the installed power. Due to the fact that it is difficult to determine when and where that happens, it is better to apply the conservative approach with the 100 % case.

The duration of a berthing operation depends strongly on the size and therefore the controllability of the ship. It can take approximately 15 minutes however in the case of less manoeuvrable ships it can take up to more than an hour. The de-berthing operation normally has a shorter duration.

A.3 Distance bow thruster to quay wall

The width of the vessel's beam is smaller at the bow than at the amidship section. For sea-going vessels this difference is larger than for inland vessels. It is important to know the distance between the bow thruster and the slope in order to determine the hydraulic loads on the slope. Roubos (2006) set up an equation for the distance between the outflow point of a duct and the quay wall for sea-going container vessels, this is given in (Eq. A-3).

$$x_{thruster} \approx 0.5 * B_s \qquad \textit{(Eq. A-3)}$$

With: $x_{thruster}$: $Distance\ between\ outflow\ thruster\ tunnel\ and\ quay\ [m]$

For other types of vessels some reference locations in the Netherlands are used for the determination of the distance between ship and the toe of the slope. Types of vessels that are important and that have to be

considered are bulk carriers and tankers, RoRo vessels and inland vessels. A lot of jetties with berthing locations parallel to the bank are constructed in the Port of Rotterdam, mainly for tankers, some bulk carriers and RoRo vessels or as berthing place without unloading-, loading equipment or terminal. Next to that along the river Waal and the river Rhine some ports where ships can stay over the night, some waiting areas before locks or movable bridges at side channels or –rivers and other berthing locations for inland vessels are observed. At these berthing locations, from Google Earth the distance between amidships and a point at the slope where the water level crosses it is determined.

If the type of waterway and therefore also the types of vessels that go through it is known, the approximate water depth can be assumed. The 'handysize' and 'handymax' bulk carriers or tankers with a draught up to 9 m according to Quist (2016) are considered, because that are the vessels that most times have a bow thruster. The RoRo terminal that is considered (Beneluxhaven) is assumed to have RoRo vessels with a draught of 12m, this is the draught for the largest RoRo vessels according to Quist (2016). The river Waal has a minimum water depth within its fairway of 2.8m according to Rijkswaterstaat (2016). However the harbors where the inland vessels can stay overnight has to be accessible for the vessels with the largest draught that use the Waal River, that are draughts of 4.4m. Again a keel clearance of 1m is assumed.

Also the slopes are assumed to be constructed as an 1 : 3 slope because these are the most applied slopes for river and canal banks.

The distance between the outflow opening of the bow thruster and the side of the vessel is different for each type of vessel. According to Blokland (personal communication) for inland vessels this is in the range of 0.7 to 3.0 times a jet diameter of 1.0 or 1.1m (D_0, which is equal to the propeller diameter D_p for tunnel thrusters). For bulk carriers and tankers it is assumed to approximately half the beam width which is comparable to a container vessel (beam widths of 20m considered for the type of bulk carriers and tankers mentioned above), for RoRo vessels this is approximately 4.0 to 5.0 times a D_0 of 2.5m. With this information the distance between the outflow opening and the toe of the slope is calculated.

	Most observed distances	Assumed water depth	Distance outflow to side of midship	Distance outflow to toe of slope
Bulk carriers / tankers	25m	10m	~10.0m	5.00m
	35m	12m	~10.0m	9.00m
	50m	12m	~10.0m	24.00m
RoRo vessels	30m	13m	10.0m – 12.5m	1.00m
Inland vessels	12m	2.8m	0.7m – 3.3m	4.30m
	20m	5.4m	0.7m – 3.3m	4.50m
	40m	5.4m	0.7m – 3.3m	24.50m

Table 34 - Distance between outflow opening and toe of an embankment

Appendix B - Material stability

Stability theories by Izbash, Shields and Hoan, used as basis for many design criteria.

B.1 Izbash

This approach is actually relatively easy to understand and is based on the balance of all the forces acting on a single grain. These forces are presented in Figure 69 and (Eq. B-1). A distinction is made between the active forces (the load) and the passive forces (the strength). The active forces are representative for the flow and the turbulence that act on the grain and consist of the drag force (F_D), the lift force (F_L) and the shear force (F_S). The passive forces consist of the strength of the grain which is represented by the gravity (W) and the friction between the grains (F_F). When the sum of the active forces becomes bigger than the sum of the passive forces the grain starts to move and the stability criterion is trespassed.

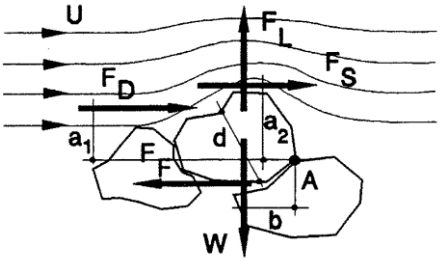

Figure 69 - Forces on a single grain

Load *(Eq. B-1)*

$$F_D = 0.5 * C_D \rho_W U_b^2 A_D$$
$$F_F = 0.5 * C_F \rho_W U_b^2 A_F$$
$$F_L = 0.5 * C_L \rho_W U_b^2 A_L$$

Strength

$$W = (\rho_s - \rho_w) g D_{50}^3$$
$$F_F = f * W$$

With:
$C_{D;F;L}$: $Coefficients$ $[-]$
ρ_W: $Water\ density$ $[m^3/s]$
U_b: $Velocity\ near\ bottom$ $[m/s]$
$A_{D;F;L}$: $Area\ of\ grain\ where\ force\ acts\ on$ $[m2]$
ρ_s: $Grain\ density$ $[m^3/s]$
D_{50}: $Median\ grain\ diameter$ $[m]$
f: $Friction\ coefficient$ $[-]$

Every active force is proportional to the flow velocity squared. As can be derived from the description of the theory given above and the equations it can be concluded that there should be a critical value of the flow velocity at which a grain is no longer stable and starts to move. This critical velocity is used to derive a dimensionless relation between load and strength. That is achieved by balancing the horizontal forces ($\Sigma H=0$) with each other, the vertical forces with each other ($\Sigma V=0$) and the moment equilibrium ($\Sigma M=0$) around the corner of the grain (point A in Figure 69). This leads to (Eq. B-2).

$$u_c^2 = K\Delta g d \qquad \textit{(Eq. B-2)}$$

$$u_c = 1.2\sqrt{2\Delta g d}$$

$$\Delta = \frac{\rho_s - \rho_w}{\rho_w}$$

With: $u_c: Critical\ velocity\ near\ bed\ [m/s]$
$K: Coefficient\ [-]$
$d:\ Nominal\ grain\ diameter\ [m]$

Finally Izbash experimentally determined the coefficient K and formulated (Eq. B-2). The experiments were performed with big stones in shallow water however the following obscurities should be considered:

- The place where the velocity is defined is unclear and because of the set-up of the experiments it can be assumed that the velocity near the bed has to be used.
- The way the diameter is defined is unclear as well and because of the set-up of the experiments it can be assumed that the nominal diameter of a stone has to be used.

According to Schiereck (2012) and the description of the theory it is recommended to use the Izbash approach for water jets. This approach is applicable to non-uniform flow cases and cases where there is no equilibrium considered between the forces due to the flow and the bed friction. In most design cases the Izbash equation with stability parameters according to Blokland (1997) is used.

$$d_{n50} \geq \beta_{Iz,cr} * \frac{m_h * U_{b,max}^2}{2 * g * \Delta} \qquad \textit{(Eq. B-3)}$$

With: $u_c: Critical\ velocity\ near\ bed\ [m/s]$
$K: Coefficient\ [-]$
$d:\ Nominal\ grain\ diameter\ [m]$

B.2 Shields

This approach is based on the equilibrium of forces and a relation between load and strength as well. Nonetheless this theory is derived for an area that consists of more than one grain. This is taken into account in the friction force which is now the shear force on an area of the bed and is the active force or the load in the derived equation. When this shear force becomes bigger than the stability criterion multiple grains start to move away.

Shields used the shear velocity and the particle Reynolds number to derive a relation between the dimensionless shear stress and the bed strength. This relation is given in (Eq. B-4) and represents a stability criterion which holds that the critical Shields parameter is given as function of the critical shear velocity.

$$\Psi_c = \frac{\tau_c d^2}{(\rho_s - \rho_w) g d^3} = \frac{u_{*c}^2}{\Delta g d} \qquad \textit{(Eq. B-4)}$$

With: $\Psi_c:\ Shields\ stability\ parameter\ [-]$
$\tau_c:\ Critical\ shear\ stress\ [N/m2]$
$u_{*c}:\ Critical\ shear\ velocity\ [m/s]$

The shear velocity is actually the shear stress with the dimensions of velocity. The particle Reynolds number is defined as an indicator for the amount of protruding of a grain into the turbulent boundary layer. Shields

assumes that uniform flow occurs and therefore assumes a logarithmic vertical velocity profile with a fully developed boundary layer. The used velocity is the depth averaged velocity.

Relation between Shields and Izbash
Verhagen (2001) derived and explained the relation between the Izbash and Shields stability equations because the guidelines in PIANC (1997) did not take the extra induced turbulence by bow thrusters into account. This extra turbulence is included in the bed stability relations.

As also described above Izbash derived a relation between the velocity near the bed and the moment of incipient motion of the grains. With experimental data and curve fitting he found an Izbash coefficient. Shields derived a relation between the momentum loss and the force from the bed on the flow. For this he used a logarithmic velocity profile which describes uniform flow. This indicates that the velocity is probably determined at different locations. The difference in locations is proven and shown in Figure 70. Shields uses the average flow velocity that takes place at 0.4 times the water depth and Izbash uses the local velocity just above the bed. This relations is found by equating both stability relations and reformulating it for the velocity.

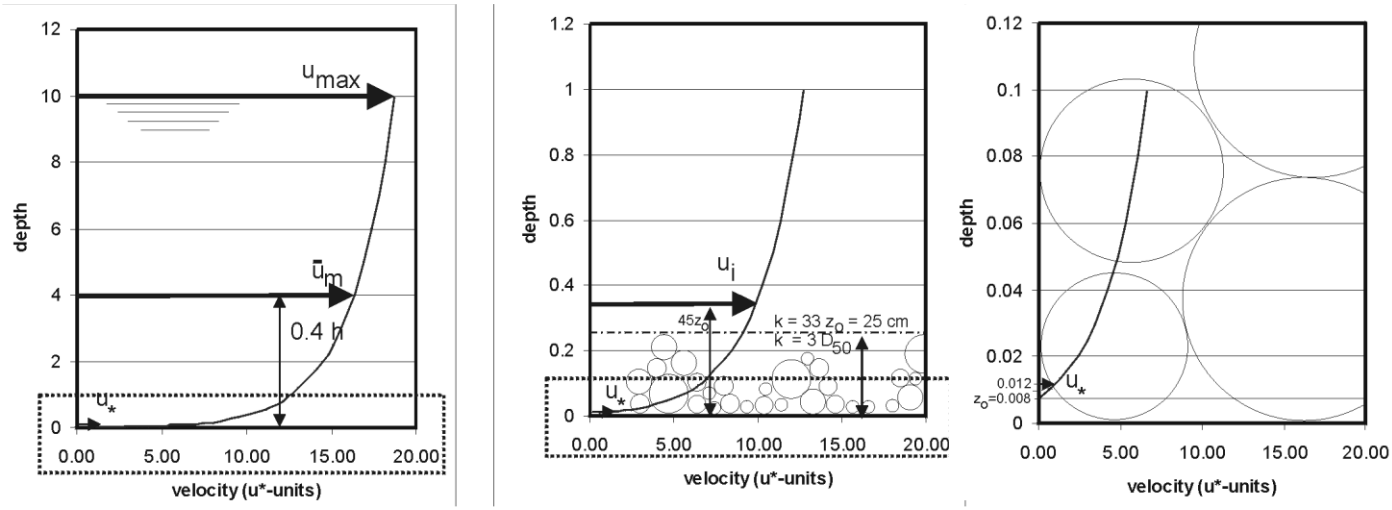

Figure 70 - Velocity profile on different scales (Verhagen, 2001)

B.3 Hoan
The function given above in (Eq. 2-17) used the value of the relative turbulence intensity. There is a possibility a problem occurs with that value because there is almost no current nearby the reattachment point. However there is a high turbulence intensity at that point and this can lead to a value of the relative turbulence intensity that goes to infinity. According to Schiereck (2012) it is therefore recommended to use the value of the kinetic energy of the turbulent velocity and apply an equation of the form given in (Eq. B-5). This relation uses the time averaged velocity and an extra term is added to take the turbulence effects into account.

$$\Psi_c = \frac{\left(\bar{u}+\alpha\sqrt{k}\right)^2}{\Delta g d} \qquad \textit{(Eq. B-5)}$$

One of the criteria for the use of such an equation is that the time-averaged velocity should be measured or determined at the right location. Also the turbulent kinetic energy has to be measured and the value of the coefficient α needs to be determined with lab tests.

Hoan (2008) developed a relation for the Hoan mobility parameter that is shown in (Eq. B-6). The load part represents that the average is taken over the complete water depth, this is indicated with the brackets and subscript ‘h’. Within this part a distinction is made between the values near the bed and near the surface.

Where the values near the bed contribute more to the load. Following from the tests performed by Hoan (2008) the value of α should be 3.5 in order to determine the Hoan mobility parameter.

$$\Psi_{Hoan} = \frac{\langle(\bar{u}+\alpha\sqrt{k_u})^2 * \sqrt{1-z/h}\rangle_h}{\Delta g d_{n50}} \qquad \textit{(Eq. B-6)}$$

$$k_u = \sigma(u) = \sqrt{\overline{u'^2}}$$

With: Ψ_{Hoan}: $Hoan\ mobility\ parameter\ [-]$
α: $Coefficient\ [-]$
z: $Distance\ above\ the\ bed\ [m]$
k_u: $Kinetic\ energy\ of\ turbulent\ velocity\ in\ u-direction\ [J]$

Appendix C - Equilibrium scour depth

In 2014 Roelse conducted a research to develop a method to predict the equilibrium scour depth at a slope with piles that is affected by a bow thruster current. The equation that is formulated consists of two parts, the jet diffusion mechanism and the pile obstruction mechanism.

C.1 Jet diffusion mechanism

The scour caused by the propeller jet only, is given in the jet diffusion mechanism and is first part of (Eq. C-3). The bow thruster jet contains high turbulence intensities and therefore it was assumed that the Hoan mobility parameter should be used for the best prediction. However for this parameter detailed data of the flow field just above the slope is needed and this was not available during that research and therefore the maximum velocity just above the slope is used to replace the Hoan mobility parameter. This maximum slope velocity is the hydraulic load on the slope mentioned before. With this maximum slope velocity the densimetric slope Froude number is formulated as shown in (Eq. C-1).

To make a distinction between material transport and no transport a critical densimetric slope Froude number is formulated as well. This contains the bed slope velocity at which the first grains start to move which is defined as the critical bed slope velocity. If the densimetric slope Froude number exceeds the critical densimetric slope Froude number the jet diffusion mechanism is initiated and scour occurs.

$$Fr_{slope} = \frac{U_{slope}}{\sqrt{g*\Delta*d_{50}}} \qquad \textit{(Eq. C-1)}$$

$$Fr^2{}_{slope,crit} = \frac{U^2{}_{slope,crit}}{g*\Delta*d_{50}}$$

With: Fr_{slope}: $Densimetric\ slope\ Froude\ number$ $[-]$
U_{slope}: $Flow\ velocity\ just\ above\ slope$ $[m/s]$
Δ: $Relative\ density$ $[-]$
d_{50}: $Median\ grain\ size$ $[m]$

C.2 Pile obstruction mechanism

In the case there are piles on the slope this gives additional scour next to the scour of the jet diffusion mechanism. Piles induce higher flow velocities and higher turbulence intensities and therefore more erosion of the slope material, this pile obstruction mechanism is indicated as the second part of (Eq. C-3). The equation for this mechanism is formulated for the uniform flow case first and after that factors to take account of the effects of non-uniform flow are added in the factor K as shown in (Eq. C-2).

$$K = K_{gr} * K_u * K_{shape} * K_g * K_d \qquad \textit{(Eq. C-2)}$$

$$K_u = 2 * \frac{U_{slope}}{U_{slope,crit}} - 1 \qquad \text{for} \quad 0.5 * U_{slope,crit} < U_{slope} < U_{slope,crit}$$

With: K_{gr}: $Sediment\ grading\ factor$ $[-]$
K_u: $Velocity\ correction\ factor$ $[-]$
K_{shape}: $Shape\ grading\ factor$ $[-]$
K_g: $Pile\ group\ correction\ factor$ $[-]$
K_d: $Sediment\ grading\ factor$ $[-]$

The pile obstruction mechanism initiates when the densimetric slope Froude number becomes higher than the 0.5 times the critical densimetric slope Froude number. Therefore this mechanism occurs already before the jet diffusion mechanism occurs.

C.3 Calculation method for equilibrium scour depth

Combining both the jet diffusion and pile obstruction mechanism gives the equation to predict the equilibrium scour depth as shown in (Eq. C-3). This method is only validated for the situation with a horizontal bed and not for a sloping bed yet. Therefore also the values presented for the coefficients are determined with already existing data from research with a horizontal bed.

$$\frac{h_{se}}{D_0} = \alpha_2 * \left(Fr_{slope}^2 - Fr_{slope,crit}^2\right)^{\beta_2} + \gamma * K * \frac{D_{pile}}{D_0} * tanh\left(\frac{h}{D_{pile}}\right) \qquad \textit{(Eq. C-3)}$$

If $Fr_{slope} > Fr_{slope,crit}$

With:
h_{se}: $Equilibrium\ scour\ depth\ [m]$
D_0: $Propeller\ diameter\ [m]$
Fr_{slope}: $Densimetric\ slope\ Froude\ number\ [-]$
$Fr_{slope,crit}$: $Critical\ densimetric\ slope\ Froude\ number\ [-]$
K: $Coefficient\ for\ all\ correction\ factors\ [-]$
D_{pile}: $Pile\ diameter\ [m]$
h: $Water\ depth\ [m]$
α_2: $(= 0.32)\ Coefficient\ to\ be\ validated\ by\ experimental\ data\ [-]$
β_2: $(= 0.53)\ Coefficient\ to\ be\ validated\ by\ experimental\ data\ [-]$
γ: $(= 1.2)\ Coefficient\ to\ be\ validated\ by\ experimental\ data\ [-]$

Appendix D - Plan view and cross section of model set up

For test scenario T5 a plan view and a cross section are shown. This is the test scenario with the largest distance between model vessel and the toe of the slope and a slope of 1:3. What is not presented in the plot is that the model vessel has to shift a few centimetres extra perpendicular to the slope, in order to take into account the thickness of the plates with the glued stones which will be mounted on top of the slope.

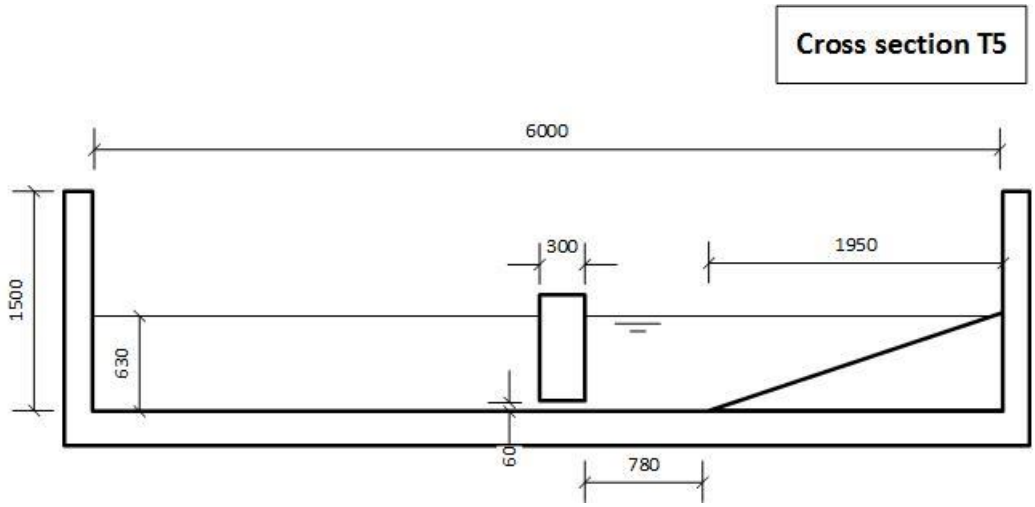

Figure 71 – Cross section of test scenario T5

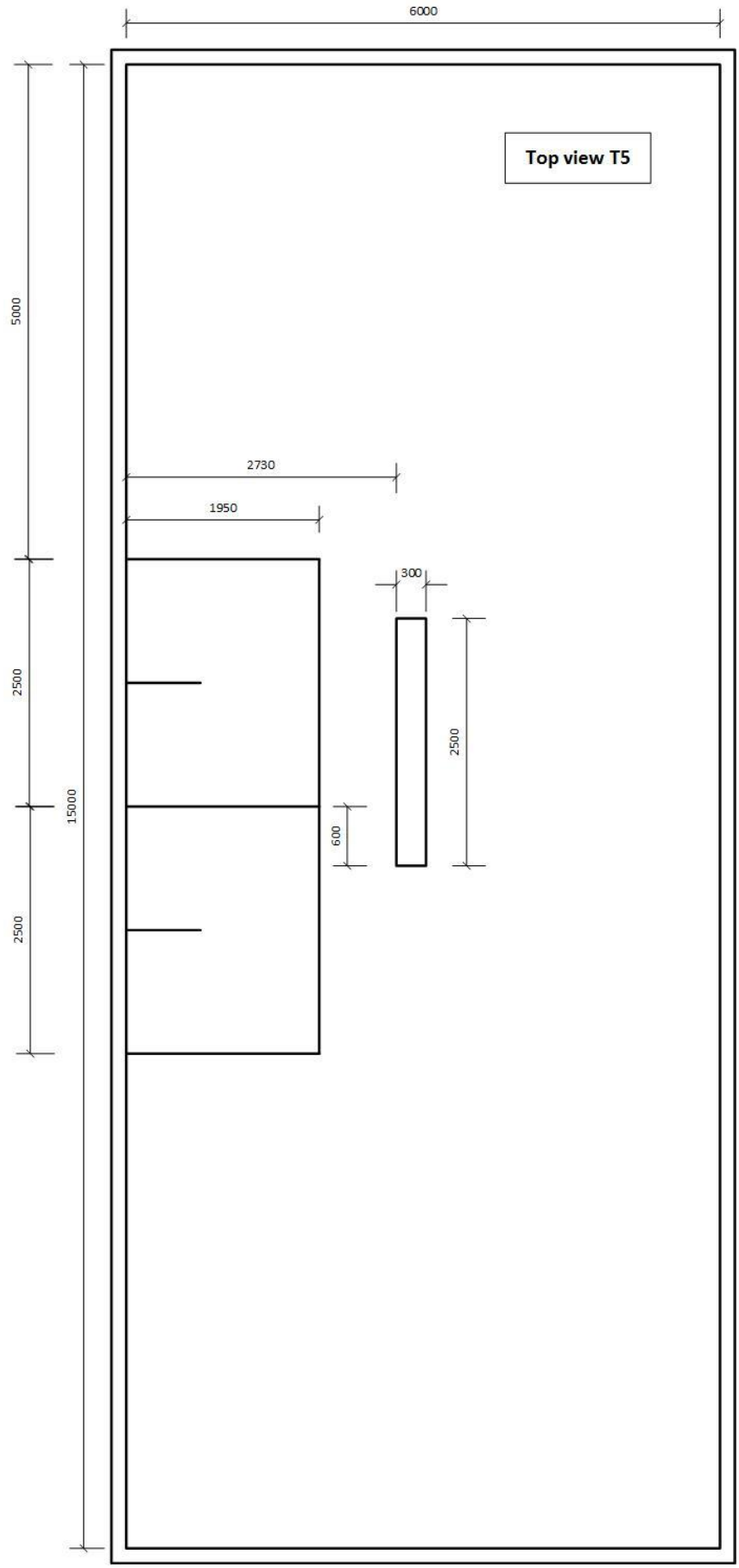

Figure 72 - Top view of test scenario T5

Appendix E - Sieve analysis stones stability tests

A sieve analysis is performed of the stones used for the stability tests. These stones were applied in the top layer of loose stones during the stability test of test scenario T6. A layer with a thickness of 2 times d_{n50} was built on top of the plates with glued stones. The stones were sold by KPS Delft and classified as Yellow Sun 11 – 22 mm. Before the stones were used for the construction of the loose top layer they were sieved at Deltares with a minimum sieve diameter of 11 mm and a maximum sieve diameter of 18 mm. After the tests were conducted a sample of the loose stones was sieved at the Concrete Lab of the TU Delft. The diameters of the sieves used are given in Table 35. The curve of the analysis of the sieving is shown in Figure 73.

Sieve number	Sieve diameter
#1	8 mm
#2	10 mm
#3	14 mm
#4	16 mm
#5	20 mm

Table 35 - Sieve diameters used for the sieving of the stones

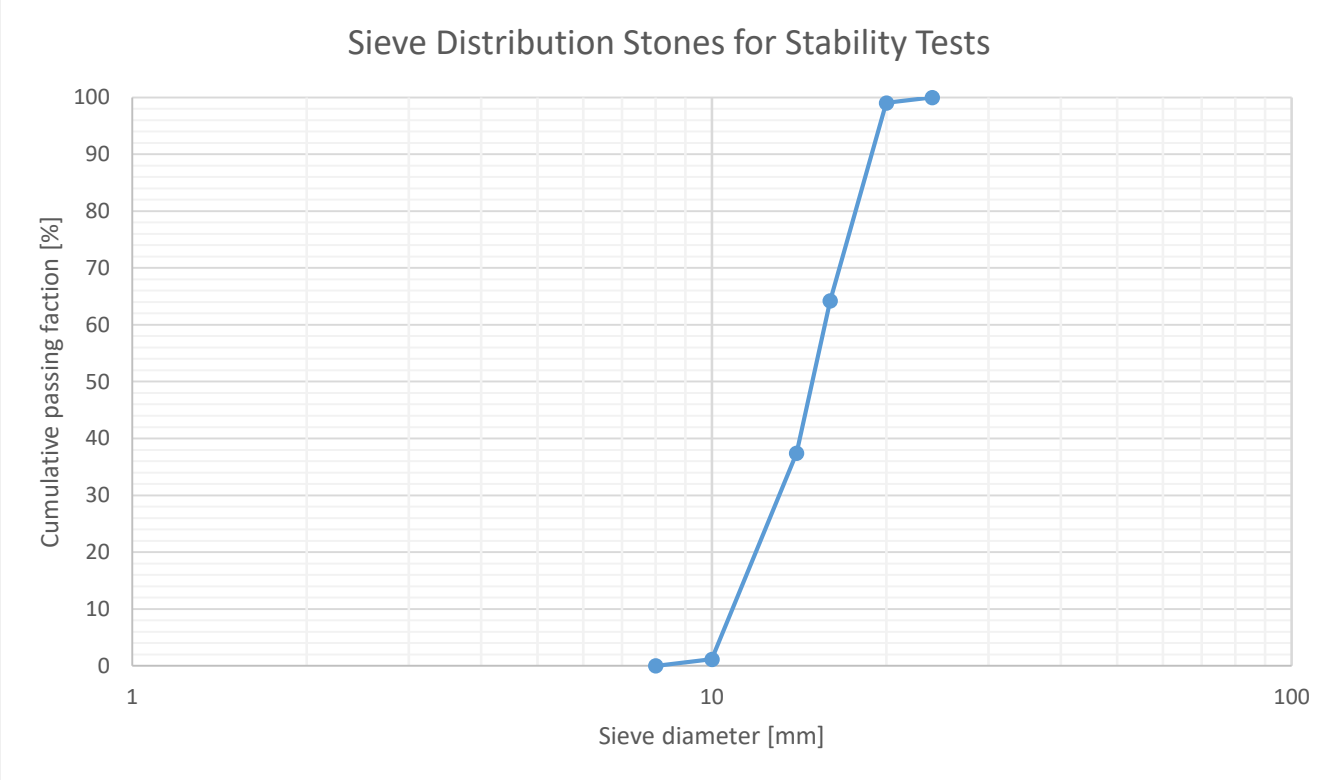

Figure 73 - Sieve distribution curve of the stones used during the stability tests of test scenario T6

From the sieve distribution curve follows that the d_{50} is equal to 15 mm. This value will be used during the analysis of the results of the stability tests. Furthermore the d_{15} is equal to 12 mm and the d_{85} is equal to 18 mm. This makes the relation d_{85}/d_{15} equal to 1.5.

Appendix F - Test results

In this appendix all measurement results are presented for each test scenario of the type II tests. For the test scenarios of the type II tests with velocity measurements (T1 – T10 except T6) this includes a top view of all measured time-averaged slope velocities, a top view of all measured absolute turbulence intensities, a plot of the centre slope velocities in x'- and y-direction, a plot of the centre absolute turbulence intensities in x'- and y-direction, a plot for the time-averaged sideward velocities in x'- and y-direction and a plot for the sideward absolute turbulence intensities in x'- and y-direction. For the test scenario with stability measurements (T6) this includes a plot of the amount of stone movements per step for all runs and the movement directions of the stones per step for each run.

Test Scenario T1

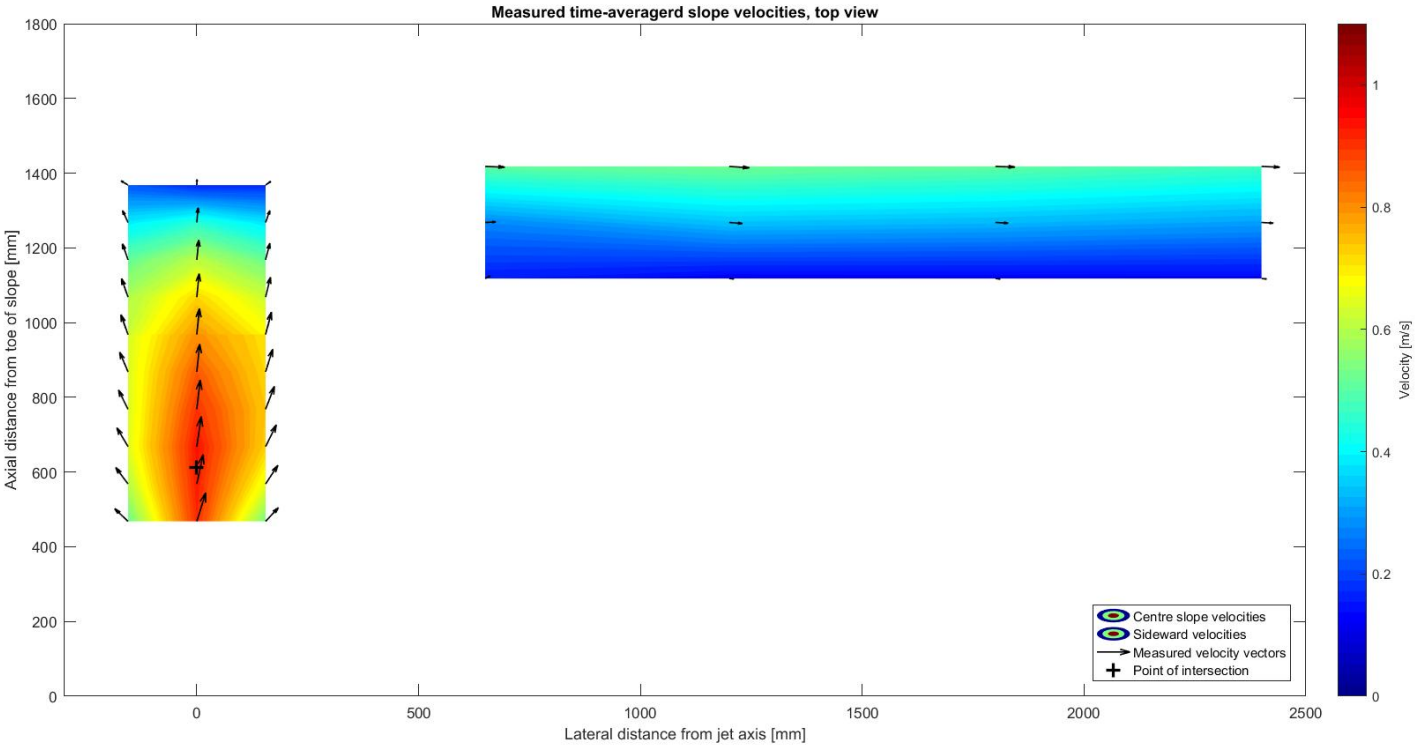

Figure 74 - Top view all measured slope velocities (Ux' and Uy combined) for T1

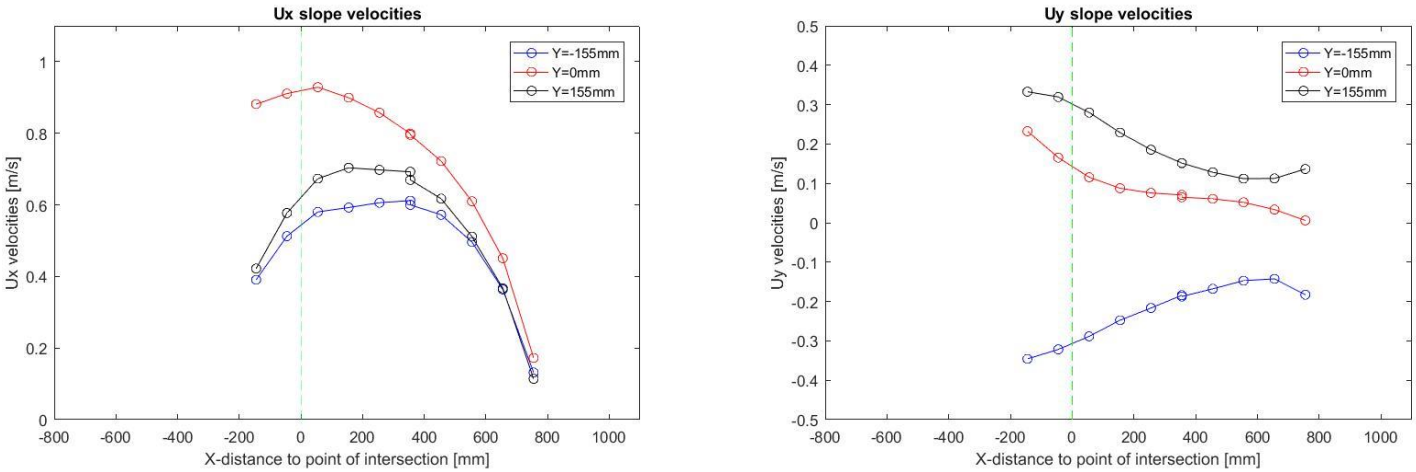

Figure 75 - Time-averaged velocities Ux' and Uy at center slope for T1

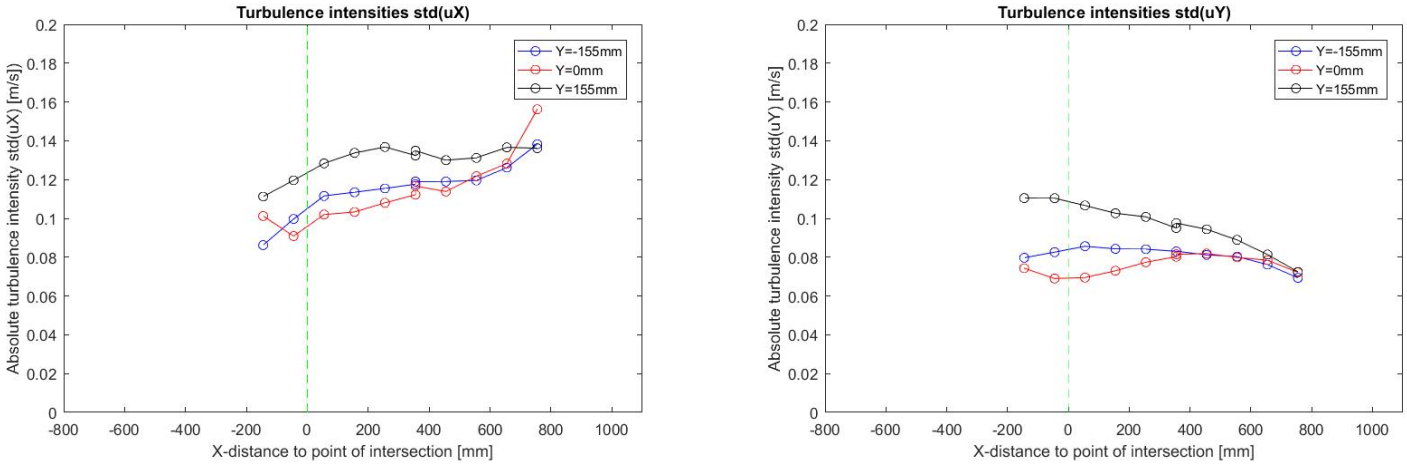

Figure 76 - Absolute turbulence intensities center slope x'- and y-direction for T1

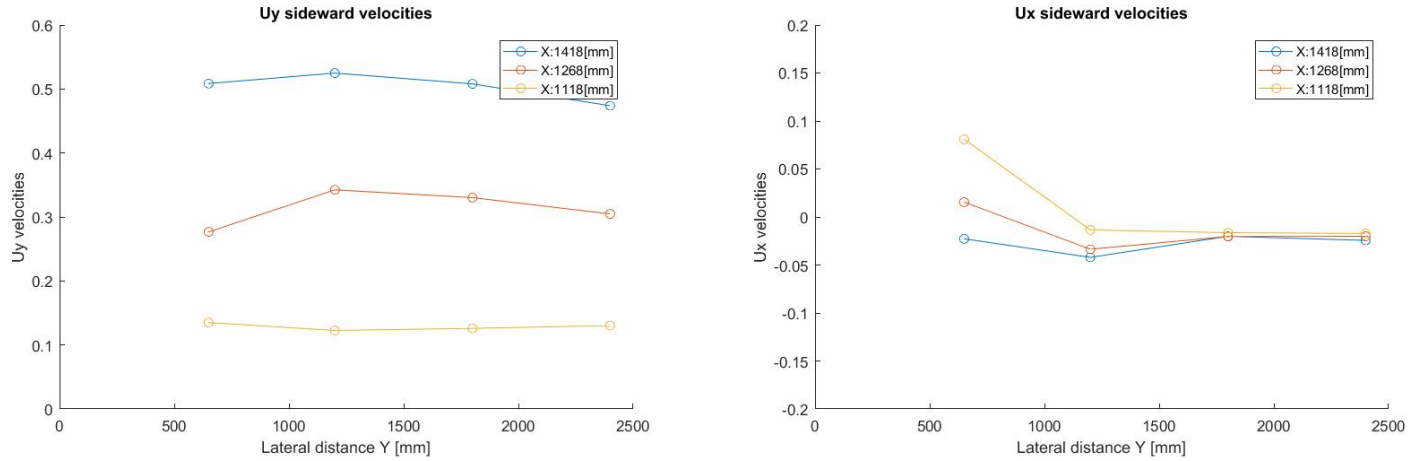

Figure 77 - Sideward time-averaged slope velocities Ux' and Uy for T1

Test Scenario T2

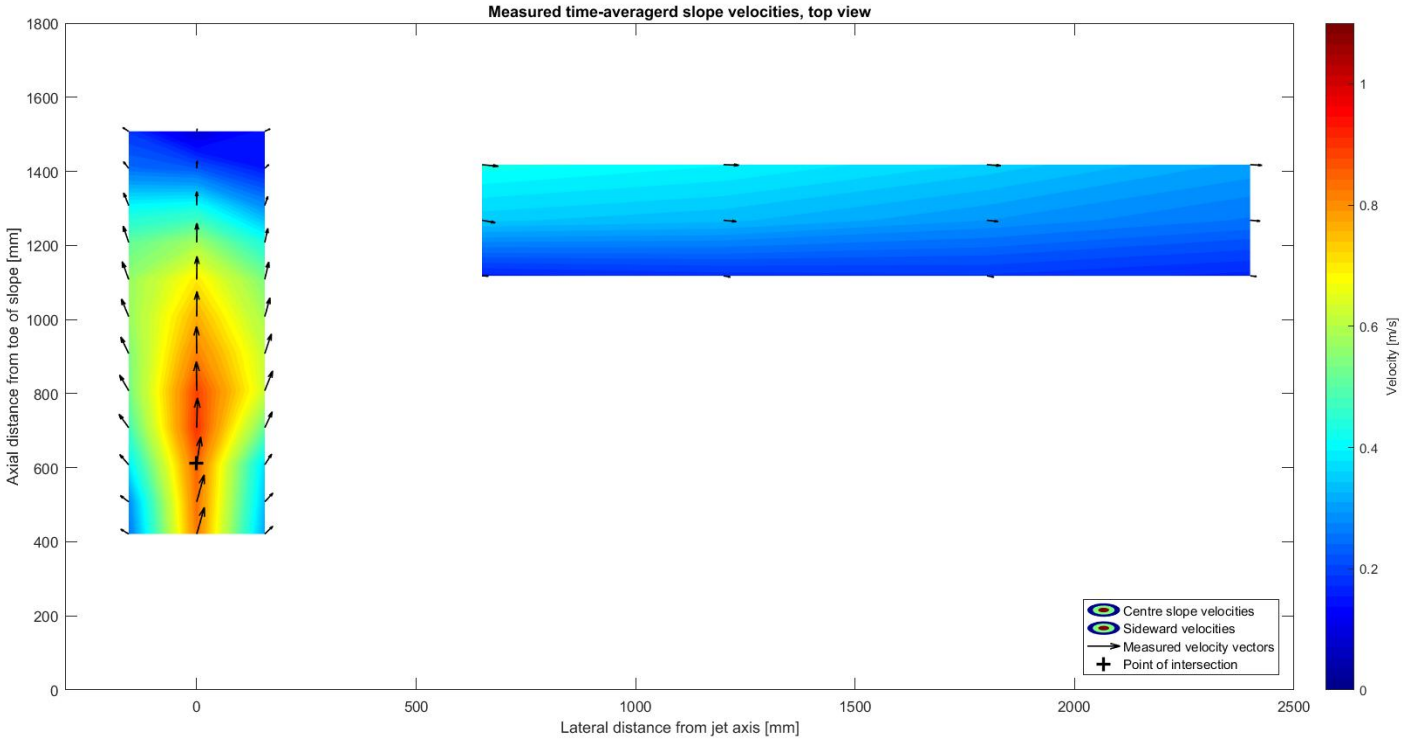

Figure 78 - Top view all measured slope velocities (Ux' and Uy combined) for T2

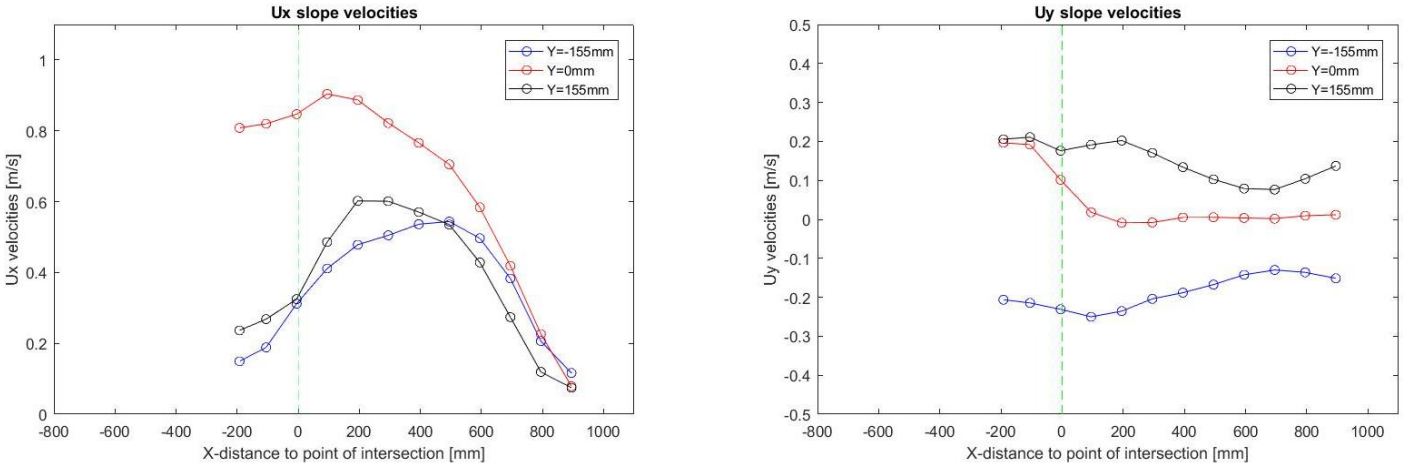

Figure 79 - Time-averaged velocities Ux' and Uy at center slope for T2

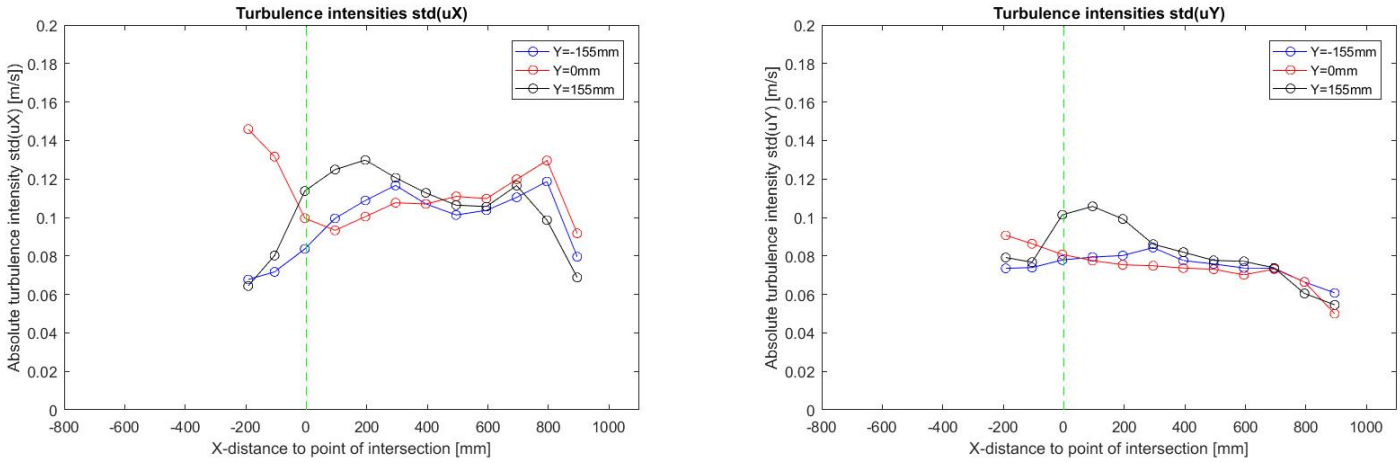

Figure 80 - Absolute turbulence intensities center slope x'- and y-direction for T2

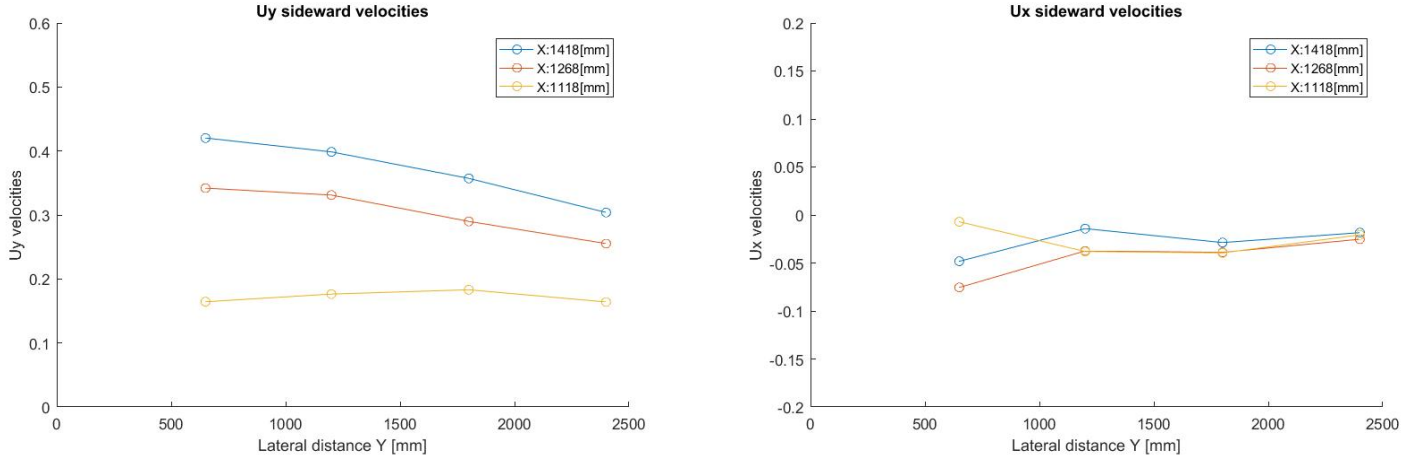

Figure 81 - Sideward time-averaged slope velocities Ux' and Uy for T2

Test Scenario T3

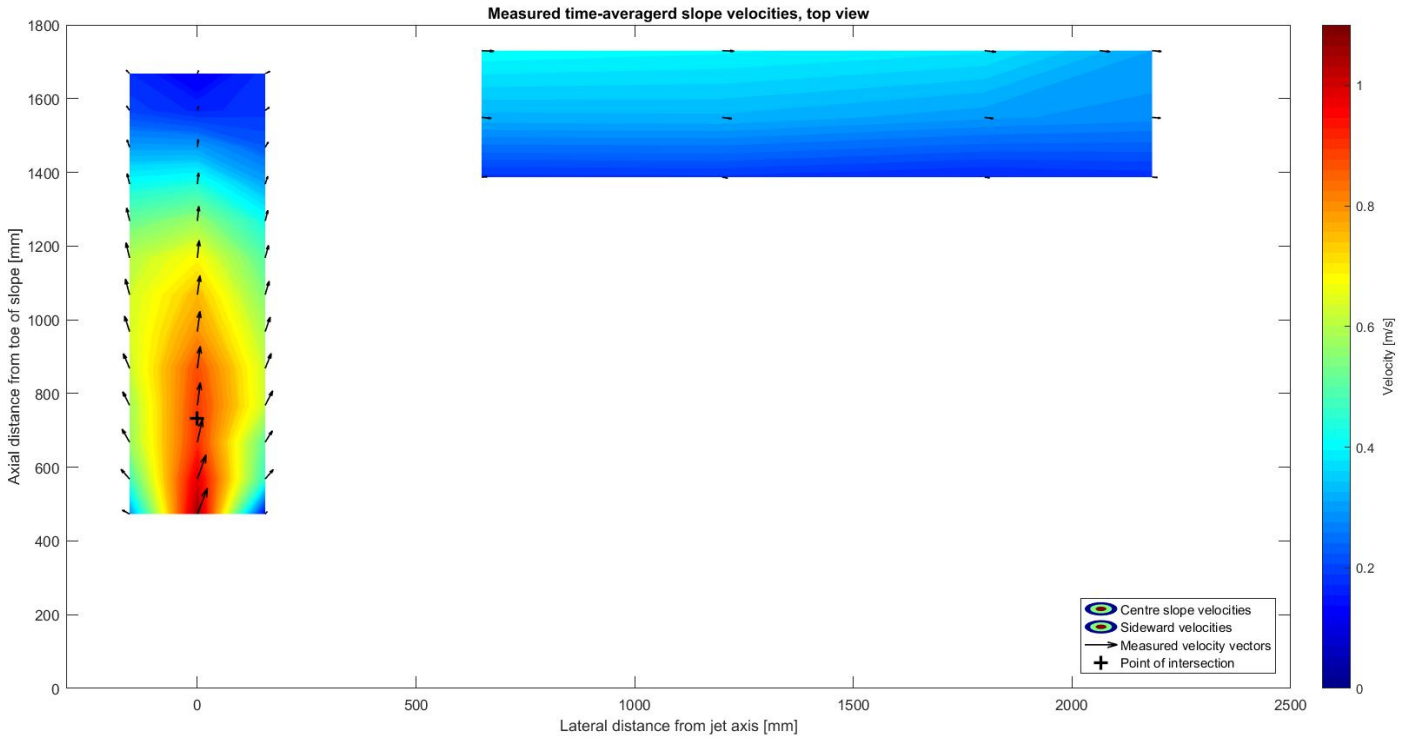

Figure 82 - Top view all measured slope velocities (Ux' and Uy combined) for T3

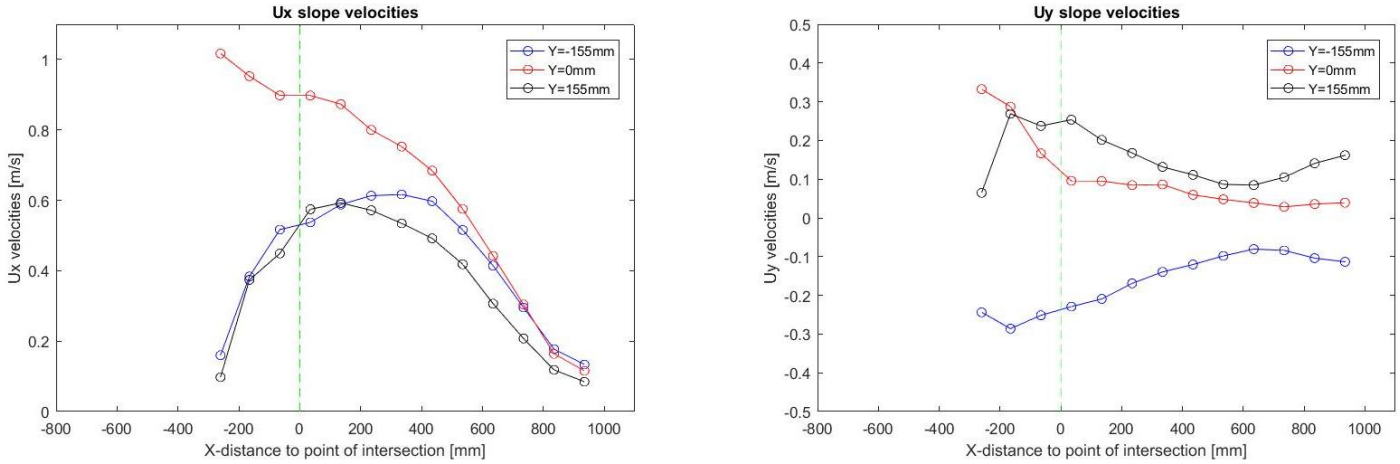

Figure 83 - Time-averaged velocities Ux' and Uy at center slope for T3

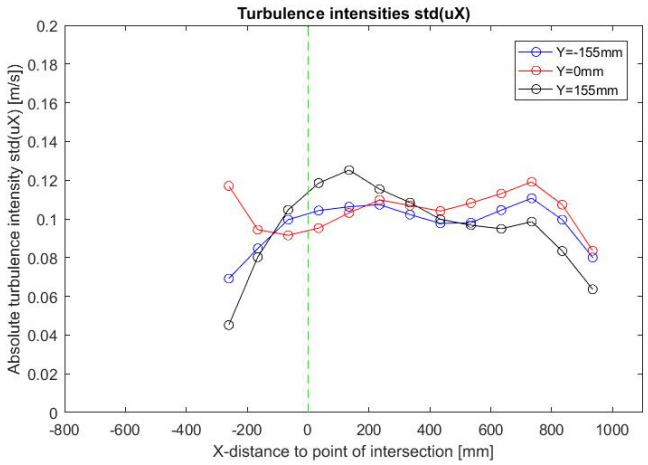

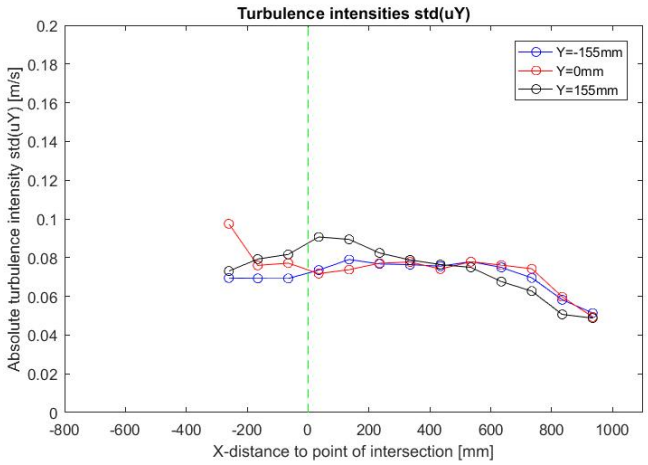

Figure 84 - Absolute turbulence intensities center slope x'- and y-direction for T3

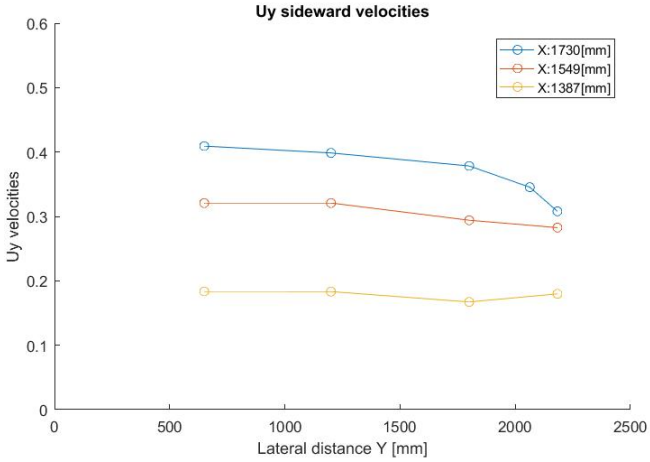

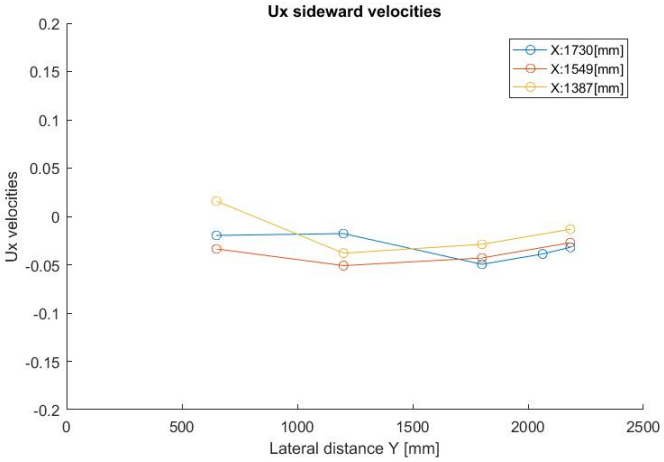

Figure 85 - Sideward time-averaged slope velocities Ux' and Uy for T3

Test Scenario T4

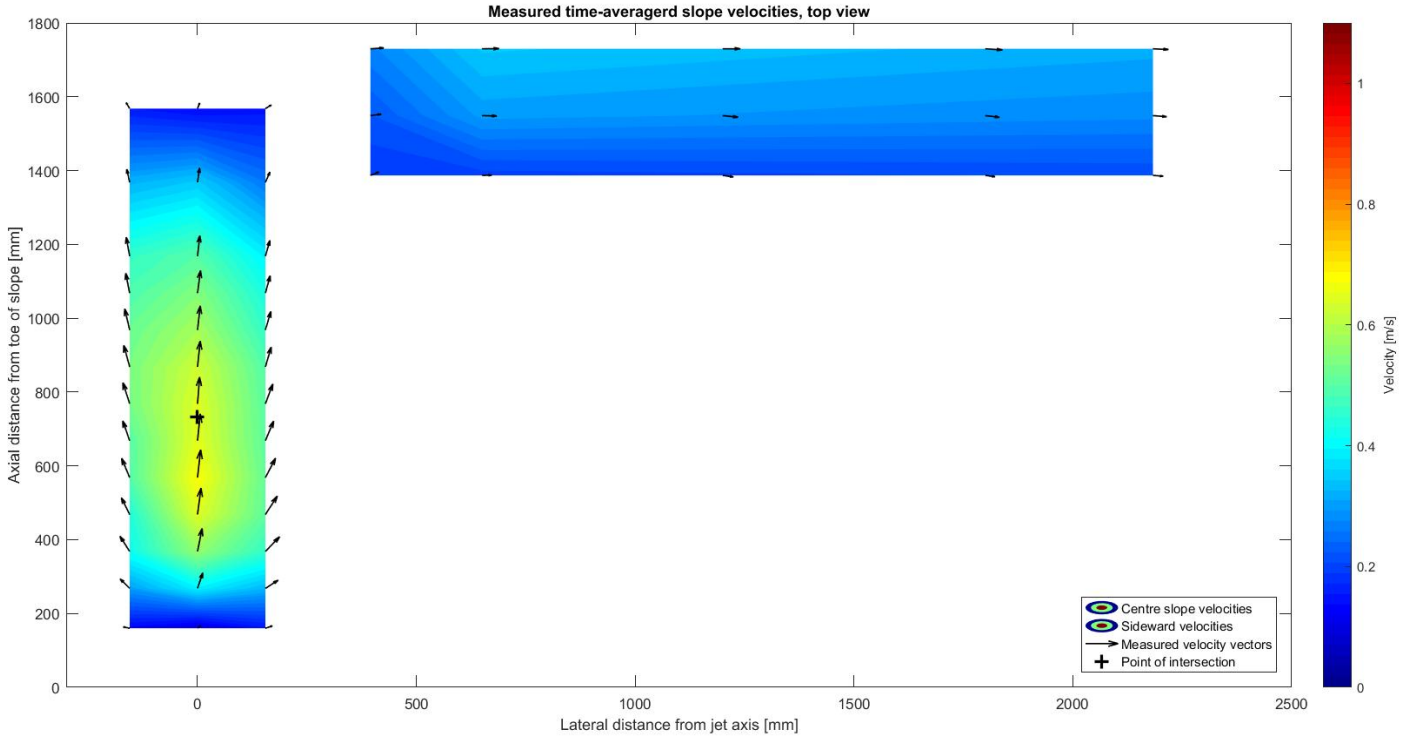

Figure 86 - Top view all measured slope velocities (Ux' and Uy combined) for T4

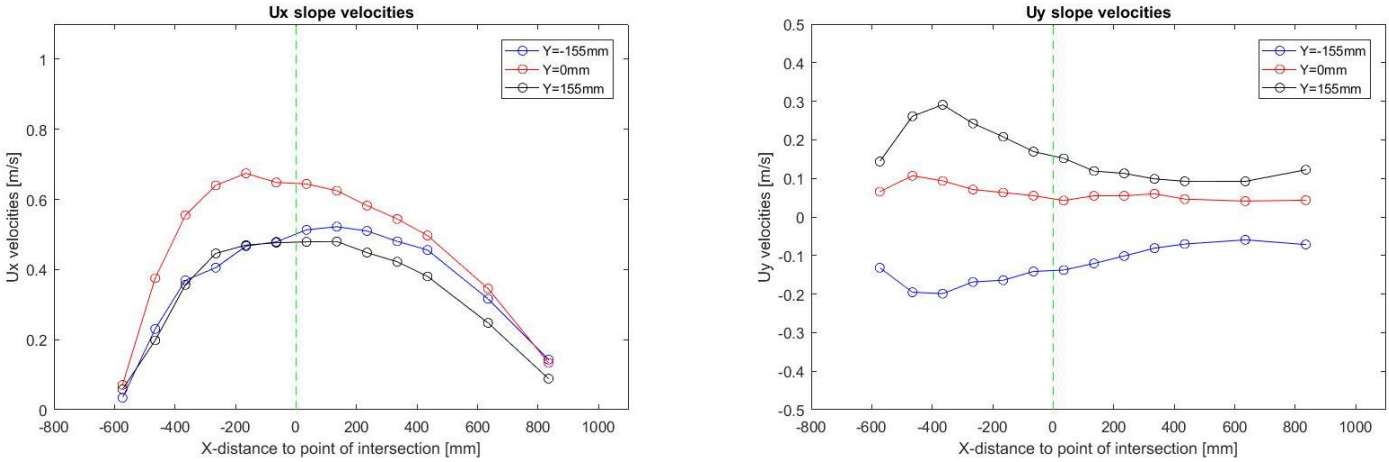

Figure 87 - Time-averaged velocities Ux' and Uy at center slope for T4

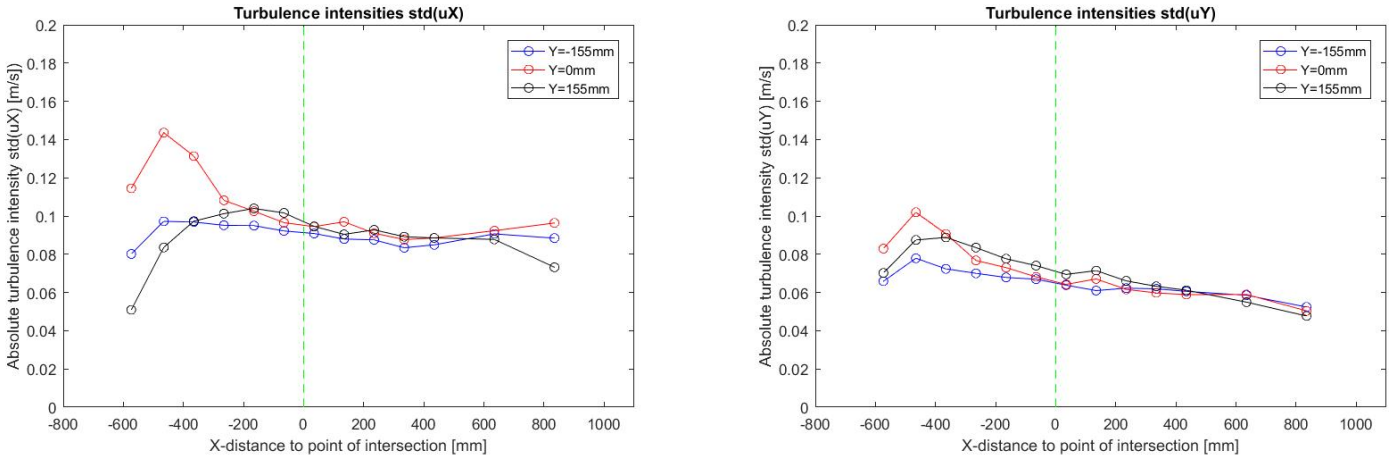

Figure 88 - Absolute turbulence intensities center slope x'- and y-direction for T4

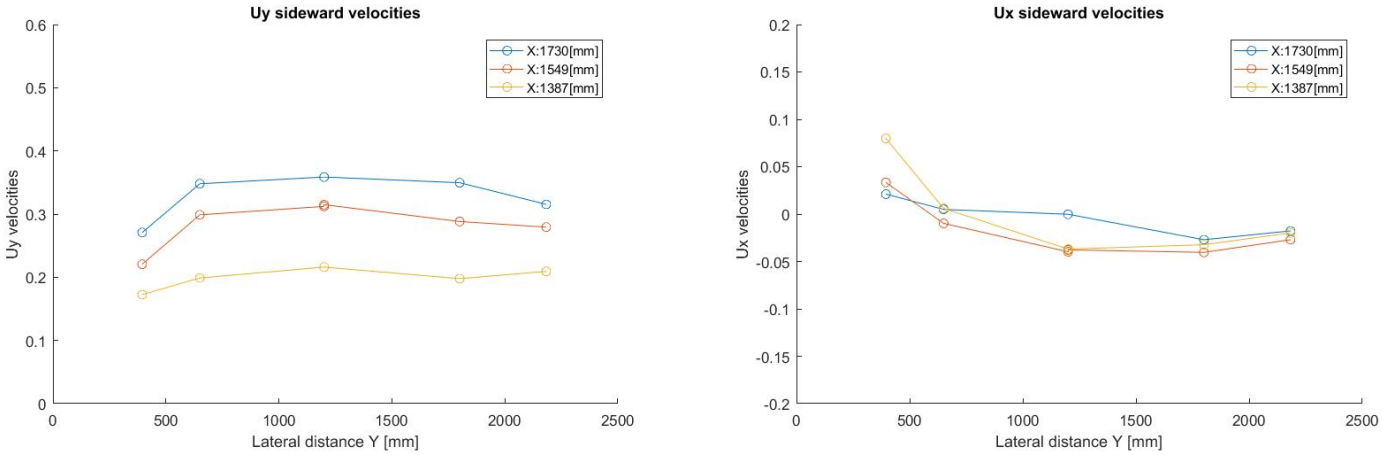

Figure 89 - Sideward time-averaged slope velocities Ux' and Uy for T4

Test Scenario T5

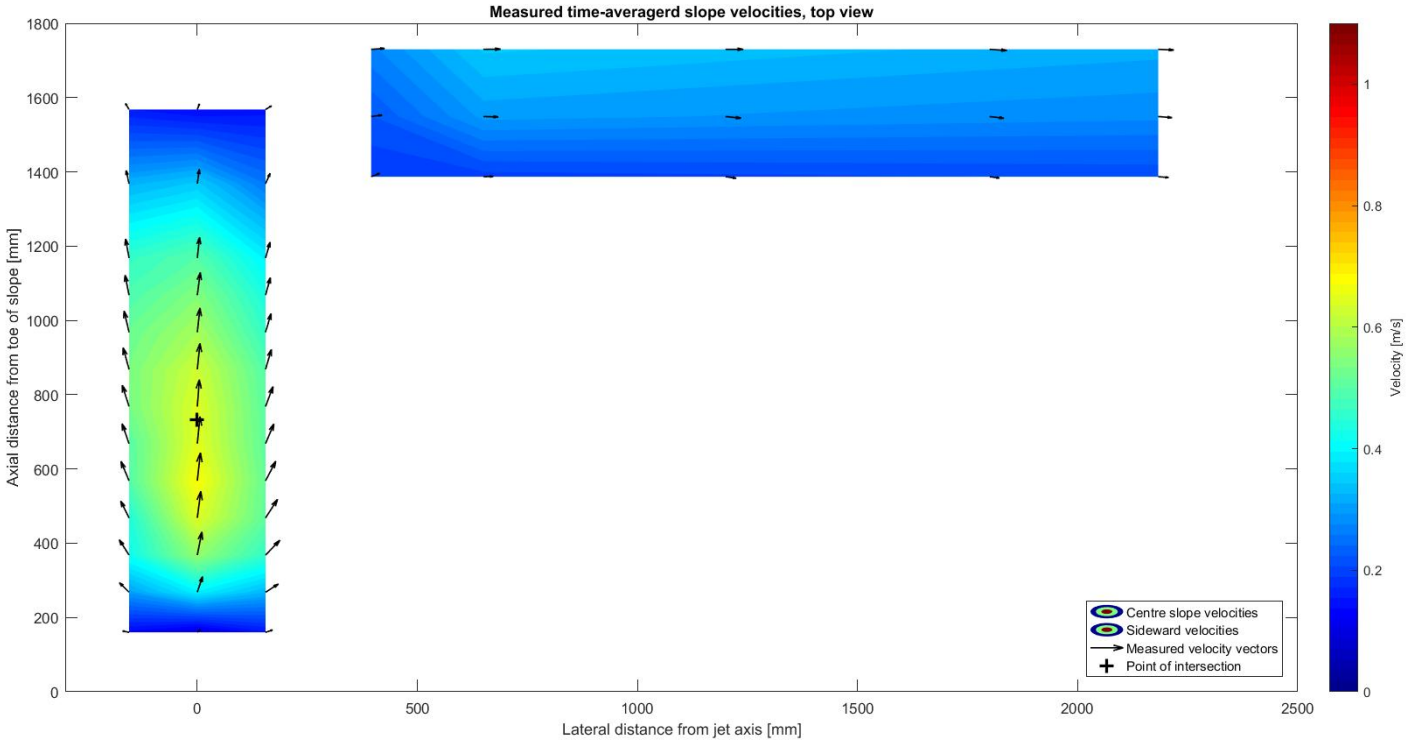

Figure 90 - Top view all measured slope velocities (Ux' and Uy combined) for T5

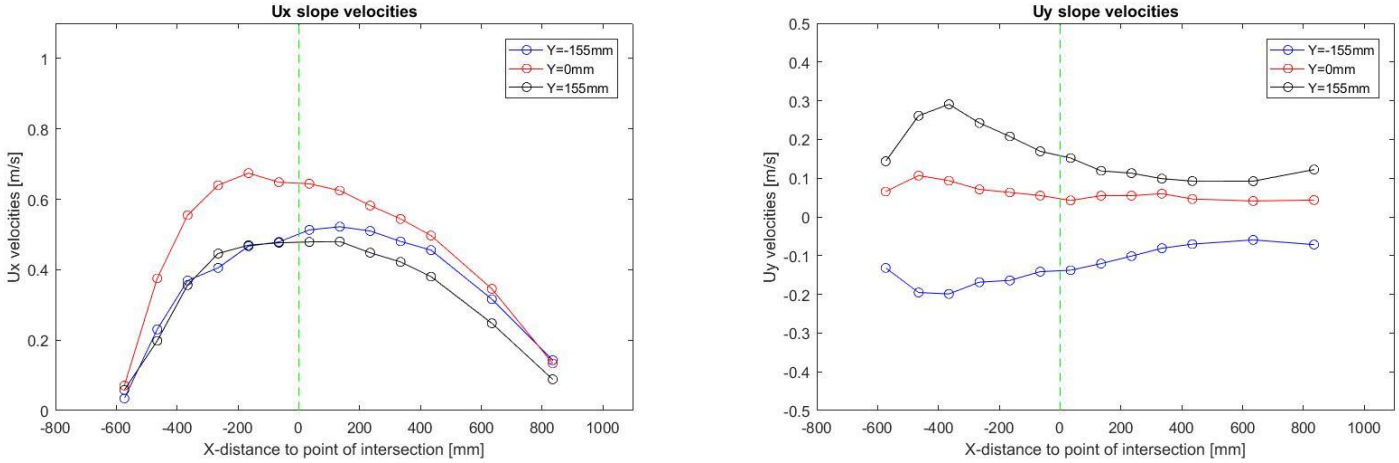

Figure 91 - Time-averaged velocities Ux' and Uy at center slope for T5

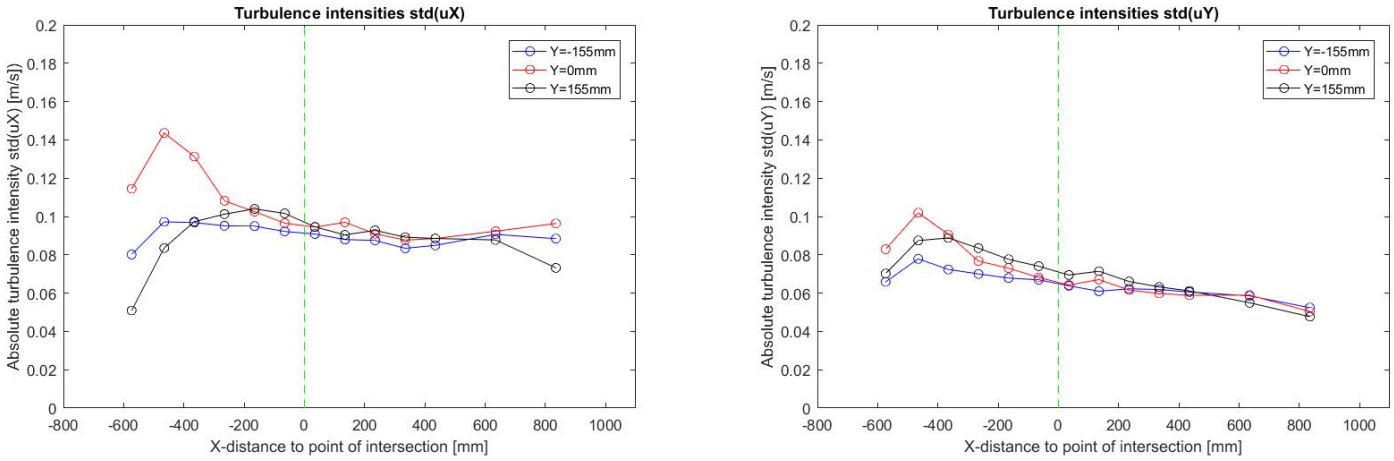

Figure 92 - Absolute turbulence intensities center slope x'- and y-direction for T5

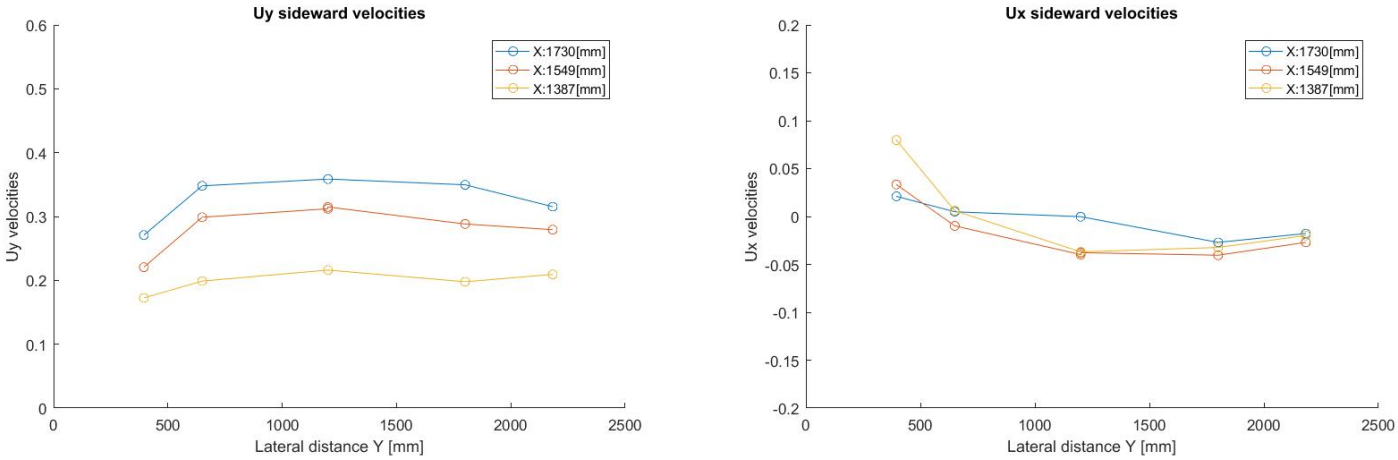

Figure 93 - Sideward time-averaged slope velocities Ux' and Uy for T5

Test Scenario T6

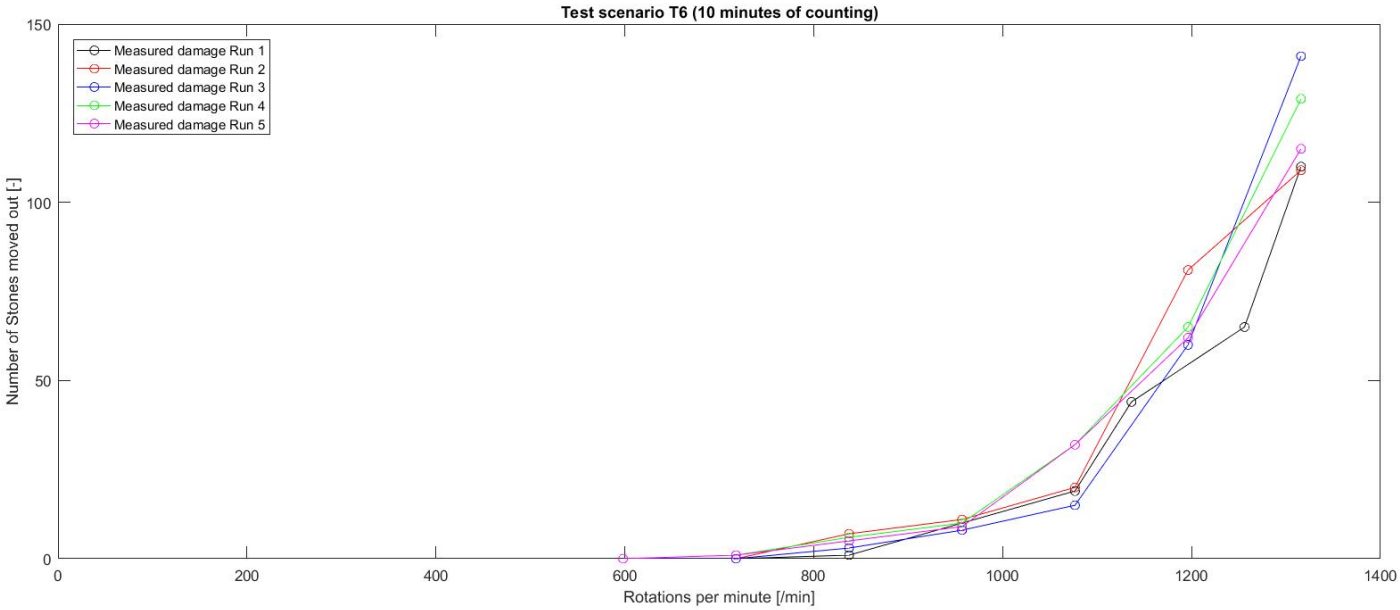

Figure 94 - Number of stone movements per step of all runs for T6

Test Scenario T7

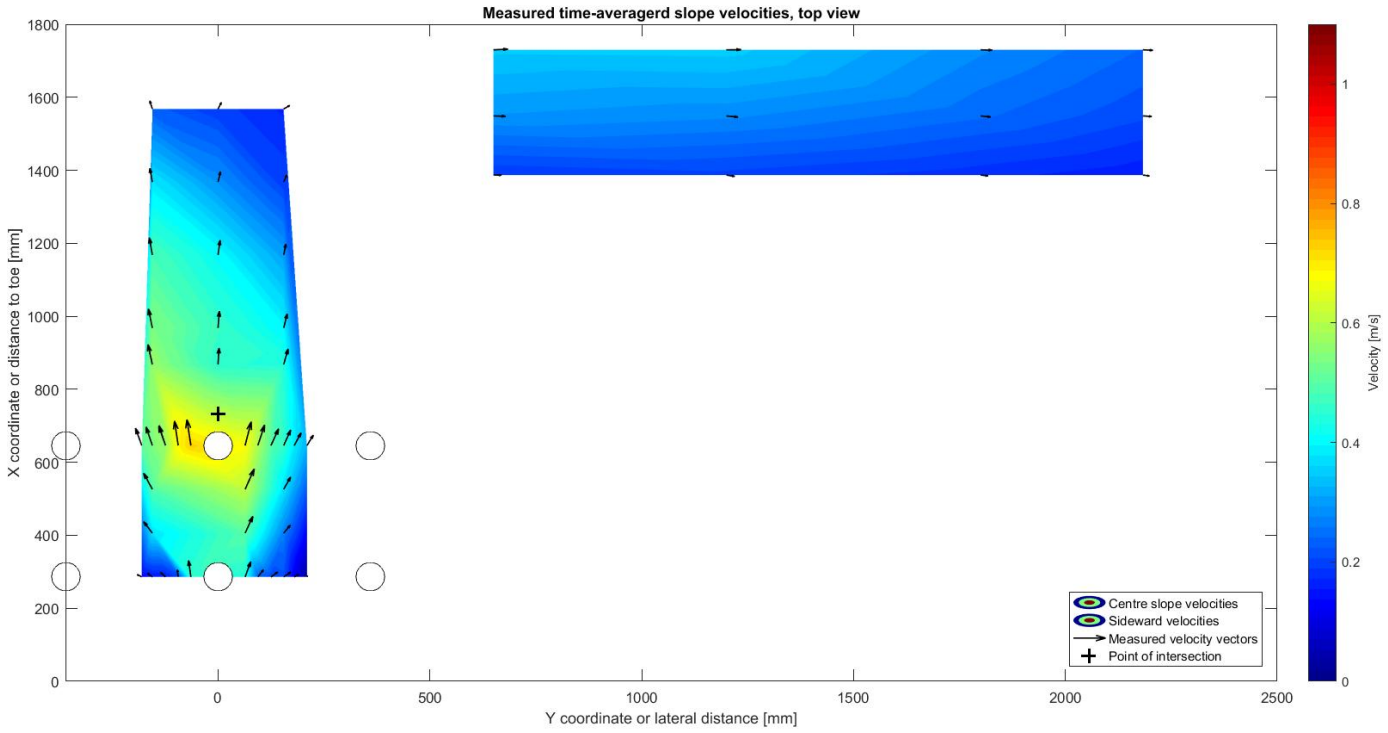

Figure 95 - Top view all measured slope velocities (Ux' and Uy combined) for T7

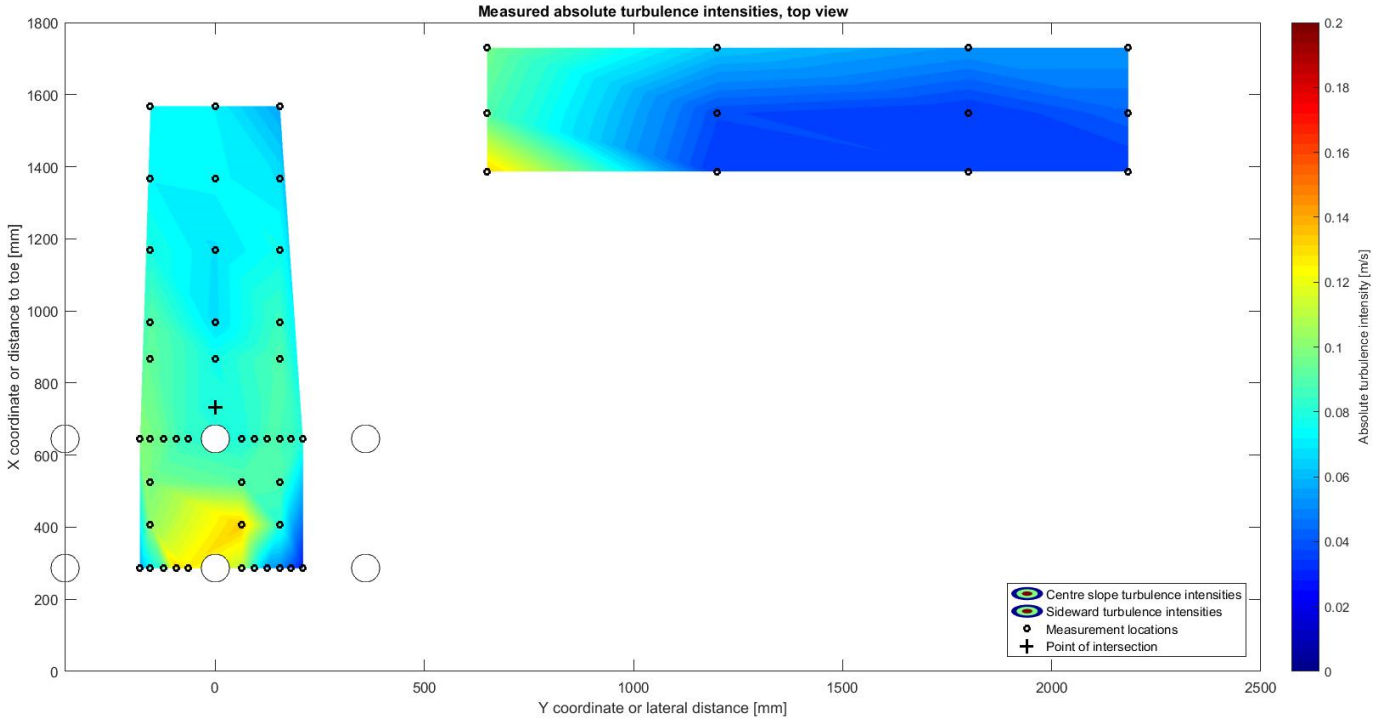

Figure 96 - Top view all measured absolute turbulence intensities in x'-direction (std(Ux')) for T7

Test Scenario T8

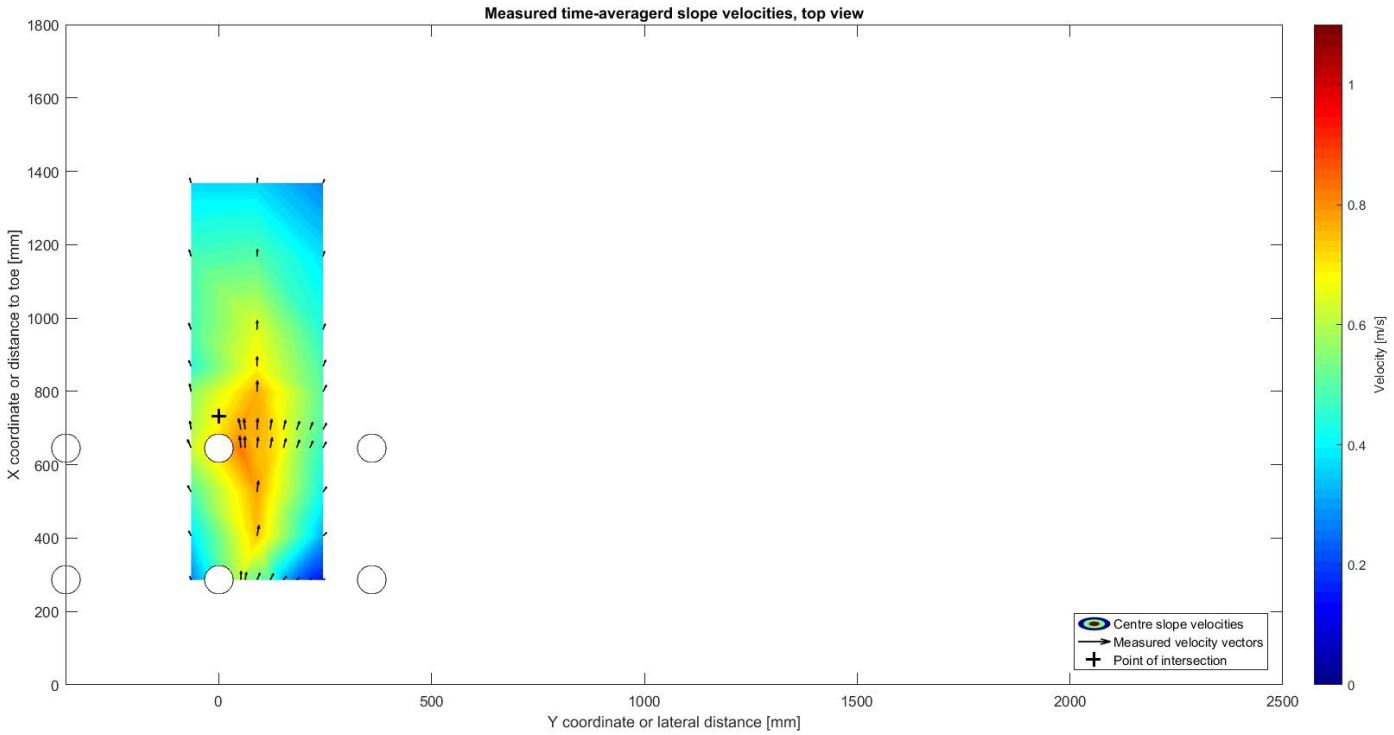

Figure 97 - Top view all measured slope velocities (Ux' and Uy combined) for T8

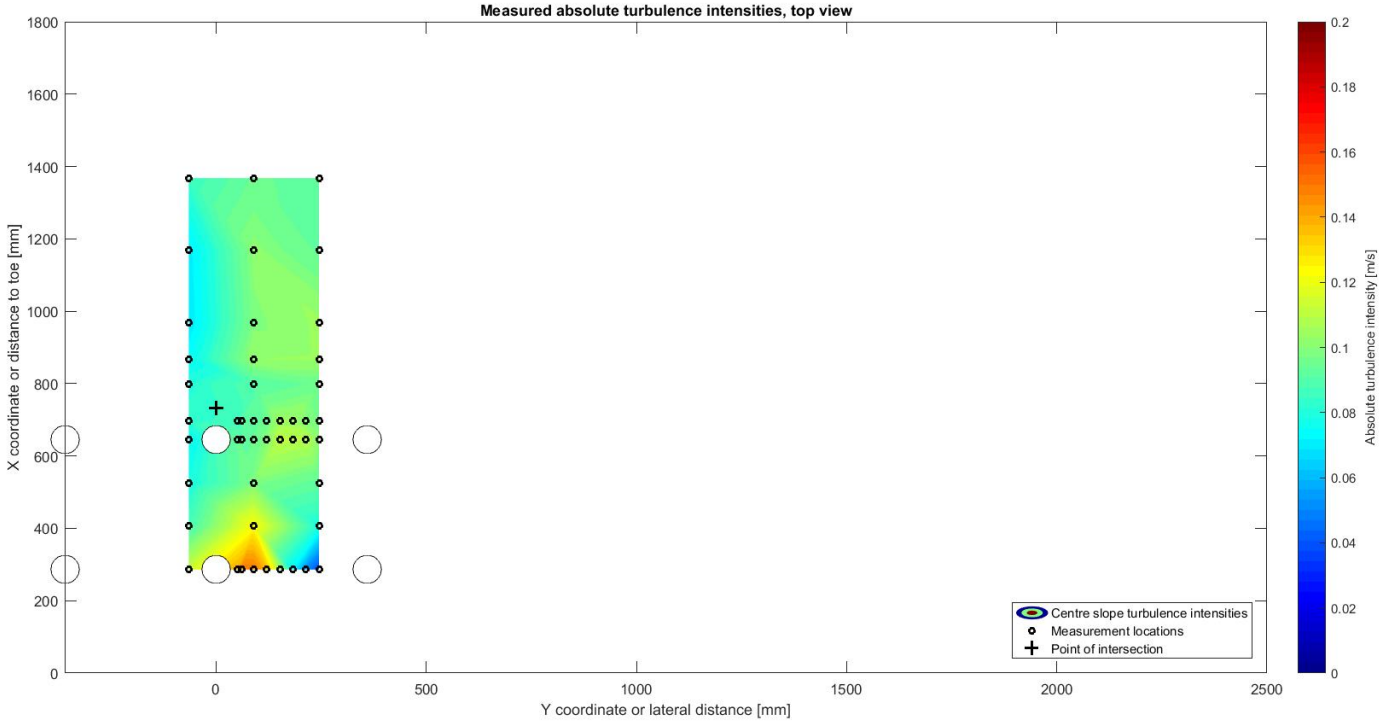

Figure 98 - Top view all measured absolute turbulence intensities in x'-direction (std(Ux')) for T8

Test Scenario T9

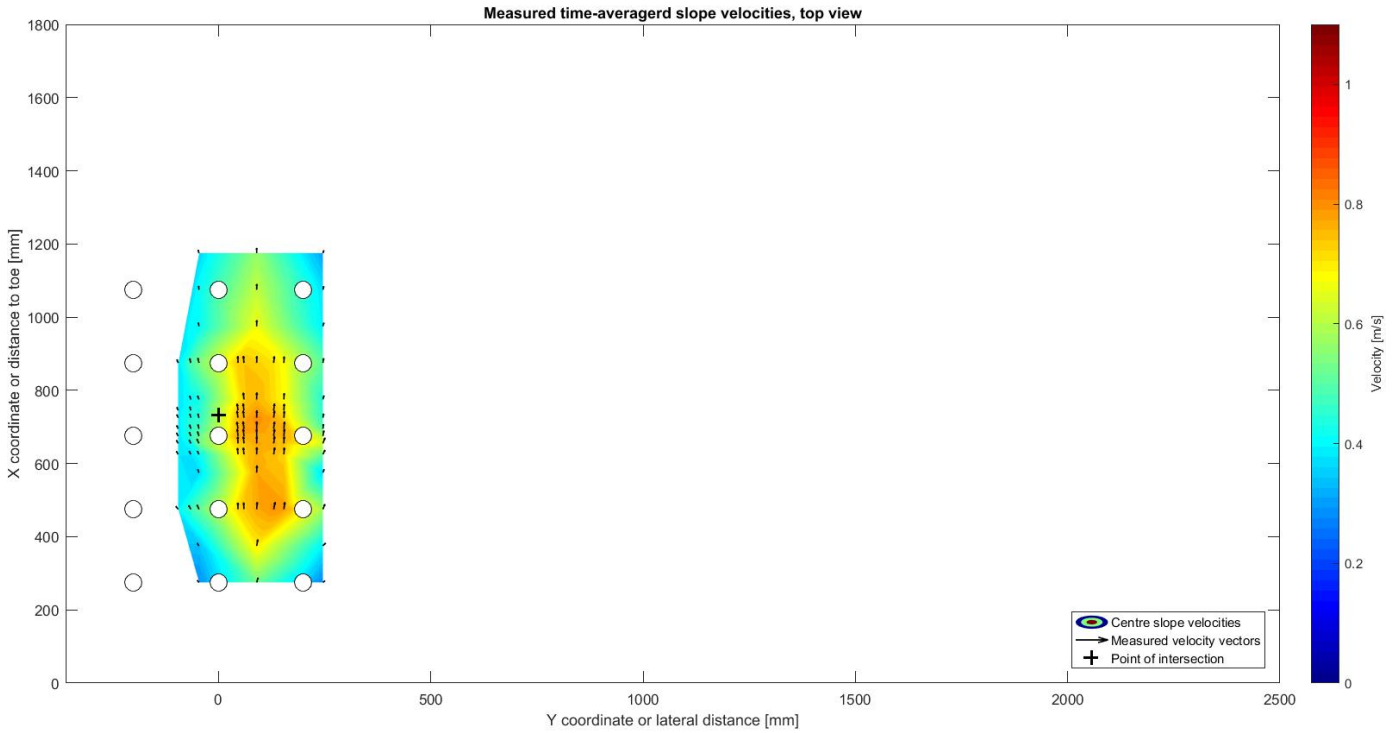

Figure 99 - Top view all measured slope velocities (Ux' and Uy combined) for T9

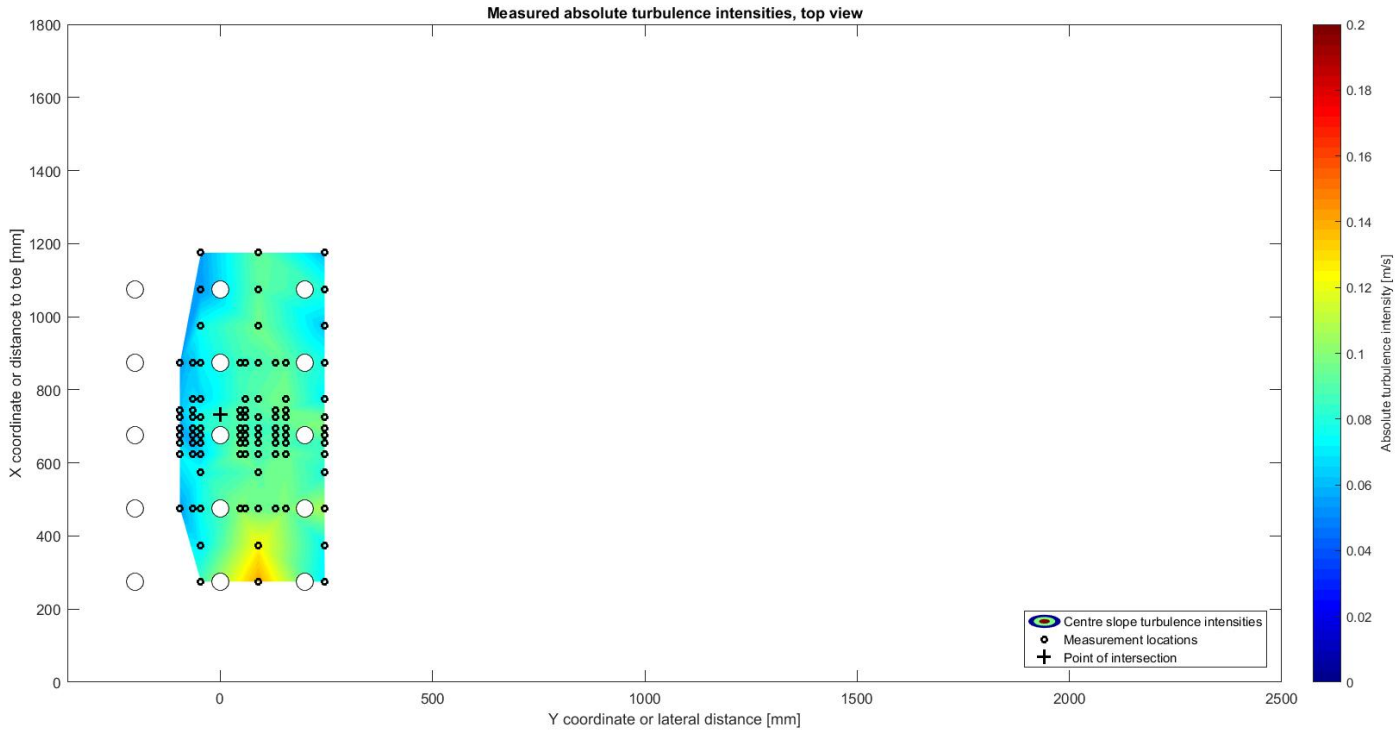

Figure 100 - Top view all measured absolute turbulence intensities in x'-direction (std(Ux')) for T9

Test Scenario T10

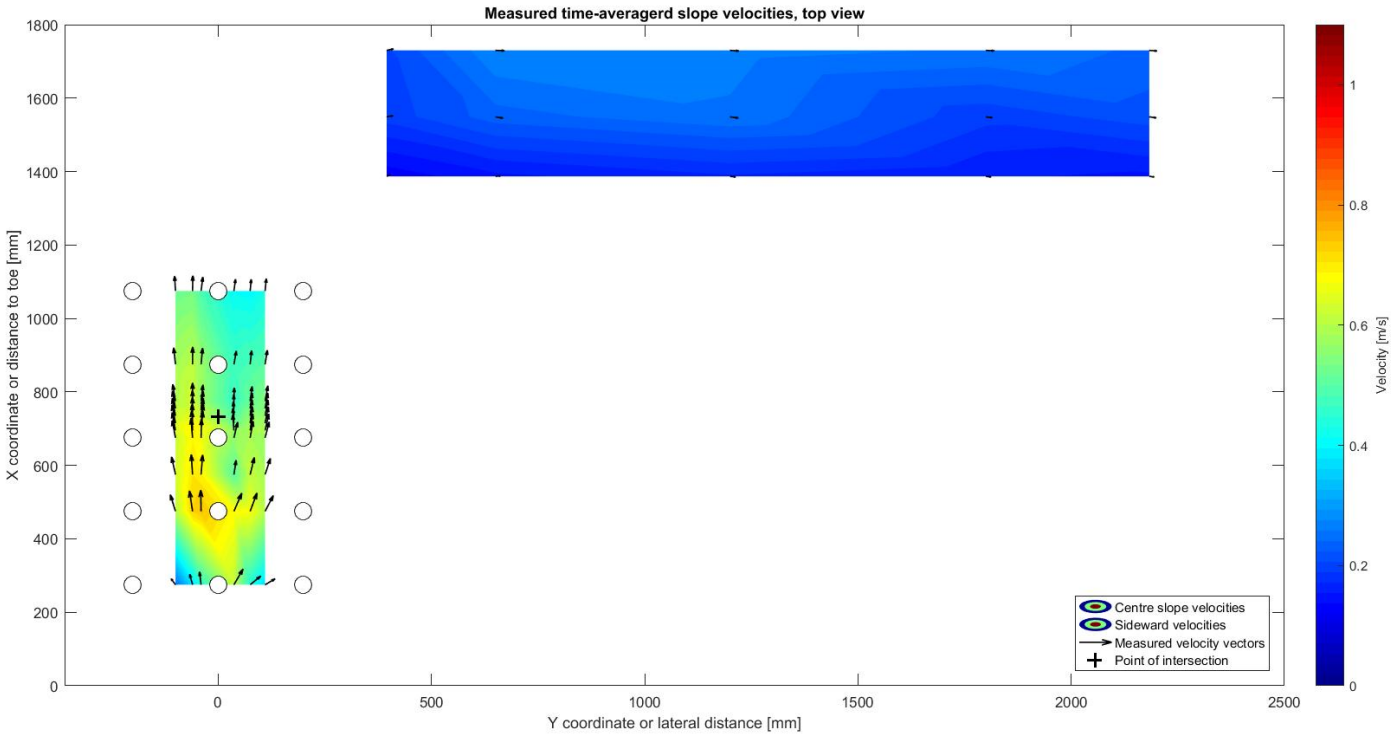

Figure 101 - Top view all measured slope velocities (Ux' and Uy combined) for T10

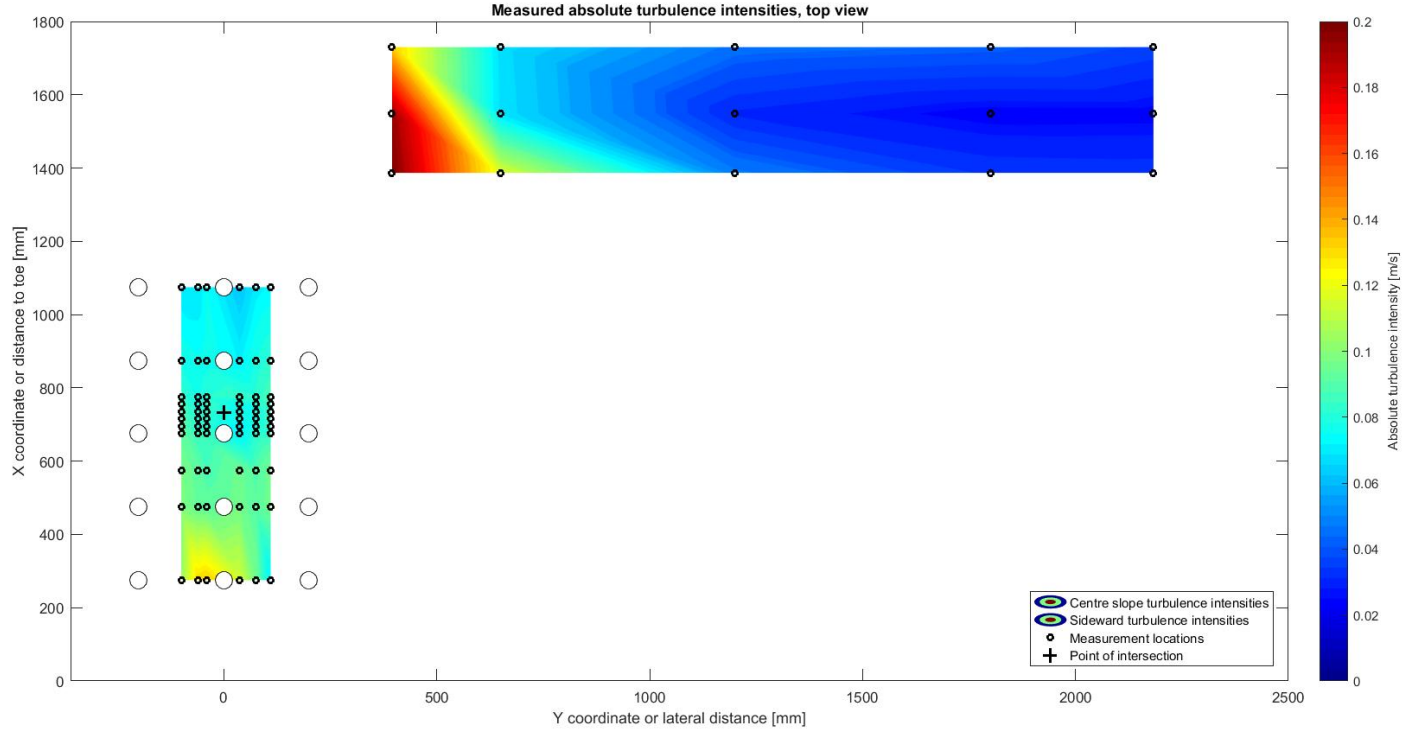

Figure 102 - Top view all measured absolute turbulence intensities in x'-direction (std(Ux')) for T10

Appendix G - Comparison to test results by Van Doorn (2012)

The first test scenario T1 has a similar model set up as the first test scenario tested by Van Doorn in 2012. The reason for this is that the model set ups tested in this research are an extension of the model set ups tested by Van Doorn (2012). It is therefore important to make a comparison to the data obtained by both researches for the same test scenario.

Both set ups contained an equal slope angle, axial distance and roughness of the sloping bed. Next to that a similar bow thruster and model vessel is used. There are only three differences and that are the basin dimensions, the measurement equipment and the water level. The basin used was much larger as already discussed in chapter 3. The measurement equipment for this research consisted of multiple EMSs where for the other research an Acoustic Doppler Velocimeter was used. The water level during this research was set at 0.63 m where for the first test scenario by Van Doorn the water level was set at 0.42 m. In addition, the wrong transformation of the measured velocities to the slope velocities perpendicular and parallel to the slope is corrected as well. Therefore the following corrections are applied on the data by Van Doorn (2012) before presented in Figure 103:

- First the correct transformation is applied on the measured velocities by Van Doorn in order to obtain the correct slope velocities. This transformation is discussed in section 2.2.1 and also reported by De Jong (2014).
- Secondly, the slope velocities are multiplied with a factor 1.08 to correct for the influence of the difference in water depth. Van Doorn (2012) investigated the influence of the difference in the water depth and found that there was a factor of 1.08 increase in slope velocities for this increase in water level. This factor is based on a different water level and different slope angle and takes the effect of both into account. Nevertheless this is used to multiply it with the values of the time-averaged velocity measured by Van Doorn.

The measured time-averaged $U_{x'}$ velocities and the absolute turbulence intensities of both researches are plotted in Figure 103.

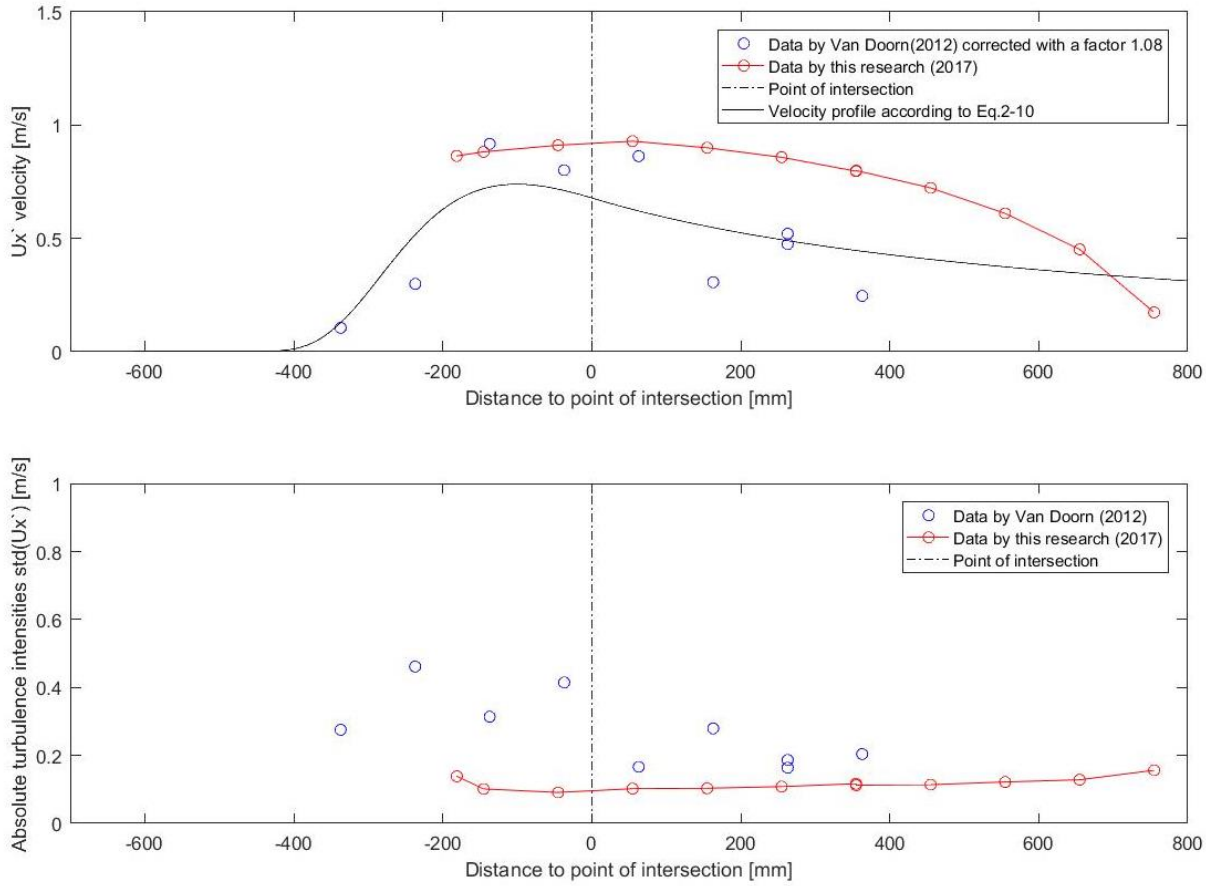

Figure 103 - Comparison between test results by Van Doorn (2012) and this research for test scenario T1

As can be observed from the plots is that there are some differences between the data obtained by both researches. Due to the smaller water depth it was not possible by Van Doorn to measure as high on the slope as during this research. Nevertheless it was possible during his measurements to measure closer to the toe of the slope. The measured maximum time-averaged slope velocity measured by Van Doorn (2012) shows a value that is nearly equal to the value of the maximum slope velocity of this research. However the location is before the point of intersection instead of after it. Next to that, the slope velocities measured by Van Doorn are smaller higher on the slope and are closer to the velocities according to equation (Eq. 2-10) higher on the slope. Also, the measurement points are not located on a fluent curve and have larger variations between sequential points. This makes the measurements by Van Doorn less reliable.

The absolute turbulence intensities of both researches show large differences. Where the other research shows turbulence intensities of 0.2 to 0.4 m/s, this research shows only intensities of 0.1 to 0.2 m/s. This probably has to do with the measurement equipment used. Another research by Schokking (2002) with a similar EMS as used for this research shows similar absolute turbulence intensities as shown in Figure 104. A possible explanation of the differences in measured absolute turbulence intensities is the higher effective measuring frequency of an Acoustic Doppler Velocimeter and the smaller measurement volume of an Acoustic Doppler Velocimeter. Due to this the ADV is able to measure also the smaller vortices and can therefore lead to a larger measured absolute turbulence intensity.

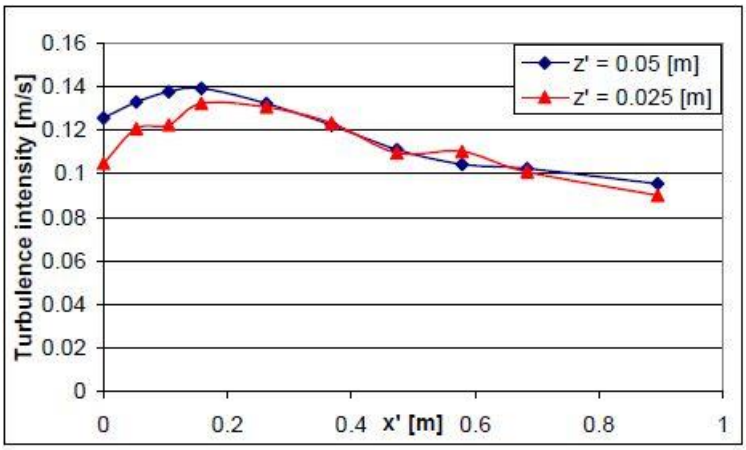

Figure 104 - Absolute turbulence intensities on slope measured during scale model tests by Schokking (2002)

Appendix H – Unconfined jet calculation method for slopes

This Appendix discusses the calculation of the velocity profile according to unconfined jet calculation method for hydraulic bed loads on a slope. For this an adaptation of the original equation is needed. The original formula is adapted in order to determine what velocities are expected along the slope caused by the propeller jet.

$$U_{x,r} = A * \left(\frac{D_p}{x}\right)^a * U_0 * exp\left(-\frac{1}{2C_2^2} * \frac{r^2}{x^2}\right) \quad \textit{(Eq. H-1)}$$

For x<L the 'r' is replaced by a factor that is a function of the axial distance and the slope angle in order to determine the jet velocities at locations on the slope before the point of intersection of the jet axis and the slope at x=L. The situation is presented in .

$$r = \frac{1}{m} * (L - x) \quad \textit{(Eq. H-2)}$$

$$\frac{r}{x} = \frac{1}{m} * \left(\frac{L}{x} - 1\right) \quad \textit{(Eq. H-3)}$$

$$U_{x<L,slope} = A * \left(\frac{D_0}{x}\right)^a * U_0 * exp\left(-\frac{b}{m^2} * \left(\frac{L}{x} - 1\right)^2\right) \quad \textit{(Eq. H-4)}$$

For x > L the jet axis has hit the slope and the propeller jet flows upwards along the slope, therefore r = 0:

$$U_{x>L,slope} = A * U_0 * \left(\frac{D_0}{x}\right)^a * 1 \quad \textit{(Eq. H-5)}$$

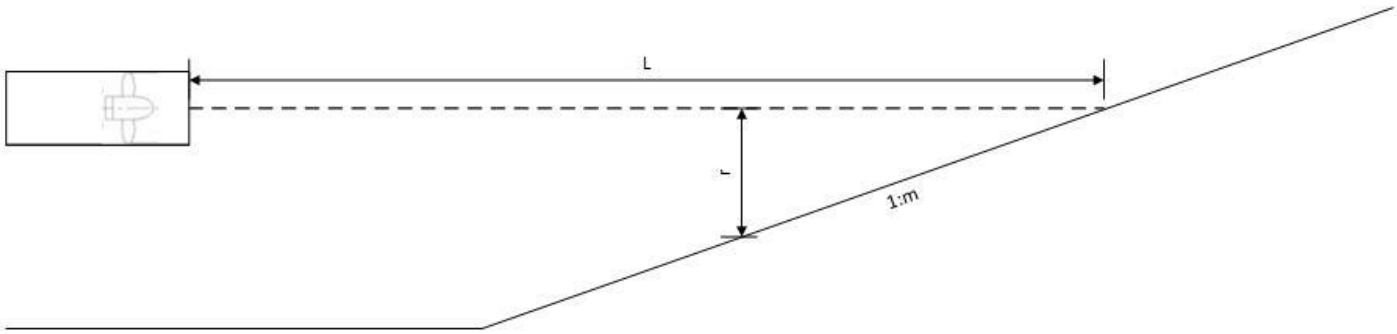

Figure 105 - Dutch Calculation method hydraulic bed loads for a slope situation